Understanding the Deactivation of the Iron Molybdate Catalyst and its Influence on the Formox Process

Raun, Kristian Viegaard

Publication date:
2018

Document Version
Publisher's PDF, also known as Version of record

Understanding the Deactivation of the Iron Molybdate Catalyst and its Influence on the Formox Process

Ph.D. Thesis

Kristian Viegaard Raun

Department of Chemical and Biochemical Engineering

Technical University of Denmark

September 2018

Preface

This thesis entitled “Understanding the Deactivation of the Iron Molybdate Catalyst and its Influence on the Formox Process” is submitted in partial fulfilment of the requirements for the Doctor of Philosophy degree (PhD) at the Technical University of Denmark (DTU). The thesis accounts for the most significant results achieved from the independent scientific research that I, Kristian Viegaard Raun, have conducted as part of the PhD study. To fulfil the requirements for completing a PhD I also followed courses, did teaching, dissemination and the public defence of the thesis. The work was completed at the Combustion and Harmful Emission Control (CHEC) Research Centre at the Department of Chemical and Biochemical Engineering (KT) in close collaboration with Haldor Topsoe A/S (HTAS), from October 2015 to September 2018. The research project was supervised by Professor Anker Degn Jensen (DTU), Assistant Professor Martin Høj (DTU) and Senior Principal Scientist Max Thorhauge (HTAS).

This PhD project is part of the larger research project entitled “Next Generation Methanol to Formaldehyde Selective Oxidation Catalyst” that focused on understanding the iron molybdate catalyst currently used for selective oxidation of methanol to formaldehyde and development of new catalysts. The project is a collaboration between KT at DTU, HTAS and Karlsruhe Institute of Technology (KIT). The financial support from The Independent Research Council under grant number DFF – 4184-00336 is gratefully acknowledged.

During the PhD project, I have supervised Max Schumann, Jeppe Johannessen and Kaylee McCormack in their student projects. Thank you for your contribution to the PhD project. Furthermore, I gratefully acknowledge Professor Jan-Dierk Grunwaldt (KIT) for fruitful discussions during the PhD project.

I would like to thanks the CHEC technicians Anders Kjersgaard and Nikolaj Nissen who assisted in rebuilding the single pellet setup, and the workshop at KT especially Lars Møller, Michael Lindaa and Søren Vestergaard Madsen who also assisted in rebuilding the setup.

I would also like to thank all my fellow PhD students at KT and especially my two office-mates Lars Schwarzer and Giovanni Cafaggi. You have all contributed to a good and fun working environment.

Kristian Viegaard Raun

Kongens Lyngby

September 30th, 2018

Abstract

The industrial production of formaldehyde from methanol is an important chemical process. The majority of the produced formaldehyde is processed into higher-valued synthetic resins, making formaldehyde an important chemical building block. In 2017 approximately 52 million ton were produced, and the demand is increasing.

Formaldehyde is primarily synthesized industrially by selective oxidation of methanol over an iron molybdate catalyst. The industrial catalyst is composed of $Fe_2(MoO_4)_3$ with an excess of MoO_3 corresponding to a molar ratio of Mo/Fe of 2-3. However, the process lifetime is only 1-2 years due to loss of molybdenum from the catalyst leading to a loss of selectivity and pressure drop increase over the bed due to transport and downstream deposition of the volatilized molybdenum. The relative short lifetime of the process leaves great room for improvements.

This thesis is dedicated to study the performance of the iron molybdate catalyst under reaction conditions and propose strategies to stabilize the catalyst and mitigate molybdenum transport taking both catalyst preparation and reactor design into account.

The first part of the thesis investigates the catalytic performance of a synthesized iron molybdate catalyst with a particle size of 150-300 μm during selective oxidation of methanol to formaldehyde for a period up to 25 days. The structural and compositional changes of the catalyst were characterized and it was shown that free MoO_3 quickly (around 10 hours) volatilized leaving a MoO_3-depleted catalyst. At longer operating time, also the $Fe_2(MoO_4)_3$ lost molybdenum successively forming $FeMoO_4$ and finally Fe_2O_3. However, even at significant changes in the catalyst composition, it maintained a rather satisfactory selectivity towards formaldehyde (above 92 %). Surprisingly, formation of β-MoO_3 was observed after 25 days, indicating that this species might be stable to some extent under reaction conditions.

The second part of the thesis investigates volatilization and loss of MoO_3 from industrial catalyst pellets under varying reaction conditions for a period up to 10 days. Molybdenum was shown to volatilize, leaving a depleted zone starting at the pellet surface and moving inwards with time. The rate of volatilization was shown to be enhanced by increasing methanol concentration and operating temperature, while water was shown to inhibit the rate of volatilization. The experimental data was used to develop and validate a dynamic single pellet mathematical model, which considers the diffusion and oxidation of methanol, the reversible volatilization reaction between molybdenum (MoO_3) and methanol, and the diffusion of all gaseous species including the volatile molybdenum species through the pellet. The model calculates the loss of Mo as a function of the position in the pellet, time on stream and reaction conditions and compared favorably with the experimental data.

In the third part of the thesis the developed single pellet model is implemented in a reactor model, where transport of the volatilized MoO_3 and deposition downstream in the reactor bed takes place. As methanol is converted through the bed, the volatilized Mo species decompose into MoO_3 and methanol in the void space between the pellets due to the reverse volatilization reaction. The deposition decreases the void space leading to pressure drop buildup, which is calculated as a function of the catalyst shape and molybdenum content, reaction conditions and time on stream. The reactor model is fitted to experimental measurements of increasing pressure drop in a pilot scale reactor at Haldor Topsøe A/S. Finally the model is used to predict the effect of different strategies to extend the process lifetime. By reducing the molybdenum content or changing the shape of the catalyst pellets from open to filled cylinders in the initial part of the reactor, optimization of the pressure drop increase is achieved.

This thesis contributes with new insight into the structural changes and catalytic performance of the iron molybdate catalyst under reaction conditions over a time period long enough to achieve significant degradation. The developed catalyst pellet model implemented into a reactor model was used to analyze different strategies to extend the process lifetime with respect to catalyst preparation. Redesigning the catalyst in the initial part of the reactor was shown to potentially extend the lifetime of the formaldehyde process significantly.

Resumé (Summary in Danish)

Industriel produktion af formaldehyd fra metanol er en vigtig kemisk proces. Størstedelen af den producerede formaldehyd omsættes til syntetiske resiner, hvilket gør formaldehyd til et vigtig kemisk mellemprodukt. I 2017 blev der produceret ca. 52 millioner tons, og efterspørgslen er stigende.

Industrielt fremstilles formaldehyd primært via selektiv oxidation af metanol over en jernmolybdat-katalysator. Den industrielle katalysator består af $Fe_2(MoO_4)_3$ med et overskud af MoO_3 svarende til et molforhold mellem Mo/Fe på 2-3. Processens levetid er imidlertid kun 1-2 år på grund af tab af molybdæn fra katalysatoren, hvilket fører til tab af selektivitet og tryktabsstigning over katalysatorlejet på grund af transport og afsætning af flygtig molybdæn i lejet. Den relative korte proceslevetid efterlader store muligheder for forbedringer.

Denne afhandling undersøger jernmolybdat-katalysatorens ydeevne ved reaktionsbetingelser. Strategier til at stabilisere katalysatoren og nedbringe molybdæntransport undersøges med henblik på både katalysatorfremstilling og procesdesign.

I den første del af afhandlingen undersøges jernmolybdat-katalysatorens ydeevne til selektivt at oxidere metanol til formaldehyd i en periode på 25 dage. Her anvendes katalysatorpartikler i sigtefraktionen 150-300 µm hvor der ikke diffusionsbegrænsninger. Ændringer i katalysatorens struktur og sammensætning blev karakteriseret, og det blev påvist, at overskud af MoO_3 hurtigt (ca. 10 timer) afdamper og efterlader en MoO_3-udtømt katalysator. Over længere driftstid afdamper molybdæn fra $Fe_2(MoO_4)_3$ under dannelse af $FeMoO_4$ og ved yderligere afdampning dannes Fe_2O_3. Katalysatoren bibeholdt imidlertid en tilfredsstillende selektivitet (over 92 %) selv efter signifikante ændringer i katalysatorsammensætningen til højt jernindhold. Mod forventning blev dannelse af β-MoO_3 observeret efter 25 dage, hvilket indikerer at denne molybdænfase i en vis grad er stabil ved reaktionsbetingelser.

Den anden del af afhandlingen undersøger afdampning og tab af MoO_3 fra industrielle katalysatorpiller, hvor diffusionsbegrænsninger er betydelige, ved varierende reaktionsbetingelser i en periode på op til 10 dage. Molybdæn viste sig at afdampe og efterlade en udtømt zone, der startede ved pillens overflade og bevægede sig indad over tid. Hastigheden

af afdampningen steg ved øget metanolkoncentration og driftstemperatur, mens øget vandkoncentration inhiberede afdampningen. De eksperimentelle data blev anvendt til at udvikle og validere en dynamisk, matematisk enkeltpille-model, der betragter diffusion og oxidation af metanol, den reversible afdampningsreaktion mellem molybdæn (MoO_3) og metanol og diffusion af alle komponenter i gasfasen, herunder de afdampede molybdæn komponenter, gennem pillen. Modellen beregner tabet af MoO_3 som funktion af positionen i pillen, driftstid og reaktionsbetingelser. Modellen kunne tilfredsstillende beskrive de eksperimentelle observationer.

I den tredje del af afhandlingen implementeres enkeltpille-modelen i en reaktormodel, hvor transport af den afdampede molybdæn og senere aflejring i katalysatorlejet finder sted. Når metanol omdannes over lejet, dekomponerer den afdampede molybdæn til MoO_3 og metanol i hulrummet mellem pillerne. Aflejringen reducerer hulrummets volumen, hvilket fører til tryktabsstigning, der beregnes som funktion af katalysatorens geometri og molybdænindhold, reaktionsbetingelserne og driftstiden. Reaktormodellen blev fittet til eksperimentelle målinger af tryktabsstigning i en pilotskala reaktor ved Haldor Topsøe A/S. Endeligt bruges modellen til at forudsige effekten af forskellige strategier til at forlænge processens levetid. Ved at reducere katalysatorens molybdænindhold eller ændre dens geometri fra åbne til fyldte cylindre i den første del af reaktoren opnås optimering af tryktabsstigningen.

Denne afhandling bidrager med ny indsigt i jernmolybdat-katalysatorens strukturelle ændringer og ydeevne ved reaktionsbetingelser over en længere periode hvor signifikant nedbrydning af katalysatoren opnås. Den udviklede katalysatorpille-model implementeret i en reaktormodel kan bruges til at analysere forskellige strategier til at forlænge processens levetid med hensyn til katalysatorfremstilling og procesdesign. Det blev påvist at ændringer i katalysatoren i den første del af reaktoren potentielt kan forlænge formaldehydprocessens levetid betydeligt.

Contents

Nomenclature

Abbreviations and Acronyms

DME	Dimethyl Ether
DMM	Dimethoxymethane
ML	Mono Layer
SEM	Scanning Electron Microscopy
STEM	Scanning Transmission Electron Microscopy
TEM	Transmission Electron Microscopy
XRD	X-ray Diffraction
µ-CT	Micro Computed Tomography

Arabic Letters

a_A	Activity of component A	-
A_p	Surface area of the pellet	[m^2]
C_A	Concentration of component A	[mol/m^3]
d	Diameter	[m]
$D_{e,A}$	Effective diffusion coefficient of component A	[m^2/s]
D_p	Hydraulic diameter of the pellet	[m]
k_A	Rate constant of reaction A	[s^{-1}] [L/kg/s]

k_g	Mass transfer coefficient	[m/s]
K	Constant	
L	Length of reactor or pellet	[m]
M_A	Molar mass of component A	[g/mol]
n_A	Reaction order of component A	-
N_A	Amount of substance A	[mol]
p	Pressure	[bar]
Q	Standard volumetric flow rate	[m^3/s]
r	Distance in pellet	[m]
r_A	Reaction rate of component A	[mol/m^3/s]
R	Gas constant	8.314 [J/mol/K]
R_h	Radius of hole in pellet	[m]
R_p	Radius of pellet	[m]
t	time	[s]
T	Temperature	[K]
v_s	Superficial velocity	[m/s]
V	Volume of reactor	[m^3]

Greek Letters

Δp	Pressure drop	[bar]
ε	Porosity	-
ρ_A	Density of component A	[kg/m^3]
ϕ	Volumetric fraction	-
μ	Dynamic viscosity	[Pa·s]

Subscripts and Superscripts

b	Bulk
dep	Deposition
h	Hole
i	Chemical compound i
p	Pellet
Ref	Reference stage

Chapter 0
Introduction to the Thesis

This chapter gives an overview of the structure of the PhD thesis, the publications made, and the student projects that were supervised. The thesis is part of the project "Next Generation Methanol to Formaldehyde Selective Oxidation Catalyst", funded by The Independent Research Council in Denmark, which includes two PhD projects at DTU and contributions from Haldor Topsøe A/S and Karlsruhe Institute of Technology.

Publications and Conference Contributions

International Peer-Reviewed Journals

Kristian Viegaard Raun, Lars Fahl Lundegaard, Jacques Chevallier, Pablo Beato, Charlotte Clausen Appel, Kenneth Nielsen, Max Thorhauge, Anker Degn Jensen and Martin Høj: "Deactivation Behavior of an Iron-Molybdate Catalyst During Selective Oxidation of Methanol to Formaldehyde", Catalysis Science and Technology, 2018, Volume 8, Issue 18, pp. 4626-4637.

Articles in Preparation

Kristian Viegaard Raun, Jeppe Johannessen, Kaylee McCormack, Charlotte Clausen Appel, Sina Baier, Max Thorhauge, Martin Høj and Anker Degn Jensen: "Modeling of the Molybdenum Loss in Iron Molybdate Catalyst Pellets for Selective Oxidation of Methanol to Formaldehyde"

Kristian Viegaard Raun, Max Thorhauge, Martin Høj and Anker Degn Jensen: "Modeling of Molybdenum Transport and Pressure Drop Increase in the Fixed Bed Reactor used for Selective Oxidation of Methanol to Formaldehyde over Iron Molybdate Catalyst"

Oral Conference Contributions

Kristian Viegaard Raun, Max Schumann, Martin Høj, Bjarke T. Dalslet , Pablo Beato, Christian D. Damsgaard, Jacques Chevallier, Jan-Dierk Grunwaldt, Anker Degn Jensen: "Studies of Deactivation of Methanol to Formaldehyde Selective Oxidation Catalyst". Presented at: The 25th North American Catalysis Society Meeting 2017 (NAM25), 2017, Denver, USA.

Kristian Viegaard Raun, Max Schumann, Martin Høj, Bjarke T. Dalslet, Pablo Beato, Christian D. Damsgaard, Jacques Chevallier, Jan-Dierk Grundwaldt, Kenneth Nielsen, Anker Degn Jensen: "Studies of Deactivation of Methanol to Formaldehyde Selective Oxidation Catalyst". Presented at: The 13th European Congress on Catalysis (EUROPACAT), 2017, Florence, Italy.

Kristian Viegaard Raun, Jeppe Johannessen, Martin Høj, Max Thorhauge, Charlotte Clausen Appel, Anker Degn Jensen: " Modeling of the Molybdenum Loss in Iron Molybdate Catalyst Pellets used for Selective Oxidation of Methanol to Formaldehyde". Presented at: The 25th International Conference on Chemical Reaction Engineering (ISCRE25), 2018, Florence, Italy.

Kristian Viegaard Raun, Jeppe Johannessen, Martin Høj, Max Thorhauge, Charlotte Clausen Appel, Anker Degn Jensen: " Modeling of the Molybdenum Loss in Iron Molybdate Catalyst Pellets used for Selective Oxidation of Methanol to Formaldehyde ". Presented at: The 18th Nordic Symposium on Catalysis (NCS), 2018, Copenhagen, Denmark.

Poster Conference Contributions

Non

Supervision of Students Projects

Max Schumann, Master's thesis: "Synthesis and Characterization of Iron Molybdate Catalysts for the Selective Oxidation of Methanol to Formaldehyde", April, 2016.

Jeppe Johannessen, Master's thesis: "Deactivation of FeMo-based catalysts for oxidation of methanol to formaldehyde", June, 2017.

Kaylee McCormack, Special Project (30 ECTS): "Deactivation of iron-molybdate catalyst for methanol to formaldehyde oxidation", January, 2018.

Structure of PhD thesis

Each chapter of the thesis is written in a manner that it can be read individually. The experimental chapters 2, 3 and 4 include a short literature section, to establish the necessary knowledge for the respective chapter. There is therefore some inevitable overlap between the chapters. The final chapter 5 concludes the research conducted during the work of the PhD project. A short description of each chapter is given below:

Chapter 1: Is a literature survey, including an overview of the different industrial processes for production of formaldehyde and the relevant process of this project named the Formox process, synthesis of the iron molybdate catalyst, mechanisms and kinetics of the selective oxidation of methanol and the deactivation behavior of the catalyst system.

Chapter 2: Is the published paper "Deactivation Behavior of an Iron-Molybdate Catalyst During Selective Oxidation of Methanol to Formaldehyde", where the deactivation behavior and structural changes in the iron molybdate catalyst were followed under reaction conditions for up to 600 h on stream for a powder catalyst.

Chapter 3: Is the manuscript for the paper "Modeling of the Molybdenum Loss in Iron Molybdate Catalyst Pellets for Selective Oxidation of Methanol to Formaldehyde", where the loss of molybdenum from industrial iron molybdate catalyst pellets were measured at varying reaction conditions. A dynamic 1D mathematical model for a single pellet in which methanol oxidation to formaldehyde and simultaneous Mo volatilization takes place was developed and fitted the experimental measured data.

Chapter 4: Is the manuscript for the paper "Modeling of Molybdenum Transport and Pressure Drop Buildup in the Fixed Bed Reactor used for Selective Oxidation of Methanol to Formaldehyde over Iron Molybdate Catalyst", where the single pellet model developed in chapter 3 is implemented in a reactor model simulating a single reactor tube including pressure drop increase. The reactor model is fitted to experimental data measured on a pilot plant setup provided by Haldor Topsøe A/S. Furthermore, the model is used to simulate an industrial reactor for a period of two years. The model is finally used to predict the effect of optimizing the catalyst design.

Chapter 5: Conclusion and future work on the PhD thesis.

Chapter 1
Introduction

Formaldehyde (CH_2O) is one of the most important industrial intermediate chemicals. It is an aldehyde prepared from methanol and due to its high reactivity it has a wide range of applications in chemical processes. In 2017 approximately 52 million ton were produced, and with an estimated annual growth rate of over 5 %, the demand is increasing[1]. Formaldehyde is used by the industry to produce a large number of products, where formaldehyde resins account for approximately 75 % of the consumption [2].

Formaldehyde occurs in low concentrations in nature, where it is produced from organic material by photochemical processes in the atmosphere or as a metabolic product in animals and plants. Pure formaldehyde at room temperature and atmospheric pressure is a color- and odorless [3] gas characterized by an irritating effect to the eyes and throat. Due to formaldehydes ability to polymerize, it is commercially available as an aqueous solution of 37-50 wt.% known as formalin [3]. Methanol is usually present (0.5-1.5 wt.%) in the final product[4]. Formaldehyde gas and formalin are toxic and may cause cancer [5].

The first attempt to synthesize formaldehyde was in 1859 by Butlerov, where he tried to prepare formaldehyde by hydrolyzing methylene acetate. However, formaldehyde was first truly synthesized in 1867, where Hoffman oxidized methanol vapor with air over a heated platinum spiral. In 1882 industrial production became possible. Kekulé described the preparation of pure formaldehyde by oxidation of methanol with air using a metal catalyst and Tollens discovered a method to regulate the methanol-air ratio and affecting the yield. Today all industrial production of formaldehyde is still based on conversion of methanol using modern heterogeneous catalysts [6].

1.1 Industrial processes to production of formaldehyde

Today formaldehyde is industrially produced from methanol by two major reactions. The first reaction is partial (selective) oxidation of methanol (1.1) and the second reaction is methanol dehydrogenation (1.2) [3]:

$$CH_3OH + ½O_2 \rightarrow CH_2O + H_2O \qquad \Delta H = -156\frac{kJ}{mol} \tag{1.1}$$

$$CH_3OH \rightarrow CH_2O + H_2 \qquad \Delta H = -85\frac{kJ}{mol} \tag{1.2}$$

In the industry the reactions are catalyzed by silver or metal oxide catalysts. Silver catalyzes both reactions while metal oxides catalyze only the partial oxidation reaction (1.1). Formaldehyde is industrially produced from methanol by the following heterogeneous catalytic processes [6]:

1. Partial oxidation and dehydrogenation of methanol over crystalline silver or silver gauze in the presence of sub-stoichiometric amounts of air, small amount of steam and excess of methanol at 600 – 650 °C. (Single pass conversion = 77 – 87 %, unconverted methanol is recovered by distillation and recycled.)
2. Selective oxidation of methanol over iron – molybdenum oxide catalyst with excess of air at 250 – 400 °C. (Conversion = 98 – 99 %)

The second process using an iron-molybdenum oxide catalyst is dominant in the industrial production of formaldehyde due to high single pass conversion and selectivity. In this study, the focus will be on this process, called the Formox process. In the literature the modified iron-molybdenum oxide catalyst is in general called iron molybdate catalyst, due to its preparation from iron and molybdate ions.

1.2 Formox process

In the Formox process an excess of air (~10 % MeOH, 10 % O_2 in N_2) is used to ensure high conversion of methanol (98 - 99 %)[3]. The relatively low concentration of oxygen is obtained by mixing recycle gas to the feed stream, which keep the risk of explosion low [4]. The temperature should be below 400 °C to limit side reactions, such as formation of CO/CO_2 and to assure the stability of the catalyst [7]. The yield is between 88 - 91 % [3]. However, the lifetime of the catalyst is only between 1 to 2 years, which is a major issue [8].

The selective oxidation of methanol to formaldehyde is an exothermic reaction (ΔH = -156 kJ/mol, see (1.1)). To control the temperature a multitubular reactor is used for the process and the reactor temperature is 250 - 400 °C at atmospheric pressure [9]. However, a significant pressure drop through the bed can occur, due to the mobility of molybdenum yielding narrow zones in the bed. The feed gas is preheated to 150 - 200 °C before entering the reactor. In the first part of the reactor the gas is heated to approximately 250 °C in an inert zone. In the second zone the reaction takes place over the iron molybdate catalyst. To heat the inlet gas in the initial zone of the reactor and to remove some of the produced heat in the second catalytic zone, the reactor has a boiling oil bath (≈ 290 °C) on the shell side of the reactor. When the gas enters the second zone of the re-

actor (catalytic bed), it is quickly heated due to the highly exothermic reaction (typically to 350 - 400 °C). This is called the hot spot of the reactor [10]. The gas is afterwards slowly cooled due to slower reaction rate and the surrounding oil bath. The axial temperature profile in the reactor is difficult to control and hotspots higher than 400 °C can easily occur. Nowadays the catalyst in the initial part of the second zone is diluted (app. 50 %) to avoid thermal run away [8].

Figure 1.1 shows a simplified flow diagram of the Formox process. Initially fresh air and tail gas from the absorption column is mixed and preheated by the product stream, followed by introduction to an evaporator where methanol is mixed with the gas to a single feed gas stream. The feed stream is introduced to the reactor. In the reactor methanol is catalytically converted to formaldehyde. The excess heat from the reactor is used to produce steam, which partly is used to evaporate methanol in the evaporator. The outlet stream of the reactor is cooled before being introduced to an absorption column. Water is introduced to the top of the column and formaldehyde in the gas stream is absorbed in the water forming aqueous formaldehyde (formalin), which is the final product. Some of the tail gas from the absorber is recycled.

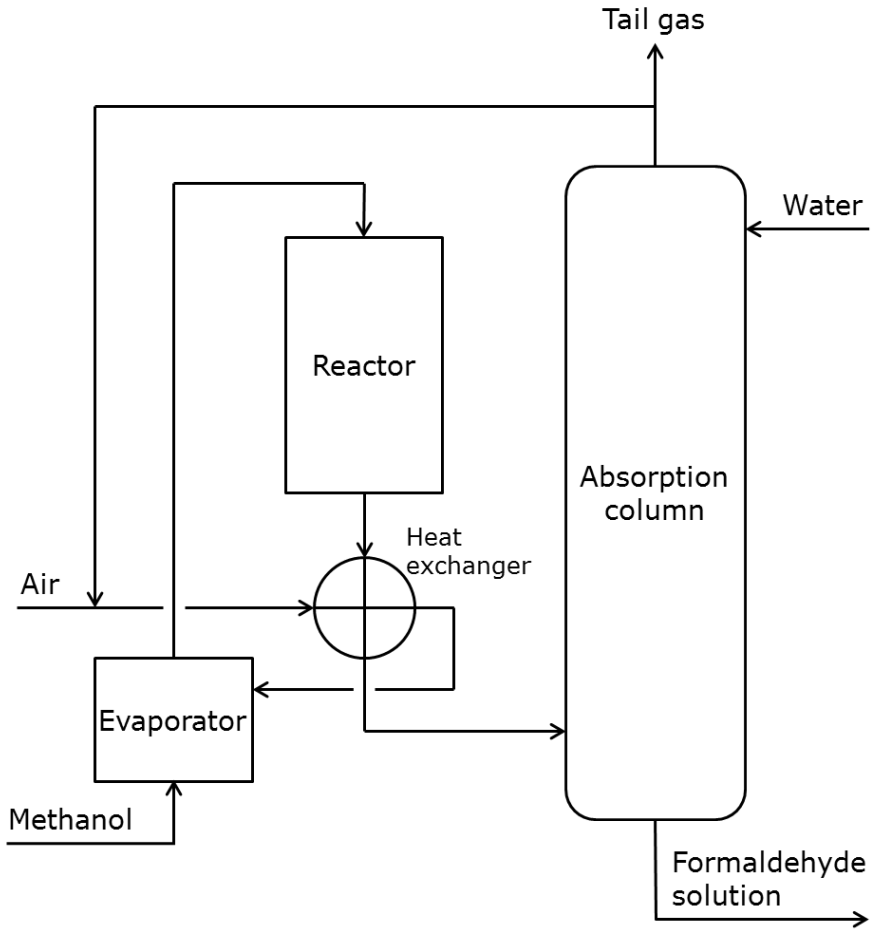

Figure 1.1 – Flow diagram of formaldehyde production by the Formox process.

1.3 Iron-molybdate catalyst

Metal oxides such as iron oxide (Fe_2O_3) and molybdenum oxide (MoO_3) can form crystalline phases where both metal atoms are included in the crystal structure (called mixed metal oxides) such as the main phase in the iron-molybdate catalyst ferric molybdate ($Fe_2(MoO_4)_3$) or the ferrous molybdate phase ($FeMoO_4$).

The industrially used iron-molybdate catalyst (Mo/Fe ratio = 2-3) consists primarily of two crystal phases of $Fe_2(MoO_4)_3$ and MoO_3 [11]. To achieve the $Fe_2(MoO_4)_3$ phase the Mo/Fe ratio must be equal to or larger than the stoichiometric ratio of 1.5. For higher Mo/Fe ratios (> 1.5) both the $Fe_2(MoO_4)_3$ and the MoO_3 crystal phases will be present in the catalyst. Some physical properties of the pure and mixed oxides are shown in Table 1.1.

Table 1.1 – Physical properties of pure oxide phases. [6, 13–15]

	Mol. Weight [g/mol]	**Color**	**Melting point [°C]**	**Density [g/cm³]**
$Fe_2(MoO_4)_3$	591.56	Brown-yellow-green	956	4.5
$FeMoO_4$	215.78	Light green	1115	5.6
Fe_2O_3	159.69	Red-brown	1539	5.25
MoO_3	143.94	White-yellow	802	4.70
MoO_2	127.94	Dark blue-violet	~1800	4.70

1.3.1 Ferric molybdate

Ferric molybdate ($Fe_2(MoO_4)_3$) is the more Mo containing (Mo/Fe = 1.5) and oxidized (Fe^{3+}) iron molybdate phase. The unit cell is monoclinic in space group P_{21a} with a = 1.5707 nm, b = 0.9231 nm, c = 1.8204 nm and β = 125.25°. The structure consists of corner sharing tetrahedra and octahedra with molybdenum and iron atoms in the centers respectively and oxygen in the corner positions. The average bond length is 1.754 ±0.004 and 1.990 ±0.005 Å for Mo-O and Fe-O respectively [15]. It is seen that the structure is relatively open (Figure 1.2).

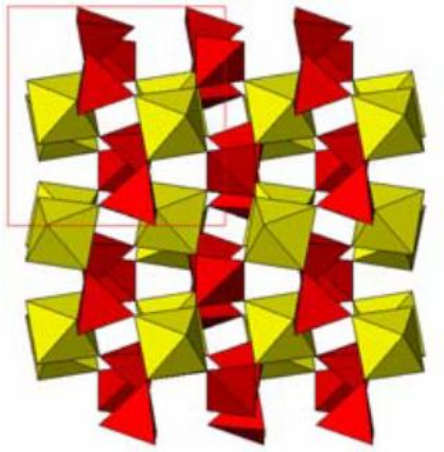

Figure 1.2 – The ferric molybdate structure with Mo in tetrahedral and Fe in octahedral coordination shown in idealized form as built up by regular polyhedral. The red and yellow polyhedral have Mo and Fe, respectively in the center, and oxygen in the corner positions. Each oxygen is shared by two polyhedral and therefore 2-coordinated. The structure is viewed along the (100) direction. Adapted from [15].

1.3.2 Ferrous Molybdate

Ferrous molybdate ($FeMoO_4$) is the less Mo containing (Mo/Fe = 1) and reduced (Fe^{2+}) iron molybdate phase. At ambient pressure the phase can have two different structures depending on the temperature under formation[14]. At low temperature α-$FeMoO_4$ can form. The unit cell is monoclinic in space group C_{2m} with lattice parameters a = 0.9807 nm, b = 0.8950 nm, c = 0.7659 nm and β = 114.02°. At about 400 °C α-$FeMoO_4$ starts to transform to β-$FeMoO_4$. The coordination of Fe is nearly octahedral and Mo is tetrahedral. The unit cell is in space group C_{2m} with lattice parameters a = 1.0301 nm, b = 0.9402 nm, c = 0.7053 nm and β = 106.28°. House et al. [16] studied the reduction of $Fe_2(MoO_4)_3$ under reaction conditions at 350 °C and observed the formation of β-$FeMoO_4$.

1.3.2.1 Iron oxide

Iron (III) oxide (α-Fe_2O_3) known as hematite is the most common iron oxide phase. It has a R_{3c} space group, with lattice parameters a = 0.5036 nm and c = 1.3749 nm, and six formula units per unit cell. The phase has a rhombohedrally centered hexagonal structure with a close-packed oxygen lattice. Two thirds of the octahedral sites are occupied by Fe(III) ions [17].

1.3.2.2 Molybdenum trioxide

Molybdenum trioxide (MoO_3) is the oxidized form (Mo^{6+}) of molybdenum oxide. The phase can form several structures depending on preparation conditions. α-MoO_3 is the thermodynamically stable phase. It has an orthorhombic structure in space group P_{bnm} with lattice parameters a = 0.39628 nm, b = 1.3855 nm, c = 0.36964 nm and β = 90°. It comprises of layers built from linked, distorted MoO_6 octahedra and possesses terminal Mo=O bonds [18]. Molybdenum trioxide can mainly form two other metastable structures, typically synthesized at low temperature.

McCarron III et al. [19] studied β-MoO_3 which is a three-dimensional structure, built by corner-shared octahedral MoO_6 units. Oxygen atoms are multiply bonded to Mo atoms and only the surface positioned octahedral units possesses unshared corner oxygen atoms forming terminal Mo=O bonds. β-MoO_3 transform to α-MoO_3 at around 450 °C.

Olenkova et al. [20] studied the hexagonal molybdenum oxide (h-MoO_3) which is a hydrated form of molybdenum trioxide ($MoO_3 \bullet H_2O$). The structure is build up by disordered MoO_6 octahedral units forming double-chains. At common corners the chains are linked forming polyhedrons. Each polyhedron has a free corner where the water molecule is incorporated into the structure. Other small molecules can likewise be incorporated in the structure. Lunk et al. [21] studied the decomposition process of h-MoO_3 by differential thermal analysis. At 320 °C water in the structure were released and at 425 °C the remaining decomposed phase recrystallized to α-MoO_3.

1.3.2.3 Molybdenum dioxide

Molybdenum dioxide (MoO_2) is the reduced form (Mo^{4+}) of molybdenum oxide. The unit cell is monoclinic in space group P_{21c} with lattice parameters a = 0.56109 nm, b = 0.48562 nm, c = 0.56285 nm and β = 120.95°. It consist of chains of distorted MoO_6 octahedra [18].

1.3.3 Interaction between the crystal phases in iron-molybdate catalyst

The MoO_3 phase in the iron molybdenum catalyst is rather mobile at the reaction temperature (250 – 400 °C) leading to thermal spreading. Molybdenum oxide can also interact with iron oxide forming different Fe-Mo oxide phases such as $Fe_2(MoO_4)_3$. In the following section, different studies of this subject are discussed.

Huang et al. [22] studied the interaction between Fe_2O_3 and MoO_3 grains after different heat treatments. Via solid-state reaction at the intergranular contact surface between MoO_3 and Fe_2O_3, MoO_3 can spread onto the surface of Fe_2O_3 during heat treatment. This phenomenon is called “thermal spreading”. The driving force is the surface free energy and the reaction takes place on the entire Fe_2O_3 surface. The Fe_2O_3 grains were analyzed by XPS and SEM after heat treatment (300, 400, 500 and 600 °C for 5 h). At 300 °C some MoO_3 was present on the surface of the Fe_2O_3 grains. At 400 °C $Fe_2(MoO_4)_3$ was detected at the surface. At 500 °C the outer shell of the initial Fe_2O_3 grain was converted to $Fe_2(MoO_4)_3$ with MoO_3 on the surface and Fe_2O_3 in the core. At 600 °C no more MoO_3 was available and the grain was converted to a thick shell of $Fe_2(MoO_4)_3$ and a core of Fe_2O_3. This experiment demonstrates that molybdenum is mobile in the Fe-Mo oxide system allowing formation of the $Fe_2(MoO_4)_3$ phase. At full conversion the composition of the grain is dependent of the

Mo-Fe ratio. For an Mo/Fe ratio below 1.5 (sub-stoichiometric of $Fe_2(MoO_4)_3$), a grain will consist of a shell of $Fe_2(MoO_4)_3$ and a core of Fe_2O_3. For an Mo/Fe ratio above 1.5, a grain will consist of $Fe_2(MoO_4)_3$ with a layer of MoO_3 at the surface. The mobility of molybdenum was observed down to 300 °C and compared with the operating temperature of the formaldehyde process (250 – 400 °C), it is reasonable to assume that molybdenum is mobile at the reaction conditions. The industrial catalyst is prepared with the $Fe_2(MoO_4)_3$ and MoO_3 phase. However, for the studied catalyst system containing Fe_2O_3 and MoO_3, the formation of the $Fe_2(MoO_4)_3$ phase was not observed below 400 °C.

Brookes et al. [23] studied the core-shell material MoO_3/Fe_2O_3 with 3 monolayers (ML) of Mo at the surface. The material was prepared by doping 3 ML equivalents (eq) of MoO_3 onto the surface of Fe_2O_3 particles, and the material was calcined for 2 hours at varying temperatures (300-600 °C). The evolution of the surface structure with respect to calcination can be seen in Figure 1.3. The initial non-calcined material consists of a Fe_2O_3 core with a 3 ML shell of MoO_3. After calcination at 400 °C the MoO_3 shell formed a monolayer shell with the excess MoO_3 forming nanocrystallites. It was proposed by the author that the formation of a monolayer occurs already at 300 °C. The excess MoO_3 nanocrystallites react with the Fe_2O_3 core forming $Fe_2(MoO_4)_3$ when heated to 500 °C. The $Fe_2(MoO_4)_3$ phase is at the surface of the Fe_2O_3 core but underlie the top surface layer of MoO_3. The observation by Brookes et al. are in good agreement with the observations by Huang et al. discussed above.

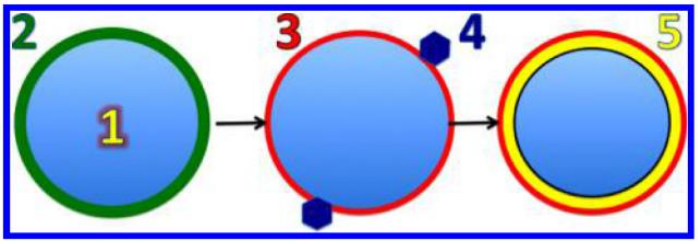

Figure 1.3 – The evolution of the surface structure of the 3 ML catalyst as function of calcination temperature. On the left, the surface consist of an amorphous MoO_3 layer (2), supported on the Fe_2O_3 core (1), which is the structure at temperatures below 400 °C. In the middle, is shown the structure at ~400 °C with both nano-crystallites of MoO_3 (4) at the surface of the catalyst and the surface of MoO_3 present (3). Finally, in the right-hand panel, is shown the structure after calcination at 500 °C, in which the nanoparticles of MoO_3 have mostly converted to $Fe_2(MoO_4)_3$ (yellow layer 5), but with the active monolayer of MoO_3 overlaying it [23].

Xu et al. [24] studied the surface phase composition of iron molybdate catalysts with different Mo/Fe ratios (1.54, 1.86 and 2.36) prepared by co-precipitation and calcination at different temperatures (400 - 700 °C for 4 h). For all tested Mo/Fe ratios and calcination temperatures the core of the catalyst remained nearly unchanged consisting of the $Fe_2(MoO_4)_3$ phase. For the molybdate rich catalysts (Mo/Fe ratios of 1.86 and 2.36) an MoO_3 phase was observed at the catalyst surface due to segregation. For high calcination temperatures (700 °C) the MoO_3 phase formed needle-like crystals. Figure 1.4 shows SEM images of catalysts with a Mo/Fe ratio of 2.36 after calcination at 500 (left) and 700 °C (right). EDX and XPS analysis confirmed that the needle-like structures was dominated by MoO_3.

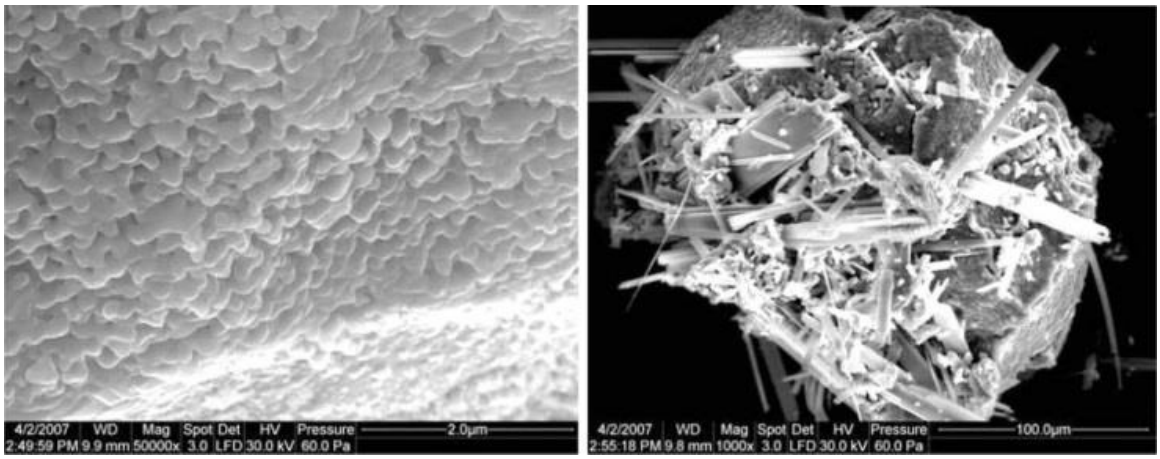

Figure 1.4 – SEM images of iron-molybdate catalyst. Mo/Fe ratio = 2.36. Calcination time = 4 h. Calcination temperature: Left = 500 °C and right = 700 °C [24].

The different studies of the interaction between the phases in iron molybdate catalysts show that molybdenum is relatively mobile and the mobility is enhanced by elevated temperatures. In the core crystal phase consisting of both iron oxide and molybdenum oxide, molybdenum can move to potential Mo-poor regions. The crystal structure of $Fe_2(MoO_4)_3$ seems to be the most thermodynamic favorable structure between iron oxide and molybdenum oxide in oxidizing atmosphere, however other structures can also be formed such as $FeMoO_4$. Excess of molybdenum oxide forms an monolayer (MoO_3) on the catalyst core phase ($Fe_2(MoO_4)_3$) due to thermal spreading. Due to segregation, further excess of molybdenum oxide forms a separate crystal phase of pure MoO_3. The excess crystal phase of MoO_3 grows into needle-like crystals at high temperatures (700 °C) [24]. However, in an industrial process the catalyst is only exposed to elevated temperatures of 250 - 400 °C, and the formation of the observed needlelike crystals are not likely to occur directly from the catalyst as observed in the study.

1.4 Phases in the iron-molybdate system and their catalytic properties

As the iron molybdate catalyst cycles through the reaction mechanism (discussed in section 1.4.5 and 1.4.6) mainly two different sites are exposed to the gas phase. Initially the MoO_3 including a terminal oxygen is exposed. As methanol is converted to formaldehyde and water, which desorb from the catalyst surface and leaves a vacancy at the terminal oxygen yielding a MoO_2 like structure. Furthermore, as the catalyst deactivates due to loss of molybdenum, the catalyst core phase of $Fe_2(MoO_4)_3$ is exposed, and for high degree of deactivation the core phase can potentially change crystal structure to $FeMoO_4$ and Fe_2O_3. Equation (1.3) shows the crystal phases in the iron molybdate system at varying molybdate content. Table 1.2 shows an overview of the selectivity of the different phases discussed above.

$$\text{High Mo}: \ MoO_3 > Fe_2(MoO_4)_3 > FeMoO_4 > Fe_2O_3 \ :\text{Low Mo} \tag{1.3}$$

Table 1.2 - Selectivity of different phases in the iron molybdate oxide system.

Material	Selectivity towards
MoO_3	Formaldehyde [25–27]
MoO_2	Primarily CO and small amounts of CO_2 [25, 26]
$Fe_2(MoO_4)_3$	Primarily formaldehyde [26–28]
$FeMoO_4$	CO [9, 26]
Fe_2O_3	CO_2 [26, 27, 29]

1.4.1 Synergy effect between iron and molybdate in the catalyst

As it can be seen from Table 1.2, MoO_3 has high selectivity towards formaldehyde but low activity, and $Fe_2(MoO_4)_3$ has moderate selectivity towards formaldehyde but high activity. However, the industrial iron molybdate catalyst consists of both phases and achieves both high selectivity and activity.

Bowker et al. [30] studied the effect of doping hematite with surface layers of Mo by incipient wetness impregnation. It was observed that even low loadings of only 0.25 ML of Mo yielded greatly enhanced selectivity towards formaldehyde and CO and decreased selectivity towards the full combustion product CO_2. However, by increasing the about of Mo dosed on the surface (seven ML) this catalyst did not achieve as high selectivity as the commercial iron molybdate catalyst. The author explained the lower selectivity by no formation of a pure Mo oxide ML on the surface, which is essential for high selectivity.

Söderhjelm et al. [15] studied the synergy between the MoO_3 and $Fe_2(MoO_4)_3$ phase in the iron molybdate catalyst. They tested catalysts with different Mo/Fe ratios (Pure Fe_2O_3, 0.2, 0.5, 1, 1.5, 2.2 and pure MoO_3). They achieved the highest selectivity and activity for the catalyst with a Mo/Fe ratio of 2.2. This catalyst consisted of a bulk phase of $Fe_2(MoO_4)_3$ and a surface layer phase of MoO_3. They concluded that there is a synergy effect between the active surface layer (MoO_3) and the underlying sublayers ($Fe_2(MoO_4)_3$) of the catalyst. The catalyst is as selective towards formaldehyde as pure MoO_3, which is less active, and

almost as active as pure $Fe_2(MoO_4)_3$, which is less selective. The synergy between the two phases in the iron molybdate catalyst thus yields a catalyst with both relatively high selectivity and activity.

Bowker et al. [31] Furthermore, studied the effect of increasing iron content in the catalyst on the selectivity. As the iron content increases the selectivity towards CO compared to formaldehyde increases. The author concludes that no iron atoms should be present in the surface layer of the catalyst to achieve the highest selectivity.

1.4.2 Preparation of iron molybdate catalyst

Iron molybdate catalysts can be prepared by several methods such as "kneading and evaporation" [32], where e.g. ammonium molybdate is dissolved in water and added gradually to e.g. iron nitrate powder, followed by evaporation of water and calcination. Iron molybdate catalysts can also be prepared by solid state reactions between molybdenum oxide and iron oxide at elevated temperature [23] and different precipitation methods such as hydrothermal synthesis [33] and co-precipitation [13]. Nowadays industrial iron molybdate catalysts are generally synthesized by co-precipitation followed by calcination. Furthermore, hydrothermal synthesis has in the recent years been investigated, achieving active and selective catalysts [33].

Several precipitation syntheses are reported in the literature. In general the catalyst is prepared from an ammonium heptamolybdate solution and iron chloride or iron nitrate solutions [13], [32]. The precipitate is further filtered and washed with distilled water until the pH of the filtrate reaches 7. The solid is then dried and calcined at 400-500 °C to obtain the correct crystal phases ($Fe_2(MoO_4)_3$ and MoO_3). The surface area of the catalyst is typically 5-8 m^2/g [34].

With respect to co-precipitation the precipitation solution is filtrated and the filter cake consisting of iron-molybdate oxide is washed, dried and calcined at approximately 500 °C to obtain the final catalyst [32].

With respect to hydrothermal synthesis the solution of the iron and molybdate precursor is loaded in an autoclave for thermal treatment at typically 150 °C to obtain the correct crystal phases ($Fe_2(MoO_4)_3$ and MoO_3). The molybdate phase forms a molybdenum-rich layer at the bulk catalyst surface ($Fe_2(MoO_4)_3$). The precipitation solution is finally filtered, washed and dried [33]. No calcination is needed to obtain the right crystal phases.

An iron molybdate catalyst with an approximately stoichiometric ratio of $Fe_2(MoO_4)_3$ (~1.5) has a bright green color and a catalyst with a significant excess of molybdenum (e.g. Mo/Fe ratio = 3) has a yellow color [33].

1.4.3 Effect of pH in preparation media

During precipitation of iron molybdate catalysts iron ions and molybdate ions are initially dissolved in aqueous media. In this section the effect of pH on the properties of the ions in the precipitation solution and the particle size of the precipitated crystals will be discussed.

Pernicone [35] studied the effect of pH in the precipitation solution on the catalytic properties of iron molybdate catalysts. As described in section 1.3.3, the Mo/Fe ratio must be above 1.5 to obtain the active MoO_3 phase at the catalyst surface. The prepared and tested catalyst in the study had a Mo/Fe ratio of 2.

It is commonly known that iron ions forms complex ions with water which is in equilibrium with hydronium as follows:

$$[Fe(H_2O)_6]^{3+}_{(aq)} \leftrightarrow [Fe(H_2O)_5OH]^{2+}_{(aq)} + H^{+}_{(aq)} \qquad (1.4)$$

However, based on magnetic measurements on the antiferromagnetic interaction between iron ions, Pernicone [35] suggested that more complex ions are present such as:

Figure 1.5 – Iron complexes between two iron atoms and water.

Dewangan et al. [36] reported that the polymolybdate anions in a solution is dependent on its pH value. At pH above 6 Mo(VI) is found as colorless $[MoO_4]^{2-}$ ions. At decreasing pH $[MoO_4]^{2-}$ is condensed and gives an extensive range of polymolybdates. At low pH (< 1) molybdate precipitate as $MoO_3 \cdot 2H_2O$. The relationship between pH and molybdate anion species is as follows:

$$[MoO_4]^{2-} \xrightarrow{pH<6} [Mo_7O_{24}]^{6-} \xrightarrow{pH=1.5-2.9} [Mo_8O_{16}]^{4-} \xrightarrow{pH<1} MoO_3 \bullet 2H_2O \qquad (1.5)$$

Hydrothermal treatment (220 °C for 7 hours) of precipitated $MoO_3 \bullet 2H_2O$ yields the formation of α-MoO_3. During precipitation the iron ions react with molybdate anions and precipitate as Fe-Mo oxide.

Belhekar et al. [11] observed that the crystal size of iron molybdate catalyst prepared by precipitation including an industrial catalyst (Mo/Fe ratio = 2-3) depends on the preparation conditions including control of pH during mixing. For catalysts prepared by mixing aqueous solutions of ferric nitrate and ammonium paramolybdate followed by pH adjustment to 1.8, the crystal phases became fairly large (> 3 μm) with a surface area of 4.2 m^2/g and had varying shapes. However, with pH control during the mixing (pH = 1.8) the two phases became small (< 0.3 μm) with a surface area of 10.3 m^2/g and had uniform shape. The preparation includes calcination at 400 °C in air for 12 hours.

1.4.4 Kinetics of the selective oxidation of methanol to formaldehyde

The kinetics of selective oxidation of methanol over metal-oxide catalysts has been studied for almost the past century; from patenting the first process to several kinetic studies to DFT calculations performed by powerful computers of nowadays. In this section some of the studies through time and their findings will be discussed.

In 1921 Bailey and Craver [37] patented a process to oxidize methanol into formaldehyde over a vanadium oxide catalyst in presence of oxygen, at ambient pressure and temperatures between 275 – 400 °C, following the reaction:

$$CH_3OH + ½O_2 \rightarrow CH_2O + H_2O \tag{1.6}$$

The process had only a moderate single pass conversion (68 %) with a selectivity of 90 %.

In 1931 Adkins and Peterson [38] investigated the process over an iron and molybdenum oxide catalyst, and furthermore a stoichiometric iron-molybdate catalyst (Mo/Fe = 1.5). They concluded that pure molybdenum oxide was fully selective (100 %) but had low activity (single pass conversion = 38 %), and that the iron oxide had high activity but almost exclusively induced the formation of carbon dioxide. However, when combining the two oxides into iron-molybdate catalyst an active and selective catalyst was obtained (single pass yield = 90 %).

Bowker et al. [39] used a pulse flow reactor combined with temperature-programmed desorption (TPD) to investigate the reactor over iron molybdate and MoO_3, and they observed that conversion started at 150 and 270 °C respectively. These observations are in good agreement with Adkins and Petersons [38] that iron molybdate is more active than MoO_3.

1.4.5 Active site

Rellán-Piñeiro and López [40] performed DFT calculations on the selective oxidation of methanol to formaldehyde on different surfaces including α-MoO_3.

The selective oxidation of methanol towards formaldehyde takes place at the molybdate rich surface of the catalyst As shown schematically in Figure 1.6. Each molybdenum atom is surrounded by four bridging oxygen atoms in the layer and one terminal oxygen atom.

The active site consists of a molybdenum atom and its related terminal oxygen. The active site is bifunctional and has both acidic and basic properties. The molybdenum atom has acidic properties and the terminal oxygen atom has basic properties.

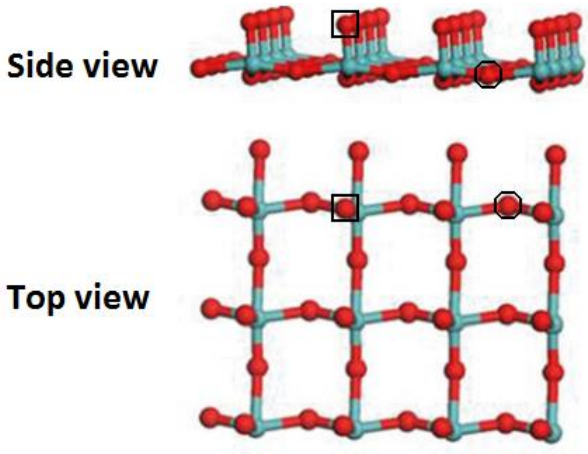

Figure 1.6 – Model of α-MoO_3(010), side and top view. Blue atoms: Molybdenum. Red atoms: Oxygen. □: Terminal oxygen atom. ○: Bridge oxygen atom [40].

1.4.5.1 Role of iron in the catalyst

Even though the active part of the iron molybdate catalyst is the surface layer of MoO_3, it is commonly known that the activity increases with iron present in the sublayers of the catalyst. In the DFT study by Rellán-Piñeiro and López [40], they also studied the influence of iron atoms in the sublayers of the catalyst. Iron in the sublayer can accept part of the electronic excess, which allows for a buffering effect on the oxygen content of the active molybdenum atom site. This effect makes formation of vacancies easier yielding higher activity. The selectivity is high due to low adsorption energy of formaldehyde compared to methanol. Furthermore, they concluded that iron atoms in the surface layer will decrease the selectivity, because iron sites bind formaldehyde strongly which may lead to further oxidation.

1.4.6 Reaction mechanism

In 1967 Bhattacharyya and Janakiram [41] used a flow reactor to study the kinetics of the oxidation of methanol catalyzed by vanadium pentoxide. By fitting their measurements of the reaction rate to a previous suggested rate expression by Mars and van Krevelen [42], they concluded that the catalyzed reaction follows the Mars-van Krevelen mechanism.

The mechanism of selective oxidation of methanol to formaldehyde over iron molybdate is, however, not fully understood. But, some agreement is found in the literature. The mechanism can be divided into three overall steps;

- Dissociative adsorption of methanol forming methoxy and hydroxyl groups Dehydrogenation of the methoxy group forming adsorbed formaldehyde
  Desorption of formaldehyde to the gas phase The excess hydrogen forms water molecules with lattice oxygen from the catalyst.
- The formed water desorbs to the gas phase.
- The catalyst is reoxidized by oxygen from the gas phase.

In 1969 Pernicone et al. [43] studied the conversion of methanol to formaldehyde over iron-molybdate catalyst, and proposed that lattice oxygen participated in the reaction mechanism, which is consistent with the Mars-van Krevelen mechanism [42] as follows:

$$CH_3OH(g) + *_{ox} + O_{cat} \leftrightarrow CH_3O*_{ox} + HO_{cat} \quad (1.7)$$

$$CH_3O*_{ox} + O_{cat} \leftrightarrow CH_2O*_{red} + HO_{cat} \quad (1.8)$$

$$CH_2O*_{red} \leftrightarrow CH_2O(g) + *_{red} \quad (1.9)$$

$$2HO_{cat} \rightarrow H_2O(g) + O_{cat} + *_{ox} \quad (1.10)$$

$$*_{red} + ½O_2(g) \rightarrow O_{cat} \quad (1.11)$$

Where $*_{ox}$ is the oxidized active site (Mo^{6+}) and $*_{red}$ is the reduced active site (Mo^{4+}). O_{cat} is a terminal oxygen atom in the catalyst lattice. The rate limiting step is reported to be the dehydrogenation of the methoxy group (1.8) [44].

Figure 1.7 shows the proposed mechanism steps based on the DFT study performed on the mechanism of converting methanol to formaldehyde by Rellán-Piñeiro and López [40]. The proposed mechanism is in good agreement with the mechanism proposed by Pernicone.

Step 1: Initially methanol adsorb to the MoO_3 surface through a hydrogen bond between the acidic hydrogen in methanol and the terminal oxygen of the catalyst.

Step 2: Abstraction of the acidic hydrogen in the methanol by the terminal oxygen forming a hydroxyl group bonded to the molybdenum center. The methoxy fragment binds to the same molybdenum center.

Step 3: One of the hydrogen atoms on the methoxy fragment is transferred to either a free terminal oxygen atom forming a hydroxyl group (Figure 1.7 a) or to a hydroxyl group forming water (Figure 1.7 b). The formaldehyde fragment interact with a neighboring site forming a configuration where formaldehyde is bonded to the neighboring site. This step is the rate limiting step.

Step 4: Formaldehyde and water desorbs to the gas phase leaving a fully oxidized site and an oxygen vacancy site.

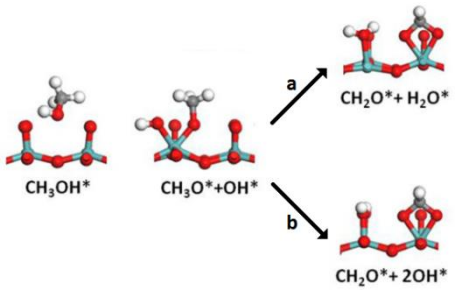

Figure 1.7 – DFT based mechanism of oxidative dehydrogenation of methanol to formaldehyde on MoO_3 catalysts [40].

With respect to the transferred hydrogen atom in step 3, two pathways are proposed. It can bond to a hydroxyl group and form a water molecule adsorbed to the original molybdenum center (Figure 1.7 a) or it can bond to a second terminal oxygen and form a second hydroxyl group (Figure 1.7 b). In the first case two sites are included in the overall mechanism, one with adsorbed water and one with adsorbed formaldehyde. In the second case two sites with adjacent hydroxyl groups and one with adsorbed formaldehyde is included (total three sites). The formed water molecule includes the original terminal oxygen atom. Desorption of water from the molybdenum center removes the original terminal oxygen atom and leaves a vacancy. The removal of the terminal oxygen atom from the catalyst surface could be further investigated using isotopically labeled oxygen and/or methanol to track the specific oxygen atoms. The site is reoxidized with oxygen from the gas phase. The reoxidization mechanism is discussed later in this section.

To get a quantitative overview of the kinetics of the process, Bowker [45] has proposed a number of simple rules which dictate for high selectivity:

Rule 1: Surface terminal oxygen is the active oxidizing species, which is replenished from the gas phase, by a Mars-van Krevelen mechanism.

Rule 2: Bulk oxygen becomes mobile enough at the reaction temperature to reoxidize the vacancy at the catalyst surface. Much of the oxygen can be removed from the bulk, and thus act as a "buffer" to surface reduction.

Rule 3: It is the segregated molybdenum oxide on the surface of iron molybdate catalyst that dictates the selectivity towards formaldehyde.

Rule 4: It is the highest oxidation state (Mo^{6+}) of the molybdenum atoms that form the selective site.

1.4.7 Selectivity

As described in section 1.4.5 and 1.4.6 the selective site towards formaldehyde is the highest oxidation state of molybdenum (Mo^{6+}). As described in section 1.4.6 molybdenum is reoxidized to regenerate the Mo^{6+} site during the mechanism forming formaldehyde. However, the reduced site (Mo^{4+}) is active and selective towards CO formation [25], decreasing the overall selectivity towards formaldehyde. The reduced site (Mo^{4+}) is more reactive and is able to strip off all hydrogen atoms from the adsorbed methanol molecule. A high rate of surface reoxidation is therefore crucial to achieve a high overall selectivity towards formaldehyde. Bowker [25] reported that at >320 °C the reoxidation of the molybdenum oxide occurs fast and that the selectivity towards formaldehyde increases compared to lower temperatures.

Brookes et al. [46] furthermore studied the MoO_3/Fe_2O_3 catalyst by X-ray absorption fine structure (XAFS), which provide surface sensitive information. Under *In situ* catalysis studies during formaldehyde production, it was observed that a single overlayer of O_h Mo units remained at the surface at all times in the oxidation state Mo^{6+}. These observations confirm that oxygen from the gas phase rapidly reoxidize the catalyst surface and that the selective Mo^{6+} is present at the surface yielding high selectivity of this catalyst.

1.4.8 Reoxidation of the catalyst

House et al. [16] studied the reaction under anaerobic and aerobic conditions, and observed that oxygen in the gas phase is not directly involved in the reaction, which is agreement with the Mars-van Krevelen mechanism [42]. The surface oxygen in the catalyst is used in the oxidation reaction and the gas phase oxygen is used to reoxidize the catalyst surface. Furthermore, at temperatures above 250 °C (reaction conditions = 250 – 400 °C) the bulk lattice oxygen become readily mobile and is available for reoxidizing the surface by diffusing through the catalyst. The reoxidation mechanism is not fully understood. However, Coquet and Willock [47] have performed a DFT study where they conclude that oxygen molecules in the gas phase can adsorb to the vacancy site (Mo^{4+}) by oxidizing the molybdenum atom. Adsorption of molecular oxygen result in O_2, O_2^- or O_2^{-2} surface species depending on the geometry of adsorption.

Brookes et al. [48] found from pulse flow experiments performed under anaerobic conditions that diffusion of oxygen in the lattice is hindered in MoO_3. However, by incorporating Fe into the subsurface layers the oxygen becomes much more mobile, which enables it to counter the reduction at the surface during oxygen starvation and easy reoxidation during surplus. Similar results are seen by Bowker et al. [49]

1.4.9 Kinetic models

Deshmukh et al. [44] studied the intrinsic steady-state kinetics of the selective oxidation of methanol towards formaldehyde including the most important side reactions. The reaction rates by were modeled by Langmuir-Hinshelwood expressions. The reactions taken into account was the main reaction of methanol to formaldehyde, and side reactions; formaldehyde to carbon monoxide, methanol to dimethyl ether (DME), formaldehyde from DME, and dimethoxymethane (DMM) from formaldehyde and methanol. The reaction scheme can be seen in Figure 1.8. A commercial iron molybdate catalyst was tested in a differential quartz reactor (0.11 mg catalyst and reactor inner diameter = 5 mm) varying the feed composition and temperature (methanol = 0 – 15 mol%, oxygen = 0 – 10 mol%, water = 0 – 4 mol% and inert nitrogen. Temperature = 230 – 290 °C). To study the reactivity of formaldehyde towards side products, methanol was pre-converted to formaldehyde in a pre-reactor.

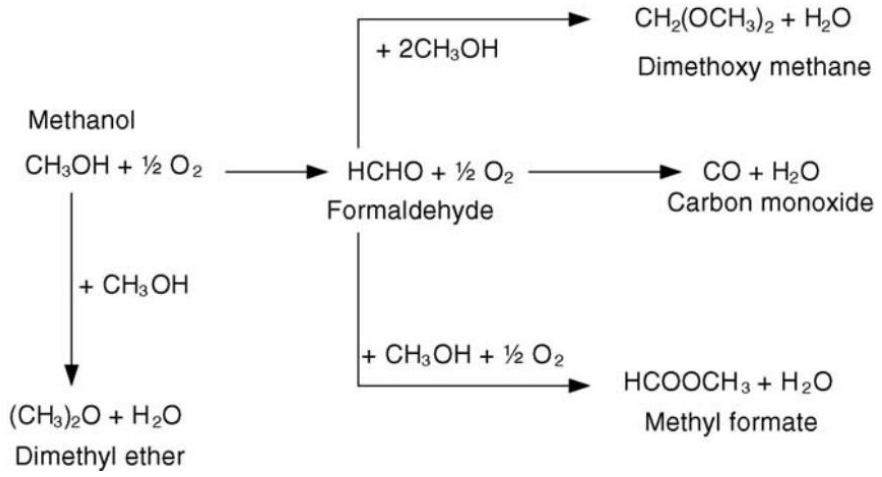

Figure 1.8 – Reaction scheme of main and side reactions of the partial oxidation of methanol to formaldehyde [44].

At low methanol concentration (<5 mol%) the methanol partial oxidation rate was approximately first order in both methanol and oxygen. However, methanol and oxygen showed Langmuir-Hinshelwood kinetics, which indicates saturation of the catalyst surface at higher concentrations (>5 % MeOH and >3 % O_2 respectively). Water in the feed gas had an inhibiting effect, which decreased at higher water partial pressures and temperature (>4 mol% and >250 °C).

With respect to the oxidation rate of formaldehyde to CO, it showed a positive Langmuir-Hinshelwood type dependency on the oxygen concentration and a first order dependency on the formaldehyde concentration.

With respect to side products, a very low yield (< 0.5 mol%) of dimethyl ether, dimethoxymethane and methyl formate were observed. The formation of dimethyl ether showed a first order dependency on the methanol concentration. Furthermore, dimethyl ether and oxygen can form formaldehyde. The oxidation of dimethyl ether to formaldehyde showed a nearly zero order dependency on the DME concentration. The reaction between methanol and formaldehyde to DMM showed a first order dependency on both methanol and formaldehyde.

1.4.10 Summary of section 1.4

The surface of the iron-molybdate catalyst is dominated by a molybdenum oxide rich layer, with Mo mainly in oxidation state 6+ at sufficiently oxidizing conditions. It is on this layer the catalytic mechanism takes place. Molybdenum is volatile at the reaction conditions and excess molybdate is present to replenish Mo loss from the catalyst surface. The mechanism is not fully understood; however, in the literature the majority proposes a Mars-van Krevelen redox mechanism [42]. Furthermore, Rellán-Piñeiro and López studied the mechanism by DFT calculations [40] and concluded that the activity of MoO_3 is linked to the formation of vacancies at reasonable energy costs. Furthermore, Fe atoms in the subsurface layer can accept some of the electronic excess during the redox mechanism which increases the activity while keeping the selectivity high. The rate limiting step is calculated by DFT [40] to be the dehydrogenation of the methoxy fragment during the conversion between methanol and formaldehyde.

1.5 Deactivation and Mo volatilization

Deactivation and volatilization of Mo is partly covered in the main chapters of the thesis (Chapter 2, 3 and 4). However, in order to be able to read the introduction section alone it has been included here as well. There is therefore some overlap of information between this section (1.5) and the main chapters.

Molybdenum forms volatile species with methanol under reaction conditions, which can leave behind molybdenum poor zones in the catalyst bed [8, 44]. Besides the ferric molybdate phase ($Fe_2(MoO_4)_3$) present in the fresh catalyst, the reduced ferrous phase ($FeMoO_4$) can be present in the spent catalyst. At substantial molybdenum loss Fe_2O_3 can be formed. Due to segregation of molybdenum in ferric molybdate, this phase tends to have an over stoichiometric Mo/Fe ratio on the surface [24].

Popov et al. [50] studied the deactivation and Mo volatilization from an iron molybdate catalyst system (Mo/Fe = 1.5-2.5 and MoO_3) under varying conditions of MeOH in air. They used a fixed bed reactor with a circulation loop and a trap for volatile Mo compounds placed downstream in the setup. They concluded that the rate of Mo volatilization is mainly affected by the methanol concentration and suggested the formation of the volatile compounds such as $MoO_2(OCH_3)_2$, $MoO_2(OH)(OCH_3)$, $MoO_2(OCH_3)$ and $MoO_2(OH)$. They observed that the volatile Mo species condensed as a blue film on the reactor tube inner surface at the reactor outlet. Furthermore, they observed brown formations on the catalyst at reaction temperatures of 350 °C, which they characterized to be iron oxide by XRD. During their experiments they measured the catalyst activity by the rate of methanol conversion. They concluded that loss of Mo from the catalyst surface is the main reason for deactivation of the catalyst. The effect of varying the space time was also investigated and it was found that for space times above 0.01 sec, the concentration of volatile Mo compound was independent on the space time at constant MeOH concentration. This indicates that equilibrium of the Mo volatilization reaction is quickly reached.

Burriesci et al. [9] studied spent catalyst pellets from an industrial plant. They observed that pellets from the initial part of the catalyst bed were subject to loss of MoO_3 in accordance with the observations of Popov et al. [50]. However, no significant loss of Mo from the pellets close to the inlet of the bed was observed, which might have been due to a low inlet temperature to avoid thermal run away. Furthermore, they paid close attention to the pellets after the hotspot in the reactor and observed formation of needlelike MoO_3 crystals on the surface of the pellets. It was suggested that growth of these whisker crystals on the surface of the pellets after the hotspot were the reason for the pressure drop buildup observed in industrial plants due to occupation of the void space between the pellets.

Smith et al. [51] studied the morphological transformations of a single crystal MoO_3 surface under continuous flow of a MeOH-air mixture. They observed like Popov et al. [50] a blue Mo-rich film during their experiments. Using XRD it was revealed that the film layer consisted of $Mo_2O_5(OCH_3)_2$. Two pathways for its formation were suggested. In the first pathway MeOH forms surface methoxy and hydroxyl groups upon adsorption on the MoO_3 surface and a molybdenum oxide hydroxide molecule desorbs into the gas phase. This desorbed molecule then reacts with methanol in the gas phase forming $Mo_2O_5(OCH_3)_2$. In the second pathway surface molybdenum methoxides desorb directly as the observed molybdenum oxide-methoxide. The authors suggested that the second pathway was the most plausible [51] and this was also suggested by Ivanov and Dimitrov [10] and follows:

$$2MoO_3 + 2MeOH \rightarrow Mo_2O_5(OCH_3)_2 + H_2O \qquad (1.12)$$

Dias et al. [52] studied the catalytic effect of varying the number of MoO_3 mono layers (ML) on top of iron molybdate. Their data show that 5 ML on the catalyst surface is relatively active and selective towards CH_2O. However, as the Mo ML is decreasing to 0.5 ML the catalyst become less active. This observation of the effect of Mo ML on the catalyst surface confirms the conclusion made by Popov et al. [50], that loss of activity is due to loss of Mo from the catalyst surface.

Ivanov and Dimitrov [10] performed experiments on single, industrial like reactor tubes (inner diameter = 20 mm and length = 80 cm) for 15 months in the temperature range 200-340 °C (MeOH = 6.2 %, O_2 = 11 % in N_2). Catalyst pellets at different positions through

the bed were characterized by Mössbauer spectrometry, XRD, chemical analysis and surface area measurements. Their data show that the catalyst pellets placed ¼ into the bed (temperature = 225-245 °C) were subjected to loss of Mo from the pellet surface, which decreased the activity of the catalyst, due to loss of MoO_3 which is in god agreement with the observations by Dias et al. [52] and Popov et al. [50]. Furthermore, at high temperatures (T> 300 °C), they observed a reddish-brown coloration of the pellet surface due to formation of $FeMoO_4$ and Fe_2O_3. Formation of $FeMoO_4$ and Fe_2O_3 is also observed elsewhere [3,13–17]. After the hots spot needle-like MoO_3 crystals were observed similar to the observations of Burriesci et al. [9].

Andersson et al. [8] studied catalyst pellets extracted from an industrial plant after half and full lifetime (10.2 % MeOH and ~9 % O_2 in N_2). Formation of $FeMoO_4$ and Fe_2O_3 were observed in accordance with the observations by Popov et al. [50], Burriesci et al. [9] and Ivanov and Dimitrov [10]. Catalyst sections throughout the bed were characterized by BET, Fourier transform Raman (FT-Raman) spectroscopy, X-ray diffraction (XRD), elemental analysis with atomic absorption spectroscopy (AAS) and activity measurements. The analysis showed that after half and full process lifetime approximately the first ¼ and ⅓ of the catalyst bed was depleted for the excess MoO_3 phase, respectively. Moreover, it was observed that Mo depleted pellets were subject to increased pore volume and decreased activity, which support the conclusions of Dias et al. [52] and Popov et al. [50]. The deposition of Mo downstream in the reactor predominantly occurred in the void space between the pellets after the hotspot, which is also observed by Ivanov and Dimitrov [10]. However, Burriesci et al. [9] contrarily observed that the catalyst at the inlet of the catalyst bed, were not subject to loss of Mo. Andersson et al. [8] attributed this to the lower MeOH inlet concentration (6 vol.%). Furthermore, the initial part of the bed in the study by Andersson et al. [8] were diluted with inert rings, allowing for higher inlet temperature leading to faster volatilization of Mo from the catalyst, which might also be part of the explanation.

The Mo volatilization and downstream formation of needlelike MoO_3 crystals in the void space between the catalyst pellets leads to increased pressure drop over the reactor, which is one main reasons for the rather short lifetime of only 1-2 years, after which the catalyst load must be replaced [8]. Another reason for replacement of the catalyst is loss of selectivity, which is also related to Mo depletion and formation of less selective iron rich phases [16]. In an industrial plant the catalyst loses activity over time due to loss of Mo, which is compensated for by increasing the reactor temperature.

1.6 Promoters

Industrial iron molybdate catalyst may contain small amounts of promoters like chromium, aluminum, cobalt, tungsten, nickel, tellurium, magnesium and tin. Introduction of promoters can affect the activity, selectivity and stability of the catalyst. The short lifetime (1-2 years) of the iron-molybdate catalyst remains an unsolved problem, and a potential beneficial effect on the stability is the most significant improvement which could be achieved by introducing promoters.

In general not much research has been published with respect to introduction of different promoters to the iron molybdate catalyst. However, some research has been performed with respect to chromium, aluminum and tungsten.

Klissurski et al. [57] studied the effect of introducing chromium in a ratio (Mo/(Fe+Cr) of 2.5/(0.5+0.5). The catalyst was prepared by co-precipitation forming an orthorhombic crystal phase of the type $Me_2(MoO_4)_3$ (Me = Fe, Cr) and MoO_3, being isostructural to the non-doped iron molybdate catalyst. The doped catalyst had commensurable activity and selectivity compared to the commercial (no Cr) catalyst. Furthermore, the stability was tested at 400 – 420 °C for 100 hours. The activity and selectivity of the doped catalyst remained practically constant, while the activity of the commercial catalyst with no Cr decreased by 20 %. The stability test shows that the chromium doped catalyst had increased stability compared to the non-doped commercial catalyst.

Pesheva et al. [58] studied the effect of introducing chromium and aluminum to the iron molybdate catalyst. They concluded that both promoters increased the stability the catalyst. However, the selectivity was not mentioned. Furthermore, they stated that the stability is related to the reducibility of the promoter, yielding the following stability sequence:

$$MoFeO < MoFeCrO < MoFeCrAlO \tag{1.13}$$

Ivanov et al. [59] studied the effect of introducing different amounts of tungsten (0-15.9 wt.% WO_3) to the iron molybdate catalyst. The catalyst was prepared by co-precipitation forming a crystal phase of $Fe_2(Mo_xW_{1-x}O_4)_3$ and $(Mo_xW_{1-x})O_3$, being isostructural to the non-doped catalyst. At a reaction temperature of 350 °C, they achieved the highest yield of formaldehyde (93.4 %) with a tungsten content of 4.9 wt.%, compared to the yield of the non-doped catalyst of 90.2 %. Unfortunately, they did not study tungsten's effect on the deactivation of the catalyst.

1.7 Conclusion

Formaldehyde (CH_2O) is produced industrially from methanol. The most common process is the Formox process, where methanol is selectively oxidized over iron an molybdate catalyst. The reaction conditions are 250–400 °C and atmospheric pressure. The reaction is exothermic and takes place in a multitubular reactor. The conversion of the process is 98–99 % and the yield is 88–91 %. Iron molybdate catalysts consist of two phases being $Fe_2(MoO_4)_3$ and MoO_3. Due to segregation of Mo and thermal spreading a surface enrichment of MoO_3 occurs on the $Fe_2(MoO_4)_3$ phase. The MoO_3 rich surface yields a highly selective catalyst towards formaldehyde and the presence of iron atoms in the subsequent sublayers yield a relatively high reaction rate.

In the literature the majority propose that the catalyzed selective oxidation of methanol occurs by a Mars-van Krevelen mechanism where the terminal oxygen at the catalyst surface takes part in the reaction, leaving an oxygen vacancy on the catalyst surface. The vacancy is later reoxidized by oxygen from the gas phase bringing the catalyst back to its original state. The rate-limiting step is believed to be the breaking of the C-H bond in the methoxide species adsorbed on the catalyst surface.

At the reaction temperature (250 °C–400 °C) the MoO_3 phase in the catalyst forms volatile species with methanol, which leaves Mo depleted catalyst pellets. The activity of the catalyst decreases as MoO_3 is volatilized from the MoO_3 rich surface. At temperatures >300 °C Mo in the $Fe_2(MoO_4)_3$ phase furthermore becomes volatile, leading to formation of non-selective iron rich species such as $FeMoO_4$ and at significant Mo depletion Fe_2O_3. To counter the deactivation phenomena an excess of MoO_3 is present in the industrial catalyst (Mo/Fe ratio = 2-3). The excess MoO_3 forms individual pure crystals. In the industrial reactor the volatilization of MoO_3 occurs in the first part of the catalytic bed. As MeOH is converted through the bed, the volatile Mo-species in the gas phase decomposes by the reverse reaction to MeOH and MoO_3 that precipitates. The precipitation mainly occurs in the void space between the catalyst pellets downstream in the bed, leading to pressure drop buildup. The lifetime of the Formox process is only 1-2 years, which is due to either pressure drop buildup or loss of selectivity.

Industrial iron molybdate catalysts may contain small amounts of promoters like chromium, wolfram and aluminum. The promotors may increase the activity and to a low degree the stability. To the author's knowledge there are no reports of methods to significantly increase the catalyst stability and life-time, which continues to be the main challenges.

1.8 References

[1] Merchant Research & Consulting ltd, "World Formaldehyde Production to Exceed 52 Mln Tonnes in 2017," 2016. [Online]. Available: https://mcgroup.co.uk/news/20140627/formaldehyde-production-exceed-52-mln-tonnes.html.

[2] IHS Chemical, "IHS analysis report Forecast: global formaldehyde market demand after five years," 2013.

[3] A. M. Bahmanpour, A. Hoadley, and A. Tanksale, "Critical review and exergy analysis of formaldehyde production processes," *Rev. Chem. Eng.*, vol. 30, no. 6, 2014.

[4] R. Günther, W. Disteldorf, A. O. Gamer, and A. Hilt, "Ullmann's encyclopedia of industrial chemistry," *Weinheim*, 2012.

[5] "www.kemibrug.dk." [Online]. Available: http://www.kemibrug.dk/KBA/CAS/121619/. [Accessed: 01-Dec-2015].

[6] G. Reuss, W. Disteldorf, A. O. Gamer, and A. Hilt, "Formaldehyde," in *Ullmann's Encyclopedia of Industrial Chemistry*, Wiley-VCH Verlag GmbH & Co. KGaA, 2000.

[7] A. P. V. Soares, M. F. Portela, and A. Kiennemann, "Methanol Selective Oxidation to Formaldehyde over Iron-Molybdate Catalysts," *Catal. Rev.*, vol. 47, no. 1, pp. 125–174, Oct. 2005.

[8] A. Andersson, M. Hernelind, and O. Augustsson, "A study of the ageing and deactivation phenomena occurring during operation of an iron molybdate catalyst in formaldehyde production," *Catal. Today*, vol. 112, pp. 40–44, 2006.

[9] N. Burriesci, F. Garbassi, M. Petrera, G. Petrini, and N. Pernicone, "Solid State Reactions in Fe-Mo Oxide Catalysts for Methanol Oxidation During Aging in Industrial Plants.," *Stud. Surf. Sci. Catal.*, vol. 6, pp. 115–126, 1980.

[10] K. I. Ivanov and D. Y. Dimitrov, "Deactivation of an industrial iron-molybdate catalyst for methanol oxidation," *Catal. Today*, vol. 154, no. 3–4, pp. 250–255, 2010.

[11] A. a. Belhekar, S. Ayyappan, and A. V. Ramaswamy, "FT-IR studies on the evolution of different phases and their interaction in ferric molybdate—molybdenum trioxide catalysts," *J. Chem. Technol. Biotechnol.*, vol. 59, no. 4, pp. 395–402, 1994.

[12] W. M. (ed) Haynes, *CRC Handbook of chemistry and physics*, 96th ed. CRC Press, 2015.

[13] A. P. V. Soares, M. F. Portela, and A. Kiennemann, "Methanol Selective Oxidation to Formaldehyde over Iron-Molybdate Catalysts," *Catal. Rev. Eng.*, vol. 47, no. 1, pp. 125–174, 2005.

[14] B. Y. A. W. Sleight, "Magnetic, Mossbauer, and Structural Studies on Three Modifications of FeMoO4," vol. 348, no. 6, pp. 2–7, 1968.

[15] E. Soderhjelm, M. P. House, N. Cruise, J. Holmberg, M. Bowker, J.-O. Bovin, and A. Andersson, "On the Synergy Effect in MoO3-Fe-2(MoO4)(3) Catalysts for Methanol Oxidation to Formaldehyde," vol. 2, pp. 145–155, 2008.

[16] M. P. House, A. F. Carley, and M. Bowker, "Selective oxidation of methanol on iron molybdate catalysts and the effects of surface reduction," *J. Catal.*, vol. 252, pp. 88–96, 2007.

[17] L. MacHala, J. Tuček, and R. Zbořil, "Polymorphous transformations of nanometric iron(III) oxide: A review," *Chem. Mater.*, vol. 23, no. 14, pp. 3255–3272, 2011.

[18] K. Lohbeck, H. Haferkorn, W. Fuhrmann, and N. Fedtke, "Manganese and Manganese Alloys," *Ullmann's Encycl. Ind. Chem.*, no. group 12, pp. 413–454, 2005.

[19] E. M. I. McCarron, "β-Mo03: a Metastable Analogue of W03," *J. Chem. Soc., Chem. Commun.*, vol. 101, pp. 336–338, 1986.

[20] I. P. Olenkova, L. M. Plyasova, and S. D. Kirik, "Crystal structure of 'hexagonal' MoO3," *React. Kinet. Catal. Lett.*, vol. 16, no. 1, pp. 81–85, 1981.

[21] H. J. Lunk, H. Hartl, M. A. Hartl, M. J. G. Fait, I. G. Shenderovich, M. Feist, T. A. Frisk, L. L. Daemen, D. Mauder, R. Eckelt, and A. A. Gurinov, "'Hexagonal molybdenum trioxide' - Known for 100 years and still a fount of new discoveries," *Inorg. Chem.*, vol. 49, no. 20, pp. 9400–9408, 2010.

[22] Y. Huang, L. Cong, J. Yu, P. Eloy, and P. Ruiz, "The surface evolution of a catalyst jointly influenced by thermal spreading and solid-state reaction: A case study with an Fe2O3–MoO3 system," *J. Mol. Catal. A Chem.*, vol. 302, no. 1–2, pp. 48–53, 2009.

[23] C. Brookes, P. P. Wells, G. Cibin, N. Dimitratos, W. Jones, D. J. Morgan, and M. Bowker, "Molybdenum Oxide on Fe 2 O 3 Core–Shell Catalysts: Probing the Nature of the Structural Motifs Responsible for Methanol Oxidation Catalysis," *ACS Catal.*, vol. 4, pp. 243–250, 2014.

[24] Q. Xu, G. Jia, J. Zhang, Z. Feng, and C. Li, "Surface phase composition of iron molybdate catalysts studied by UV Raman spectroscopy," *J. Phys. Chem. C*, vol. 112, no. 25, pp. 9387–9393, 2008.

[25] M. Bowker, A. F. Carley, and M. House, "Contrasting the Behaviour of MoO3 and MoO2 for the Oxidation of Methanol," *Catal. Letters*, vol. 120, no. 1–2, pp. 34–39, 2007.

[26] B. R. Yeo, G. J. F. Pudge, K. G. Bugler, A. V. Rushby, S. Kondrat, J. Bartley, S. Golunski, S. H. Taylor, E. Gibson, P. P. Wells, C. Brookes, M. Bowker, and G. J. Hutchings, "The surface of iron molybdate catalysts used for the selective oxidation of methanol," *Surf. Sci.*, vol. 648, pp. 163–169, 2016.

[27] C. Brookes, P. P. Wells, N. Dimitratos, W. Jones, E. K. Gibson, D. J. Morgan, G. Cibin, C. Nicklin, D. Mora-Fonz, D. O. Scanlon, C. R. A. Catlow, and M. Bowker, "The Nature of the Molybdenum Surface in Iron Molybdate. The Active Phase in Selective Methanol Oxidation," *J. Phys. Chem. C*, vol. 118, no. 45, pp. 26155–26161, 2014.

[28] M. Carbucicchio and F. Trifiró, "Surface and Bulk Redox Processes in Iron-Molybdate-Based," *J. Catal.*, vol. 85, pp. 77–85, 1976.

[29] C.-T. Wang and R. J. Willey, "Oxidation of methanol over iron oxide based aerogels in supercritical CO2," *J. Non. Cryst. Solids*, vol. 225, pp. 173–177, 1998.

[30] M. Bowker, C. Brookes, A. F. Carley, M. P. House, M. Kosif, G. Sankar, I. Wawata, P. P. Wells, and P. Yasenevaz, "Evolution of active catalysts for the selective oxidative dehydrogenation of methanol on Fe2O3 surface doped with Mo oxide," *Phys. Chem. Chem. Phys.*, vol. 15, no. 29, pp. 11988–12003, 2013.

[31] M. Bowker, M. House, A. Alshehri, C. Brookes, E. K. Gibson, and P. P. Wells, "Selectivity determinants for dual function catalysts: applied to methanol selective oxidation on iron molybdate," *Catal. Struct. React.*, vol. 1, no. 2, pp. 95–100, 2015.

[32] K. H. Hassan and P. C. H. Mitchell, *Evaluation of different methods to prepare the Fe2O3/MoO3 catalyst used for selective oxidation of methanol to formaldehyde*, vol. 175. Elsevier Masson SAS, 2010.

[33] A. M. Beale, S. D. M. Jacques, E. Sacaliuc-Parvalescu, M. G. O'Brien, P. Barnes, and B. M. Weckhuysen, "An iron molybdate catalyst for methanol to formaldehyde conversion prepared by a hydrothermal method and its characterization," *Appl. Catal. A Gen.*, vol. 363, no. 1–2, pp. 143–152, 2009.

[34] S. Chapman, C. Brookes, M. Bowker, E. Gibson, and P. P. Wells, "FDCATAL16 Design and Stabilisation of a High Area Iron Molybdate Surface for the Selective Oxidation of Methanol to Formaldehyde," *Faraday Discuss.*, 2015.

[35] N. Pernicone, "MoO3-Fe2(MoO4)3 catalysts for methanol oxidation," *J. Less Common Met.*, vol. 36, no. 1–2, pp. 289–297, 1974.

[36] K. Dewangan, N. N. Sinha, P. K. Sharma, A. C. Pandey, N. Munichandraiah, and N. S. Gajbhiye, "Synthesis and characterization of single-crystalline α-MoO3 nanofibers for enhanced Li-ion intercalation applications," *CrystEngComm*, vol. 13, no. 3, p. 927, 2011.

[37] G. C. Bailey and A. E. Craver, "Process of Procucing Formaldehyde," 1921.

[38] H. Adkins and W. Peterson, "The oxidation of methanol with air over iron, molybdenum, and iron-molybdenum oxides," *... Am. Chem. Soc.*, vol. 53, no. 1927, pp. 1512–1520, 1931.

[39] M. Bowker, R. Holroyd, A. Elliott, P. Morrall, A. Alouche, C. Entwistle, and A. Toerncrona, "The selective oxidation of methanol to formaldehyde on iron molybdate catalysts and on component oxides," *Catal. Letters*, vol. 83, no. 3–4, pp. 165–176, 2002.

[40] M. Rellán-Piñeiro and N. López, "The Active Molybdenum Oxide Phase in the Methanol Oxidation to Formaldehyde (Formox Process): A DFT Study," *ChemSusChem*, vol. 8, no. 13, pp. 2231–2239, 2015.

[41] S. K. Bhattacharyya and K. Janakiram, "Kinetics of the Vapor-Phase Oxidation of Methyl on Vanadium Pentoxide Catalyst," *J. Catal.*, no. 8, pp. 128–136, 1967.

[42] P. Mars and D. W. van Krevelen, "Oxidations carried out by means of vanadium oxide catalysts," *Chem. Eng. Sci.*, vol. 3, pp. 41–59, 1954.

[43] N. Pernicone, F. Lazzerin, G. Liberti, and G. Lanzavecchia, "On the mechanism of CH3OH oxidation to CH2O over MoO3-Fe2(MoO4)3 catalyst," *J. Catal.*, vol. 14, no. 4, pp. 293–302, 1969.

[44] S. a R. K. Deshmukh, M. Van Sint Annaland, and J. a M. Kuipers, "Kinetics of the partial oxidation of methanol over a Fe-Mo catalyst," *Appl. Catal. A Gen.*, vol. 289, no. 2, pp. 240–255, 2005.

[45] M. Bowker, "Rules for Selective Oxidation Exemplified by Methanol Selective Oxidation on Iron Molybdate Catalysts," *Top. Catal.*, vol. 58, no. 10, pp. 606–612, 2015.

[46] C. Brookes, M. Bowker, E. K. Gibson, D. Gianolio, K. M. H. Mohammed, S. Parry, S. M. Rogers, P. Silverwood, and P. P. Wells, "In Situ Spectroscopic Investigations of MoOx/Fe2O3 Catalysts for the Selective Oxidation of Methanol," *Catal. Sci. Technol.*, vol. 6, pp. 722–730, 2016.

[47] R. Coquet and D. J. Willock, "The (010) surface of α-MoO3, a DFT + U study," *Phys. Chem. Chem. Phys.*, vol. 7, no. 22, p. 3819, 2005.

[48] C. Brookes, M. Bowker, and P. Wells, "Catalysts for the Selective Oxidation of Methanol," *Catalysts*, vol. 6, no. 7, p. 92, Jun. 2016.

[49] M. Bowker, R. Holroyd, M. House, R. Bracey, C. Bamroongwongdee, M. Shannon, and A. Carley, "The selective oxidation of methanol on iron molybdate catalysts," *Top. Catal.*, vol. 48, no. 1–4, pp. 158–165, 2008.

[50] B. I. Popov, V. N. Bibin, and G. K. Boreskov, "Study of an iron-molybfate oxide catalyst for oxidation of methanol to formaldehyde," *Kinet. Catal.*, vol. 17, no. 2, pp. 322–327, 1976.

[51] R. L. Smith and G. S. Rohrer, "The Morphological Evolution of the MoO3 (010) Surface during Reactions in Methanol – Air Mixtures," vol. 278, pp. 270–278, 1998.

[52] A. P. S. Dias, F. Montemor, M. F. Portela, and A. Kiennemann, "The role of the suprastoichiometric molybdenum during methanol to formaldehyde oxidation over Mo–Fe mixed oxides," *J. Mol. Catal. A Chem.*, vol. 397, pp. 93–98, 2015.

[53] Y. H. Ma and S. J. Kmiotek, "Deactivation Kinetics of Ferric Molybdate," vol. 142, pp. 132–142, 1988.

[54] I. Mitov, S. Asenov, T. Tomov, and D. Klissurski, "In situ Mössbauer Study of the Interaction of Methanol with An Iron–Molybdenum Oxide Catalyst," *J. Phys. Chem. C*, vol. 111, no. 14, pp. 5389–5393, 2007.

[55] N. Pernicone, "Deactivation of Fe-Mo Oxide Catalyst in Industrial Plant and Simulation Tests on Laboratory Scale," *Catal. Today*, vol. 11, pp. 85–91, 1991.

[56] K. V. Raun, L. F. Lundegaard, J. Chevallier, P. Beato, C. C. Appel, K. Nielsen, M. Thorhauge, A. D. Jensen, and M. Høj, "Deactivation behavior of an iron-molybdate catalyst during selective oxidation of methanol to formaldehyde," *Catal. Sci. Technol.*, 2018.

[57] D. Klissurski, V. Rives, I. Mitov, and N. Abadzhjieva, "Iron-chromium-molybdenum oxide catalysts for methanol oxidation," vol. 18, pp. 265–271, 1993.

[58] Y. Pesheva, I. Mitov, D. Klissurski, and D. Mössbauer, "Study on the Stability of Molybdate Based Catalysts," in *Book of Abstracts Europacat II*, 1995.

[59] K. Ivanov, I. Mitov, and S. Krustev, "Selective oxidation of methanol on Fe–Mo–W catalysts," *J. Alloys Compd.*, vol. 309, no. 1–2, pp. 57–60, 2000.

Chapter 2

Deactivation Behavior of Iron-Molybdate Catalyst During Selective Oxidation of Methanol to Formaldehyde

Abstract

An iron molybdate/molybdenum oxide catalyst (Mo/Fe = 2) was synthesized by a hydrothermal method and the catalyst's performance and compositional changes were followed during selective oxidation of methanol to formaldehyde for up to 600 h. The activity was continuously measured for a series of experiments performed in a laboratory fixed-bed reactor with 10, 100, 250 and 600 h on stream under reaction conditions (5 % MeOH, 10 % O_2 in N_2, Temp. = 384 – 416 °C, W/F = 1.2 g_{cat} h mol^{-1}_{MeOH}). The structural and compositional changes of the catalyst were investigated by a number of techniques including: XRD, Raman spectroscopy, XPS, SEM-EDS and STEM-EDS. Methanol forms volatile species with molybdenum at reaction conditions, leading to depletion of Mo from the catalyst. Excess MoO_3 was shown to volatilize and leave the catalyst during the first 10 h on stream, leading to an initial loss in activity of 50 %. From 10 to 600 h on stream leaching of molybdenum from the remaining iron molybdate phase ($Fe_2(MoO_4)_3$, Mo/Fe = 1.5) leads to iron rich phases ($FeMoO_4$ and Fe_2O_3, Me/Fe < 1.5) and simultaneously an increase in activity to approximately 1.5 times the initial activity. Even at high degrees of molybdenum loss (Mo/Fe = 0.49) the formaldehyde selectivity remained above 92 %, and the combined CO/CO_2 selectivity was below 4 %. This is likely due to a surface layer of MoO_x on the catalyst at all times due to segregation and a surface in equilibrium with the gaseous molybdenum compounds. After 600 h on stream formation of β-MoO_3 was observed, indicating that this molybdenum oxide phase is stable to some extent under reaction conditions.

2.1 Introduction

The industrial production of formaldehyde from methanol is an important chemical process. The majority of the produced formaldehyde is processed into higher-valued synthetic resins [1], making formaldehyde an important C_1 building block. Formaldehyde polymerize at room temperature and is commercially available as an aqueous solution known as formalin (37 wt.%). The formalin production was approximately 52 million tons in 2017 [2]. Formaldehyde may be synthesized industrially by selective oxidation of methanol over an iron-molybdate/molybdenum oxide (FeMo) catalyst according to: $CH_3OH + ½O_2 \rightarrow CH_2O + H_2O$ (ΔH = -156 kJ/mol) [3]. The reaction is normally carried out in a multitubular reactor (tube length = 1 to 1.5 m) with excess of oxygen (MeOH = 10%, O_2 = 10 % in N_2) at near atmospheric pressure and 270-400 °C (yield = 88-92 % with complete methanol conversion in a single pass), known as the Formox process [1]. Since the early 1960s the inlet concentration of methanol has increased from 6.5 to ~10 % methanol, which significantly increases productivity [4]. The fresh catalyst consists of two phases $Fe_2(MoO_4)_3$ and MoO_3. The role of the two phases has been discussed in the literature and mainly two explanations have been suggested. One explanation is that the MoO_3 phase forms a thin surface layer on the $Fe_2(MoO_4)_3$ bulk phase. This molybdenum rich surface is selective towards formaldehyde while the iron in the sublayer increases the activity of the catalyst [5,6]. Pure MoO_3 has low activity. Another explanation is that $Fe_2(MoO_4)_3$ is the active phase and that MoO_3 must be present to replenish molybdenum lost from the iron molybdate surface and avoid formation of less selective iron rich phases [7-10].

Molybdenum forms volatile species with methanol and potentially water under reaction conditions, which can leave behind molybdenum poor zones in the catalyst bed [11,12]. Besides the ferric molybdate phase ($Fe_2(MoO_4)_3$) present in the fresh catalyst, the reduced ferrous phase ($FeMoO_4$) can be present in the spent catalyst. At substantial molybdenum loss Fe_2O_3 can be formed. Due to segregation of molybdenum in ferric molybdate, this phase tends to have an over stoichiometric Mo/Fe ratio on the surface [13].

The Selective oxidation of methanol to formaldehyde follows the Mars-van-Krevelen mechanism with initial reduction of the iron atoms (2.1) [14]:

$$CH_3OH + Fe_2(MoO_4)_3 \rightarrow CH_2O + H_2O + 2FeMoO_4 + MoO_3 \quad (2.1)$$

In the presence of excess MoO_3, the catalyst surface is re-oxidized without formation of iron rich species (2.2) [12]:

$$2FeMoO_4 + MoO_3 + ½O_2 \rightarrow Fe_2(MoO_4)_3 \quad (2.2)$$

However if there is shortage of MoO_3 the re-oxidation may result in the formation of hematite (2.3) [14]:

$$3FeMoO_4 + ¾O_2 \rightarrow Fe_2(MoO_4)_3 + ½Fe_2O_3 \quad (2.3)$$

The MoO_3 and $Fe_2(MoO_4)_3$ phases are primarily selective towards formaldehyde, however $FeMoO_4$ and Fe_2O_3 are reported to be selective towards CO and CO_2 respectively. Molybdenum oxide must be sufficiently available at the catalyst surface to ensure selectivity towards formaldehyde [15]. The commercial catalyst is prepared with excess MoO_3 (Mo/Fe > 1.5) to counter the loss of molybdenum [16]. Furthermore, excess MoO_3 increas-

es the mechanical strength of the catalyst pellets, preventing crumbling and the resulting reactor plugging by catalyst fines [17]. The average lifetime of the industrial catalyst is only 1–2 years depending on the operating conditions.

Full scale experiments have been performed for the total lifetime of industrial catalysts followed by characterization. At full scale the formed volatile molybdenum species flow along the reactor and as the methanol is converted, the volatile molybdenum species decompose to molybdenum oxide and accumulate near the reactor hot spot [12,18]. The precipitation of molybdenum oxide leads to significant increase in pressure drop, process shutdown and change of the catalyst. The pressure drop increase is the main reason for the short lifetime of the process, rather than decreasing selectivity.

Laboratory studies have been performed to investigate the degradation phenomena of the FeMo catalyst [9,19]. In these studies a fixed-bed reactor is operated at high space time achieving high conversion. At high degree of conversion, it is difficult to measure changes in the catalyst activity. Furthermore, Popov et al. [11] observed a saturation of the gas by volatile molybdenum species at low space time and moderate temperature. For a fixed-bed reactor operated at high space time, the gas will be saturated with the volatile molybdenum species in the first part of the catalyst bed and the subsequent part will be shielded from loss of molybdenum. The varying molybdenum loss in the reactor will lead to uneven degradation of the catalyst bed. The space time and methanol conversion must be sufficiently low to be able to measure uniform deactivation due to loss of molybdenum,

As the methanol inlet concentration and process productivity has increased through the last decades, the short lifetime of the process remains a major challenge. Even though spent catalysts from industrial reactors have been investigated, the understanding of the structural and compositional changes over time and their effect on the catalyst performance is limited. To increase the catalyst stability and the process lifetime a detailed understanding of the catalyst deactivation behavior must first be established. This work presents a study of the continuous deactivation behavior and structural changes in the FeMo catalyst during selective oxidation of methanol to formaldehyde, determined by prolonged activity tests and comprehensive characterization of spent catalyst exposed to high temperature and low space time with intermediate conversion of methanol.

2.2 Experimental

2.2.1 Catalyst preparation

The iron molybdate catalyst was prepared by hydrothermal synthesis similar to the procedure reported by Beale et al. [20]. Iron nitrate nonahydrate ($Fe(NO3)•9H2O$ – Sigma Aldrich > 98 % purity) and ammonium heptamolybdate tetrahydrate ($(NH4)4Mo7O24•7H2O$ – Sigma Aldrich > 99 % purity) were dissolved separately in equal amounts of demineralized water (2 times 150 mL). The ammonium heptamolybdate solution was dropwise added to the iron nitrate solution under vigorous stirring. Some precipitation occurred immediately after mixing. The mixture was loaded in a 400 mL Teflon-lined autoclave with a magnetic stirrer and the pH was measured (1.66). The autoclave was sealed, heated to 180 °C and kept at this temperature for hydrothermal treatment of the mixture for 12 hours. The solid product was filtered, washed with demineralized wa-

ter and dried at 60 °C overnight yielding a yellow/green powder (yield = 92 %). Finally the powder was calcined at 535 °C for 2 h. The composition of the obtained material was determined to Mo/Fe = 2.01 by inductively coupled plasma (ICP) analysis.

2.2.2 Catalyst activity measurements

The synthesized catalyst powder was pressed into a pellet, crushed and sieved to a 150-250 µm sieve fraction. A bed containing 25 mg catalyst and 170 mg SiC (150-300 µm sieve fraction) was placed between two plugs of quartz wool in a U-tube reactor (ID = 4 mm). The reactor was placed in an oven. The feed gas consisted of 10 vol.% O_2 and ~5 vol.% MeOH in N_2, which was fed at a flowrate of ~157.5 mL/min (1 bar, 273.15 K). N_2 and O_2 were introduced by mass flow controllers (Brooks) and bubbled through a flask containing MeOH (≥99.9 %, Sigma-Aldrich). The gas was saturated with MeOH and the concentration was controlled by cooling the bubble-flask in a cooling bath to 5 °C. To determine the conversion and selectivity the gas composition was measured at the outlet of the reactor by a gas chromatograph (GC)(Thermo Scientific, Trace GC Ultra). The MeOH and DME concentrations were measured using an FID-detector and the CH_2O, H_2O, CO, CO_2, O_2 and N_2 concentrations were measured using a TCD-detector. The measured concentrations were corrected for expansion of the gas due to reaction using the N_2 signal as internal standard [21]. Furthermore, the reactor inlet and outlet pressures were measured, and a thermocouple was placed inside the reactor touching the exit of the catalyst bed to measure the bed temperature. Before each experiment, the catalyst bed was thermally treated at 400 °C in air for two hours and the conversion was subsequently measured at increasing temperatures (oven temp. = 250, 300, 340 and 375 °C) under reaction conditions to obtain the first order reaction rate constant as a function of temperature. Due to fast changes in the catalyst activity under reaction condition, the oven temperature was increased without MeOH in the feed (10 % O_2 in N_2). When the oven temperature stabilized at the given temperatures, MeOH was introduced for 5 min followed by an activity measurement. The measurement at 375 °C is the first measurement of the prolonged deactivation experiment. The changes in the catalyst activity prior to the experiment are small due to the short exposure time and moderate temperature. The four initial activity measurements were subsequently used to generate an Arrhenius plot to provide the activation energy and pre-exponential factor to be used for calculation of the relative rate constant as explained in section 2.2.2.3. The experiments ran for 10, 100, 250 and 600 h respectively (oven temp. = 375 °C, 1 GC-measurement / hour). The industrial reaction temperature is 270-400 °C and the catalyst lifetime is 1-2 years. To achieve a fast deactivation rate it was decided to run the oven at 375 °C, achieving a catalyst temperature of 384 – 416 °C due to the exothermic reaction, which is at the upper limit of the industrial reaction temperature. The samples were cooled to room temperature in the reaction gas mixture to maintain the catalyst state.

2.2.2.1 GC-calibration

Both GC detectors (FID and TCD) were calibrated using gas mixtures with known concentrations, except for formaldehyde due to its ability to polymerize at room temperature. The TCD detector was calibrated for formaldehyde using Lennard-Jones parameters to calculate the viscosity and thermal conductivity for formaldehyde and reference species

(N_2, O_2, MeOH and CH_4). A linear trend between the TCD detector response factor and the thermal conductivity for the respective reference species were seen. Assuming that the response factor for formaldehyde fits the linear trend of the reference species its response factor could be estimated [22-24]. The response factor of formaldehyde was similar to the response factors for N_2, O_2 and MeOH, which have similar molar masses.

2.2.2.2 Calculation of selectivity and conversion

The selectivities and conversions were normalized to 100 % by assuming that all measured carbon species in the product stream originated from methanol in the feed according to (2.4) and (2.5):

$$Selec.(CH_2O) = \frac{P_{CH_2O}}{P_{MeOH} + P_{CH_2O} + 2P_{DME} + P_{CO} + P_{CO_2}} \cdot 100\% \tag{2.4}$$

$$Conversion = \left(1 - \frac{P_{CH_2O}}{P_{MeOH} + P_{CH_2O} + 2P_{DME} + P_{CO} + P_{CO_2}}\right) \cdot 100\% \tag{2.5}$$

2.2.2.3 Calculation of relative rate

The catalyst temperature was not constant through the experiments due to the exothermic reaction, which will affect the degree of conversion. To compensate for the changing catalyst temperature on the apparent activity in terms of conversion, a relative rate constant was calculated for each gas sampling time (1 sample per hour) in the activity measurements. The relative rate constant is the ratio between the measured rate constant and the calculated rate constant of the fresh catalyst at the catalyst temperature at the sampling time. The measured rate is calculated from the degree of conversion at the sample-time and the expected rate of the fresh catalyst is calculated from the catalyst temperature at the sample-time and the initially measured Arrhenius parameters.

The reaction order of Methanol is reported to be first order [25,26] and the relative rate constant is calculated according to (2.6-2.8) as explained above. The measured rate constant is calculated from the plug flow reactor design equation (2.6) and the expected rate constant of the fresh catalyst is determined from the Arrhenius parameters (2.7). The relative rate constant is the ratio between measured and expected rate constant of the fresh catalyst (2.8) at the reactor temperature at the time of sampling.

$$k_{Meas}(T) = -\frac{v_0}{W} \cdot \ln(1 - X) \tag{2.6}$$

$$k_{Fresh}(T) = A \cdot \exp\left(\frac{-E_a}{RT}\right) \tag{2.7}$$

$$k_{Relative} = \frac{k_{Meas}(T)}{k_{Fresh}(T)} \tag{2.8}$$

Where v_0 is the volumetric flow rate, W is the catalyst mass, X is the degree of conversion, A is the pre-exponential factor, E_a is the activation energy, R is the gas constant and T is the absolute temperature.

2.2.3 XRD

XRD data were collected using a PanAlytical Empyrean diffractometer equipped with focusing mirrors for CuKα radiation (λ = 1.541 Å) and a capillary spinner. A Ni beta filter, a pair of 0.04 radian soller slits and a beam stop was further more used. Samples were measured in sealed capillaries. Rietveld refinement was performed using the TOPAS software [27] and reference structures for $Fe(MoO_4)_3$ [ICSD 80449], $FeMoO_4$ [ICSD 43013], α-MoO_3 [ICSD 152313], β-MoO_3 [ICSD 86426] and Fe_2O_3 [ICSD 15840]. Atomic positions and stoichiometry were fixed while lattice parameters, average crystallite size and scale factors were refined.

2.2.4 Raman spectroscopy

Raman spectra were recorded with a Horiba LabRAM microscope, using 633 nm excitation. The samples were sealed in glass capillaries in order to avoid re-oxidation in air during measurements. A 50x long distance objective (Olympus) was used to focus the laser beam, with a measured power of 1 mW on the sample. Tests with higher and lower laser power were done to check for sample laser damage, which was only observed in the case of the sample run for 600 h time on stream. Reference spectra for all relevant phases are shown in Figure A.1.

2.2.5 SEM

The particles were dispersed on double sided carbon tape on an aluminium stub and the samples were coated with an electron conductive layer of carbon prior to investigation. Scanning Electron Microscopy (SEM) images were acquired in an Environmental SEM, XL30 FEG, at 15 kV and the backscattered electron signal was used.

EDX analyses in SEM were acquired without standards at 15 kV with an EDAX liquid Nitrogen cooled Si(Li) detector.

2.2.6 STEM

X-rays maps were acquired using a FEI Talos (S)TEM running at 200 kV in Scanning Transmission Electron Microscopy (STEM) mode and implanted with the ChemiSTEM technology consisting of 4 SDD X-rays detectors distributed symmetrically around the sample.

2.2.7 XPS

XPS was performed with a Theta Probe system from Thermo Fisher. The system utilizes monochromatized Al K_α X-rays with an energy of 1486.7 eV as the source and the spot size was set to 400 µm (diameter). A hemispherical analyzer was used for data acquisition and the data was analyzed with the Avantage software packages version 5.979 from Thermo Fisher.

2.2.8 ICP-OES

The catalyst samples were decomposed by fusion with potassium pyrosulphate, and dissolved by adding concentrated hydrochloric acid. The element concentration was determined using a Perkin Elmer model Optima 3000 ICP/OES analyser.

2.2.9 BET

The specific surface area (SSA) was measured on the fresh catalyst, after degassing at 350 °C under vacuum, by nitrogen adsorption at its boiling point using multipoint BET theory with four points in the p/p_0 = 0.15 to 0.3 range (Quantachrome NOVA-touch LX2).

2.3 Results

2.3.1 Activity measurements

The activity of the synthesized iron molybdate/molybdenum oxide catalyst (SSA = 4.7 m^2/g) was measured over time in the four experiments. Each of the experiments (TOS = 10, 100, 250 and 600 h) showed the same development in activity over time, showing that the activity measurements are reproducible (Figure A.2). The activation energy (57 ±2 kJ/mol) and pre-exponential factor of the catalyst was determined prior to each experiment by measuring the reaction rate constant at four temperatures and applying the Arrhenius equation (Figure A.3).

The results of the experiment for 600 h on stream are shown in Figure 2.1. The activity showed an initial decrease from ~100 to 48 % relative rate (conversion = 47 – 25 % and catalyst temp. = 398 – 384 °C, see Figure A.4), followed by an increase to ~155 % relative rate (conversion ≈ 68 %), thus exceeding the activity of the fresh catalyst. Moreover, the combined CH_2O and DME selectivity was above >96 % at all times. DME will mainly be converted to formaldehyde yielding high overall selectivity at total conversion. Small amounts of CO and CO_2 were produced with an overall increasing trend with time on stream to about 3.2 % at 600 h. Due to potential further oxidation of CH_2O, the CO and CO_2 formation would be higher at total conversion with slightly lower overall CH_2O selectivity. Initially the catalyst temperature followed the development of the activity due the exothermic reactions. However, with increasing CO and CO_2 selectivity at the end of the experiment the catalyst temperature kept increasing, since the combustion reactions are more exothermic than the selective oxidation reaction.

The activity of a comparable commercial catalyst has been measured for 100 h on stream at similar reaction conditions and a similar trend in the development of the activity and selectivity was observed.

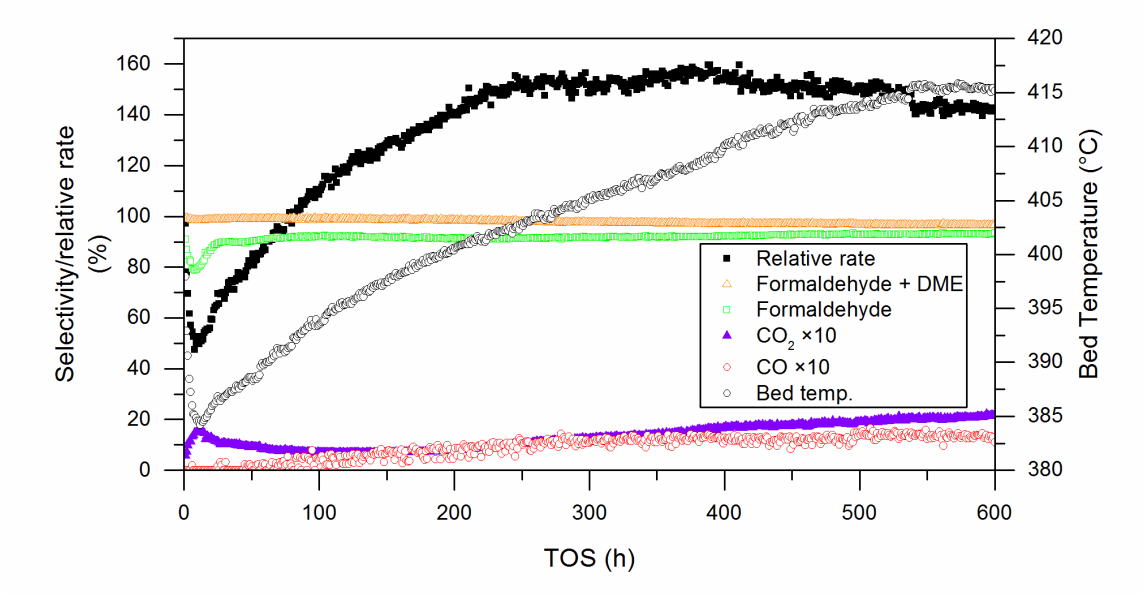

Figure 2.1 - MeOH conversion, formaldehyde selectivity, formaldehyde + DME selectivity, CO selectivity, CO_2 selectivity (C-mol.%) and catalyst temperature. Operating conditions: 25 mg catalyst mixed with 170 mg SiC, ~157.5 NmL/min gas feed: 10 % O2, ~5 % MeOH in N2. Ambient pressure. Methanol conversion = 23-70 %.

2.3.2 XRD and Raman spectroscopy

The X-ray diffraction (XRD) patterns and Raman spectra of the fresh and spent catalyst samples revealed a significant molybdenum loss over time (Figure 2.2, Figure 2.3, Figure A.5 and Figure A.6). XRD gives mainly information about the bulk of the samples, while Raman spectroscopy is performed on single positions in the sample (special resolution ~10 µm), yielding information about the local presence of the phases. The Mo/Fe ratio were estimated from the Rietveld refined phase composition under the assumptions of only stoichiometric phases and no presence of X-ray amorphous phases. The Mo/Fe ratios and phase compositions are shown in Table 2.1. The crystal size for all samples were ~200 nm. The fresh catalyst consisted of $Fe_2(MoO_4)_3$ and α-MoO_3 which is indicated by the reflections at 2θ = 12.75, 23.35 and 27.34° respectively in the XRD patterns and bands belonging to α-MoO_3 (818, 993, 665, 128, 116 cm^{-1}) and $Fe_2(MoO_4)_3$ (782, 990, 966 cm^{-1}) in the Raman spectra. The corresponding Mo/Fe ratio (XRD) of the fresh catalyst is lower than the ICP-OES measured ratio. This is most likely due to some amorphous MoO_x present on the catalyst surface, as determined by STEM line scans (see Section 3.3), which is not detected by XRD. The XRD pattern and Raman spectra of the fresh catalyst is in accordance with catalysts reported in the literature [28,29]. After 10 h on stream no MoO_3 was detected in the sample, which is due to the volatilization of MoO_3 under reaction conditions. In the Raman spectra some bands belonging to the less molybdenum rich β-$FeMoO_4$ (925, 875 cm^{-1}) started to be visible, along with $Fe_2(MoO_4)_3$, indicating slight reduction and Mo loss from the iron molybdate phase. MoO_3 has a replenishing effect on the iron molybdate phase [30,31], which is most likely the reason for the low degree of reduction in the initial 10 h on stream. After 100 h on stream reduction of $Fe_2(MoO_4)_3$ to β-$FeMoO_4$ was also detected by XRD, where β-$FeMoO_4$ is indicated by the reflection at 2θ = 26.17°. In the Raman spectra the intensity of the bands belonging to β-$FeMoO_4$ increased, while the intensity of

the $Fe_2(MoO_4)_3$ bands reduced. Similar observations of β-$FeMoO_4$ formation under redox conditions have been observed by O'Brien et al. [32].

After 250 h on stream the intensity of the reflections and bands belonging to β-$FeMoO_4$ were increased and decreased for $Fe_2(MoO_4)_3$. Furthermore, Raman bands at 162, 707 and 846 cm^{-1} became visible, indicating the formation of new phases. After 600 h the catalyst was subject to significant molybdenum loss. Most of the initial $Fe_2(MoO_4)_3$ was reduced to β-$FeMoO_4$ and a significant amount of hematite (Fe_2O_3) was present in the catalyst, which is indicated by XRD reflections at 2θ = 24.18° and 2θ = 33.17°. Furthermore, a new phase of β-MoO_3 was present indicated by reflections at 2θ = 23.02° and 2θ = 25.04°. Due to the inhomogeneous nature of the sample, Raman gave different spectra at different positions. Representative Raman spectra at two different positions are shown in Figure 2.3. At the first position (a) the new phases such as β-$FeMoO_4$ were dominant, and only trace amounts of $Fe_2(MoO_4)_3$ was detected. Bands at 846, 353, 774 and 900 cm^{-1} were assigned to the metastable β-MoO_3. However, bands at 682, 707 and 812 cm^{-1} could not be assigned. By increasing the laser power, the non-assigned bands were selectively removed (indicating a high reactivity of this phase), and by increasing the laser power further, the β-MoO_3 was transformed into the thermodynamically stable α-MoO_3 (Figure A.7). The formation of β-MoO_3 must originate from segregation of Mo from one or both of the iron molybdate phases. At the second position (b) bands belonging to Fe_2O_3 (219, 284, 396 and 1305 cm^{-1}) were detected.

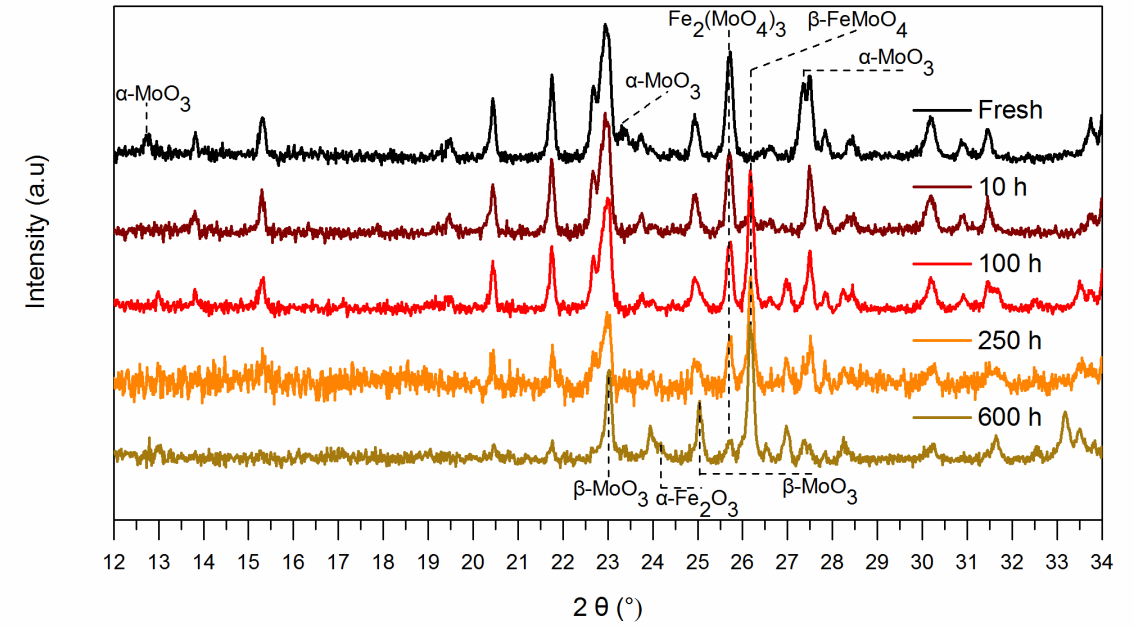

Figure 2.2 – XRD patterns of the fresh and spent Fe-Mo catalyst samples (TOS = 10, 100, 250 and 600 h).

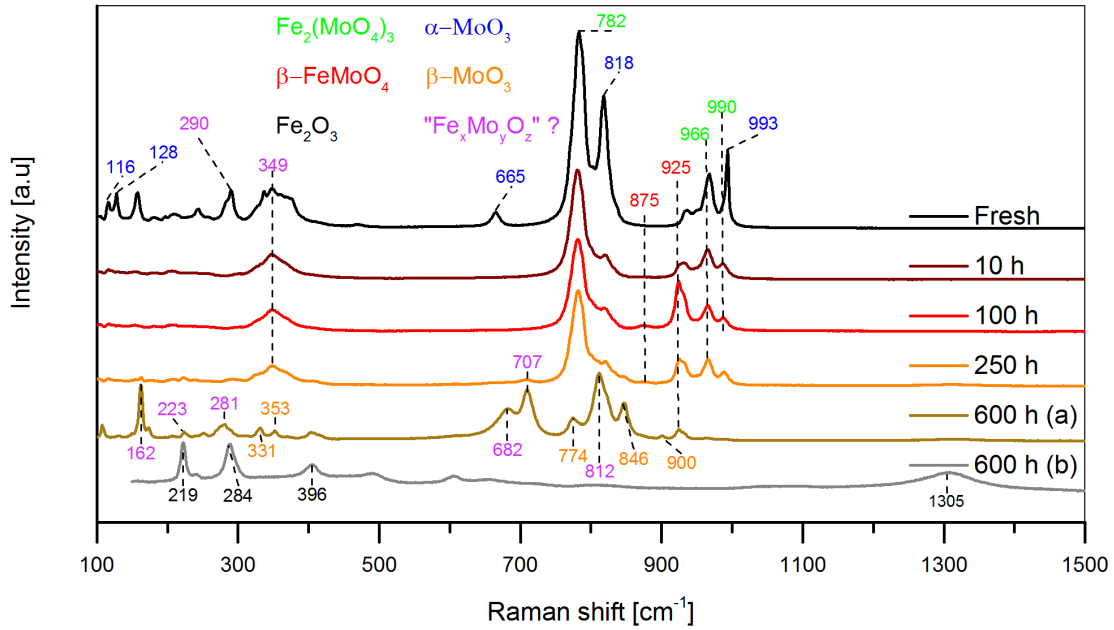

Figure 2.3 – Raman spectra of the fresh and spent Fe-Mo catalyst samples (TOS = 10, 100, 250 and 600 h). Due to the inhomogeneous nature of the catalyst after 600 h spectra from two representative spots are shown.

Table 2.1 – Characterization of the fresh and spent catalysts samples (TOS = 10, 100, 250 and 600 h) with, XRD, Raman spectroscopy, ICP-OES and XPS.

Sample	**Phases According to Raman** *Small amounts	**Phases According to XRD** Phase (wt.%)	**Mo/Fe Bulk Ratio according to:** [a] **XRD,** [b] **ICP-OES**	**Mo/Fe Surface Ratio** according to: XPS
FeMo_Fresh	α-MoO_3, $Fe_2(MoO_4)_3$	MoO_3 (17), $Fe_2(MoO_4)_3$ (83)	1.90 [a], 2.01 [b]	5.84
FeMo_10h	$Fe_2(MoO_4)_3$, β-$FeMoO_4$*	$Fe_2(MoO_4)_3$ (100)	1.50 [a]	0.81
FeMo_100h	$Fe_2(MoO_4)_3$, β-$FeMoO_4$	$Fe_2(MoO_4)_3$ (69), β-$FeMoO_4$ (31)	1.31 [a]	0.75
FeMo_250h	β-MoO_3*, $Fe_2(MoO_4)_3$, β-$FeMoO_4$	$Fe_2(MoO_4)_3$ (64), β-$FeMoO_4$ (36)	1.28 [a]	0.66
FeMo_600h	β-MoO_3, $Fe_2(MoO_4)_3$*, β-$FeMoO_4$, Fe_2O_3	β-MoO_3 (11), $Fe_2(MoO_4)_3$ (20), β-$FeMoO_4$ (33), Fe_2O_3 (36)	0.49 [a]	0.44

2.3.3 SEM and STEM images

The scanning electron microscopy (SEM) images (Figure A.8-A.17) and scanning transmission electron microscope (STEM) elemental mapping (Figure A.18-A.27), both coupled with energy dispersive X-ray spectroscopy (EDS) showed the changing morphology and elemental composition of the catalyst samples with increasing time on stream. Images of the fresh catalyst (Figure 2.4) showed the presence of irregularly shaped MoO_3 particles around ~1 µm in size. Furthermore, the major part of the sample consisted of smaller $Fe_2(MoO_4)_3$ crystals. STEM line scan (Figure 2.5) revealed a surface enrichment of Mo on the $Fe_2(MoO_4)_3$ crystals of app. 5 nm. On the images of the catalyst after 10 and 100 h on stream no MoO_3 crystals were observed (Figure 2.6 and Figure 2.7, Figure A.14-A.15 and A.20-A.23) and no surface enrichment of Mo was observed. On the images of the samples after 250 and 600 h on stream almost cubic crystals of MoO_3 were observed (Figures A.8, A.9, A.13, A.14). The observation of MoO_3 crystals after 250 and 600 h on stream indicates the formation of β-MoO_3 which has monoclinic crystal structure with dimensions very close to cubic [33]. The formation of β-MoO_3 is also shown by XRD and Raman spectroscopy after 250 and 600 h on stream. A decrease in the Mo content of the iron molybdate crystals was observed as function of time on stream. The surface region was observed to be more iron rich than the crystal bulk for those samples, which indicate that Mo segregates from the crystal bulk to the surface, where it forms volatile species with MeOH and evaporates. The iron molybdate crystals appear to disintegrate as function of time on stream. This is most likely due to the loss of Mo from the crystal lattice leading to smaller polycrystalline iron molybdate particles. The change in the morphology will most likely lead to increased surface area of the spent catalyst sample. Increased surface area of Mo poor iron molybdate system are likewise observed in the literature for synthesized systems [34].

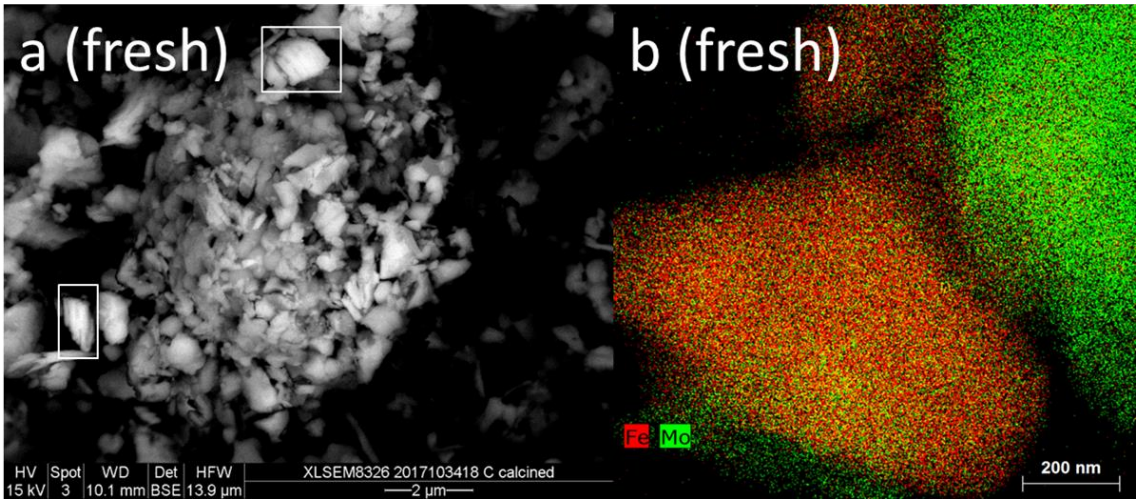

Figure 2.4 – SEM image of fresh FeMo catalyst (a), white rectangles marks MoO_3 crystals. STEM elemental mapping overlap of Fe and Mo (b).

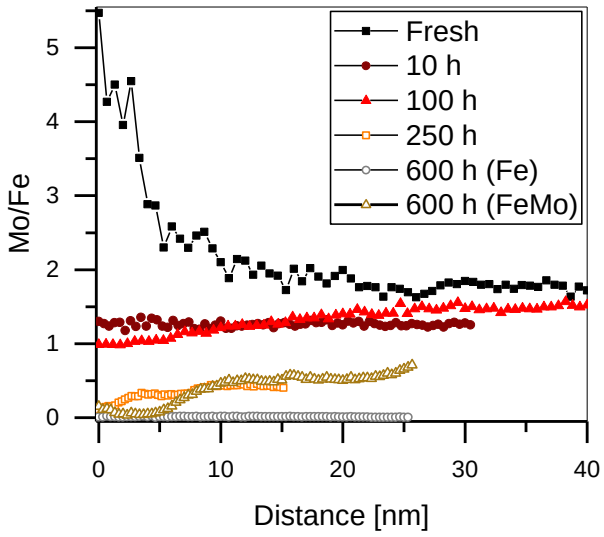

Figure 2.5 – STEM line scans of fresh and spent FeMo catalyst. 0 nm = crystal surface. The Mo/Fe atomic ratio is shown.

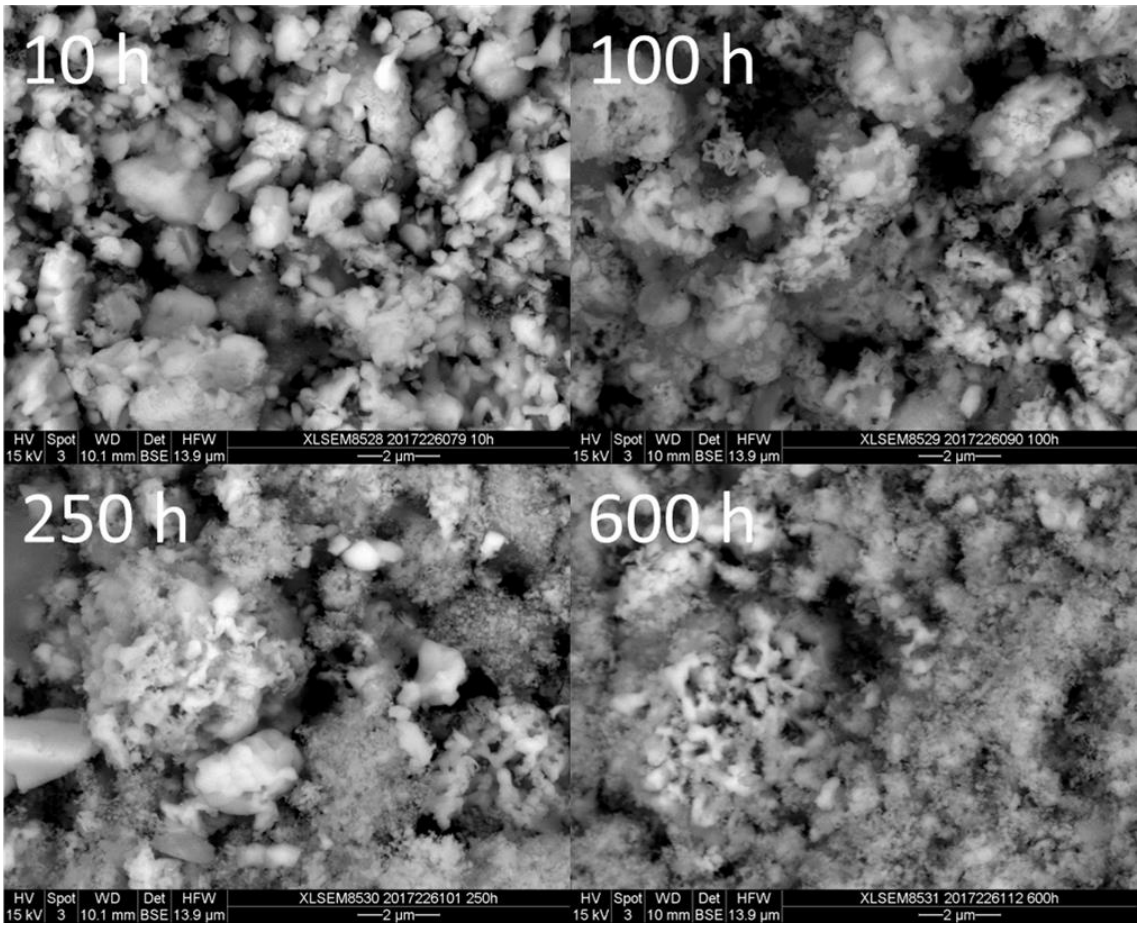

Figure 2.6 – SEM images of spent FeMo catalyst. TOS = 10 h, 100 h, 250 h and 600 h.

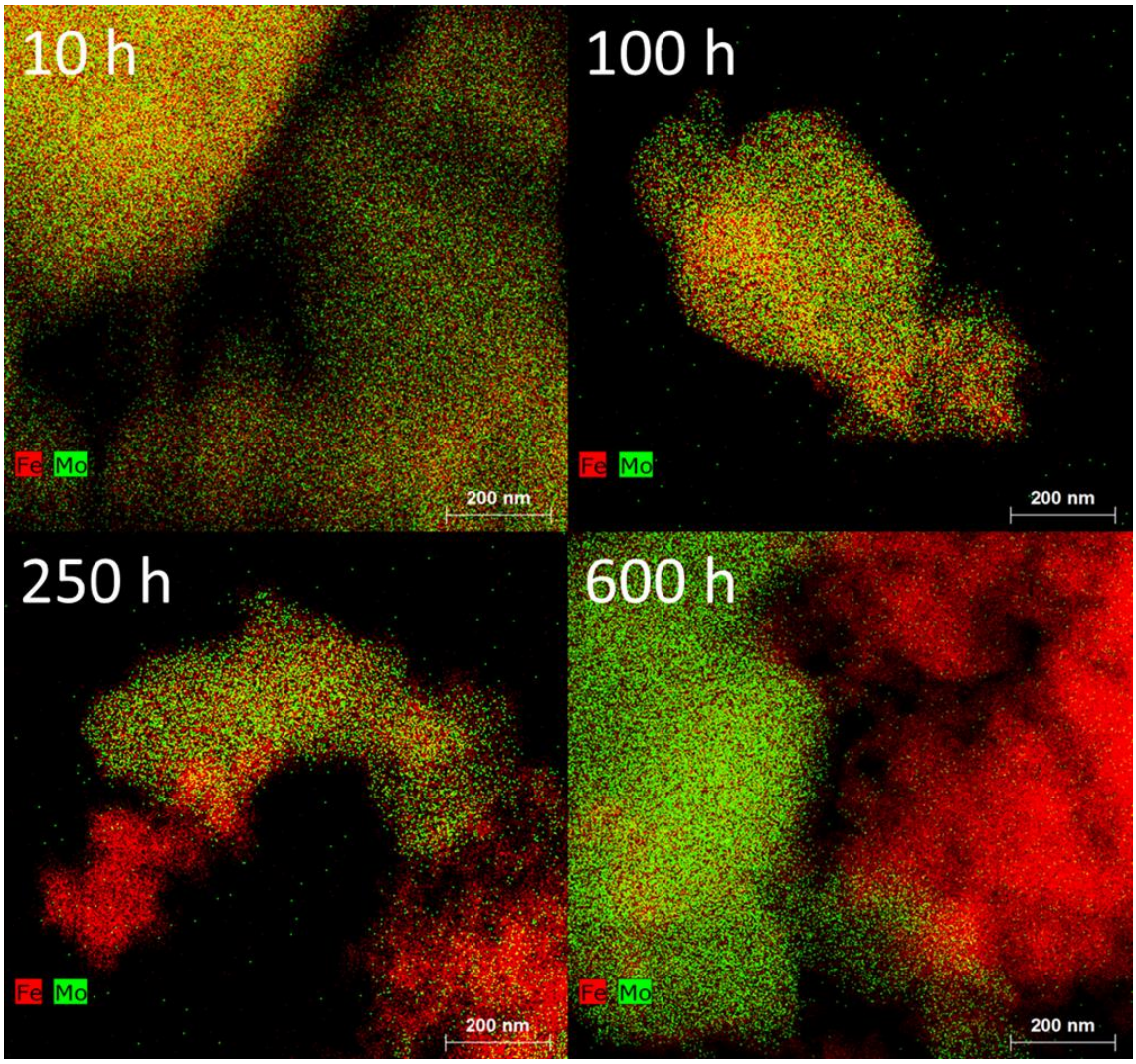

Figure 2.7 - STEM determination of atomic distributions across FeMo catalyst.
TOS = 10 h, 100 h, 250 h and 600 h.

2.3.4 XPS

X-ray photoelectron spectroscopy (XPS) of the fresh and spent catalysts revealed a significant molybdenum loss from the catalyst surface region over time. The spectra can be seen in Figure A.28. The samples were fitted to a single Mo $3d_{3/2}$-Mo $3d_{5/2}$ doublet, which indicate the presence of only one type of molybdenum (VI) oxide species. The Fe $2p_{3/2}$ peak was successfully fitted with two individual components, which indicate the presence of two iron (II and III) oxide species. However, these species overlap closely, which makes quantification of the separate species highly uncertain. The Fe $2p_{3/2}$ binding energies are reported as fitted to a single Fe $2p_{3/2}$ peak. The binding energies can be seen in Table 2.2 and the Mo/Fe ratio can be seen in Table 2.1. Similar binding energies have been reported in the literature [35,36].

Table 2.2 – Peak positions in XPS spectra of fresh and spent catalysts.

	Binding energy (eV)	
Catalysts sample	Mo $3d_{5/2}$	Fe $2p_{3/2}$
FeMo_Fresh	234.3	713.6
FeMo_10 h	231.4	709.9
FeMo_100 h	232.1	710.7
FeMo_250 h	231.5	710.2
FeMo_600 h	231.6	710.0

2.4 Discussion

The catalytic performance (Figure 2.1) and compositional changes (Table 2.1) observed for the synthesized iron molybdate catalyst (Mo/Fe = 2) reveal significant Mo loss in a period of 600 h on stream at the reaction conditions (~5 % MeOH, 10 % O_2 in N_2: W/F = 1.2 g_{cat}/mol_{MeOH}) and elevated temperature (catalyst = 384 – 416 °C). The catalyst was selective mainly towards formaldehyde throughout the experiment even at significant Mo loss and formation of iron rich species.

2.4.1 TOS = 0 - 10 h

The XRD and Raman spectroscopy show that no MoO_3 is present in the catalyst after 10 h on stream. This is due to the volatilization of MoO_3 with MeOH leading to transport of Mo out of the catalyst bed. This is possible since the experiments are performed with moderate conversion, so the MeOH concentration is significant throughout the catalyst bed. The initial migration of the excess Mo observed in this work is comparable with the migration occurring in the initial part of the catalytic zone in an industrial reactor, where excess Mo likewise volatilizes and is transported through the reactor. Activity measurements of the spent catalyst from industrial plants and industrial like experiments show a significant drop in activity when the catalyst loses its excess MoO_3 [12,18]. This activity drop is likewise observed in this work after 10 h on stream. Furthermore, Raman spectroscopy showed low intensity bands belonging to β-$FeMoO_4$, STEM line scan after 10 h on stream showed a Mo/Fe ratio corresponding to a mixture of $FeMoO_4$ and $Fe_2(MoO_4)_3$ and XPS

showed a Mo/Fe ratio of 0.81, which all indicate that the iron molybdate crystals are subject to Mo loss at the surface region.

The measured surface Mo/Fe ratio might be misleading, because XPS is not only surface layer sensitive. The signal originates from the top 1-2 nm and for the iron molybdate system approximately 20 % of the total XPS signal has been estimated to originate from the surface layer alone [35]. Thus, the true surface monolayer might have a different Mo/Fe ratio than the one measured with XPS. The rather high selectivity might suggest a Mo rich surface layer [31]. Assuming that 20 % of the XPS signal originates from a Mo surface monolayer (ML) and that the sublayers have an evenly distributed Mo/Fe ratio, the sublayer Mo/Fe ratio would be ~0.45, which correspond to a significantly iron enriched composition. However, it has been shown by Brookes et al. [31] that a layer of MoO_x on top of Fe_2O_3 can result in a selective catalyst at moderate conversion levels.

Dias et al. [28] studied the catalytic effect of varying the number of Mo ML on top of iron molybdate. Their data show that at 3 ML the catalyst is relatively active and selective towards CH_2O. However, when the Mo ML is decreased to 0.5 ML the catalyst become less active and more selective towards DME. The observations by Dias et al. support the observations in this work of increasing DME formation during the initial 10 h on stream where all MoO_3 and the surface enrichment of MoO_x on $Fe_2(MoO_4)_3$ evaporate from the catalyst, as determined by XRD, Raman spectroscopy, STEM and XPS.

In the present work, the selectivity towards CO and CO_2 was higher compared to the observed selectivity of commercial catalysts [1]. This could be due to the high temperatures (384-416 °C) where the temporary reduction of the catalyst surface during the conversion of methanol to formaldehyde becomes relative faster than the re-oxidization of the catalyst, leading to CO and CO_2 selective sites on the catalyst [37].

2.4.2 TOS = 10 - 250 h

XRD shows that the iron molybdate phase remaining after 10 h on stream is subject to further Mo loss leading to reduction and formation of β-$FeMoO_4$ with an overall bulk Mo/Fe ratio of 1.28 after TOS = 250 h. STEM line scan showed iron rich surface regions and XPS shows a Mo/Fe ratio of 0.66, which indicate further Mo loss at the surface region. The lower Mo content at the surface region compared to the bulk indicates that Mo from the bulk phase ($Fe_2(MoO_4)_3$) segregates to the surface, where it evaporates, leaving $FeMoO_4$ and Fe_2O_3 as an outer layer of the crystals. The tendency of Mo segregation to the surface is also reported elsewhere in the literature [31,38].

House et al. [34] studied the effect of varying the Mo/Fe ratio in the iron molybdate/molybdenum oxide catalyst system. Figure 2.8 shows some of the presented data with respect to conversion (Figure 2.8 (a)) and selectivity (Figure 2.8 (b)) at 190 °C, both as function of the catalyst Mo content. It can be seen that for the catalyst with very low Mo content (Mo/Fe = 0.02) the conversion is approximately half compared to the stoichiometric catalyst (Mo/Fe = 1.5). The conversion over Fe_2O_3 was app. 0 % at this temperature. The low activity of pure Fe_2O_3 is also reported elsewhere [30]. For the catalysts with low Mo contents (Mo/Fe = 0.2 and 0.5) the conversion is close to twofold higher than the stoichiometric catalyst. It should be mentioned that the change in activity is likely a surface area effect as the iron-rich catalysts have close to one order of magnitude larger sur-

face areas than the stoichiometric catalyst. SEM images in the current work show that iron molybdate crumbles, which most likely will increase the surface area of the catalyst sample. Due to the small sample size it has not been possible to verify this by e.g. N_2 adsorption using the Brunauer-Emmett-Teller (BET) theory.

Furthermore, it can be seen that for catalysts with a Mo/Fe ratio ≥0.5 that the combined formaldehyde and DME selectivity is above 90 % at conversion levels between 20-25 %. However, at increased conversion (40–50 %) the selectivity significantly decreases as function of decreasing Mo content in the catalysts indicating that the iron-rich catalysts are active in oxidizing formaldehyde to CO and CO_2. When comparing the data presented by House et al. [34] with the current work it should be mentioned that the temperatures are approximately 200 °C higher in the current work. At elevated temperature the oxidation of methanol and formaldehyde could potentially form CO and CO_2. However, this is not the case for the current work, possibly due to low coverage of formaldehyde at the higher temperature, and the two sets of data are reasonably comparable.

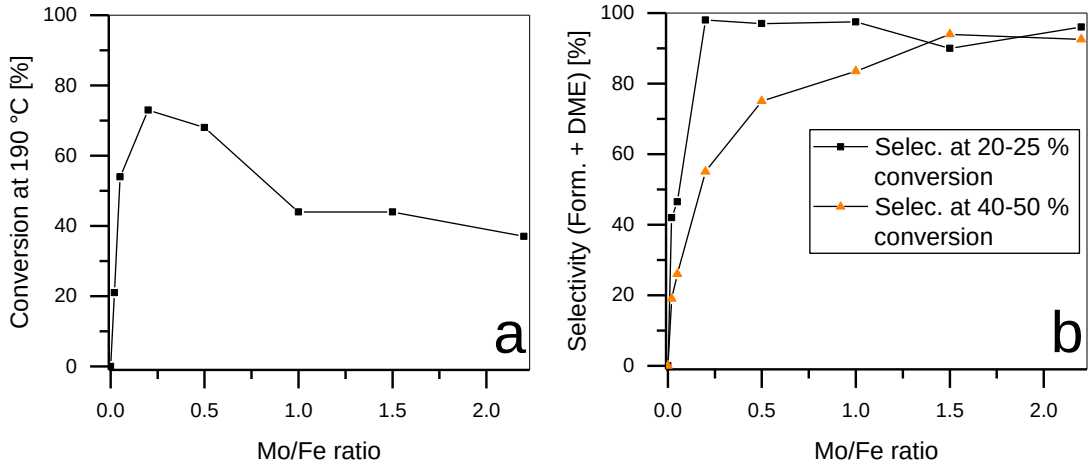

Figure 2.8 – Left: Conversion of 1 µL of methanol pulses as function of Mo content. Catalyst surface area for increasing Mo content: 16.8, 34.0, 65.6, 55.4, 38.7, 7.8 and 6.7 m^2/g.
Right: Combined formaldehyde and DME selectivity as function of Mo content (the temperature for selectivity at 20-25 % conversion is 160–200 °C and for selectivity at 40-50 % conversion is 175–215 °C). Data adapted from House et al. [34].

2.4.3 TOS = 250 – 600 h

For the sample after TOS = 600 h XRD shows the presence of $Fe_2(MoO_4)_3$, $FeMoO_4$, Fe_2O_3 and β-MoO_3 with an overall Mo/Fe ratio of 0.49, which indicates a significant loss of Mo. STEM line scans of the surface regions shows no Mo on the Fe_2O_3 crystals and an iron rich surface region for the iron molybdate crystals compared to the bulk. XPS shows a Mo/Fe ratio of 0.44, which indicates further segregation and volatilization of Mo. After 400 h on stream the activity of the catalyst starts to decrease slowly, which is probably due to formation of the less active Fe_2O_3. Furthermore, the selectivity slowly decreases, due to formation of significant amounts of iron rich surfaces. The newly formed Fe_2O_3 is selective towards CO_2. However, since Fe_2O_3 is also significantly less active the overall selectivity of the catalyst remains high, and the combined formaldehyde and DME selectivity after 600 h on stream is 97 % with the remainder being CO and CO_2. This shows that even small

amounts of molybdenum present at the catalyst surface yield a rather selective catalyst. This has also been reported elsewhere in the literature [31,35].

To the authors knowledge the formation of β-MoO_3 in the iron molybdate system under reaction conditions has not been observed elsewhere in the literature. Since no excess MoO_3 is observed after TOS = 10 h, the Mo in the formed β-MoO_3 must originate from the iron molybdate. The formation is only observed after significant Mo depletion of the iron molybdate, which might indicate that the Mo originates from the reduced phase ($FeMoO_4$) as follows (2.9):

$$FeMoO_4 + \tfrac{1}{4}O_2 \rightarrow \tfrac{1}{2}Fe_2O_3 + \beta\text{-}MoO_3 \qquad (2.9)$$

Pham et al. [39] synthesized β-MoO_3 and studied its catalytic performance compared to the thermodynamically stable α-MoO_3 under reaction conditions (6.2 % MeOH in air, W/F = 15 g_{cat} h mol^{-1}_{MeOH}) in a fixed bed reactor. They concluded that the synthesized β-MoO_3 transforms to α-MoO_3 at 350 °C. This is below the catalyst temperature in the present study, which means that the β-MoO_3 observed in this study should have quickly transformed to α-MoO_3. However, in the experiment reported by Pham et al. [39] methanol is fully converted and due to the exothermic reaction the catalyst bed might be subject to a hot spot and the actual temperature where β-MoO_3 transformed could thus be higher. Furthermore, the prepared β-MoO_3 was calcined at 350 °C as part of the synthesis procedure without transforming to the α-MoO_3. The transition temperature from β to α-MoO_3 is moreover reported in the literature with high variation from 387 °C [40] to 450 °C [41]. The data in the current work show that β-MoO_3 must be rather stable at the reaction conditions, since it does not evaporate after TOS = 600 h.

In the present work the degradation of catalyst particles in the sieve fractions 150-250 µm were shown to maintain high formaldehyde selectivity (> 97%) even at significant degradation and loss of Mo. However, this is observed at moderate conversion levels where the oxidation of formaldehyde to CO/CO_2 is limited by the short residence time in the bed. At total conversion of MeOH the further oxidation of formaldehyde would most likely be more intensive yielding lower selectivity. Brookes et al. [31] did likewise observe decreasing selectivity at increasing MeOH conversion.

When comparing the present work with the industrial process it must be taken into account that MeOH is converted to formaldehyde within a much larger catalyst pellet. MeOH is converted through the pellet and it must be expected that the degradation at the pellet core is less significant. To compare the current work and other studies in the literature on smaller catalyst particles, a degradation study of an entire pellet would be of high interest and is ongoing in our laboratory.

2.5 Conclusion

In the present study an iron molybdate/molybdenum oxide catalyst (Mo/Fe = 2) was synthesized using hydrothermal synthesis followed by calcination (535 °C / 2 h). During operation (25 mg catalyst, feed flow = ~157.5 NmL/min, ~5 % MeOH, 10 % O_2 in N_2, temp. = 384-416 °C) the activity and compositional changes in the catalyst have been investigated by comprehensive characterization. All of the excess α-MoO_3 volatilized during the initial 10 h under reaction conditions and the surface of the iron molybdate crystals were subject to loss of Mo leading to iron rich surface species. The loss of MoO_3 in the initial 10 h resulted in a 50 % decrease in activity of the catalyst. The initial decrease in activity may be due to the decreasing amount of MoO_x on the catalyst surface as reported by Dias et al. [28]. While excess molybdenum oxide is present in the catalyst, it has a replenishing effect on the iron molybdate phase.

In the period following the initial volatilization of α-MoO_3, the iron molybdate phase is subject to leaching of Mo leading to iron rich phases ($FeMoO_4$ and Fe_2O_3). The selectivity only decreases slightly throughout the experiment (TOS = 600 h) even at significant loss of molybdenum. This is due to low catalytic activity of the less selective iron rich sites and probably some Mo enrichment of the catalyst surface. After 600 h the formation of β-MoO_3 was surprisingly observed, likely originating from the β-$FeMoO_4$ phase. The β-MoO_3 appears thermally stable and significantly less volatile compared to the thermodynamically stable α-MoO_3, since β-MoO_3 still remains in the catalyst at the end of the 600 h experiment.

This work is the first time the structural changes and catalytic performance of the iron molybdate catalyst has been studied at reaction conditions over a period long enough to achieve significant degradation, yielding insights to the structural changes and the corresponding catalytic performance.

2.6 References

[1] R. Günther, W. Disteldorf, A. O. Gamer, and A. Hilt, "Ullmann's encyclopedia of industrial chemistry," Weinheim, 2012.

[2] Merchant Research & Consulting ltd, "World Formaldehyde Production to Exceed 52 Mln Tonnes in 2017," 2016. [Online]. Available: https://mcgroup.co.uk/news/20140627/formaldehyde-production-exceed-52-mln-tonnes.html.

[3] S. K. Bhattacharyya and K. Janakiram, "Kinetics of the Vapor-Phase Oxidation of Methyl on Vanadium Pentoxide Catalyst," Distribution, vol. 136, pp. 128–136, 1967.

[4] E. Soderhjelm, M. P. House, N. Cruise, J. Holmberg, M. Bowker, J.-O. Bovin, and A. Andersson, "On the Synergy Effect in MoO3-Fe-2(MoO4)(3) Catalysts for Methanol Oxidation to Formaldehyde," Top. Catal., vol. 50, no. 1–4, pp. 145–155, 2008.

[5] G. Fagherazzi and N. Pernicone, "Structural Study of a Methanol Oxidation Catalyst," J. Catal., vol. 16, no. 3, pp. 321–325, 1970.

[6] M. Rellán-Piñeiro and N. López, "The Active Molybdenum Oxide Phase in the Methanol Oxidation to Formaldehyde (Formox Process): A DFT Study," ChemSusChem, vol. 8, no. 13, pp. 2231–2239, 2015.

[7] M. Carbucicchio and F. Trifiró, "Surface and Bulk Redox Processes in Iron-Molybdate-Based," J. Catal., vol. 85, pp. 77–85, 1976.

[8] G. Alessandrini, L. Cairati, P. Forzatti, P. L. Villa, and F. Trifiro, "Chemical, Structural and Catalytic Modifications of Pure and Doped Iron(III) Molybdate," J. Less Common Met., vol. 54, no. 2, pp. 373–386, 1977.

[9] A. P. V. Soares, M. F. Portela, A. Kiennemann, and L. Hilaire, "Mechanism of deactivation of iron-molybdate catalysts prepared by coprecipitation and sol – gel techniques in methanol to formaldehyde oxidation," Chem. Eng. Sci., vol. 58, no. 7, pp. 1315–1322, 2003.

[10] M. Bowker, R. Holroyd, A. Elliott, P. Morrall, A. Alouche, C. Entwistle, and A. Toerncrona, "The selective oxidation of methanol to formaldehyde on iron molybdate catalysts and on component oxides," Catal. Letters, vol. 83, no. 3–4, pp. 165–176, 2002.

[11] B. I. Popov, V. N. Bibin, and G. K. Boreskov, "Study of an iron-molybfate oxide catalyst for oxidation of methanol to formaldehyde," Kinet. Catal., vol. 17, no. 2, pp. 322–327, 1976.

[12] A. Andersson, M. Hernelind, and O. Augustsson, "A study of the ageing and deactivation phenomena occurring during operation of an iron molybdate catalyst in formaldehyde production," Catal. Today, vol. 112, pp. 40–44, 2006.

[13] Q. Xu, G. Jia, J. Zhang, Z. Feng, and C. Li, "Surface phase composition of iron molybdate catalysts studied by UV Raman spectroscopy," J. Phys. Chem. C, vol. 112, no. 25, pp. 9387–9393, 2008.

[14] N. Burriesci, F. Garbassi, M. Petrera, G. Petrini, and N. Pernicone, "Solid State Reactions in Fe-Mo Oxide Catalysts for Methanol Oxidation During Aging in Industrial Plants.," Stud. Surf. Sci. Catal., vol. 6, pp. 115–126, 1980.

[15] B. R. Yeo, G. J. F. Pudge, K. G. Bugler, A. V. Rushby, S. Kondrat, J. Bartley, S. Golunski, S. H. Taylor, E. Gibson, P. P. Wells, C. Brookes, M. Bowker, and G. J. Hutchings, "The surface of iron molybdate catalysts used for the selective oxidation of methanol," Surf. Sci., vol. 648, pp. 163–169, 2016.

[16] A. P. V. Soares, M. F. Portela, and A. Kiennemann, "Methanol Selective Oxidation to Formaldehyde over Iron-Molybdate Catalysts," Catal. Rev., vol. 47, no. 1, pp. 125–174, 2005.

[17] J. L. Figueiredo, Progress in catalyst deactivation. 1981.

[18] K. I. Ivanov and D. Y. Dimitrov, "Deactivation of an industrial iron-molybdate catalyst for methanol oxidation," Catal. Today, vol. 154, no. 3–4, pp. 250–255, 2010.

[19] A. P. V. Soares, M. F. Portela, A. Kiennemann, and J. M. M. Millet, "Iron-molybdate deactivation during methanol to formaldehyde oxidation: Effect of water," React. Kinet. Catal. Lett., vol. 75, no. 1, pp. 13–20, 2002.

[20] A. M. Beale, S. D. M. Jacques, E. Sacaliuc-Parvalescu, M. G. O'Brien, P. Barnes, and B. M. Weckhuysen, "An iron molybdate catalyst for methanol to formaldehyde conversion prepared by a hydrothermal method and its characterization," Appl. Catal. A Gen., vol. 363, no. 1–2, pp. 143–152, 2009.

[21] M. Høj, T. Kessler, P. Beato, A. D. Jensen, and J. D. Grunwaldt, "Structure, activity and kinetics of supported molybdenum oxide and mixed molybdenum-vanadium oxide catalysts prepared by flame spray pyrolysis for propane OHD," Appl. Catal. A Gen., vol. 472, pp. 29–38, 2014.

[22] M. E. Van Leeuwen, "Derivation of Stockmayer potential parameters," Fluid Phase Equilib., vol. 99, no. 99, pp. 1–18, 1994.

[23] L. S. Tee, S. Gotoh, and W. E. Stewart, "Molecular parameters for normal fluids," Industial Eng. Chemisrty -- Fundam., vol. 5, no. 3, pp. 356–363, 1966.

[24] F. M. Mourits and F. H. A. Rummens, "Critical evaluation of Lennard-Jones and Stockmayer potential parameters and of some correlation methods," Can. J. Chem. Can. Chim., vol. 55, no. 16, pp. 3007–3020, 1977.

[25] S. a R. K. Deshmukh, M. Van Sint Annaland, and J. a M. Kuipers, "Kinetics of the partial oxidation of methanol over a Fe-Mo catalyst," Appl. Catal. A Gen., vol. 289, no. 2, pp. 240–255, 2005.

[26] V. N. Bibin and B. I. Popov, "Kinetics of Methanol Oxidation by Air on Iron-Molybdenum Oxide Catalysts," Kinet. Catal. (Engl. Transl.), vol. 10, no. 6, pp. 1091–1098, 1969.

[27] A. A. Coelho, "TOPAS and TOPAS-Academic: an optimization program integrating computer algebra and crystallographic objects written in C++," J. Appl. Cryst., vol. 51, no. 1, pp. 210–218, 2018.

[28] A. P. S. Dias, F. Montemor, M. F. Portela, and A. Kiennemann, "The role of the su-prastoichiometric molybdenum during methanol to formaldehyde oxidation over Mo–Fe mixed oxides," J. Mol. Catal. A Chem., vol. 397, pp. 93–98, 2015.

[29] M. Bowker, C. Brookes, a. F. Carley, M. P. House, M. Kosif, G. Sankar, I. Wawata, P. P. Wells, and P. Yaseneva, "Evolution of active catalysts for the selective oxidative dehy-drogenation of methanol on Fe2O3 surface doped with Mo oxide," Phys. Chem. Chem. Phys., vol. 15, no. 29, p. 12056, 2013.

[30] Y. Huang, L. Cong, J. Yu, P. Eloy, and P. Ruiz, "The surface evolution of a catalyst jointly influenced by thermal spreading and solid-state reaction: A case study with an Fe2O3–MoO3 system," J. Mol. Catal. A Chem., vol. 302, no. 1–2, pp. 48–53, 2009.

[31] C. Brookes, P. P. Wells, G. Cibin, N. Dimitratos, W. Jones, D. J. Morgan, and M. Bowker, "Molybdenum Oxide on Fe 2 O 3 Core–Shell Catalysts: Probing the Nature of the Structural Motifs Responsible for Methanol Oxidation Catalysis," ACS Catal., vol. 4, pp. 243–250, 2014.

[32] M. G. O'Brien, A. M. Beale, S. D. M. Jacques, and B. M. Weckhuysen, "A Combined Multi-Technique In Situ Approach Used to Probe the Stability of Iron Molybdate Catalysts During Redox Cycling," Top. Catal., vol. 52, no. 10, pp. 1400–1409, 2009.

[33] J. B. Parise, E. M. McCarron, A. W. Sleight, and E. Prince, “Refinement of the Structure of Beta’-MoO₃,” Mater. Sci. Forum, vol. 27–28, pp. 85–88, 1988.

[34] M. P. House, A. F. Carley, R. Echeverria-Valda, and M. Bowker, “Effect of varying the cation ratio within iron molybdate catalysts for the selectivev oxidation of methanol,” J. Phys. Chem. C, vol. 112, no. 11, pp. 4333–4341, 2008.

[35] M. Bowker, R. Holroyd, M. House, R. Bracey, C. Bamroongwongdee, M. Shannon, and A. Carley, “The selective oxidation of methanol on iron molybdate catalysts,” Top. Catal., vol. 48, no. 1–4, pp. 158–165, 2008.

[36] R. Peláez, P. Marín, and S. Ordó, “Applied Catalysis A : General Synthesis of formaldehyde from dimethyl ether on alumina-supported molybdenum oxide catalyst,” Appl. Catal. A Gen., vol. 527, pp. 137–145, 2016.

[37] F. Trifiro’, V. De Vecchi, and I. Pasquon, “Nature of the Active Component in a Fe2O3-MoO3 Catalyst I. Study on the Catalyst Reduction and Oxidation*,” J. Catal., vol. 15, pp. 8–16, 1969.

[38] M. P. House, M. D. Shannon, and M. Bowker, “Surface segregation in iron molybdate catalysts,” Catal. Letters, vol. 122, no. 3–4, pp. 210–213, 2008.

[39] T. T. P. Pham, P. H. D. Nguyen, T. T. Vo, H. H. P. Nguyen, and C. L. Luu, “Facile method for synthesis of nanosized β – MoO 3 and their catalytic behavior for selective oxidation of methanol to formaldehyde,” Adv. Nat. Sci. Nanotechnol., vol. 6, no. 4, p. 45010, 2015.

[40] T. Mizushima, K. Fukushima, H. Ohkita, and N. Kakuta, “Synthesis of β-MoO3 through evaporation of HNO3-added molybdic acid solution and its catalytic performance in partial oxidation of methanol,” Appl. Catal. A Gen., vol. 326, no. 1, pp. 106–112, 2007.

[41] E. M. I. McCarron, “β-Mo03: a Metastable Analogue of W03,” J. Chem. Soc., Chem. Commun., vol. 101, pp. 336–338, 1986.

[42] J. S. Chung, R. Miranda, and C. O. Bennett, “Mechanism of Partial Oxidation of Methanol over MoO3,” J. Catal., vol. 114, pp. 398–410, 1988.

Chapter 3

Modeling of the Molybdenum Loss in Iron Molybdate Catalyst Pellets for Selective Oxidation of Methanol to Formaldehyde

Abstract

The loss of molybdenum from industrial iron molybdate ($Fe_2(MoO_4)_3$) catalyst pellets with an excess of molybdenum oxide was studied during selective oxidation of methanol to formaldehyde for up to about 10 days on stream at varying reaction conditions (MeOH = 1.6-4.5 %, O_2 = 2.5-10 %, H_2O = 0-10.2 vol.% in N_2 and temperature = 250, 300 and 350 °C). The changing morphology and the local elemental composition in the pellets were followed for increasing time on stream. Molybdenum was shown to volatilize, leaving a depleted zone starting at the pellet surface and moving inwards with time. For temperatures ≤ 300 °C only volatilization of the excess MoO_3 phase was observed. Increasing concentration of MeOH and temperature enhanced the rate of volatilization, the oxygen concentration had negligible effect, while increasing the H_2O concentration decreased the volatilization rate. At 350 °C (MeOH = 4.5 %, O_2 = 10 %, H_2O = 0 % in N_2) Mo in the $Fe_2(MoO_4)_3$ phase was furthermore volatilized leading to the formation of the reduced ferrous molybdate ($FeMoO_4$). A dynamic 1D mathematical model for a single pellet, in which methanol oxidation to formaldehyde and simultaneous volatilization of free MoO_3 takes place, was developed. The model parameters were fitted using experimental data of the pellet weight loss while the evolution of the MoO_3 depletion layer thickness was used to validate the model. The model describes the data well and additionally predicts that deposition of MoO_3 behind the depletion layer front occurs under certain conditions, leading to a MoO_3 deposition layer, which was verified by scanning electron microscopy (SEM) combined with energy-dispersive X-ray spectroscopy (EDS). Simulations with the model show that the overall loss of molybdenum is significantly slower for large pellets compared to small pellets, which is a key parameter for the success of the industrial process.

3.1 Introduction

Formaldehyde (CH_2O) is synthesized industrially by selective oxidation of methanol over an iron molybdate catalyst with excess molybdenum oxide according to (3.1) [1]:

$$CH_3OH + ½O_2 \rightarrow CH_2O + H_2O \quad \Delta H = -156 \text{ kJ/mol} \tag{3.1}$$

The reaction is carried out in a multitubular reactor (tube length = 1 to 2 m) with stoichiometric excess of oxygen (MeOH ≈ 8-10 %, H_2O = 4-8 %, O_2 ≈ 10 % in N_2) at near atmospheric pressure with complete methanol conversion in a single pass giving a formaldehyde yield around 88-92 %, known as the Formox process [2]. The feed gas is introduced to the catalytic bed at 200-250 °C and due to the exothermic reaction a hotspot of 350-400 °C is formed in the reactor [3].

Molybdenum forms volatile species with methanol under the reaction conditions, which can deplete the catalyst pellets of Mo and leave behind molybdenum poor zones in the catalyst bed [4,5]. The Mo depleted zones become rich in iron oxide sites, which are less selective towards formaldehyde, forming more CO and potentially CO_2 [6-10]. To counter the loss of Mo, excess MoO_3 is added to the commercial catalyst, thus containing $Fe_2(MoO_4)_3$ and MoO_3 as two distinct crystalline phases [7].

In the industrial reactor the volatilization of Mo occurs mainly in the initial part of the reactor, while the volatile Mo species decompose downstream in the reactor after the hotspot. The decomposed volatile Mo species deposits as needle like crystals in the void space between the catalyst pellets [3-11], which blocks the reactor and leads to increased pressure drop.

Ivanov and Dimitrov [12] performed experiments on single, industrial like reactor tubes for 15 months in the temperature range 200-340 °C (MeOH = 6.2 %, O_2 = 11 % in N_2). Their data show that the catalyst pellets placed ¼ into the bed (temperature = 225-245 °C) were subjected to loss of Mo from the pellet surface. However, the pellet core was not affected. Furthermore, at high temperatures (> 300 °C), they observed a reddish-brown coloration of the pellet surface due to formation of $FeMoO_4$ and Fe_2O_3. Formation of $FeMoO_4$ and Fe_2O_3 is also observed elsewhere [3,13-17].

Anderson et al. [5] studied catalyst pellets extracted from an industrial plant after half and full lifetime and likewise observed the formation of $FeMoO_4$ and Fe_2O_3. Furthermore, they quantified the amount of Mo in the catalyst pellets throughout the bed. After half and full process lifetime approximately the first ¼ and ⅓ of the catalyst bed was depleted for Mo, respectively. Moreover, it was observed that Mo depleted pellets were subject to increased pore volume and decreased activity. The deposition of Mo downstream in the reactor predominantly occurred in the void space between the pellets after the hotspot, which is also observed elsewhere [3].

The Mo transport and downstream deposition leads to increased pressure drop over the reactor, which is one main reason for the rather short lifetime of only 1-2 years, after which the catalyst load must be replaced [5]. Another reason for replacement of the catalyst is loss of selectivity, which is also related to Mo depletion [14].

Popov et al. [4] studied the Mo volatilization from an iron molybdate catalyst under varying reaction conditions. They concluded that the rate of volatilization is mainly affected by

the methanol concentration and suggested the formation of the volatile compounds $MoO_2(OCH_3)_2$, $MoO_2(OH)(OCH_3)$, $MoO_2(OCH_3)$ and $MoO_2(OH)$. They observed that the volatile Mo species condensed as a blue film on the reactor tube inner surface at the reactor outlet. Smith et al. [18] observed likewise a blue Mo-rich film during their experiments with single MoO_3 crystals under continuous flow of a MeOH-air mixture. Using XRD they concluded that the film layer consisted of $Mo_2O_5(OCH_3)_2$ and suggested two pathways for its formation. In the first pathway MeOH forms surface methoxy and hydroxyl groups upon adsorption on the MoO_3 surface and a molybdenum oxide hydroxide molecule desorbs into the gas phase. The desorbed molecule then reacts with methanol in the gas phase forming $Mo_2O_5(OCH_3)_2$. In the second pathway surface molybdenum methoxides desorb directly as the observed molybdenum oxide-methoxide. The authors suggested that the second pathway was the most plausible [18] and this was also suggested by Ivanov and Dimitrov [12] and follows:

$$2MoO_2 + 2MeOH \rightarrow Mo_2O_5(OCH_3)_2 + H_2O \tag{3.2}$$

The volatilization of Mo and deposition downstream in the reactor leading to pressure drop buildup is a major unsolved issue of the iron molybdate catalysts. In our laboratories the volatilization has been studied at well-defined conditions for small catalyst particles (150-250 μm) [17], revealing that all excess MoO_3 volatilizes rapidly (TOS ≈ 10 h, MeOH = ~5 %, O_2 = 10 % in N_2 at catalyst temp = 384-398 °C) which is much faster than observed in industry. The results thus indicate that the rate of volatilization is strongly dependent on the catalyst particle size. In this work, the rate of volatilization of Mo from industrial catalyst pellets has been studied as a function of well-defined operating conditions and a single pellet model that take the relevant phenomena into account has, for the first time, been developed.

3.2 Experimental

3.2.1 Single pellet Mo loss measurements

The industrial iron molybdate catalyst pellets had a molar ratio of Mo to Fe of 2.4. The pellets were shaped as a cylinder with a hole in the middle (OD = 4.55 mm, hole diameter = 1.70 mm and length = 4.00 mm). A pellet was slid onto a thermocouple (OD = 1.5 mm) and centered in a tubular flow reactor (ID = 6.5 mm). A photo of the reactor and pellet can be seen in Figure B.1. Three identical reactors were placed in a three zone electrically heated furnace and operated in parallel containing one pellet each. The feed gas was equally distributed between the reactors using rotameters and needle valves. The feed gas composition was varied in the individual experiments between 1.6-4.5 vol.% MeOH, 2.5-10 vol.% O_2 and 0-10.2 vol.% H_2O in N_2, and was introduced at a total flowrate of 9 L/min (3 L/min per reactor, 1 bar, 273.15 K). N_2 and O_2 were introduced by mass flow controllers (Bronkhorst). Before entering the three reactors, a fraction of the gas was bubbled through two flasks in parallel containing MeOH (≥ 99.9%, Sigma-Aldrich) and demineralized water respectively (0.5-1.1 L/min for MeOH and 0-1 L/min for H_2O). The gas was saturated by MeOH and H_2O respectively and the concentrations were controlled by heating the bubble-flasks (45 °C for MeOH and 72-80 °C for H_2O). The two saturated gas flows were mixed with the remaining gas to a single feed of the desired composition before en-

tering the reactors. The respective thermocouples were placed through the pellets hole measuring the gas temperature just before the pellet (250 ±3, 300 ±3 and 350 ±3 °C). The mass of the pellets was measured before and after the experiments. To ensure precise measurements, the pellets were initially dried at 120 °C and heat-treated at 420 °C after the experiments to ensure full oxidation of the catalyst [19].

3.2.2 Scanning electron microscopy

The Mo depleted catalyst pellets were cast in epoxy polymer and cut through the middle along the radial axis to reveal the cross sectional area of the pellet. The samples were coated with an electron conductive layer of carbon prior to investigation. Scanning Electron Microscopy (SEM) images were acquired in an Environmental SEM, FEI XL30 FEG, at 15 kV using the backscattered electron signal. EDS analyses were acquired in the electron microscope without standards at 15 kV with an EDAX liquid Nitrogen cooled Si(Li) detector and a liquid Nitrogen free Thermo Silicon Drift Detector (SDD).

3.2.3 X-ray micro computed tomography

X-ray tomograms were obtained using a ZEISS XRadia 410 Versa instrument. The instrument was operated at 140 kV and 10 W using the high energy 2 (HE2) filter and a 4X objective. For measurements of the whole sample 1601 projections with 5 sec exposure time were used, which resulted in a total measurement time of 3:02 h:min. A pixel size of 4.6 µm was obtained using a 2x2 binning. Image reconstruction was performed using the built-in acquisition and reconstruction software package provided by ZEISS.

Visualization, image analysis and phase segmentation were performed using the commercial software Avizo 9.5.0 (FEI). The following procedure was used: Initially the reconstructed volume of the whole catalyst was filtered using a nonlocal means filter which was applied on the individual xy planes with a search window of 21 pixels, a local neighborhood of 5 pixels, a similarity value 0.6 and using an adaptive choice of lambda. The pellet was segmented using the magic wand tool and characterizing the different phases by the following grey scale intensity values (outer air = 0-13658, depleted phase = 13659-27152 and non-depleted phase = 27153-65535). Both phases contained some holes which were not included in the segmentation. In order to fill these non-assigned holes in the volume, the interactive watershed tool provided by the segmentation editor was used. It uses a gradient magnitude image calculated by a quick Canny method, which controls the expansion of the markers used for the watershed expansion. After this step the depleted and non-depleted phases were segmented and the materials statistics module was applied to obtain the volumetric information of the two phases.

3.3 Results and discussion

3.3.1 SEM images

The scanning electron microscopy (SEM) images of the pellets cross section coupled with energy-dispersive X-ray spectroscopy (EDS) showed the depletion of Mo with increasing time on stream. In Figure 3.1 some characteristic samples are shown and more samples are shown in the supporting information (Figures B.2 –B.7).

For the fresh pellet (Figure 3.1 (a)) a mainly light grey (Mo/Fe = 2.4 atomic ratio) appearance throughout the pellet was observed with some smaller Mo rich inclusions (white) and voids (black)(Figure B.2). For an exposed pellet (Figure 3.1 (b)) (Conditions: 4.4 % MeOH, 0 % H_2O, 10 % O_2 in N_2, 350 °C and time on stream (TOS) = 70 h) a Mo depleted, dark grey layer at the pellet surface was observed. EDS area scans at the surface region (Figure 3.2) revealed that the depleted layer had an atomic ratio of approximately Mo/Fe = 1.5, corresponding to pure $Fe_2(MoO_4)_3$. In the interior of the pellet the composition was unchanged with a Mo/Fe ratio of 2.4. For pellets exposed to 350 °C a zone with increased Mo (Mo/Fe = 2.8) compared to the fresh pellet was observed behind the depleted layer towards the center (Figure 3.2 (c)). For the pellets exposed to 350 °C and TOS ≥ 160 h (Figure 3.3), the composition in the depleted layer was approximately Mo/Fe = 1, which indicates that the initial $Fe_2(MoO_4)_3$ was reduced to the less Mo rich $FeMoO_4$ phase. Reduction of $Fe_2(MoO_4)_3$ and formation of $FeMoO_4$ is also observed elsewhere in the literature [17,20].

Water in the feed gas (10 %) slowed down the development of the depletion layer, and Mo deposition inside the pellet was not observed at ~350 °C (Figure 3.4).

For the depleted pellet treated with low oxygen concentration (Figure 3.5)(Conditions: 3.5 % MeOH, 0 % H_2O, 2.5 % O_2 in N_2, 300 °C and TOS = 288 h) white inclusions at the pellet surface region were observed, and shown by EDS to be Mo rich particles (Figure B.7). The Mo inclusions were present both in the depletion layer and further into the pellet. No inclusions were present in the first ~100 µm from the pellet surface. Volatilization of Mo has been observed to increase at lower oxygen concentration in the literature [4]. However, in this study the oxygen concentration in the feed gas was shown to have no effect on the overall mass loss of the pellet (Figure B.12). To the authors knowledge the formation of Mo inclusions at low oxygen concentration (2.5 % O_2) has not be observed elsewhere in the literature, and is not fully understood.

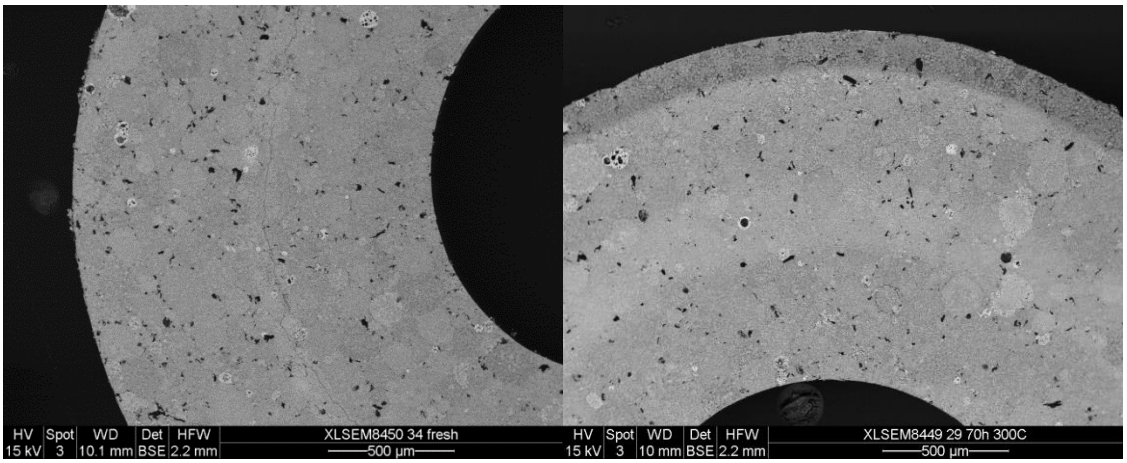

Figure 3.1 – SEM images of the cross section of fresh (a) and depleted (b) pellets (Conditions: 4.5 % MeOH, 0 % H_2O, 10 % O_2 in N_2, 300 °C and TOS = 71 h). Light grey indicates Mo rich areas, dark grey indicates Mo depleted areas and white indicate Mo rich inclusions.

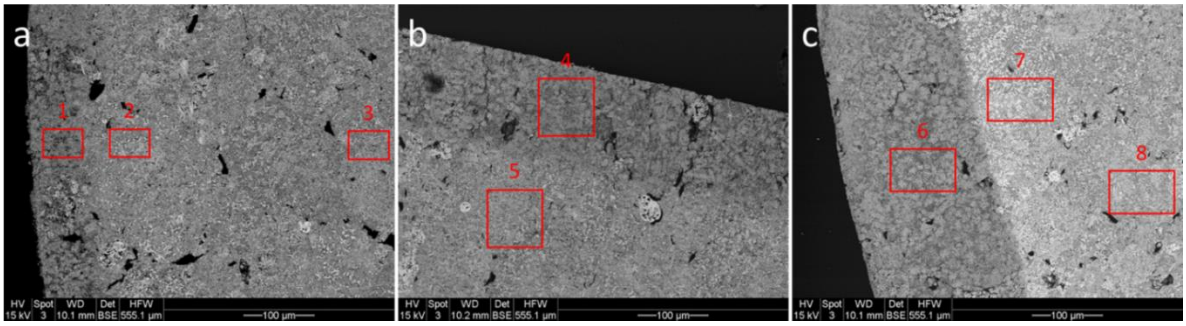

Figure 3.2 – SEM images of the cross sectional surface regions of depleted pellets treated at (a) 250 °C, (b) 300 °C and (c) 350 °C. TOS = 71-78 h, 4.4-4.5 % MeOH, 0 % H_2O, 10 % O_2 in N_2. Mo/Fe: area 1 = 1.6, area 2 = 2.5, area 3 = 2.4, area 4 = 1.5, area 5 = 2.4, area 6 = 1.6, area 7 = 2.8 and area 8 = 2.5.

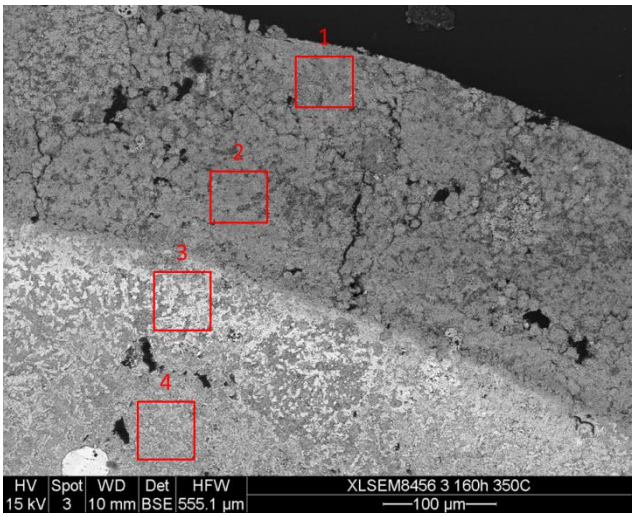

Figure 3.3 - SEM image of the cross sectional surface region of a depleted pellet treated at 350 °C for 160 h (Conditions: 4.4 % MeOH, 0 % H_2O, 10 % O_2 in N_2). Mo/Fe: area 1 = 1.1, area 2 = 1.2, area 3 = 3.0 and area 4 = 2.5.

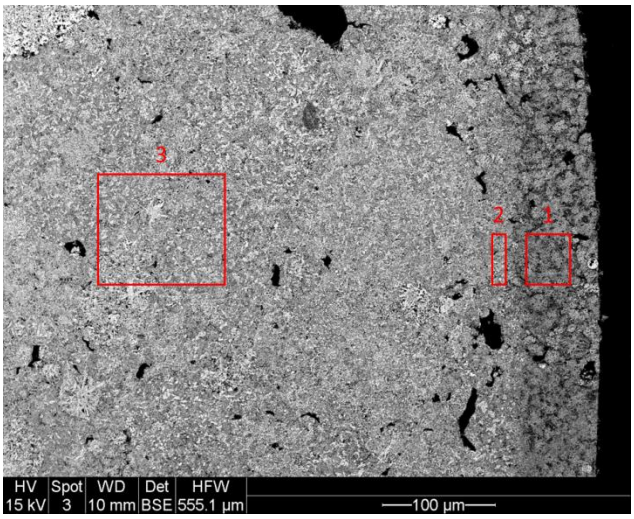

Figure 3.4 – SEM image of the cross sectional surface region in a depleted pellet treated at 350 °C for 73 h with water added to the gas phase (Conditions: 4.2 % MeOH, 9.3 % H_2O, 10 % O_2 in N_2). Mo/Fe: area 1 = 1.7, area 2 = 2.2 and area 3 = 2.5.

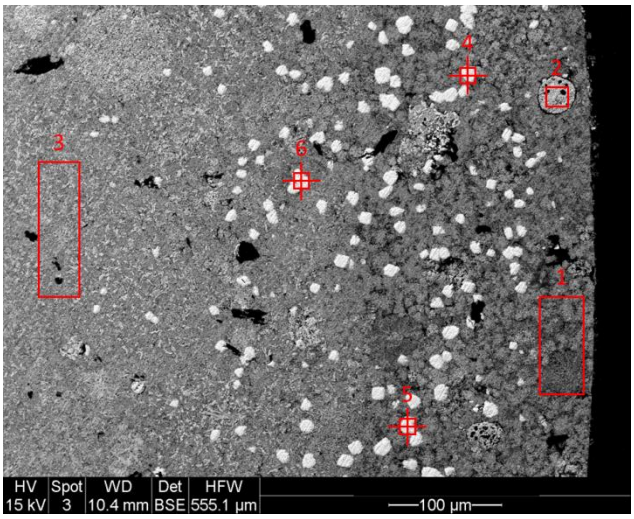

Figure 3.5 - SEM image of the cross sectional surface region in a depleted pellet treated at 300 °C for 288 h with low oxygen concentration (Conditions: 3.50 % MeOH, 0 % H_2O, 2.5 % O_2 in N_2). Mo/Fe: area 1 = 1.7, area 2 = 1.6, area 3 = 2.5, area 4 = 12.6, area 5 = 8.0 and area 6 = 5.1.

It is widely observed in the literature that Mo in the iron molybdate catalyst can form volatile species with MeOH and be transported away from the catalyst [2, 3, 7], which was also observed in the current work as blue molybdenum deposits at the reactor outlet. The SEM images combined with EDS of the depleted pellets show that the excess MoO_3 present in the catalyst forms volatile Mo species which diffuse through the pellet. At the pellet surface the Mo species leave the pellet and enter the bulk gas phase and is carried out of the reactor. The depletion layer has a rather sharp front, which indicates that the volatilization reaction is equilibrium limited and that the equilibrium is established at the front. The volatile Mo species formed at the front will also diffuse into the pellet. At ~350 °C deposition of excess Mo inside the pellet is observed. As the temperature increases the MeOH concentration through the pellet is decreasing faster due to the higher rate of reaction. The volatile Mo species likely decomposes inside the pellet pores as the MeOH concentration decreases towards the pellet center due to the equilibrium between MeOH and the Mo species according to reaction (3.2). The formation of $FeMoO_4$ is only observed at 350 °C, which indicates that $Fe_2(MoO_4)_3$ is significantly more stable than MoO_3 and that volatilization of Mo only occurs from the MoO_3 phase at moderate temperatures (≤ 300 °C) under the applied reaction conditions.

3.3.2 Mass loss of excess MoO_3 at increased TOS

As the pellets underwent Mo depletion they were likewise subject to a corresponding mass loss with increasing time on stream. Figure 3.6-3.8 show the mass loss of the catalyst pellets at increasing TOS at varying temperature, MeOH and water concentrations. The mass loss is converted to the corresponding loss of the excess MoO_3 phase assuming that only this phase forms volatile Mo species.

All applied reaction conditions showed the same trend in the mass loss rate with increasing TOS. Initially the mass loss was fast, due to the high MeOH concentration at the pellet surface, which quickly volatilizes the excess MoO_3 present there, according to (3.2). After 10-20 h on stream the rate decreases, due to the effect of decreased MeOH concentration

at the developed depletion layer front and diffusion limitations of the formed Mo species out of the pellet. These inhibiting effects increasingly slowed down the rate of depletion with time on stream.

3.3.2.1 Effect of MeOH

The MeOH concentration strongly affects the mass loss rate of the catalyst pellet (Figure 3.6). As discussed in the introduction similar results have been observed for Mo volatilization in the literature [4,18].

3.3.2.2 Effect of temperature

The volatilization rate of solid MoO_3 in the catalyst with MeOH (3.2) increases with increasing temperature (Figure 3.7). However, the rate of reaction for MeOH to formaldehyde will likewise increase, which counteract the rate of volatilization due to the decreasing MeOH concentration inside the pellet. Furthermore, the rate of diffusion of the gaseous species out of the pellet will also increase at increasing temperature. The overall loss of Mo from the pellet is affected by all these contributions and the net effect is an increased rate of Mo loss from the pellets with increasing temperature at the applied reaction conditions (MeOH = ~ 4.4 %, H_2O = 0 %, O_2 = 10 % in N_2).

3.3.2.3 Effect of H_2O

An increased H_2O concentration decreases the mass loss rate, which indicates that H_2O inhibits the volatilization reaction (3.2) (Figure 3.8). H_2O is likewise known to inhibit the oxidation of MeOH (3.1) [21], which will increase the MeOH concentration through the pellet and an increased volatilization rate might be expected. However, the mass loss measurements show this is not the case and that H_2O overall inhibits the mass loss of the pellet. This indicates that the volatile Mo species are formed during the catalytic cycle, likely as a low concentration side product.

3.3.2.4 Effect of oxygen

Varying the oxygen concentration (2.5-10 % O_2, ~2 % MeOH, 0 % H_2O in N_2) had no effect on the mass loss rate of the catalyst pellet (Figure B.3). Mo-rich inclusions are observed with SEM at an O_2 concentration of 2.5 % (Figure 3.5), indicating that Mo is mobilized but retained in the catalyst pellet as Mo-rich inclusions.

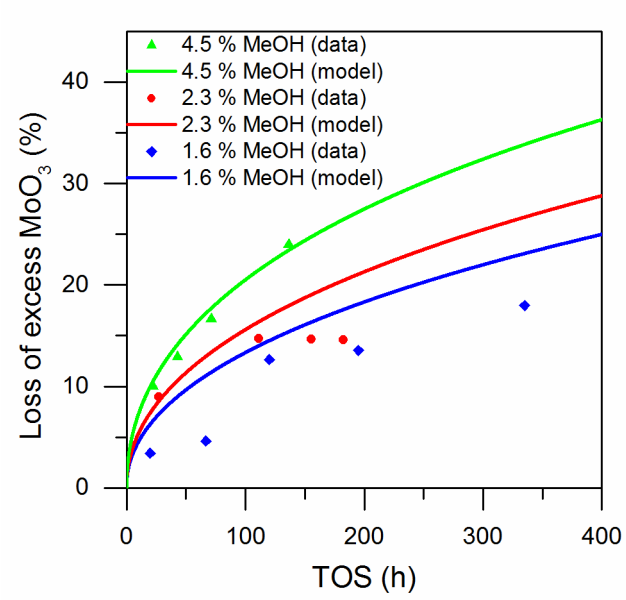

Figure 3.6 – Influence of MeOH concentration on the overall loss of excess MoO_3 in the pellets as a function of TOS. Treated at MeOH = 1.6-4.5 %, H_2O = 0 %, O_2 = 10 % in N_2 at 300 °C. Mo/Fe = 2.4. Flow rate = 3000 mL/min (1 bar, 273.15 K).

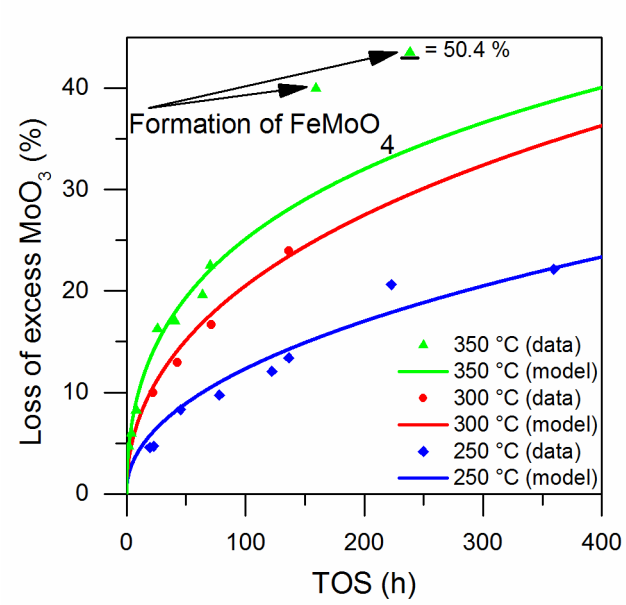

Figure 3.7 – Influence of temperature on the overall loss of excess MoO_3 in the pellets as function of TOS. Treated at MeOH = 4.4-4.5 %, H_2O = 0 %, O_2 = 10 % in N_2 at 250-350°C. Mo/Fe = 2.4. Flow rate = 3000 mL/min (1 bar, 273.15 K). Data point at 350 °C and TOS = 238 h is equal to 50.4 % loss of excess MoO_3.

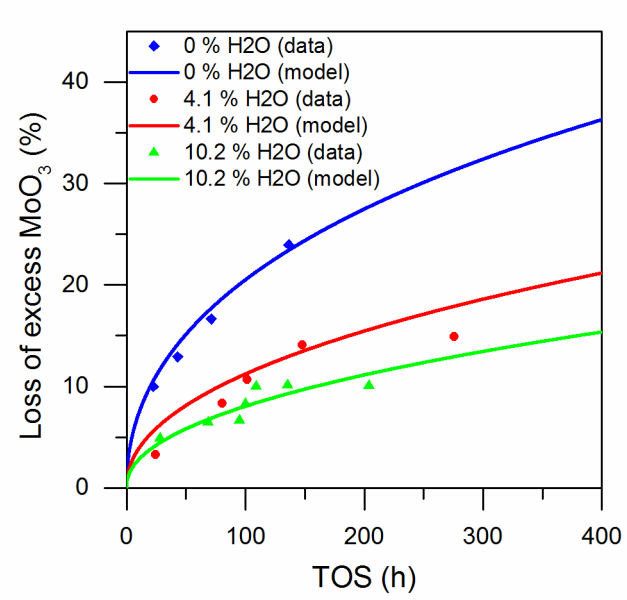

Figure 3.8 – Influence of water concentration on the overall loss of excess MoO_3 in the pellets as function of TOS. Treated at MeOH = 4.0-4.5 %, H_2O= 0-10.2 %, O_2 = 10 % in N_2 at 300 °C. Mo/Fe = 2.4. Flow rate = 3000 mL/min (1 bar, 273.15 K).

3.3.3 X-ray micro computed tomography

For non-destructive information on a whole catalyst pellet and complementary insights to SEM cross section images, X-ray micro computed tomography (µ-CT) was conducted on a depleted pellet (Figure 3.9) after 64 h on stream at 350 °C , MeOH = 4.4 %, H_2O = 0 % O_2 = 10 % in N_2. This technique revealed the MoO_3 depletion development throughout the entire pellet. Figure 3.9 shows an image of the entire axial cross section of the depleted pellet. The depletion layer has evolved evenly from the outer surface of the pellet and from the top surface facing towards the reactor inlet. Only a slight depletion has evolved from the inner surface and from the bottom surface facing away from the reactor inlet. During exposure the inner hole of the pellet was blocked by a thermocouple and the downstream end of the pellet was facing a spacer centering the pellet in the reactor (see Figure B.1). The blocking of the inner and end surface lead to only slight depletion from these surfaces. Segmentation of the depleted and non-depleted areas of the pellet showed that 20.3 vol.% (10.8 of 53.1 mm^3) of the entire pellet were subject to depletion, corresponding to a mass loss of 6.19 % at Mo/Fe = 2.4. The measured mass loss is however slightly lower (5.97 %), since some of the volatilized MoO_3 have moved inside the pellet. The depletion layer thickness in the radial direction was measured to approximately 110 µm.

Images of the cross-section in the radial plane through the pellet (Figure B.8) and a movie showing the depletion through the entire pellet can be seen in Appendix B.

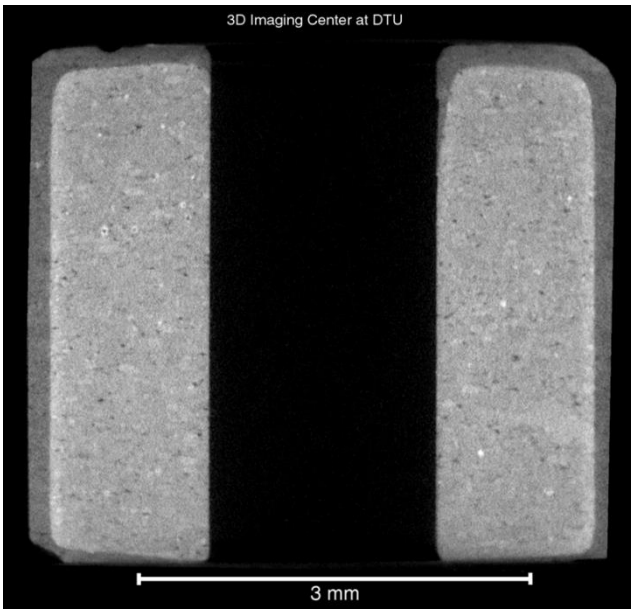

Figure 3.9 – X-ray micro computed tomography image of the entire axial cross section in a depleted pellet (Conditions: 4.4 % MeOH, 0 % H_2O, 10 % O_2 in N_2, 350 °C and TOS = 64 h). Dark grey indicates the less X-ray absorbing depleted layer and light grey indicates a higher absorbing non-depleted material, while white indicates areas of strong absorption due to Mo deposition.

3.4 Model

In this section, the single catalyst pellet model is derived describing the concentration profiles of MeOH, H_2O, solid MoO_3 and volatile Mo-species. Methanol diffuses from the bulk gas phase into the pellet at the surface, where it is primarily oxidized to formaldehyde and water, which diffuses out of the pellet. Furthermore, methanol and solid MoO_3 in the catalyst react to form the volatile Mo-species. The volatile Mo-species can either diffuse inwards or outwards the pellet or it can decompose and depositing solid MoO_3. The volatile Mo-species enters the bulk gas phase at the pellet surface. There is no diffusion of solid MoO_3, however it is removed during volatilization.

The industrial catalyst pellets are cylindrical with a hole in the middle. During experiments the pellets were placed on a thermocouple blocking the hole. Only small amounts of Mo volatilization were observed from the inner surface and the end surface facing away from the reactor inlet (Figure 3.9). Figure 3.10 shows a schematic of the cylindrical cross section.

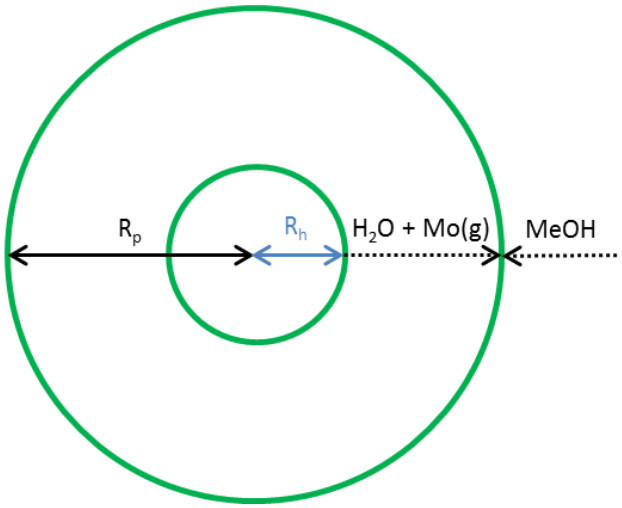

Figure 3.10 – Schematic of the catalyst pellet system with the cross sectional view of the cylindrical shape of the. The green lines are the pellet surface. The radius of the pellet is R_p and the radius of the hole in the pellet is R_h.

The following assumptions have been made during the derivation and solution of the single catalyst pellet model:

- The volatilization reaction of MoO_3 with MeOH follows the reversible reaction: $MoO_3(s) + CH_3OH(g) \rightleftarrows Mo(g)$
- The volatile Mo species is $Mo_2O_5(OCH_3)_2$
- Mo in iron molybdate is not volatile.
- No film resistance at the pellet surface.

3.4.1 Concentration profiles

3.4.1.1 Species mass balances

The concentration profiles in the pellet can be calculated by setting up a shell mole balance over a small section of the pellet, taking the diffusion in and out of the element into account, and the respective formation and accumulation at the position (B.1). The diffusion can be calculated by Fick's first law of diffusion (B.2 where the diffusion coefficient in the pellet is dependent on the porosity (B.3). Due to the volatilization of Mo in the pellet the porosity is dependent on the time due to the changing concentration of solid Mo (B.4-B.5) at a given position. The balance is reduced (B.6-B.7) and becomes Equation (3.3) (Table 3.1), where r equal to zero is at the center of the cylindrical pellet, R_h is at the inner pellet surface and R_p is at the outer surface. With respect to solid Mo there is no diffusion and the diffusion coefficient is thus equal to zero.

3.4.1.2 Rate of formation

3.4.1.2.1 MeOH and H_2O

Bibin and Popov [22] studied the kinetics of selective oxidation of MeOH over iron molybdate catalysts (3.1) and suggested a rate expression (3.4), which takes the inhibition by water and MeOH into account. Water is formed during oxidation of MeOH to formaldehyde (3.5). The selective oxidation reaction is much faster than the volatilization of solid Mo in

the catalyst. Only the contribution from the oxidation of MeOH is taken into account with respect to the rate of reaction of MeOH and H_2O.

3.4.1.2.2 Solid and volatile Mo

MeOH and solid MoO_3 in the catalyst reversibly form a volatile gaseous Mo species . The obtained mass loss data at varying conditions and TOS, reveal that water inhibits the volatilization reaction of Mo. The reaction mechanism is not fully understood and several volatile Mo species have been proposed as discussed above, of which $Mo_2O_5(OCH_3)_2$ appears to be the most likely species [4,18]. The rate expression with respect to volatilization of Mo can be described in several ways. Two rate expressions have been tested in the model and fitted to the experimental data. The first expression was a power-law rate expression, with different orders in both the forward reaction between MeOH and solid MoO_3 and backward reaction between $Mo_2O_5(OCH_3)_2$ and H_2O (3.2). This expression was found to overestimate the deposition of Mo inside the pellet at zero H_2O bulk concentration. Both the reaction rates are fast and an equilibrium is approximately reached at the depletion front. However, for zero H_2O at the pellet surface, only the forward reaction will take place, leading to almost instantaneous volatilization of Mo at the pellet surface. According to that model the formed volatile Mo-species will then mistakenly diffuse inside the pellet and decompose where water is present due to the oxidation of MeOH. To better implement the inhibiting effect of water a Langmuir-Hinshelwood type expression is used for the forward reaction and only the concentration of the volatile Mo-species is taken into account for the backward rate. Due to the limited amount of data, a temperature dependency of the water inhibition is not included. The reversible volatilization rate expression with respect to gaseous Mo, Equation (3.6), and solid Mo, Equation (3.7), is shown in Table 3.1. a_{MoO_3} has the value of one when there is solid MoO_3 present and zero when there is not.

Table 3.1 – Equations for calculation of the concentration profiles in the pellet with respect to MeOH, H_2O, volatile Mo species and solid MoO_3. With respect to MoO_3 the diffusion (D^0_{e,MoO_3}) is zero.

Concentration profile	
$$\frac{D^0_{e,i}}{\varepsilon^0}\frac{\partial C_i}{\partial r}\frac{\partial \varepsilon(r)}{\partial r}+\frac{D^0_{e,i}}{\varepsilon^0}\frac{\partial^2 C_i}{\partial r^2}\varepsilon(r) + \frac{1}{r_{hole}+r}\frac{D^0_{e,i}}{\varepsilon^0}\frac{\partial C_i}{\partial r}\varepsilon(r)+r_i=\frac{\partial C_i}{\partial t}\varepsilon(r)$$	(3.3)
Reaction rate expressions	
$$r_{MeOH}=-\frac{k_{MeOH}C_{MeOH}}{1+k_1C_{MeOH}+k_2C_{H_2O}}\rho_{FeMo} \quad \left[\frac{\text{mol}}{m^3\cdot s}\right]$$	(3.4)
$$r_{H_2O}=\frac{k_{MeOH}C_{MeOH}}{1+k_1C_{MeOH}+k_2C_{H_2O}}\rho_{FeMo} \quad \left[\frac{\text{mol}}{m^3\cdot s}\right]$$	(3.5)
$$r_{Mo(g)}=\frac{k^+a_{MoO_3}C_{MeOH}^{n_{MeOH}}}{1+K_3C_{H_2O}}-k^-C_{Mo(g)}^{n_{Mo(g)}} \quad \left[\frac{\text{mol}}{m^3\cdot s}\right]$$	(3.6)
$$r_{MoO_3}=-\frac{k^+a_{MoO_3}C_{MeOH}^{n_{MeOH}}}{1+K_3C_{H_2O}}+k^-C_{Mo(g)}^{n_{Mo(g)}} \quad \left[\frac{\text{mol}}{m^3\cdot s}\right]$$	(3.7)
Boundary conditions	
$$C_i(t,R_P)=C_i^b$$	(3.8)
$$\frac{\partial C_i(t,R_h)}{\partial r}=0$$	(3.9)
Initial concentrations for MeOH, H_2O and Mo(g)	
$$C_i(\mathrm{t}=0,r)=0$$	(3.10)
Initial concentration for MoO_3	
$$C_i(\mathrm{t}=0,r)=C_i^0$$	(3.11)

3.4.2 Boundary and initial conditions

It is assumed that there is no gas film layer at the catalyst surface and thus the MeOH and H_2O concentrations are equal to the bulk concentrations. Furthermore, it is assumed that there is no gradient at the inner catalyst surface since it is blocked by the thermocouple on which the pellet is hanging. It is assumed that there is no initial concentration of gaseous species in the pellet. The boundary and initial conditions become equations (3.8-3.11) in Table 3.1.

3.4.3 Diffusivity

The effective diffusion coefficient of MeOH, $D^0_{e,MeOH}$ (m^2/s), at a given temperature, T is estimated by:

$$D^0_{e,MeOH} = K_1\left(\frac{T^{K_2}}{T^{K_2}_{Ref}}\right) \tag{3.12}$$

Where K_1 and K_2 are constants and T_{Ref} is a reference temperature.

The effective diffusion coefficient of the gaseous Mo-species ($Mo_2O_5(OCH_3)_2$) and water is estimated using Chapman-Enskog theory for diffusion, using the MeOH as reference species:

$$D^0_{e,i} = D^0_{e,MeOH}\frac{\sqrt{1/M_{gas}+1/M_i}}{\sqrt{1/M_{gas}+1/M_{MeOH}}} \tag{3.13}$$

Where $D^0_{e,i}$ is the effective diffusion coefficient (m^2/s) and M_i is the molar weight (g/mol) of component i. M_{MeOH} and M_{gas} is the molar weight of MeOH and the entire gas (g/mol) respectively.

3.4.4 Solution procedure

Before the system of equations was solved, it was made dimensionless (B.8-B.24). The partial differential equation system was transformed to ordinary differential equations by discretization in the pellet radial dimension using a central finite difference scheme and solved using the method of lines (MoL) with the build-in Matlab solver ODE15s.

The activity of the solid MoO_3 (a_{MoO_3} see equation (3.6-3.7)) is equal to 1 if there is solid MoO_3 present and 0 if all MoO_3 has volatilized. This step changes makes the system very stiff and difficult to solve numerically. To make the system less stiff the activity is replaced by the following expression (3.14):

$$a_{MoO_3} \approx \frac{K\ C_{MoO_3}}{1+K\ C_{MoO_3}} \quad \text{for} \quad K >> C_{MoO_3} \quad \text{and} \quad K >> 1 \tag{3.14}$$

While MoO_3 is present, the expression will be close to zero order behavior. However, when the concentration of MoO_3 approaches 0 the expression will change to first order behavior. By replacing the activity by this expression the system becomes less stiff.

3.4.4.1 Estimation of pellet mass loss

The model predicts the excess MoO_3 profile through the radial direction of the pellet. The profile is converted to the remaining excess MoO_3 in the pellet, by taking the cylindrical geometry of the radial plane into account as follows:

$$\text{Excess } MoO_{3,Radial} = \int_{R_h}^{R_p} C_{MoO_3}(r) \frac{r}{R_p^2 - R_h^2} dr \tag{3.15}$$

Where $Mo(r)$ is the predicted concentration of excess MoO_3 at the position r and R_p and R_h are the outer and inner radius respectively of the pellet.

Furthermore, for comparison of the model results with the experimental data, the depletion layer thickness at the top of the pellet was assumed to be equal to the thickness in the radial plane.

3.4.5 Fitting procedure

The model predicts the profiles through the catalyst pellet of the various species and the total loss of excess MoO_3 from the pellet. The total Mo loss can simply be converted to the corresponding mass loss. The model is fitted towards the measured mass loss data shown in Figure 3.6-Figure 3.8 indicating a good fit to the data. The parameters to be fitted in the model are the reaction orders, rate constants of the rate expressions (3.4-3.7) and the adsorption equilibrium constant (K_3) with respect to water (3.6-3.7). The rate constants are fitted to the mass loss data using the built-in MATLAB optimization tool fmincon. The reaction orders and the adsorption equilibrium constant are chosen to satisfy the dynamic behavior of the solid MoO_3 profile through the catalyst pellet. The rate constants with respect to the main reaction ($k_{MeOH}, k_1 \; and \; k_2$) were fitted to methanol conversion data not enclosed here. Popov et al. studied the volatilization of Mo from the iron molybdate catalyst [4], and reported a rate constant of Mo volatilization of 4.4×10^{-3} s^{-1} at low contact time (< 0.005 s). This value was fixed and used independent of temperature. The backward volatilization rates were fitted independently for the different temperatures towards the mass loss of the pellets. The fitted rate constants and the forward volatilization rate constant are shown in Table 3.2. Since the forward volatilization rate constant, k_+, is kept constant at all temperatures, the backward rate constant decreases with increasing temperature, yielding faster overall volatilization at increased temperature. The backward rate constant ,$k\_$, follows the Arrhenius equation (Figure B.10).

Table 3.2 – Fitted reaction orders and rate constants for the single pellet model (Table 3.1).

Rate constants		
$n_{MeOH} = 1.5$		(3.16)
$n_{Mo(g)} = 1$		(3.17)
$K_3 = 65$		(3.18)
$k_+ = 4.4 \cdot 10^{-3}$ [4]	$\left[s^{-1}\right]$	(3.19)
$k\_(250\ °C) = 3{,}163 \cdot 10^3$	$\left[s^{-1}\right]$	(3.20)
$k\_(300\ °C) = 957 \cdot 10^3$	$\left[s^{-1}\right]$	(3.21)
$k\_(350\ °C) = 421 \cdot 10^3$	$\left[s^{-1}\right]$	(3.22)

3.4.6 Model predictions

3.4.6.1 Excess MoO_3 profile

Figure 3.11 shows the model predictions of the radial excess MoO_3 profiles and the measured depletion layer thickness for a representative section of the depleted pellets investigated by SEM-EDS (Figure 3.2 and Figure 3.4) and X-ray μ-CT (Figure 3.9). The model is only fitted towards the mass loss measurements, and so the corresponding prediction of the Mo profiles through the pellets can be used as independent validation of the models capability to predict the Mo depletion behavior. The model predicts the thickness of the depletion layer well and correctly predicts the deposition behavior of MoO_3 inside the pellet at high temperature and no H_2O in the feed (350 °C, MeOH = 4.4 %, H_2O = 0 %, O_2 = 10 % in N_2). With respect to the depleted pellet investigated by μ-CT, the depletion of the entire pellet was estimated to 20.3 vol.% by segmentation, which corresponds to a predicted depletion layer at a distance equal to 0.85. The depletion layer thickness measured with μ-CT is in good agreement with the model prediction (0.86).

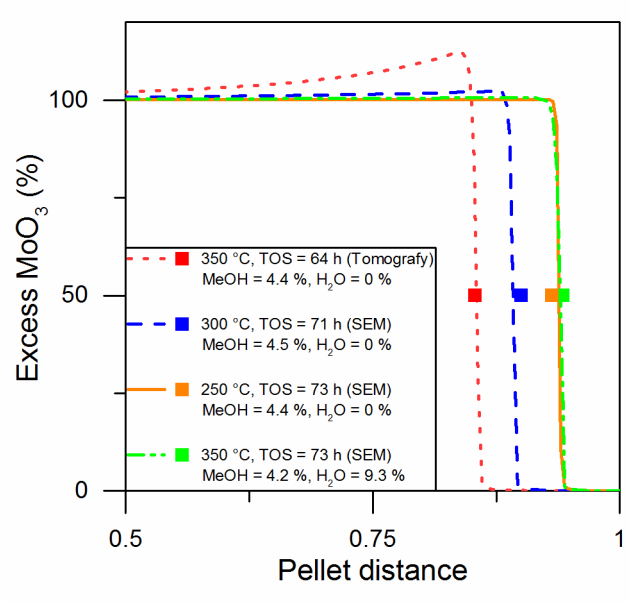

Figure 3.11 – Model prediction of MoO_3 profile (lines) and depletion layer thickness (squares) across the radial direction of the pellet. Pellet distance = 0 is equal to the inner surface and pellet distance = 1 is equal to outer surface. Initial Mo/Fe = 2.4. O_2 = 10 % and N_2 as balance.

3.4.6.2 MeOH, Mo(g), H_2O and porosity profiles

For the representative section of pellets shown in Figure 3.11, the MeOH, Mo(g), H_2O and porosity profiles are shown in Figure 3.12. For all gasous species the concentration is equal to the feed concentration at the pellet surface (pellet distance = 1) due to the assumption of no gas film resistance. MeOH is converted through the pellet forming formaldehyde along with H_2O . As expected high bulk H_2O concentration (9.3 %) inhibits the MeOH conversion (compare red and green curves at 350 C). The volatile Mo species (Mo(g)) are formed by MeOH and solid excess MoO_3 in the pellet. At the inside of the depletion front the Mo species follows the trend of MeOH. However, outside the front there is no excess MoO_3 to form the Mo species. The concentration of Mo species decreases from a maximum at the front to zero (the imposed bulk concentration) through the depleted layer. Also note that the concentration of the volatile Mo species is 12 orders of magnitude lower than the MeOH concentration. Despite this low value, it is enough to remove significant levels of MoO_3 with time. The porosity increases as the pellet is depleted of excess MoO_3, and likewise decreases when MoO_3 is deposited inside the pellet.

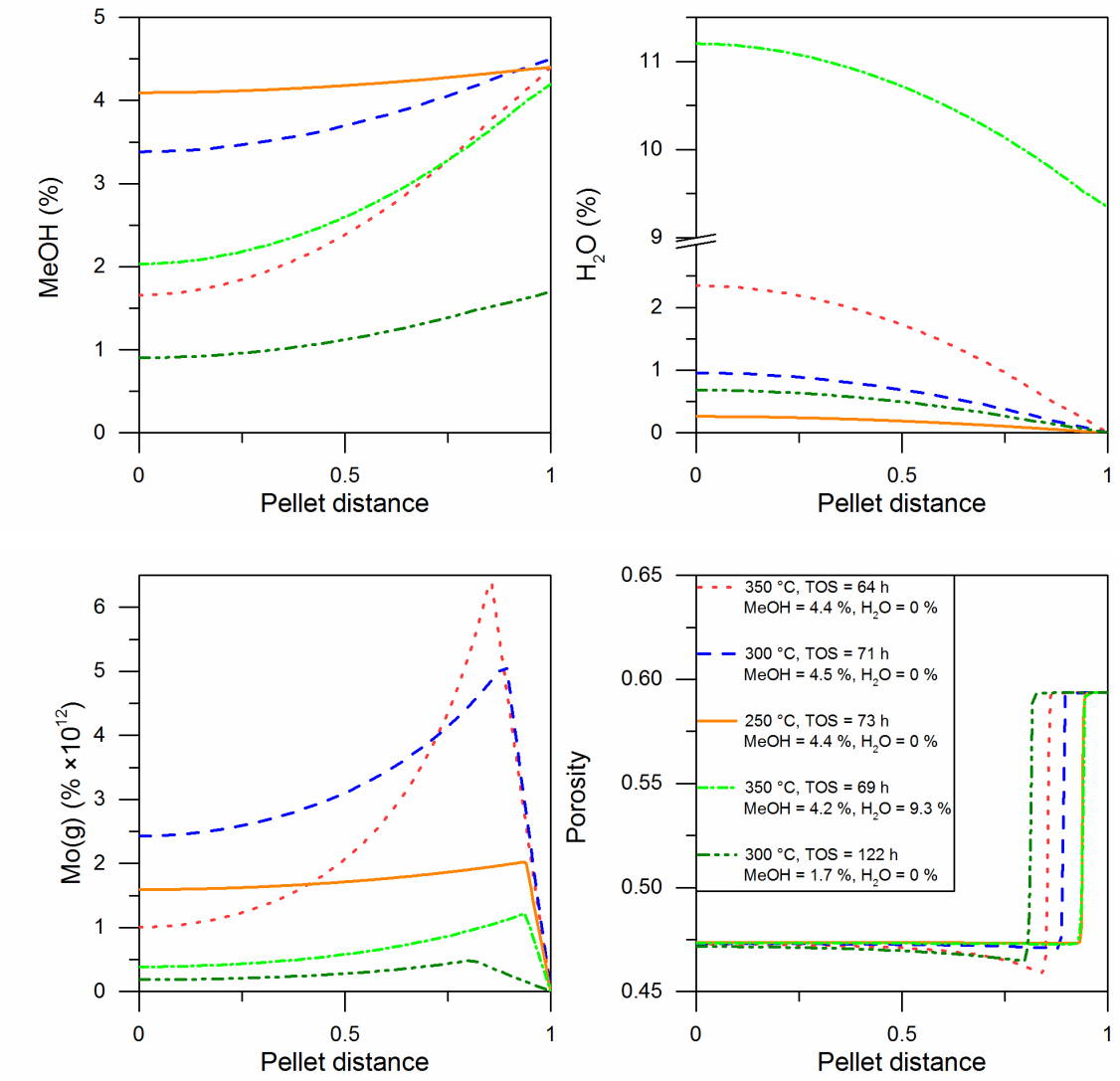

Figure 3.12 - Model prediction of MeOH, volatile Mo species (Mo(g)), H_2O and the porosity profiles across the radial direction of the pellet. Pellet distance = 0 is equal to the inner surface and pellet distance = 1 is equal to outer surface. Initial Mo/Fe = 2.4. The legend is the same for all figures.

3.4.6.3 Loss of excess Mo

The model is capable of predicting the corresponding loss of excess MoO_3 at varying reaction conditions with time on stream with reasonable accuracy (Figure 3.6-Figure 3.8). The equilibrium of the volatilization reaction (3.2) is shifted towards the volatile Mo species and the loss of excess MoO_3 in the pellet with increasing temperature (Figure 3.7). At a temperature of 350 °C and TOS above 159 h formation of $FeMoO_4$ in the depletion layer takes place, which the model does not take into account, hence the underestimation of the excess MoO_3 loss. Water inhibits the forward volatilization reaction which in turn decreases the volatilization rate with increasing water concentration (Figure 3.8). However, the forward volatilization reaction is enhanced by the MeOH concentration and the rate of volatilization increases with increasing MeOH concentration (Figure 3.6).

To further verify the model, two additional sets of data were generated (Figure 3.13 and Figure 3.14) at varying temperature and other reaction conditions (MeOH = ~2 %, H_2O = 0 % and MeOH = ~4 %, H_2O = ~10 %, both at O_2 = 10 %, in N_2). At low MeOH concentration (1.6-1.7 % MeOH (Figure 3.13)) the model slightly over predicts the loss of MoO_3. At high H_2O concentration (9.4-10.2 % H_2O (Figure 3.14)) the model prediction is rather accurate at 250 and 300 °C. However, at 350 °C the model slightly under predicts the loss of MoO_3. The inaccurate prediction at low MeOH concentration indicates that there is an effect in the volatilization of MoO_3 that the model does not account for. Furthermore, the inaccurate predictions at 350 °C indicate that there is likely a temperature dependency of the inhibiting effect of water (K_3) on the volatilization of MoO_3, which is not taken into account in the model due to the limited amount of data. Measuring a larger amount of data and including this temperature effect in the model is expected to improve the accuracy of the model at all temperatures.

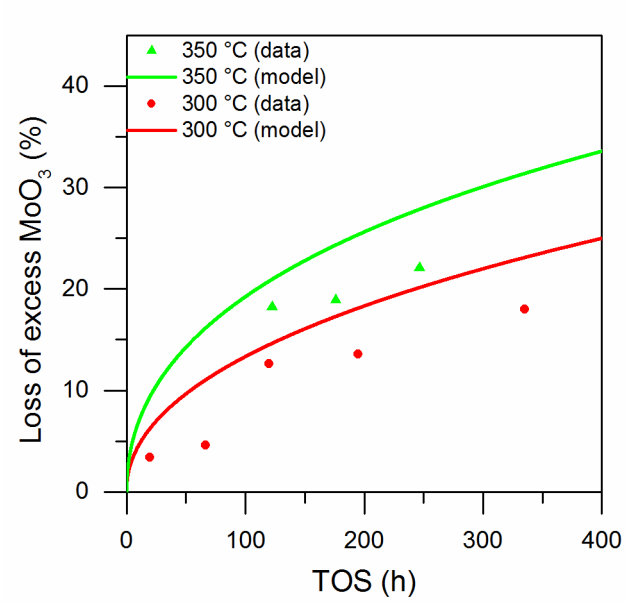

Figure 3.13 - Mass loss of excess MoO_3 in pellets at increasing TOS. Treated at MeOH = 1.6-1.7 %, H_2O = 0 %, O_2 = 10 % in N_2 at 300-350 °C. Mo/Fe = 2.4. Flow rate = 3000 mL/min (1 bar, 273.15 K).

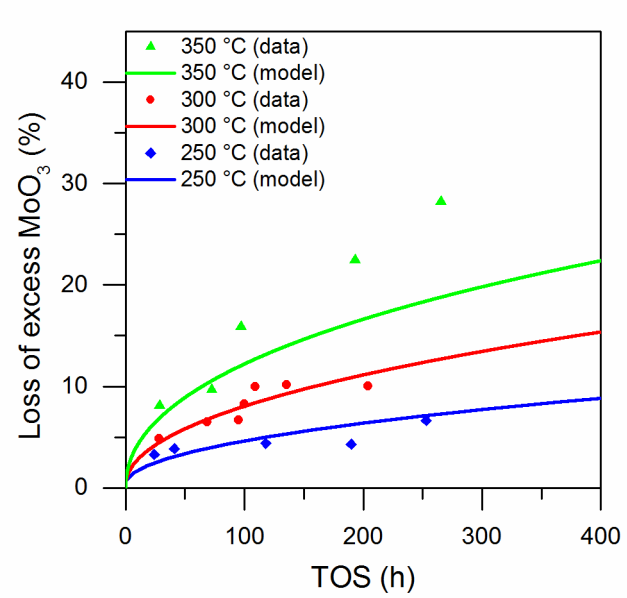

Figure 3.14 - Mass loss of excess MoO_3 in pellets at increasing TOS. MeOH = 3.6-4.2 %, H_2O = 9.4-10.2 %, O_2 = 10 % in N_2 at 250-350°C. Mo/Fe = 2.4. Flow rate = 3000 mL/min (1 bar, 273.15 K).

Figure 3.15 shows a comparison of the measured and predicted mass loss for the applied reaction conditions. 90 % of the predictions are within 7 % of the measurements, which confirms that the model predictions are in good agreement with the measured data. The two data points in Figure 3.7 where $FeMoO_4$ were formed are not included.

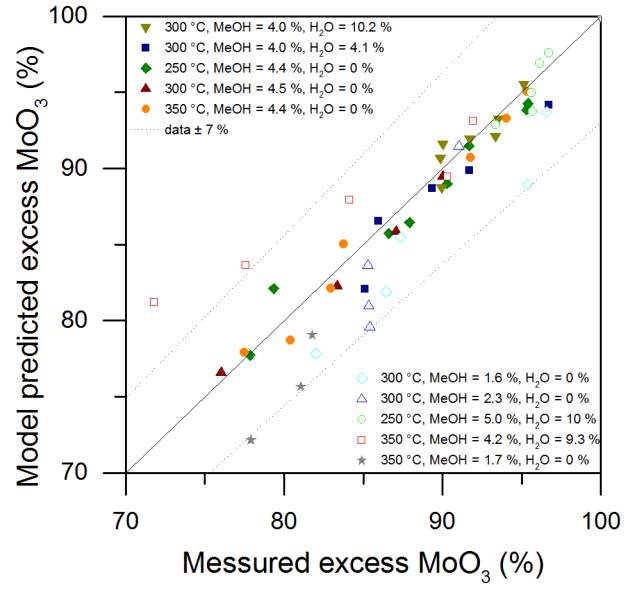

Figure 3.15 – Comparison of predicted vs measured excess MoO_3 in pellet.

3.5 Discussion

3.5.1 Effect of catalyst pellet size

As reported by the authors [17], excess MoO_3 volatizes completely from small catalyst particles within hours (TOS = 10 h, sieve fraction 150-250 nm, initial Mo/Fe = 2). Howev-

er, in the current work Mo volatilization from catalyst pellets is significantly slower. The significant difference in the overall rate of Mo volatilization is mainly due to the difference in the size between the small particles and the catalyst pellets. For the small catalyst particles the depletion layer only has to develop a small distance to reach the center of the particle and completely volatilize all excess MoO_3. However, for the larger pellets the depletion layer must develop a larger distance through the pellet, and the time to completely volatilize all MoO_3 in the pellet will be significantly higher.

To demonstrate the effect of the catalyst pellet size, the model has been used calculate the loss of excess MoO_3 at varying pellet size (MeOH = 5 %, H_2O = 5 % at 300 °C). The pellets size has been scaled with respect to volume keeping the ratio between the dimensions constant (pellet length, inner and outer radius). The loss of excess Mo can be seen in Figure 3.16. The pellet size affects the overall depletion of Mo and by increasing the pellet volume to 200 % the depletion is decreased from 21.5 to 17.2 % after 400 h on stream (corresponding to a decrease of 20 %).

However, increasing the pellet size might lead to other process challenges, such as difficult packing of the catalyst in the reactor tubes and non-intended high temperatures in the pellet center. Furthermore, the overall process selectivity might be affected, due to higher formaldehyde concentration inside larger pellets leading to increased oxidation of formaldehyde to CO [23].

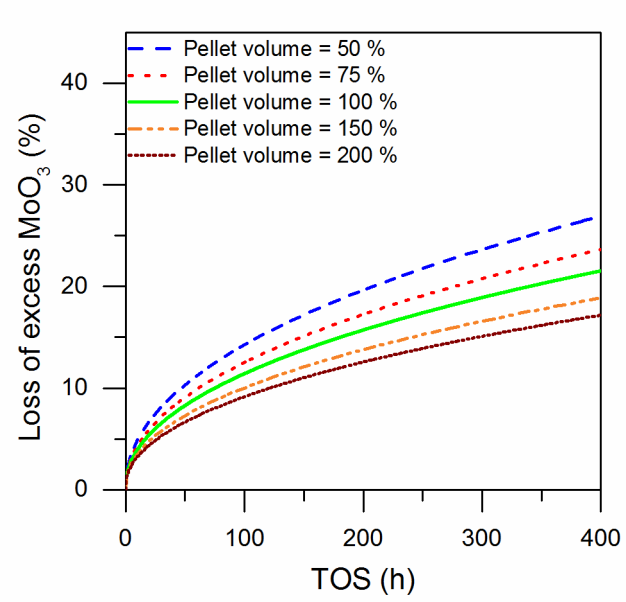

Figure 3.16 – Predicted mass loss of excess MoO_3 in pellets at increasing TOS. The ratios of the pellet dimensions are constant (pellet length, inner and outer radius).
MeOH = 5 %, H_2O = 5 % at 300°C. Initial Mo/Fe = 2.4.

3.6 Conclusion

The influence of temperature and concentration of methanol and water on the molybdenum loss from iron molybdate catalyst pellets ($Fe_2(MoO_4)_3$ with excess MoO_3 corresponding to a molar Mo/Fe ratio of 2.4) used in the oxidation of methanol to formaldehyde was investigated experimentally. The volatilization and diffusion of molybdenum, leads to a layer depleted of excess MoO_3 evolving from the surface of the catalyst pellet. The rate of

depletion is increased by MeOH and temperature, due to the volatilization reaction between MeOH and solid MoO_3 in the catalyst. Water in the gas phase inhibits the volatilization reaction and the rate of depletion. A 1D dynamic single particle model was furthermore developed and compared to experimental data. The model simultaneously calculates the formation of formaldehyde in the pellet, the volatilization of Mo and subsequent transport of the volatile Mo species into and out of the pellet as function of time. The model parameters were fitted to the overall mass loss of the pellets at varying reaction conditions and time on stream, using a feed composition of 1.6-4.5 % MeOH, 0-10.2% H_2O, 10 % O_2 balance N_2 at 250 – 350 °C. The model is capable of describing the molybdenum loss and corresponding depletion layer thickness of a single catalyst pellet. The model shows a significant effect of pellet size on the overall rate of MoO_3 volatilization and the use of pellets in the industrial process is required to dampen the loss of Mo. Incorporation of the single pellet model into a reactor model could be a useful tool to predict the loss of Mo and the associated pressure drop development in a reactor and estimation of process lifetime at varying reaction conditions and is ongoing in our group.

3.7 References

[1] H. Adkins and W. Peterson, "The oxidation of methanol with air over iron, molybdenum, and iron-molybdenum oxides," … Am. Chem. Soc., vol. 53, no. 1927, pp. 1512–1520, 1931.

[2] R. Günther, W. Disteldorf, A. O. Gamer, and A. Hilt, "Ullmann's encyclopedia of industrial chemistry," Weinheim, 2012.

[3] N. Burriesci, F. Garbassi, M. Petrera, G. Petrini, and N. Pernicone, "Solid State Reactions in Fe-Mo Oxide Catalysts for Methanol Oxidation During Aging in Industrial Plants.," Stud. Surf. Sci. Catal., vol. 6, pp. 115–126, 1980.

[4] B. I. Popov, V. N. Bibin, and G. K. Boreskov, "Study of an iron-molybfate oxide catalyst for oxidation of methanol to formaldehyde," Kinet. Catal., vol. 17, no. 2, pp. 322–327, 1976.

[5] A. Andersson, M. Hernelind, and O. Augustsson, "A study of the ageing and deactivation phenomena occurring during operation of an iron molybdate catalyst in formaldehyde production," Catal. Today, vol. 112, pp. 40–44, 2006.

[6] B. R. Yeo, G. J. F. Pudge, K. G. Bugler, A. V. Rushby, S. Kondrat, J. Bartley, S. Golunski, S. H. Taylor, E. Gibson, P. P. Wells, C. Brookes, M. Bowker, and G. J. Hutchings, "The surface of iron molybdate catalysts used for the selective oxidation of methanol," Surf. Sci., vol. 648, pp. 163–169, 2016.

[7] C. Brookes, P. P. Wells, N. Dimitratos, W. Jones, E. K. Gibson, D. J. Morgan, G. Cibin, C. Nicklin, D. Mora-Fonz, D. O. Scanlon, C. R. A. Catlow, and M. Bowker, "The Nature of the Molybdenum Surface in Iron Molybdate. The Active Phase in Selective Methanol Oxidation," J. Phys. Chem. C, vol. 118, no. 45, pp. 26155–26161, 2014.

[8] J. M. Tatibouët, "Methanol oxidation as a catalytic surface probe," Appl. Catal. A Gen., vol. 148, pp. 213–252, 1997.

[9] W. H. Cheng, “Methanol and formaldehyde oxidation study over molybdenum oxide,” J. Catal., vol. 158, no. 2, pp. 477–485, 1996.

[10] J. S. Chung, R. Miranda, and C. O. Bennett, “Mechanism of Partial Oxidation of Methanol over MoO3,” J. Catal., vol. 114, pp. 398–410, 1988.

[11] B. I. Popov and N. G. Skomorokhova, “Changes in activity, selectivity and surface area along an iron-molybdenum catalyst bed after its industrial application,” React. Kinet. Catal. Lett., vol. 18, no. 1–2, pp. 101–105, 1982.

[12] K. I. Ivanov and D. Y. Dimitrov, “Deactivation of an industrial iron-molybdate catalyst for methanol oxidation,” Catal. Today, vol. 154, no. 3–4, pp. 250–255, 2010.

[13] Y. H. Ma and S. J. Kmiotek, “Deactivation Kinetics of Ferric Molybdate,” vol. 142, pp. 132–142, 1988.

[14] M. P. House, A. F. Carley, and M. Bowker, “Selective oxidation of methanol on iron molybdate catalysts and the effects of surface reduction,” J. Catal., vol. 252, pp. 88–96, 2007.

[15] I. Mitov, S. Asenov, T. Tomov, and D. Klissurski, “In situ Mössbauer Study of the Interaction of Methanol with An Iron–Molybdenum Oxide Catalyst,” J. Phys. Chem. C, vol. 111, no. 14, pp. 5389–5393, 2007.

[16] N. Pernicone, “Deactivation of Fe-Mo Oxide Catalyst in Industrial Plant and Simulation Tests on Laboratory Scale,” Catal. Today, vol. 11, pp. 85–91, 1991.

[17] K. V. Raun, L. F. Lundegaard, J. Chevallier, P. Beato, C. C. Appel, K. Nielsen, M. Thorhauge, A. D. Jensen, and M. Høj, “Deactivation behavior of an iron-molybdate catalyst during selective oxidation of methanol to formaldehyde,” Catal. Sci. Technol., 2018.

[18] R. L. Smith and G. S. Rohrer, “The Morphological Evolution of the MoO3 (010) Surface during Reactions in Methanol – Air Mixtures,” vol. 278, pp. 270–278, 1998.

[19] T. Ressler, J. Wienold, R. E. Jentoft, and T. Neisius, “Bulk structural investigation of the reduction of MoO3with propene and the oxidation of MoO2with oxygen,” J. Catal., vol. 210, no. 1, pp. 67–83, 2002.

[20] M. P. House, A. F. Carley, R. Echeverria-Valda, and M. Bowker, “Effect of varying the cation ratio within iron molybdate catalysts for the selectivev oxidation of methanol,” J. Phys. Chem. C, vol. 112, no. 11, pp. 4333–4341, 2008.

[21] S. a R. K. Deshmukh, M. Van Sint Annaland, and J. a M. Kuipers, “Kinetics of the partial oxidation of methanol over a Fe-Mo catalyst,” Appl. Catal. A Gen., vol. 289, no. 2, pp. 240–255, 2005.

[22] V. N. Bibin and B. I. Popov, “Kinetics of Methanol Oxidation by Air on Iron-Molybdenum Oxide Catalysts,” Kinet. Catal. (Engl. Transl.), vol. 10, no. 6, pp. 1091–1098, 1969.

[23] Anthony G. Dixon, “Integrated Multiscale Modeling of Fixed Bed Reactors: Studying the Reactor under Dynamic Reaction Conditions,” in Florence (ISCRE25), 2018.

Chapter 4

Modeling of Molybdenum Transport and Pressure Drop Increase in the Fixed Bed Reactor used for Selective Oxidation of Methanol to Formaldehyde using Iron Molybdate Catalysts

Abstract

A dynamic reactor model for a single reactor tube, in which methanol oxidation to formaldehyde over an iron molybdate with excess molybdenum oxide catalyst takes place simultaneously with transport of MoO_3 from the catalyst through the reactor, was developed. A previously developed dynamic 1D mathematical model for a single ring-shaped cylindrical catalyst pellet, in which volatilization of MoO_3 takes place, was implemented in the developed reactor model. Known axial profiles in a pilot scale reactor with respect to MeOH and H_2O concentration and temperature were used as input to the model. MeOH forms volatile Mo-species with solid MoO_3 in the catalyst pellets, which diffuses to the bulk gas phase and is transported through the reactor, leading to MoO_3 depleted pellets. Volatilization of MoO_3 from the pellets was shown to occur at the initial part of the reactor. As MeOH is converted down the reactor the volatile Mo-species decomposes via the reverse reaction that formed them. Deposition of MoO_3 downstream in the reactor decreases the void space between the catalyst pellets leading to increased pressure drop. The hydraulic diameter of the pellets and the porosity of the MoO_3 deposition were fitted to experimental data obtained in a pilot plant unit containing a single reactor tube. Furthermore, the model was used to simulate a tube under industrial conditions for one year (feed composition 8.4 % MeOH, 4 % H_2O, 10 % O_2 in N_2, bed length = 1.00 m and a temperature of 190-346 °C). Finally the model was used to simulate two cases where catalyst pellets with no excess MoO_3 or shaped as filled out cylinders are used in the initial 0.21 m of the catalyst bed. The results show that this significantly decreases the rate at which the pressure drop is increased. The model is a first step towards a useful tool to predict MoO_3 transport, pressure drop increase and estimation of process lifetime at varying reaction conditions.

4.1 Introduction

Selective oxidation of methanol with air to formaldehyde was performed by von Hoffman over platinum in 1868 [1]. Commercial heterogeneous catalytic reactors were developed in the eighteen hundred eighties using copper gauze and with silver catalysts in 1910, due to higher yield. In 1931, Adkins and Peterson [2] discovered the use of iron molybdate oxide ($Fe_2(MoO_4)_3$) as catalyst according to (4.1) [3]:

$$CH_3OH + ½O_2 \rightarrow CH_2O + H_2O \quad (\Delta H = -156 \text{ kJ/mol}) \tag{4.1}$$

Nowadays the most common process for formaldehyde production uses the iron molybdate catalyst in a fixed-bed-reactor known as the Formox process [4]. Fresh air, recycle gas and methanol is mixed to a single feed stream (MeOH = 8-10 %, H_2O = 4-8 %, O_2 = 10 % in N_2) and introduced to the reactor at 150-200 °C. The reactor is a multitube heat exchange reactor consisting of thousands of tubes (tube diameter ~2 cm and length = 1 – 1.5 m [4]), with circulating boiling oil on the shell side (260-320 °C depending on the shell side pressure) to remove excess heat from the reaction [5]. The tubes are loaded with different layers of material. The upper layer consists of inert material, which will further heat the feed gas to 200-250 °C before entering the catalytic bed. The catalytic bed consists of two layers (~0.5 m each). In the first layer the catalyst is diluted (~50 %) with inert material to avoid thermal runaway. Most of the methanol is converted in this layer and due to the exothermic reaction a hotspot is formed (350-400 °C). In the last non-diluted catalyst layer the remaining methanol is completely converted. The process is carried out at near atmospheric pressure and the yield is 88-92 % [4].

The iron molybdate catalyst consist of two phases $Fe_2(MoO_4)_3$ and MoO_3 [6]. Molybdenum trioxide forms volatilize species with methanol in the feed gas which depletes the catalyst from MoO_3 [7] under the formation of less selective iron rich sites [8-13]. The following reaction have been suggested in the literature to account for the volatilization of solid MoO_3 in the catalyst under reaction conditions (4.2) [14,15]:

$$2MoO_3 + 2CH_3OH \leftrightarrow Mo_2O_5(OCH_3)_2 + H_2O \tag{4.2}$$

To counter the loss of Mo and maintain sufficient selectivity, an excess of MoO_3 is present in the commercial catalyst (molar ratio Mo/Fe ≈ 2-3).

In 1980 Burriesci et al. [16] studied spent catalyst pellets at varying positions from an industrial plant, by measuring the loss of MoO_3 through the initial (~0.40 m) part of the catalytic bed (total bed length = 0.7 m). The plant was operated at a MeOH feed concentration up to 9 %. They observed that pellets sampled 0.06 – 0.13 m into the bed was subject to loss of approximately half of the initially present MoO_3 (Figure 4.1 (a)). As methanol is converted through the reactor the volatile Mo species decompose via the reverse reaction (4.2) forming needlelike crystals between the catalyst pellets, which is also observed elsewhere [14,17-19] and discussed further later in this section. Samples of the entire mass at 0.19 – 0.40 m were subject to increased MoO_3 content.

In 2006 Andersson et al. [19] similar to Burriesci et al. [16] studied spent pellets from an industrial plant, however pellets were sampled after half and full process lifetime. Furthermore, over the decades the process design has been optimized to achieve a longer lifetime, which mainly includes dilution of the initial part of the catalytic bed with inert

rings to avoid thermal run away and increased MeOH inlet concentration to increase the productivity [20]. In the work of Andersson et al. [19] the initial part of the catalytic bed (total catalytic bed length = 1.03 m) was diluted (dilution = 55 vol.% at 0-0.50 m in the bed and Mo/Fe = 2.43 in the catalyst pellets), followed by a non-diluted part (with Mo/Fe = 2.29 in the catalyst pellets at 0.50-1.03 m in the bed). The plant was operated at a MeOH feed concentration of 10.2 %. They observed that pellets from the initial diluted layer over time were subject to complete loss of excess MoO_3 and that the depletion evolved through the bed (Figure 4.1 (b)). Their observations deviates from the observations by Burriesci et al. [16] with respect to the pellets placed closest to the inlet, where Burriesci et al. [16] did not observed loss of Mo. Andersson et al. [19] explains this by the difference in the MeOH inlet concentration. Furthermore, the temperature and H_2O concentration also affects the volatilization of MoO_3 (see chapter 3), which is not provided in their studies.

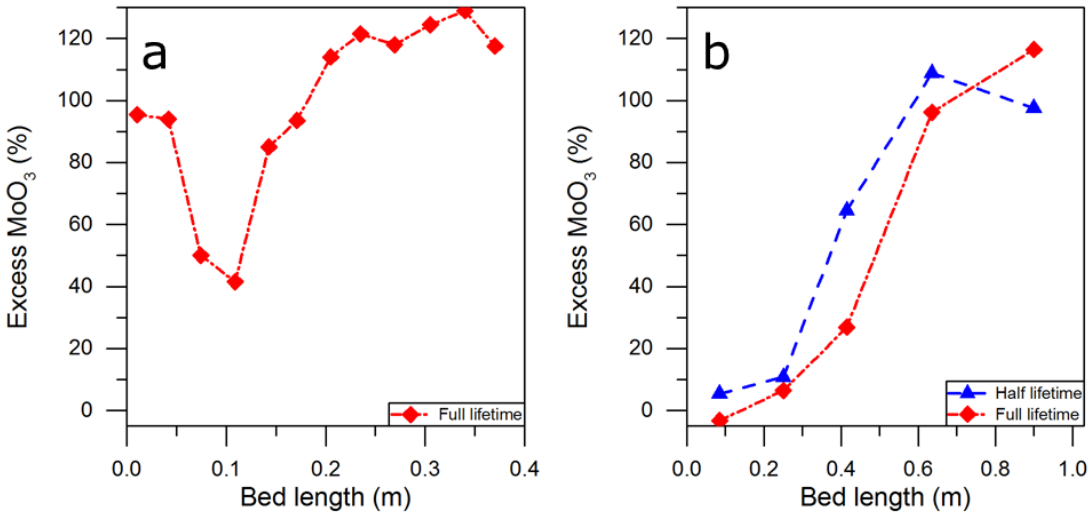

Figure 4.1 – Relative MoO_3 content of a catalyst bed. a: First ~0.40 m of a catalyst bed (total bed length = 0.70 m). Mo/Fe ≈ 2.5. Temperature =250-400 °C. Data adapted from Burriesci et al. [16]. b: (total bed length = 1.03 m). At 0-0.50 m Mo/Fe = 2.4 and at 0.50-1.03 m Mo/Fe = 2.3. Data adapted from Andersson et al. [19].

As mentioned above the volatile Mo-species is observed to deposit in the void space between the catalyst pellets downstream in the reactor [14,16-19]. Burriesci et al. [16] reported an image (Figure 4.2) which shows a spent pellet from a position after the hot spot, where deposition occurs. The needlelike crystals are seen inside the hole of the pellet and the authors mentioned that crystals on the outer surface probably separated during discharge of the pellets from the reactor. It is furthermore seen that some void space is present between the needlelike crystals. The pressure drop increase in the industrial reactor is due to the formation of the MoO_3 deposit, which decreases the void space between the pellets and increases the pressure drop over the bed. The evolving pressure drop is one of the reasons of the relatively short process lifetime of only 1-2 years.

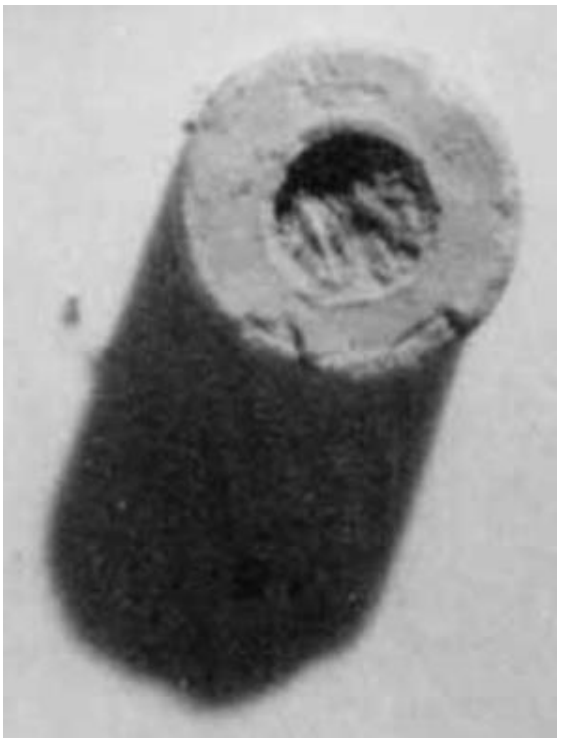

Figure 4.2 – Picture of an iron molybdate catalyst pellet with deposition of molybdenum oxide inside the hole of the pellet. Adapted from [16].

In our group we have studied experimentally and modeled the Mo loss from a single iron molybdate/molybdenum oxide pellet under well-defined reaction conditions (see chapter 3). It was observed that the loss was strongly dependent on the MeOH concentration corresponding to a reaction order of 1.5, and inhibited by H_2O. Moreover, the observations on pellets were compared with a previous study on catalyst sieve fractions (150-300 μm) [13], and it was demonstrated that concentration gradients due to diffusion limitations through the catalyst pellet strongly limited the overall volatilization. The developed single particle model was capable of predicting the observations of Mo volatilization at varying reaction conditions (temperature and MeOH, O_2 and H_2O concentrations).

In this work we present an implementation of our previous single pellet model (see chapter 3) into a reactor model and show simulation results for the vaporization and downstream deposition of MoO_3 and the development of the pressure drop over time. A study on catalyst modifications to minimize the rise in pressure drop is also presented. To the knowledge of the authors this is the first time that such a model is presented in the literature.

4.2 Experimental

4.2.1 Pressure drop measurements in pilot plant

The industrial catalyst pellets were shaped as a cylinder with a hole in the middle (outer diameter = 4.55 mm, hole diameter = 1.70 mm and length = 4.00 mm) and had a Mo/Fe atomic ratio of 2.6. The pellets were placed in a single tube pilot plant reactor with inner diameter = 21.18 mm, length = 1.5 m and with a 4.00 mm central thermopocket capable of measuring the axial temperature profile along the bed. Before the catalytic part of the bed a layer of inert rings (outer diameter = 4.5 mm, inner diameter = 2.5 mm, length = 4.00 mm and bed height = 0.195 m) were placed to preheat the gas mixture and ensure complete evaporation of methanol (MeOH) and H_2O. The initial part of the catalytic bed (0.44 m) was diluted by inert material (34.4 vol.% catalyst) followed by a non-diluted part (0.51 m), and a bottom layer of 0.1 m inert rings, yielding a total bed length of 1.245 m. The reactor was cooled using fluidized sand on the shell side of the reactor. Fresh air and N_2 were mixed and introduced to an evaporator along with MeOH and H_2O to obtain a feed gas of 8.4 % Methanol, 4 % H_2O and 10 % O_2 in N_2, which was fed to the reactor at a flowrate of 1.8 m^3/h (at 1 bar, 273.15 K). To determine the conversion and selectivity, the gas composition was measured at the outlet of the reactor by a gas chromatograph (GC) (Agilent 7890A). The reactor was pressurized and the outlet pressure was controlled to obtain an inlet pressure of 1.45 bar absolute.

4.2.2 Model

In this section, the reactor model for a single reactor tube with plug flow of gas (PFR) is derived, describing the transport of Mo and the resulting pressure drop increase. The PFR reactor tube is modeled as a series of CSTR reactors (Figure 4.3). In the individual CSTR reactor the bulk gas phase conditions are calculated with respect to methanol, temperature and volatile Mo-species. The temperature and methanol profiles through the PFR reactor are known from calculations performed by Haldor Topsøe A/S using in-house software. It is further assumed to be constant in the individual CSTR reactor. The concentration of the volatile Mo-species in the bulk gas phase is calculated from the loss of Mo in the respective catalyst pellets in the relevant CSTR reactor volume and the inlet and outlet to/from the reactor. The equilibrium concentration of volatile Mo-species is calculated from the temperature and known MeOH concentration and if the bulk phase in a given CSTR reactor is oversaturated with respect to the volatile Mo-species, it decomposes to MoO_3 in the reactor void space at a rate calculated form the rate of deposition to surfaces by external mass transfer.

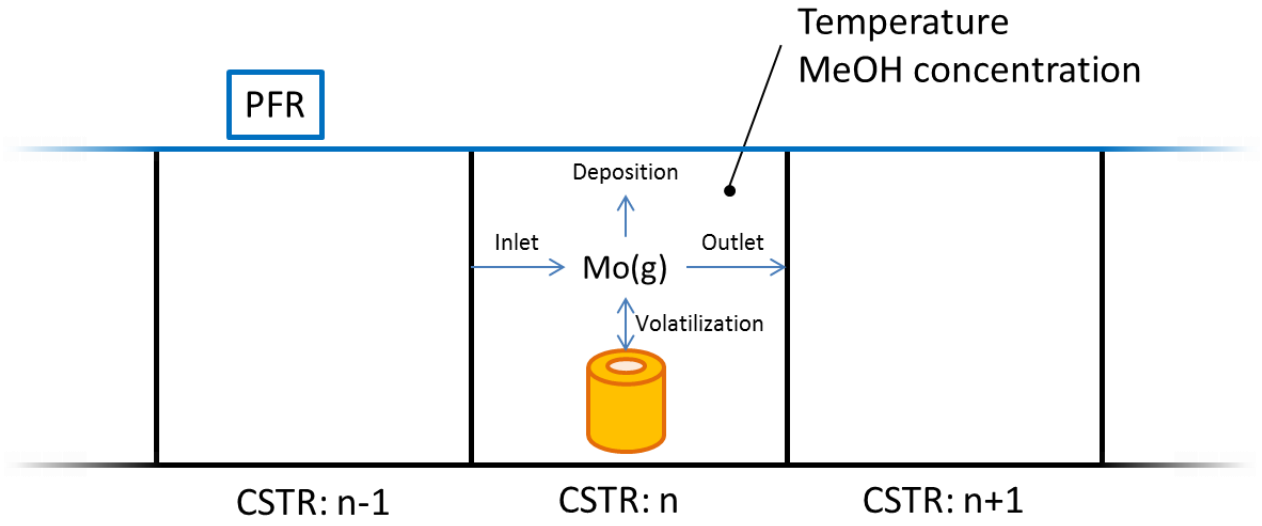

Figure 4.3 – A schematic of the PFR modeled as a series of CSTRs. The temperature and MeOH concentration are known in the individual CSTR from elsewhere. The volatile Mo-species Mo(g) concentration is calculated from the Mo volatilization from the catalyst pellets in the reactor, the inlet and outlet flow, and the rate of deposition.

4.2.3 Bulk concentration of volatile Mo-species (Mo(g))

Solid MoO_3 in the catalyst is volatilized according to reaction (4.2), and the reaction rate $r_{Mo(g)}$ is as follows (4.3) (see chapter 3):

$$r_{Mo(g)} = \frac{k^{+} a_{MoO_3} C_{MeOH}^{n_{MeOH}}}{1 + K_3 C_{H_2O}} - k^{-} C_{Mo(g)}^{n_{Mo(g)}} \qquad (4.3)$$

Where k^{+}, k^{-} and K_3 are the rate constants for the forward and backward reaction and the adsorption equilibrium constant of H_2O respectively. a_{MoO_3} is the activity of solid MoO_3 in

the catalyst (1 if there is MoO_3 and zero if there is none) and C_i is the concentration of component i with the reaction order n_i.

At equilibrium the rate is zero, and the equilibrium concentration of the volatile Mo-species can be calculated as function of the known MeOH and H_2O concentrations as follows (4.4):

$$C_{Mo(g),sat} = \left(\frac{k^+ a_{MoO_3} C_{MeOH}^{n_{MeOH}}}{k^- \left(1 + K_3 C_{H_2O}\right)} \right)^{\frac{1}{n_{Mo(g)}}} \tag{4.4}$$

4.2.4 Deposition of Mo(g) in reactor void space

If the bulk phase is oversaturated, deposition in the reactor void space will occur. The rate of deposition is driven by the difference in the concentration of volatile Mo-species and the saturation concentration in each CSTR. The deposition rate is calculated from the mass transfer from the bulk to the catalyst surface. Under this condition, there is no release of Mo(g) from the catalyst pellets, and the rate of deposition is thus given by:

$$r_{Mo,dep} = \frac{dC_{Mo,dep}}{dt} = k_g A_p (C_{Mo(g)} - C_{Mo(g),sat}) \tag{4.5}$$

Where $r_{Mo,dep}$ is the rate of deposition of Mo(g) to Mo(s) (mol/m³ reactor/s), k_g is the mass transfer coefficient (m/s), A_p is the external catalyst surface area per reactor volume (m²/m³ reactor) and $C_{Mo,dep}$ is the concentration of deposited (solid) MoO_3 (mol/m³ reactor). k_g and A_p are calculated in Appendix C (Equations C.1-C.6).

The void space is decreased as deposition of MoO_3 increasingly occupy some of the void space between the pellets in each CSTR . The respective reactor void space ε can be calculated as follows (4.6):

$$\varepsilon = \varepsilon_0 - \frac{C_{Mo,dep}}{1 - \varepsilon_{dep}} \frac{M_{MoO_3}}{\rho_{MoO_3}} \tag{4.6}$$

Where ϵ_0 is the initial void space at zero MoO_3 deposition, M_{MoO_3} is molar weight of MoO_3 (g/mol), ρ_{MoO_3} is the density (kg/m³) of MoO_3 respectively, and ϵ_{dep} is the (meso)porosity of the deposited MoO_3.

As seen in Figure 4.2 the deposit of MoO_3 forms needle like crystals and that some void space is present between the crystals. However, the bulk gas flow through such area will be highly limited due to the closed structure of these crystals. To account for the inaccessible space between the deposited crystals a "(meso)porosity" factor ϵ_{dep} is taken into account while calculating the development in the reactor void space at increasing deposition, which is used to fit the rate of pressure drop increase in the reactor.

4.2.5 Transport of Mo(g) through reactor bed

Two regimes can be occurring in the individual CSTR reactor as mentioned in section 4.2.4. Either the bulk concentration of Mo(g) is under-saturated and volatilization of Mo from the pellets to the bulk concentration is occurring, or the bulk gas is over-saturated and deposition of MoO_3 is occurring. For both regimes the concentration of the Mo(g) species is depending on the inlet from the previous reactor and the outlet to the next reactor. If volatilization from the pellets occurs the moles of volatile Mo is calculated according to equilibrium with time in the bulk gas of the given CSTR, $N^b_{Mo(g)}$ is given by (4.7):

$$\frac{\partial N^b_{Mo(g)}}{\partial t} = Q_{in}C^{in}_{Mo(g)} - Q_{out}C^b_{Mo(g)} - A_p V D_{e,Mo(g)} \left.\frac{\partial C_{Mo(g)}}{\partial x}\right|_S \left(1-\phi_{dil,n}\right) \tag{4.7}$$

Where Q_i is the volumetric flow rate (m^3/s) in or out of the reactor and $\phi_{dil,n}$ is the volumetric dilution fraction in the given CSTR. The last term accounts for the transport of Mo(g) from the catalyst pellets to the bulk gas due to the concentration gradient at the pellet surface.

If deposition occurs the bulk concentration is decreased according to equation (4.5) and the change in moles is given by (4.8):

$$\frac{\partial N^b_{Mo(g)}}{\partial t} = Q_{in}C^{in}_{Mo(g)} - Q_{out}C^b_{Mo(g)} - k_g A_p V (C_{Mo(g)} - C_{Mo(g),sat}) \tag{4.8}$$

The concentration of Mo(g) in the bulk phase can be calculated from the number of moles as follows (4.9):

$$C^b_{Mo(g)} = \frac{N^b_{Mo(g)}}{V\varepsilon} \tag{4.9}$$

Initially there is no volatile Mo-species or deposited MoO_3 in the reactor. The initial condition in each CSTR is thus given by :

$$C^b_{Mo(g)}(0) = 0,\ C_{Mo,dep}(0) = 0 \tag{4.10) (4.11}$$

The model is made dimensionless as shown in Appendix C (Equations C.7-C.17) and solved with the built-in Matlab solver ODE15s.

4.2.6 Pressure drop increase

The pressure drop through a packed bed reactor can be calculated by Ergun's equation (4.12). In this model the reactor is modeled by a series of N CSTR reactors. However, the pressure drop through the reactor is calculated as series of N PFR reactors using the conditions in the respective CSTR reactor:

$$\Delta p_n = \frac{150\mu L}{D_p^2}\frac{(1-\varepsilon_n)^2}{\varepsilon_n^3}v_s + \frac{1.75L\rho}{D_p}\frac{(1-\varepsilon_n)}{\varepsilon_n^3}v_s^2 \tag{4.12}$$

Where Δp_n is the pressure drop (Pa) in reactor n, μ is the dynamic viscosity of the gas (Pa*s), L is the length of the nth CSTR reactor (m), D_p is the hydraulic diameter of the catalyst pellets (m), ε_n is the void fraction in the reactor, v_s is the superficial velocity (m/s) and ρ is the density of the gas (kg/m^3).

The hydraulic diameter of the catalyst pellets is fitted towards the initial pressure drop through the reactor.

The correlations for the dynamic viscosity are shown in Appendix C (C.18).

The density of the gas is dependent on the pressure in the reactor and is given by:

$$\rho = p\frac{M}{RT} \tag{4.13}$$

Where p is the pressure (Pa), R is the gas constant (Pa*m3/mol/K), T is the temperature (K) and M is the molar mass (kg/mol).

The pressure in the center of a given CSTR reactor is given by:

$$p_n = p_{outlet} + \frac{\Delta p_n}{2} + \sum_{i=n+1}^{N}\Delta p_i \tag{4.14}$$

Here p_{outlet} is the outlet pressure in the reactor and $\sum_{i=n+1}^{N}\Delta p_i$ is the sum of the pressure drops in the CSTR reactors between reactor n and the outlet of the reactor tube. The pressure drop over reactor n (Δp_n) is divided by two to obtain the average pressure in that reactor.

The profiles of MeOH and temperature through the reactor are calculated elsewhere as discussed in section 4.3.1. As the catalyst is depleted for MoO_3 its performance changes as shown in chapter 2. However, for the present simulations the catalyst performance is assumed unchanged leading to constant profiles of MeOH, H_2O concentrations and temperature through the reactor at all time.

4.2.7 Pellet model

The single pellet model previously derived (see chapter 3), is a dynamic 1D mathematical model, in which methanol oxidation to formaldehyde and simultaneous volatilization of MoO_3 takes place. It is assumed that only the excess MoO_3 phase is able to volatilize and thus that no Mo are volatilized from the $Fe_2(MoO_4)_3$ phase. However, it was shown experimentally (see chapter 3) that Mo does volatilize from the $Fe_2(MoO_4)_3$ phase, forming $FeMoO_4$ at harsh conditions of high temperature (> 350 °C) and no H_2O in the bulk gas. For the purpose of the reactor simulations in this work the volatilization of Mo from the $Fe_2(MoO_4)_3$ phase is neglected, since such conditions are never reached. At elevated temperatures at the hotspot of the reactor H_2O will be present and only smaller amounts of Mo will volatilize from the $Fe_2(MoO_4)_3$ phase. In the industrial reactor the gaseous species diffuse through the entire external pellet surface. However, in the previous work (see chapter 3) the inner surface of the ring-shaped pellets where blocked due to a thermocouple placed through the hole in the pellet, which did not allow for any mass transfer at this surface. To fit the single pellet model to the experimental data, the boundary condition at the inner surface was therefore set to not allow any mass transfer. In this work the respective boundary condition is changed to allow mass transfer, so transfer of gaseous species is allowed at the entire pellet surface, which is the case in the industrial reactor (C.19).

4.3 Results and discussion

In this section the reactor model will be fitted to experimental data measured in the pilot plant. The fitted model will be used to run a simulation of an industrial reactor at reaction conditions. Afterwards the model will be used to simulate two case studies of improving the reactor design for extending the lifetime of the process by decreasing the rate of pressure drop increase.

The model described in section 4.2 uses known axial MeOH concentration and temperature profiles through the reactor. The profiles for the pilot plant reactor and an industrial reactor are calculated by Haldor Topsøe A/S internal reactor design program and is shown in section 4.3.1.

4.3.1 MeOH and temperature profile through reactor

In this work two reactors are simulated. The first reactor is the pilot plant as described in section 4.2.1 and the second reactor is an industrial reactor. The reactor tube in the pilot plant is cooled by sand on the shell side, however in an industrial plant there is oil on the shell side, which cools the reactor tube more efficiently. Figure 4.4 shows the MeOH concentration and temperature profile for an experiment performed in the single tube pilot plant, where the first 0.44 m of the catalytic bed is diluted (34.4 vol.%). Figure 4.5 shows the same profiles for an industrial reactor tube, where the first 0.50 m of the industrial reactor is diluted (30 vol.%). The difference between the diluted bed and the non-diluted bed is clearly seen on the profile for the reactor (Figure 4.5).

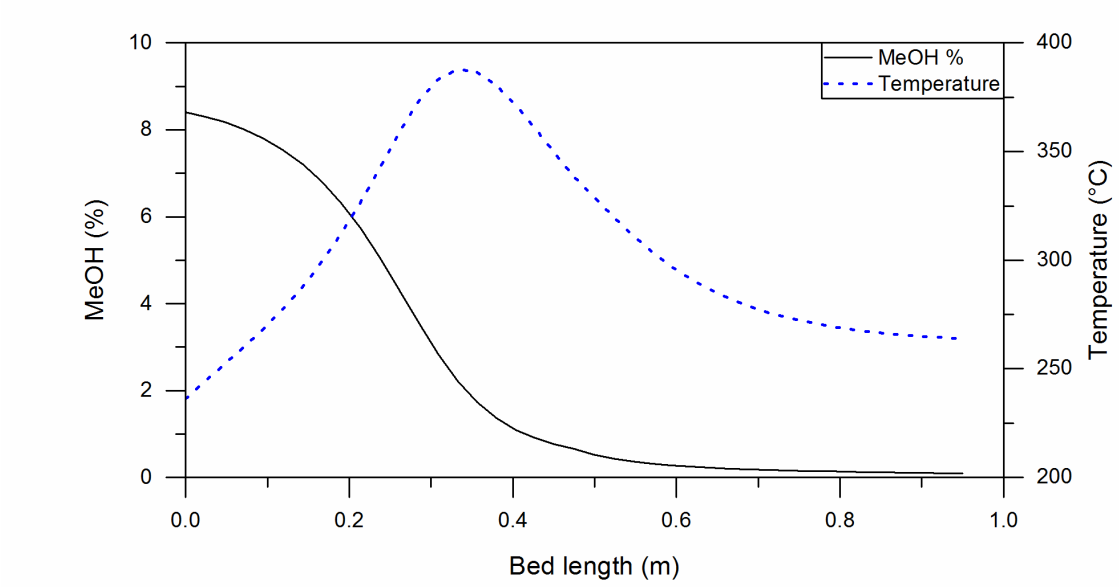

Figure 4.4 – MeOH concentration and temperature profile through the catalytic part of the bed in a pilot plant reactor. Diluted part = 0-0.44 m (34.4 vol.%).

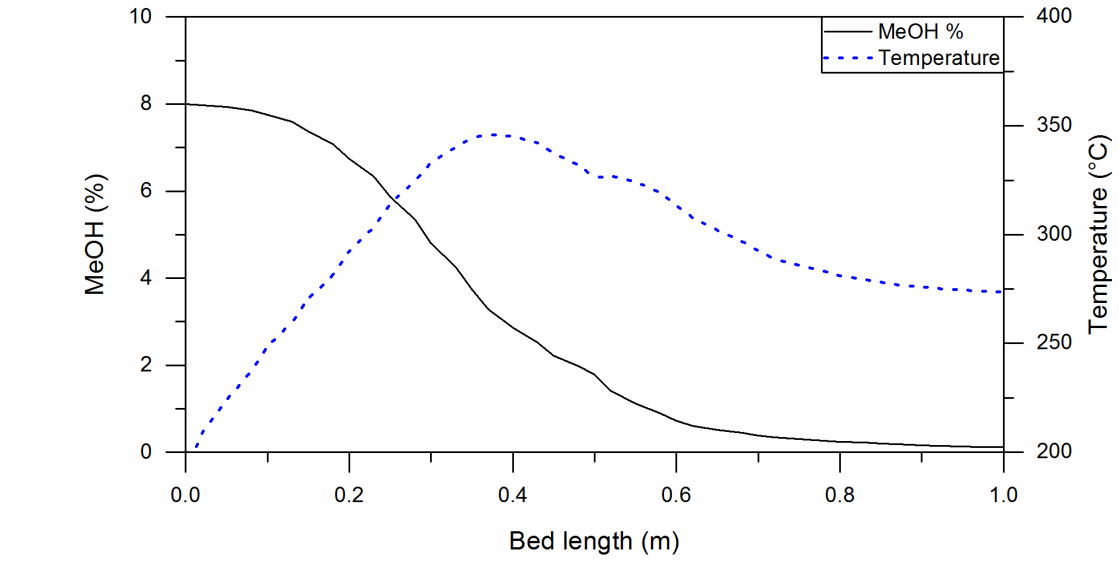

Figure 4.5 – MeOH concentration and temperature profile through the catalytic part of the bed in an industrial scale reactor. Diluted part = 0-0.50 m (30 vol.%).

4.3.2 Fitting procedure

The fitting parameters in the reactor model are the hydraulic diameter of the catalyst particles (4.12) and the porosity of the deposited MoO_3 (4.6) . An experiment in the pilot plant reactor with a runtime of 20 days on stream was used to fit the model. The hydraulic diameter was fitted towards the experimentally measured initial pressure drop in the reactor (intercept Figure 4.6). Li and Ma [21] reported a method to calculate the hydraulic diameter of non-spherical particles. Using this method, the catalyst pellets (outer diameter = 4.55 mm, inner diameter = 1.70 mm and length = 4.00 mm) should have a hydraulic diameter of 2.06 mm (Equations C.20–C.22). However, the fitted hydraulic diameter is 2.91 mm. The difference between the calculated and fitted diameter might be due to the inert pellets (outer diameter = 4.5 mm, inner diameter = 2.5 mm) used to dilute the catalyst bed. The inert pellets have a larger hole, and the pressure drop over these pellets is lower compared to catalyst pellets.

As MoO_3 deposits downstream in the bed it decreases the void space and increases the pressure drop over the reactor. The rate at which the pressure drop increases is dependent on the volume that the deposit occupies, which is calculated according to equation (4.6) as function of the (meso)porosity of the deposit. This (meso)-porosity is fitted towards the pressure drop increase over the reactor (slope Figure 4.6). The fitted porosity of the MoO_3 deposit is 0.52, which seems reasonable compared to the observed needlelike MoO_3 deposit material in Figure 4.2.

Unfortunately the data from the experiment performed in the pilot plant at Haldor Topsøe A/S is not available. However, it showed an initial pressure drop of 960 Pa and a linear trend of 35.3 Pa $days^{-1}$ in the pressure drop increase. Figure 4.6 shows the predicted pressure drop in the pilot plant over 20 days. It is seen that the fitted model predicts an initial pressure drop and rate of pressure drop increase similar to the experimentally observed.

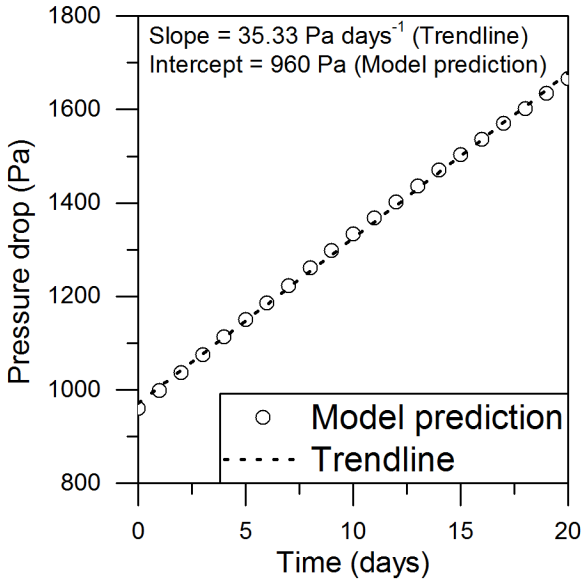

Figure 4.6 – Predicted pressure drop over time at conditions similar to experimental conditions in the pilot plant (Table 4.1), MeOH and temperature profiles are seen in Figure 4.4, outlet pressure = 1.35 bar absolute. Catalytic bed length = 95 cm (34.4 vol.% dilution of initial 0.44 m). Total bed length = 1.245 m.

Table 4.1 – Parameters and discretization inputs used for model simulations.

Parameter	**symbol**	**Value**	
	Catalyst pellet		
Pellet outer diameter	d_p	$4.55 \cdot 10^{-3}$ m	
Pellet inner diameter	d_h	$1.7 \cdot 10^{-3}$ m	
Pellet length	L_p	$4 \cdot 10^{-3}$ m	
Pellet hydraulic diameter	D_p	$5.6 \cdot 10^{-3}$ m	
	Reactor	Pilot plant	Industrial reactor
Reactor length	L	0.95 m	1.00 m
Pressure at outlet	p_0	1.35 bar	1.3 bar
Initial void space	ε_{Void}	0.523	0.523
Porosity of deposited MoO_3	ε_{dep}	0.52	0.52
Numbers of CSTRs	$n_{Reactor}$	14	14

4.3.3 Industrial reactor simulation

The fitted model was used to simulate a base case of an industrial reactor tube for 2 years. The length of the catalytic bed was 1.00 m where the first 0.50 m was diluted by inert pellets (30 vol.%). The outlet pressure is 1.3 bar and the MeOH concentration and temperature profiles through the reactor can be seen in Figure 4.5.

The simulation (Figure 4.7–Figure 4.8) shows the development of the excess MoO_3 content in the pellets through the catalyst bed, the decrease in void space due to deposition of MoO_3 and the resulting pressure drop increase. The development of the excess MoO_3 inside the catalyst pellets is seen in Figure 4.7 (a). In the first part of the bed (0–0.36 m) the rate of Mo volatilization is relatively fast and this part of the bed is almost completely depleted of excess MoO_3 after one year on stream, which is in good agreement with the observation made by Andersson et al. [19]. However, it is noted that in the very first part closest to the inlet (0–0.07 m) the catalyst is not fully depleted even after two years on stream. As discussed in section 4.1 Burriesci et al. [16] observed slower rate of volatilization at the inlet in agreement with the simulations. The rate of volatilization is affected by several contributions (MeOH and H_2O concentration and temperature (see chapter 3)) and even though the MeOH concentration is highest at the inlet, the temperature is low (inlet temperature = 190 °C), resulting in a relatively slow rate of volatilization.

As the first part of the bed (0–0.36 m) is depleted, the volatilization of MoO_3 from this part of the bed slows down. As a result, the bulk gas at the middle of the bed (0.36–0.64 m) is no longer saturated and an S-shaped depletion front develops and moves through the bed. Similar observations are seen by Andersson et al. [19] as discussed in section 4.1. In the

last part of the reactor (0.64–1.00 m) no volatilization of MoO_3 takes place, which is due to the low concentration of MeOH (0.6–0.1 vol.%) and trace amounts of the volatile Mo species.

The volatilized Mo species is transported through the catalyst bed in the bulk gas. As MeOH is converted the volatile Mo species precipitates in the void space surrounding the pellets leading to decreased void space in the bed (0.36–1.00 m)(Figure 4.7 (b)). As the overall volatilization rate of MoO_3 decreases at increasing TOS, due to depletion in the first part of the bed, so does the bulk concentration of the volatile Mo species. The part where deposition of the volatile Mo species takes place therefore moves closer to the outlet of the bed, due to the decreasing concentration of the volatile Mo species.

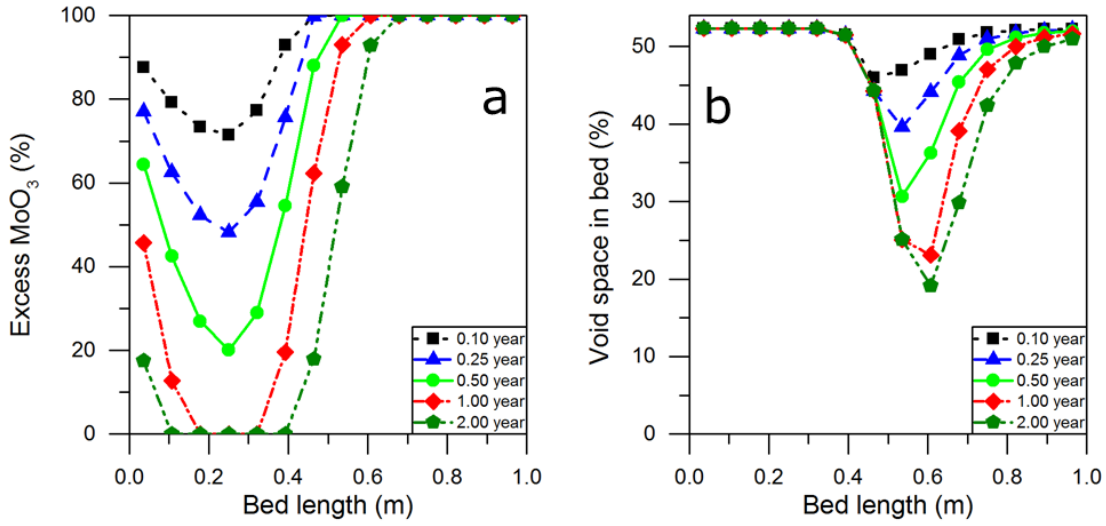

Figure 4.7 – Development of MoO_3 content (a) and void space (b) in the industrial reactor. Total bed length = 1.00 m, diluted part 0-0.50 m. Initial Mo/Fe: 2.4. Outlet pressure = 1.3 bar. MeOH and temperature profiles are seen in Figure 4.5.

The pressure drop increases as function of the decreasing void space over time as described in section 4.2.6 (4.12). Figure 4.8 shows the pressure drop increase of the base case discussed in this section and two other cases discussed in section 4.3.4 For the base case a roughly linear trend in the pressure drop increase is seen in the period up to 1.3 years from 0.096 to 0.41 bar, after which the rate of pressure drop increase slows down significantly.

As the catalyst bed is depleted for MoO_3, the concentration of the volatile Mo species decreases and the position of where MoO_3 is deposited moves downstream the bed as seen in Figure 4.7 (b). Furthermore, only 10 % of the entire deposit amount is occurring in the period between one and two years, which causes the lower rate at which the pressure drop is increased in the period after 1.3 years of 0.41 to 0.44 bar (Figure 4.8).

Moreover, it is noted that as the volatilization over time starts to takes place further into the bed (Figure 4.7 (a)), it exceeds the position of where earlier deposition occurred (Figure 4.7 (b)). The model does not take re-volatilization of the deposit into account, which most likely takes place to some degree. However, the needlelike Mo crystals are much larger than the ones present in the catalyst, yielding a much smaller surface to volume ratio, hence a lower overall rate of volatilization is expected. Furthermore, the struc-

ture of the deposit seen in Figure 4.2 would most likely limit the accessibility of the deposited crystals. However, the model might be improved by incorporating the possibility of re-volatilization of the deposited Mo crystals. Furthermore, the model does not take the decrease in catalytic activity due to depletion of MoO_3 into account (see chapter 2, Figure 2.1, TOS = 0-10 h). As the depletion layer develops through the pellet it simultaneously loss activity. This leads to a higher MeOH concentration in the center of the pellet over time, hence a higher rate of MoO_3 volatilization. However, due to the models prediction of a low MeOH concentration inside the center of the pellet even at significant degrees of MoO_3 depletion, the model hence predict a low rate of volatilization in the center. This is most likely not the case at higher degrees of depletion, and the model might underestimate the rate of volatilization at the center of the pellets. The model might furthermore be improved by taking the deactivation of the depleted layer in pellets into account.

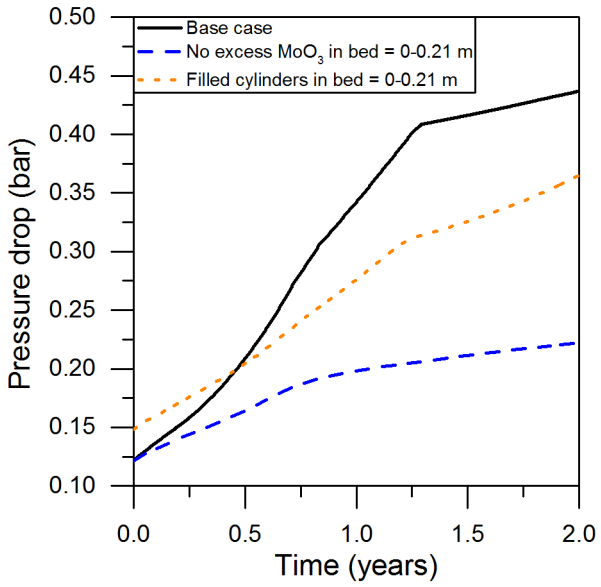

Figure 4.8 – Pressure drop simulations through the catalytic bed for the base case industrial scenario and two design optimization scenarios. Total bed length = 1.00 m, diluted part 0-0.50 m. Mo/Fe = 2.4. Outlet pressure = 1.3 bar. MeOH and temperature profiles are seen in Figure 4.5.

4.3.4 Catalyst design optimization cases

In this section the developed model is used to simulate the effect on the pressure drop of two catalyst optimization strategies (Figure 4.8). Even though changing the catalyst would yield a difference in the catalytic performance, the concentration and temperature profiles through the reactor are assumed to be similar to the one of the base case (Figure 4.5).

With respect to the first strategy, it has been observed by the authors (see chapter 3) that the $Fe_2(MoO_4)_3$ phase is rather stable and loss of Mo is limited at temperatures < 300 °C, in agreement with in the literature [14]. Furthermore, the authors have previously shown that at lower conversion the iron molybdate catalyst maintains its selectivity even when all excess MoO_3 is volatilized and only the $Fe_2(MoO_4)_3$ is present [13]. To decrease the rate of volatilization and extend the lifetime of the process, using catalyst pellets with no excess MoO_3 at the inlet of the reactor might be an interesting option. At the inlet the temperature is moderate and the formaldehyde concentration is low, so a good selectivity can still be expected even if some $Fe_2(MoO_4)_3$ is converted to $FeMoO_4$. By removing some of the MoO_3

that would migrate through the reactor, the rate at which the pressure drop will increase is decreased. A simulation of the first optimization strategy (Figure 4.8) where no excess MoO_3 is present in the initial part of the bed (0.21 m where the temperature is below 300 °C) shows that the rate of pressure drop increase significantly lower than for the base case. The pressure drop is only 0.22 bar after two year, which corresponds to a decrease of 49 % compared to the base case showing the potential of this strategy. However, it should be mentioned that excess of MoO_3 in the catalyst provides mechanical strength, which is necessary to avoid disintegration of the pellets. If the MoO_3 deficient pellets disintegrate the resulting powder would block the reactor and increase the pressure drop. Other additives to increase the mechanical strength of the pellets should thus be considered.

With respect to the second strategy, the authors have shown [13], (see chapter 3) that the pellet size/shape affects the rate of the Mo depletion. However, larger pellets are less effective due to diffusion limitations of MeOH into the pellet and might be less selective because of diffusion limitations of formaldehyde out of the pellet [22]. The pellet size and shape furthermore affects the productivity of the process. E.g. the currently used ring-shaped pellets allow for higher flowrate and hence higher productivity [23]. Taking this into account, only the catalyst pellets in the first part of the bed (0–0.21 m) have been modified. The modified pellets have been shaped as filled cylinders with the same outer diameter and length as the ring-shaped pellets in the base case and through the remaining bed (4.55 and 4.00 mm respectively). By only reshaping the pellets in the initial part of the bed the selectivity would not be significantly affected, due to the low conversion level (bulk conversion < 15 %) and furthermore the temperature is moderate (< 300 °C). The simulation of the second strategy shows that the initial pressure drop is 0.15 bar, which is 22 % higher than the base case. By filling the pellets in the first part of the bed the pressure drop increase over this zone, hence the increase of initial pressure drop over the entire bed. However, the rate at which the pressure drop increases is lower than the base case, and after 0.46 year the pressure drop is lower than in the base case. The pressure drop is 0.37 bar after two years, which is 16 % lower compared to the base case.

The transport of Mo through the bed, and the resulting pressure drop increase, is significantly affected by the methanol concentration and temperature profile through the bed. The current model uses pre-calculated profiles and assumes that these are constant throughout the lifetime of the process. For the model to be a truly useful tool for predicting Mo transport, pressure drop increase and process lifetime at varying reaction conditions, it would need to include a dynamic calculation of the MeOH concentration and temperature profiles through the bed, as the catalytic performance changes as function of MoO_3 volatilization [13]. However, the case studies above using the current model show that the Formox process using iron molybdate catalysts has possibilities for optimization with respect to pressure drop increase and potential improvement of the process lifetime. As discussed in the introduction (section 4.1) the process lifetime is dependent on the rate at which the pressure drop is increased in the reactor and the loss of selectivity. The model does not predict the selectivity of the process and only focusing on decreasing the pressure drop would most likely lead to insufficient selectivity. To extend the process lifetime both selectivity and pressure drop must be taken into account and this work presents a first step towards a useful tool to predict Mo transport and pressure drop increase at varying reaction conditions.

4.4 Conclusion

A mathematical model of the MoO_3 volatilization, transport and deposition through a reactor tube used for selective oxidation of methanol to formaldehyde over iron molybdate/molybdenum oxide catalysts and corresponding pressure drop increase was derived. The model incorporates a previously developed single pellet model for the loss of MoO_3. MoO_3 in the catalyst pellets upstream in the reactor form volatile species, which are transported through the reactor, decomposes and deposits MoO_3 in the void space between the downstream pellets, leading to pressure drop increase. The model parameters being the hydraulic diameter of the pellets in the bed and the porosity of the deposited MoO_3 were fitted towards experimental pressure drop data. The data were obtained from a single tube pilot plant for up to 20 days on stream. The fitted model was used to simulate the Mo transport in the catalyst bed and corresponding pressure drop increase for a base case industrial reactor for up to two years at industrial reaction conditions (Feed composition: 8 % MeOH, 4 % H_2O and a bed temperature of 190-346 °C).

The model was furthermore used to investigate if a lower pressure drop increase could be obtained by either removing the excess MoO_3 from the catalyst or shape the pellets as filled cylinders, in the initial 0.21 m of the reactor (total length = 1.00 m). Simulations showed that such strategies could decrease the pressure drop after two years on stream by about 49 and 16 % respectively. The reactor model uses pre-calculated, fixed profiles of MeOH concentration and temperature through the reactor. By including concentration and temperature profiles in the model as dynamic calculations it would be capable of simulation varying reaction conditions and not only known conditions. An extended model, fully dynamic model would be a useful tool to predict the volatilization of MoO_3 and to test strategies to minimize the associated pressure drop development in an industrial reactor and hence maximize the process lifetime at varying reaction conditions. The developed model is the first step towards such a model.

4.5 References

[1] A. P. V. Soares, M. F. Portela, and A. Kiennemann, "Methanol Selective Oxidation to Formaldehyde over Iron-Molybdate Catalysts," Catal. Rev. Eng., vol. 47, no. 1, pp. 125–174, 2005.

[2] H. Adkins and W. Peterson, "The oxidation of methanol with air over iron, molybdenum, and iron-molybdenum oxides," J. Am. Chem. Soc., vol. 53, no. 1927, pp. 1512–1520, 1931.

[3] S. K. Bhattacharyya and K. Janakiram, "Kinetics of the Vapor-Phase Oxidation of Methyl on Vanadium Pentoxide Catalyst," J. Catal., no. 8, pp. 128–136, 1967.

[4] R. Günther, W. Disteldorf, A. O. Gamer, and A. Hilt, "Ullmann's encyclopedia of industrial chemistry," Weinheim, vol. Chapter 4, p. Chapter 4, 2012.

[5] M. P. House, "The Selective Oxidation Of Methanol Over Iron Molybdenum Catalysts," PhD, School of Chemistry, Cardiff University, 2007.

[6] A. M. Bahmanpour, A. Hoadley, and A. Tanksale, "Critical review and exergy analysis of formaldehyde production processes," Rev. Chem. Eng., vol. 30, no. 6, pp. 583–604, 2014.

[7] B. I. Popov, V. N. Bibin, and G. K. Boreskov, "Study of an iron-molybfate oxide catalyst for oxidation of methanol to formaldehyde," Kinet. Catal., vol. 17, no. 2, pp. 322–327, 1976.

[8] B. R. Yeo, G. J. F. Pudge, K. G. Bugler, A. V. Rushby, S. Kondrat, J. Bartley, S. Golunski, S. H. Taylor, E. Gibson, P. P. Wells, C. Brookes, M. Bowker, and G. J. Hutchings, "The surface of iron molybdate catalysts used for the selective oxidation of methanol," Surf. Sci., vol. 648, pp. 163–169, 2016.

[9] C. Brookes, P. P. Wells, N. Dimitratos, W. Jones, E. K. Gibson, D. J. Morgan, G. Cibin, C. Nicklin, D. Mora-Fonz, D. O. Scanlon, C. R. A. Catlow, and M. Bowker, "The Nature of the Molybdenum Surface in Iron Molybdate. The Active Phase in Selective Methanol Oxidation," J. Phys. Chem. C, vol. 118, no. 45, pp. 26155–26161, 2014.

[10] J. M. Tatibouët, "Methanol oxidation as a catalytic surface probe," Appl. Catal. A Gen., vol. 148, pp. 213–252, 1997.

[11] W. H. Cheng, "Methanol and formaldehyde oxidation study over molybdenum oxide," J. Catal., vol. 158, no. 2, pp. 477–485, 1996.

[12] J. S. Chung, R. Miranda, and C. O. Bennett, "Mechanism of Partial Oxidation of Methanol over MoO3," J. Catal., vol. 114, pp. 398–410, 1988.

[13] K. V. Raun, L. F. Lundegaard, J. Chevallier, P. Beato, C. C. Appel, K. Nielsen, M. Thorhauge, A. D. Jensen, and M. Høj, "Deactivation behavior of an iron-molybdate catalyst during selective oxidation of methanol to formaldehyde," Catal. Sci. Technol., vol. 8, no. 18, pp. 4626–4637, 2018.

[14] K. I. Ivanov and D. Y. Dimitrov, "Deactivation of an industrial iron-molybdate catalyst for methanol oxidation," Catal. Today, vol. 154, no. 3–4, pp. 250–255, 2010.

[15] R. L. Smith and G. S. Rohrer, “The Morphological Evolution of the MoO3 (010) Surface during Reactions in Methanol – Air Mixtures,” vol. 278, pp. 270–278, 1998.

[16] N. Burriesci, F. Garbassi, M. Petrera, G. Petrini, and N. Pernicone, “Solid State Reactions in Fe-Mo Oxide Catalysts for Methanol Oxidation During Aging in Industrial Plants.,” Stud. Surf. Sci. Catal., vol. 6, pp. 115–126, 1980.

[17] B. I. Popov and N. G. Skomorokhova, “Changes in activity, selectivity and surface area along an iron-molybdenum catalyst bed after its industrial application,” React. Kinet. Catal. Lett., vol. 18, no. 1–2, pp. 101–105, 1982.

[18] Y. H. Ma and S. J. Kmiotek, “Deactivation Kinetics of Ferric Molybdate,” vol. 142, pp. 132–142, 1988.

[19] A. Andersson, M. Hernelind, and O. Augustsson, “A study of the ageing and deactivation phenomena occurring during operation of an iron molybdate catalyst in formaldehyde production,” Catal. Today, vol. 112, pp. 40–44, 2006.

[20] E. Soderhjelm, M. P. House, N. Cruise, J. Holmberg, M. Bowker, J.-O. Bovin, and A. Andersson, “On the Synergy Effect in MoO3-Fe-2(MoO4)(3) Catalysts for Methanol Oxidation to Formaldehyde,” vol. 2, pp. 145–155, 2008.

[21] L. Li and W. Ma, “Experimental Study on the Effective Particle Diameter of a Packed Bed with Non-Spherical Particles,” Transp. Porous Media, vol. 89, no. 1, pp. 35–48, 2011.

[22] Anthony G. Dixon, “Integrated Multiscale Modeling of Fixed Bed Reactors: Studying the Reactor under Dynamic Reaction Conditions,” in Florence (ISCRE25), 2018.

[23] E. Soderhjelm, M. P. House, N. Cruise, J. Holmberg, M. Bowker, J.-O. Bovin, and A. Andersson, “On the Synergy Effect in MoO3-Fe-2(MoO4)(3) Catalysts for Methanol Oxidation to Formaldehyde,” Top. Catal., vol. 50, no. 1–4, pp. 145–155, 2008.

Chapter 5
Conclusion and Further Work

The understanding of the iron molybdate catalyst used for selective oxidation of methanol to formaldehyde and the process challenges with respect to pressure drop increase have been further developed through the research conducted in this PhD thesis. A mathematical model was used to predict the effect by optimizing the catalyst and process design. However, additional research must be conducted to validate the plausible effects by changing the design.

The structural and compositional changes of the catalyst in a sieve fraction of 150–250 μm were followed for a prolonged period of up to 25 days, where volatilization of Mo in the catalyst occurred and significant Mo depletion was achieved. The catalyst maintained a rather satisfactory selectivity towards formaldehyde (above 92 %) even when all excess MoO_3 was volatilized and formation of $FeMoO_4$ and Fe_2O_3 from the $Fe_2(MoO_4)_3$ phase occurred. During formation of iron rich species loss of selectivity would be expected. The maintained selectivity was explained by the moderate conversion level (25–47 %), where only some formaldehyde is formed and is available for further oxidation towards the irreversible combustion products CO and CO_2. This result might suggest that the presence of the excess MoO_3 phase is redundant at lower conversion levels, which is the case in the initial part of the industrial reactor. However, this research is only conducted on sieve fractions (150–250 μm) of the catalyst where diffusion limitations are limited. Loss of selectivity might be more pronounced in larger catalyst pellets due to the formation of $FeMoO_4$ and Fe_2O_3 because of diffusion limitations of formaldehyde out of the pellet. Furthermore, MoO_3 increases the pellets mechanical strength which must be sufficiently high to avoid disintegration of the pellets and blocking of the reactor by catalyst powder. Further research on a larger scale, at least on single pellet scale, would be necessary to verify if this observation might be usable industrially. Furthermore, formation of β-MoO_3 was observed in the catalyst material after 25 days on stream, where the initially present α-MoO_3 was volatilized already after ~0.4 days on stream. This might indicate that β-MoO_3 is significant less volatile under the reaction conditions. Preparation and testing of an $Fe_2(MoO_4)_3$/β-MoO_3 catalyst would be of high interest with respect to decreasing the rate of which Mo is volatilized from the catalyst.

Volatilization of Mo from single iron molybdate/molybdenum oxide pellets was investigated at varying reaction conditions. The effect of MeOH, H_2O and O_2 concentration, and temperature were measured over time. The rate of volatilization was increased at increasing MeOH concentration and temperature, and inhibited by the H_2O concentration. The O_2 concentration did not affect the overall loss of Mo from the pellet. A dynamic 1D mathematical model for a single pellet, in which methanol oxidation to formaldehyde and simultaneous volatilization of excess MoO_3 takes place, was developed and positively verified towards the experimental data. At increased temperature (350 °C) and no H_2O in the bulk gas volatilization from the $Fe_2(MoO_4)_3$ phase was observed experimentally, which the developed model does not take into account. However, such conditions are not occurring industrially, and the loss of Mo from this phase is insignificant under reaction conditions where some H_2O will be present in the bulk gas due to H_2O being present in the feed gas and formation of H_2O during the main reaction of selective oxidation of methanol towards formaldehyde. The amount of data that was measured to verify the model was to some degree limited, which leads to some uncertainty in the model parameter estimation. Furthermore, the temperatures effect on H_2O inhibition of the volatilization was not implemented in the model due to the limited amount of data. Further measurements at other conditions and especially at varying combinations of temperature and H_2O concentration would be necessary to further develop and limit model parameter uncertainties.

The developed and verified single pellet model was implemented in a derived mathematical reactor model, in which the MoO_3 transport through a reactor tube and the corresponding pressure drop increase takes place. The single pellet model is used to predict the volatilization of MoO_3 and formation of volatile Mo upstream in the reactor. The volatile Mo species are transported through the reactor and deposits as MoO_3 in the void space between the pellets downstream, leading to pressure drop increase. The reactor model parameters were fitted towards experimental data obtained in a pilot plant unit at Haldor Topsøe A/S. The reactor model uses pre-calculated MeOH concentration and temperature profiles through the reactor. However, for the model to be a truly useful tool for estimation of the pressure drop by changing the process design and/or conditions, it should be capable of calculating these profiles independently. Furthermore, the model is used to simulate full lifetime of the process where the performance of the catalyst changes due to loss of Mo, which neither the single pellet model or the reactor model takes into account. Moreover, the model parameters are only fitted towards experimental data measured over a period of 20 days. It would be advantageously to e.g. measure the pressure drop of and industrial reactor under controlled conditions for full process lifetime to validate the model. It would likewise be advantageously to validate the depletion of MoO_3 through the catalyst bed with data either obtained in the pilot plant at Haldor Topsøe A/S or from industrial measurements, from where the effect of having the volatile Mo species in the bulk gas downstream in the reactor could be quantified. This is not possible in the single pellet reactor used to measure the rate of volatilization at DTU.

The combined and verified single pellet and reactor model was used to simulate the pressure drop in a base case study of a typical industrial reactor. Furthermore, the model was used to simulate two cases of optimization strategies, of which both deal with modifying the catalyst in the initial part of the reactor, where the risk of losing selectivity due to changes in the catalyst geometry is lowest. For the first strategy the excess MoO_3 was removed from the catalyst pellets and for the second strategy the pellets were shaped as

filled cylinders, which significantly increase the diffusion limitation of the volatile Mo species out of the pellet. Simulations showed decrease in the rate of which the pressure drop increases for both cases. However, the model only considers one of the reasons why a change of the catalyst load in an industrial plant might be necessary, that is the pressure drop. By removing MoO_3 or changing the pellet geometry the selectivity might be negatively affected [1-3] or it might lose its mechanical strength. For the two proposed optimization strategies, further research by e.g. pilot plant testing is necessary to verify if the model prediction is correct and if the selectivity of the entire process is satisfying.

The volatilization of Mo from the iron molybdate continues to be an issue in the Formox process. Other catalyst systems (mainly molybdates and vanadates) have been studied with the purpose of replacing the current catalyst [4]. However, the synthesis of a stable, active and selective catalyst continues to be an unsolved challenge. Since there is no obvious candidate to entirely replace the current catalyst, one strategy might be to only replace the current catalyst where it performs less effectively. The current catalyst performed well in the last part of the bed, where its stability is no issue and it has high selectivity towards formaldehyde, even at the high conversion. Other more stable catalysts typically lack high selectivity at high conversion. However, in the first part of the bed the reaction conditions are moderate with low temperature and conversion. A new more stable catalyst would only need to perform better than the current one at these conditions to overall improve the process, by replacement of the initial part of the catalyst bed.

Based on the experiments carried out during the work of this PhD thesis, insights into the complex system of the Formox process has been revealed. Optimizing and extending the lifetime of this process requires a deep understanding of the iron molybdate catalyst and the process design. The behavior of the catalyst at the different conditions through the reactor varies significantly and a combination of catalyst and process design is necessary to extend the lifetime of the process at its current stage. It is believed by the author that such optimizations are possible by further research, where this thesis is a first step towards such optimizations.

5.1 References

[1] Anthony G. Dixon, “Integrated Multiscale Modeling of Fixed Bed Reactors: Studying the Reactor under Dynamic Reaction Conditions,” in Florence (ISCRE25), 2018.

[2] A. P. V. Soares, M. F. Portela, A. Kiennemann, and L. Hilaire, “Mechanism of deactivation of iron-molybdate catalysts prepared by coprecipitation and sol – gel techniques in methanol to formaldehyde oxidation,” Chem. Eng. Sci., vol. 58, no. 7, pp. 1315–1322, 2003.

[3] M. Bowker, R. Holroyd, A. Elliott, P. Morrall, A. Alouche, C. Entwistle, and A. Toerncrona, “The selective oxidation of methanol to formaldehyde on iron molybdate catalysts and on component oxides,” Catal. Letters, vol. 83, no. 3–4, pp. 165–176, 2002.

[4] A. Andersson, J. Holmberg, and R. Häggblad, “Process Improvements in Methanol Oxidation to Formaldehyde: Application and Catalyst Development,” Top. Catal., vol. 59, no. 17–18, pp. 1589–1599, 2016.

Appendix A

A-1 Raman spectra

Relevant reference phases.

The Raman spectra of β-MoO_3 are shown in the literature[1] and the other relevant spectra are shown in Figure A.1.

1 T. M. McEvoy and K. J. Stevenson, *Langmuir*, 2005, **21**, 3521–8.

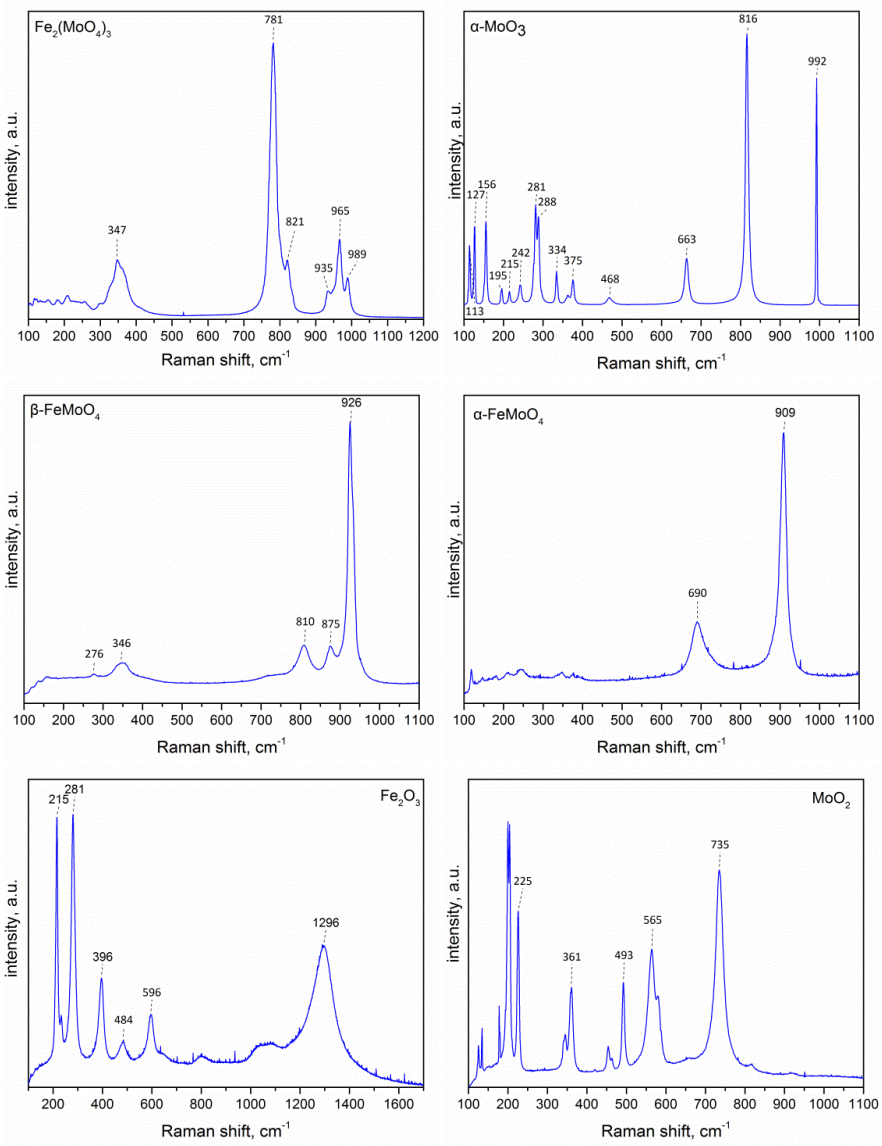

Figure A.1 – Raman spectra of $Fe_2(MoO_4)_3$, α-MoO_3, β-$FeMoO_4$, α-$FeMoO_4$, Fe_2O_3 and MoO_2.

A-2 Activity measurement

Comparison of relative rate between all activity experiments, Arrhenius plot and C-mol balances and selectivities.

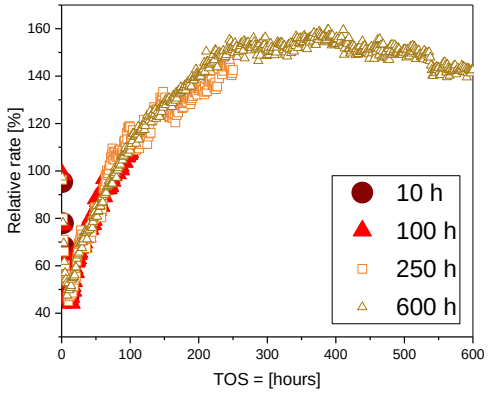

Figure A.2 – Relative rates of the catalyst for all activity experiments TOS = 10, 100, 250 and 600 hours.

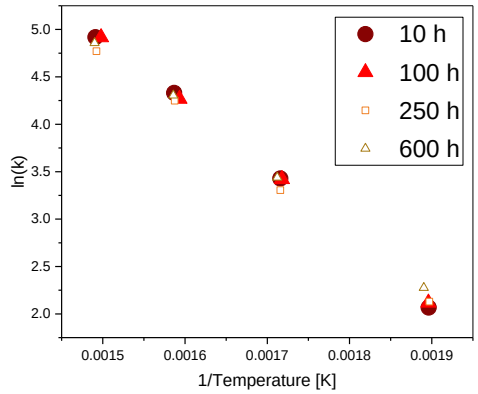

Figure A.3 – Arrhenius plot of rate constants measured prior to all activity experiments of the catalyst.

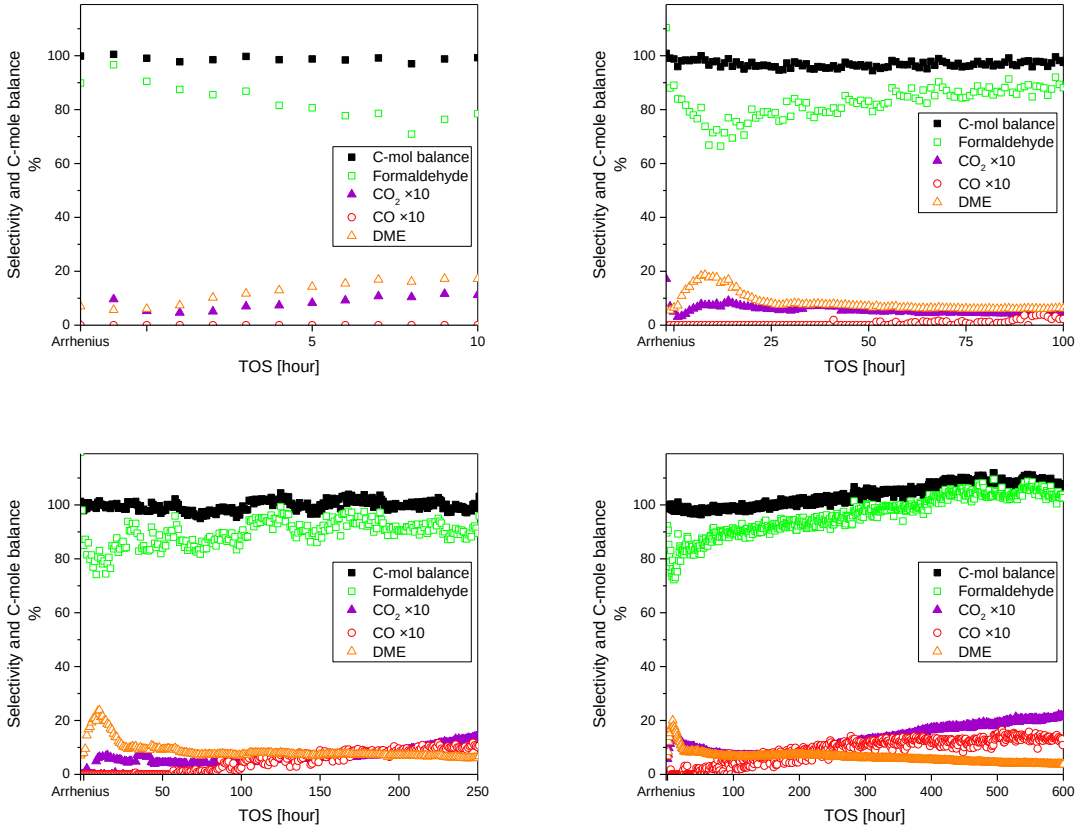

Figure A.4 – Carbon mole balances and selectivities of activity experiments TOS = 10, 100, 250 and 600 hours.

A-3 XRD patterns and Raman spectra

Zoom-ins of the most relevant spectral ranges

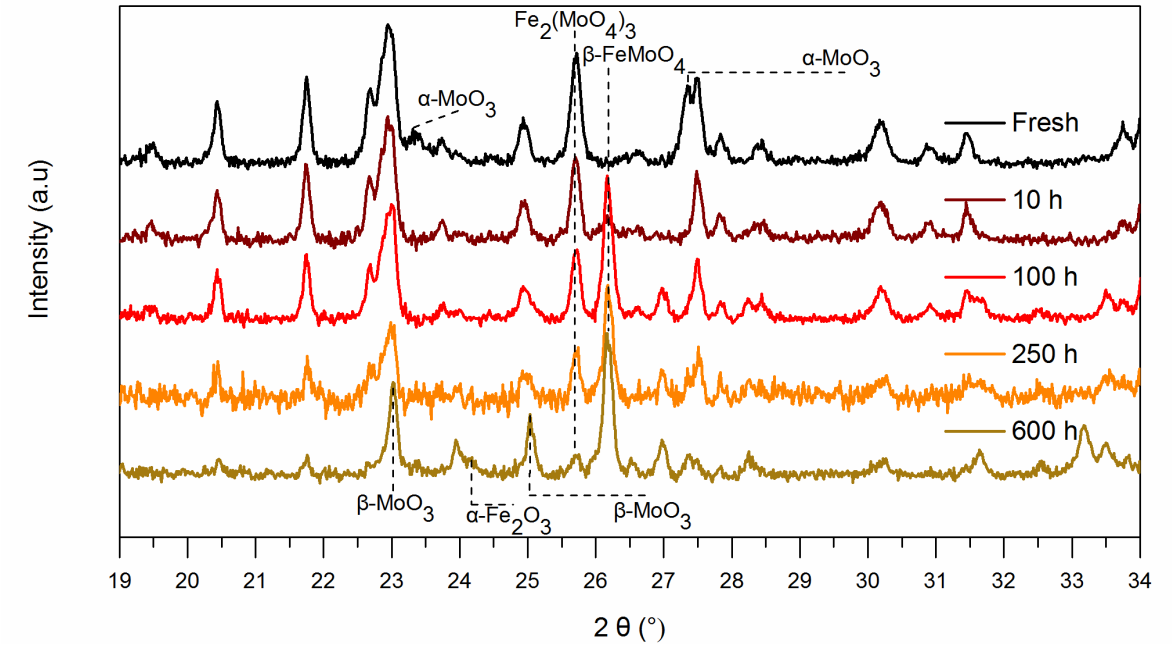

Figure A.5 – Zoom-in of Figure 2: XRD patterns of the fresh and spent FeMo catalyst samples (TOS = 10, 100, 250 and 600 h).

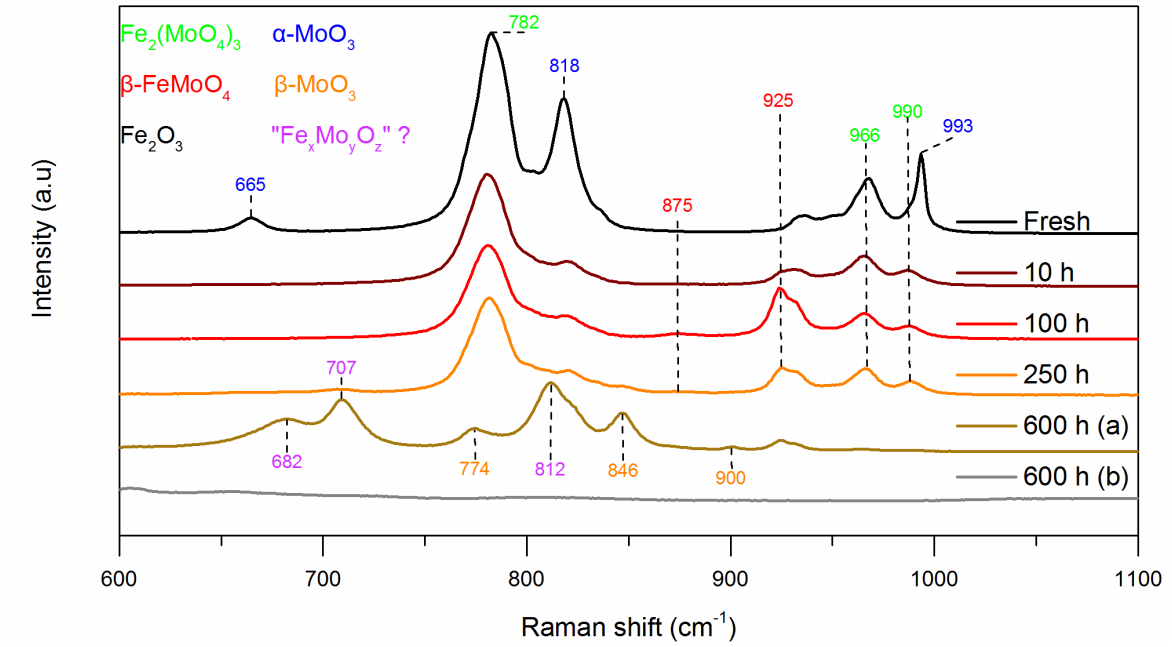

Figure A.6 – Zoom-in of Figure 3: Raman spectra of the fresh and spent FeMo catalyst samples (TOS = 10, 100, 250 and 600 h). Due to the inhomogeneous nature of the catalyst after 600 h spectra from two representative positions are shown.

A-4 Raman spectroscopy

Test for sample laser damage at increasing laser power for the sample run for 600 h on stream.

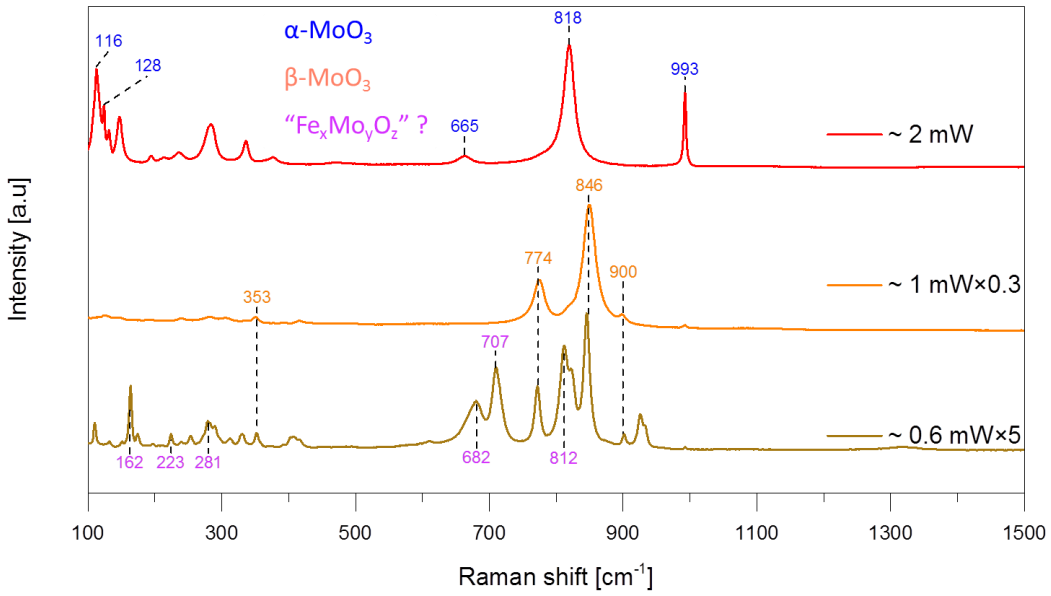

Figure A.7 – Raman spectra of the spent FeMo catalyst sample (TOS = 600 h) at varying laser power.

Figure A.7 shows Raman spectra of the spent FeMo catalyst after 600 h on stream at increasing laser power. At a laser power of 0.6 mW the bands at 846, 353, 774 and 900 cm^{-1} were assigned to the metastable β-MoO_3. However, bands at 682, 707 and 812 cm^{-1} could not be assigned. By increasing the laser power to 1 mW, the non-assigned bands were selectively removed (indicating a high reactivity of this phase), and by increasing the laser power further to 2 mW, the β-MoO_3 was transformed into the thermodynamically stable α-MoO_3

A-5 SEM

EDS analysis and Images

Fresh catalyst (a) Mo/Fe: Area 1 = 1.43 Area 2 = 7.19 Area 3 = 9.03 Area 4 = 7.51	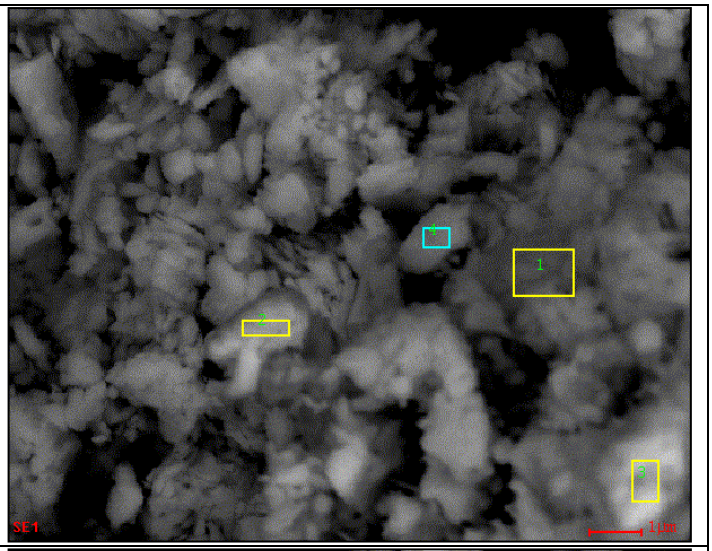
Fresh catalyst (b) Mo/Fe: Area 1 = 6.47 Area 2 = 4.48 Area 3 = 1.40 Area 4 = 1.52 Area 5 = 1.56	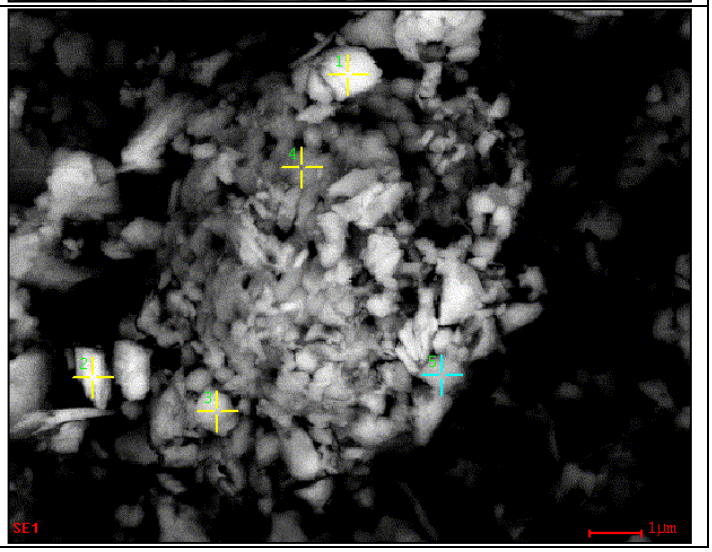

Figure A.8 – SEM-EDS of fresh catalyst.

Spent catalyst TOS = 10 h Mo/Fe: Area 1 = 1.22 Area 2 = 1.44 Area 3 = 1.46	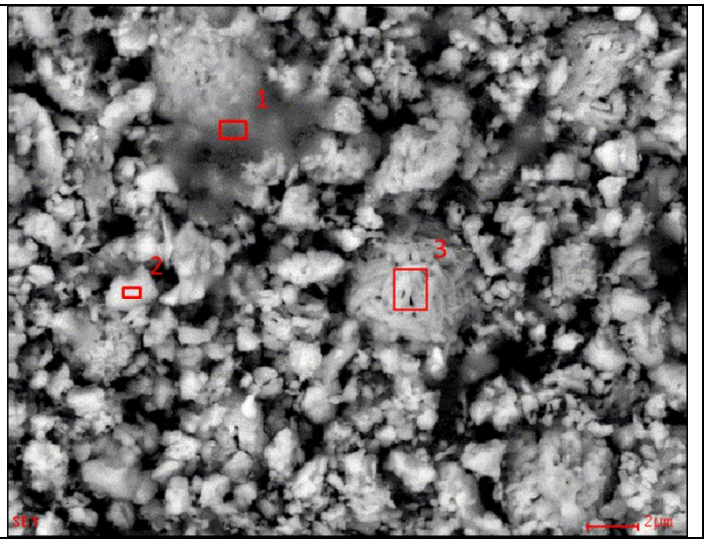

Figure A.9 – SEM-EDS of spent catalyst TOS = 10 h.

Spent catalyst TOS = 100 h Mo/Fe: Area 1 = 0.67 Area 2 = 1.11	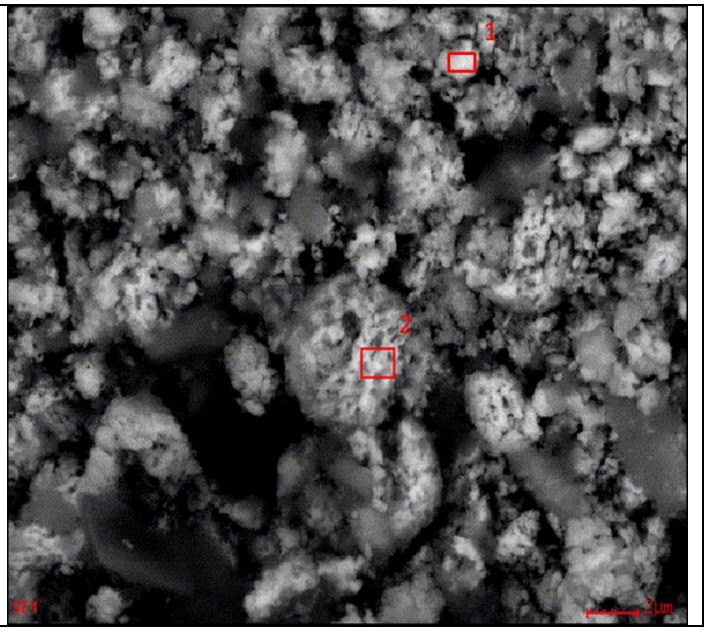

Figure A.10 – SEM-EDS of spent catalyst TOS = 100 h.

Spent catalyst TOS = 250 h (a) Mo/Fe: Area = 2.07	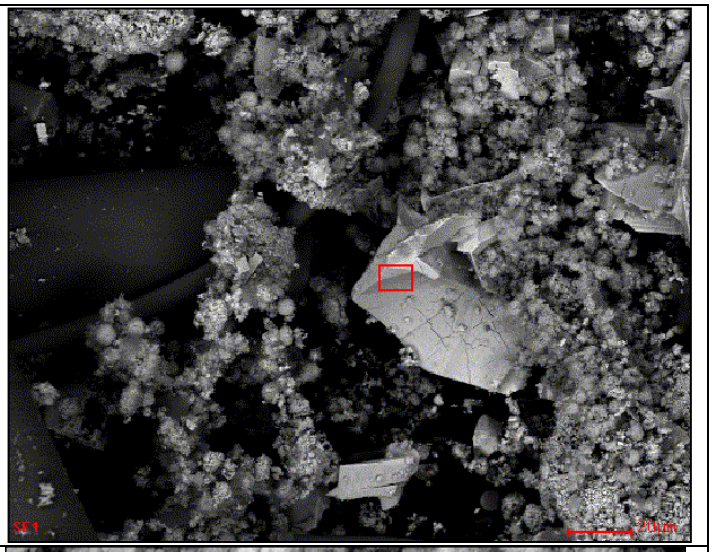
Spent catalyst TOS = 250 h (b) Mo/Fe: Area 1 = 0.015 Area 2 = 1.09 Area 3 = 2.33 Area 4 = 0.66 Area 5 = 0.037 Area 6 = 0.091	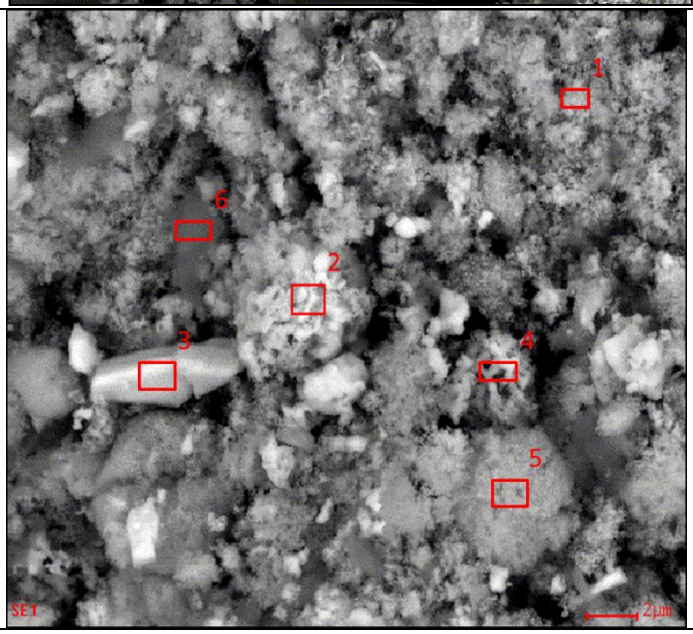

Figure A.11 – SEM-EDS of spent catalyst TOS = 250 h.

Spent catalyst TOS = 600 h (a) Mo/Fe: Area 1 = 0.56 Area 2 = 0.55 Area 3 = 0.025	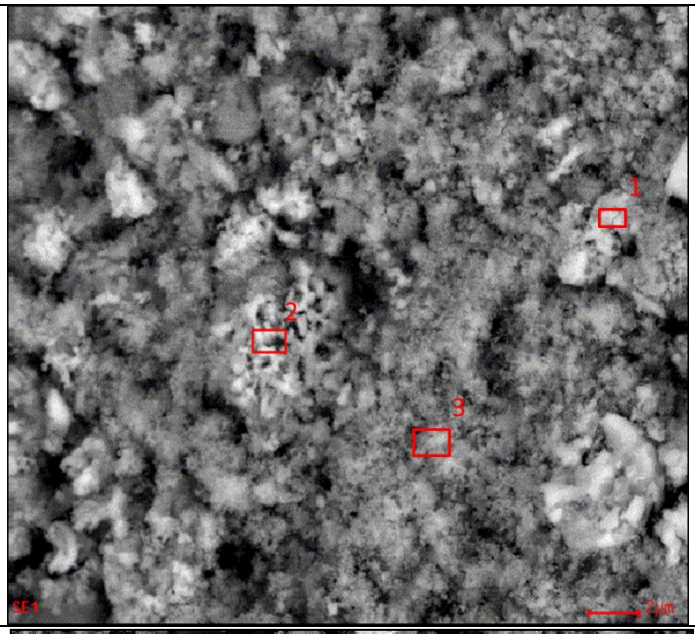
Spent catalyst TOS = 600 h (b) Mo/Fe: Area = 8.37	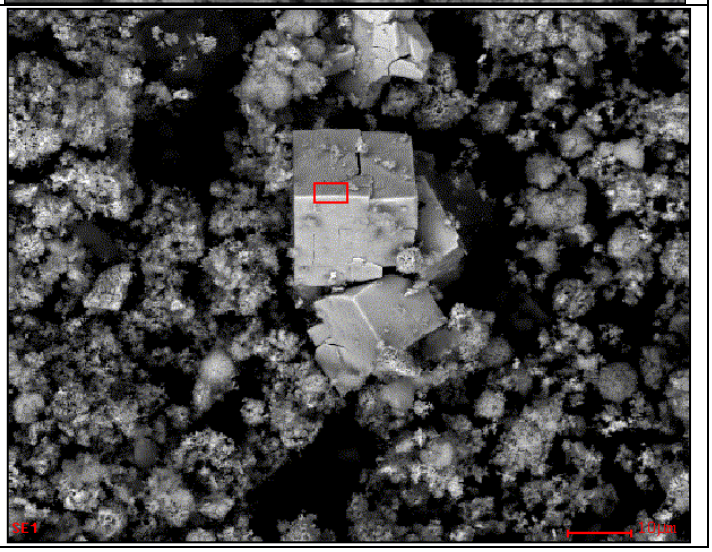

Figure A.12 – SEM-EDS of spent catalyst TOS = 600 h.

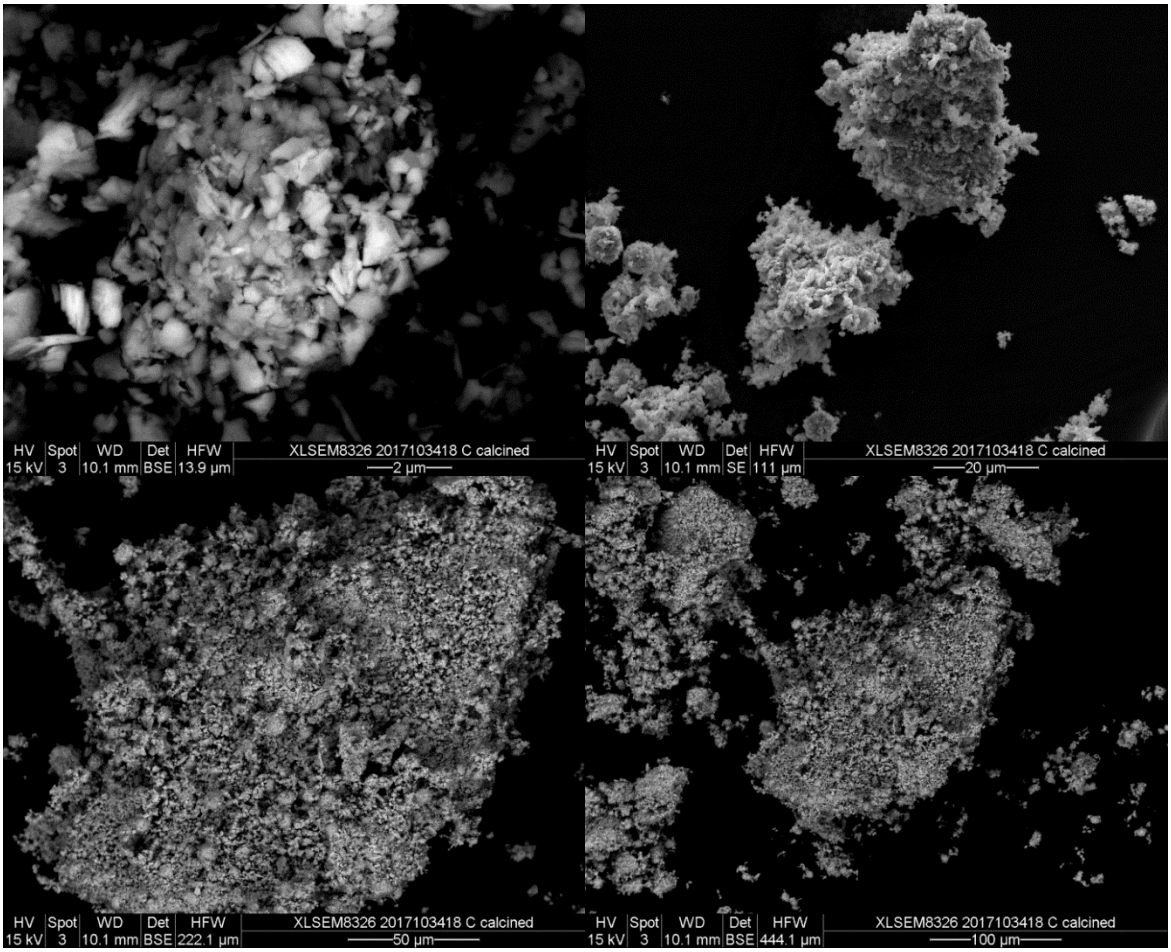

Figure A.13 – SEM images of fresh catalyst.

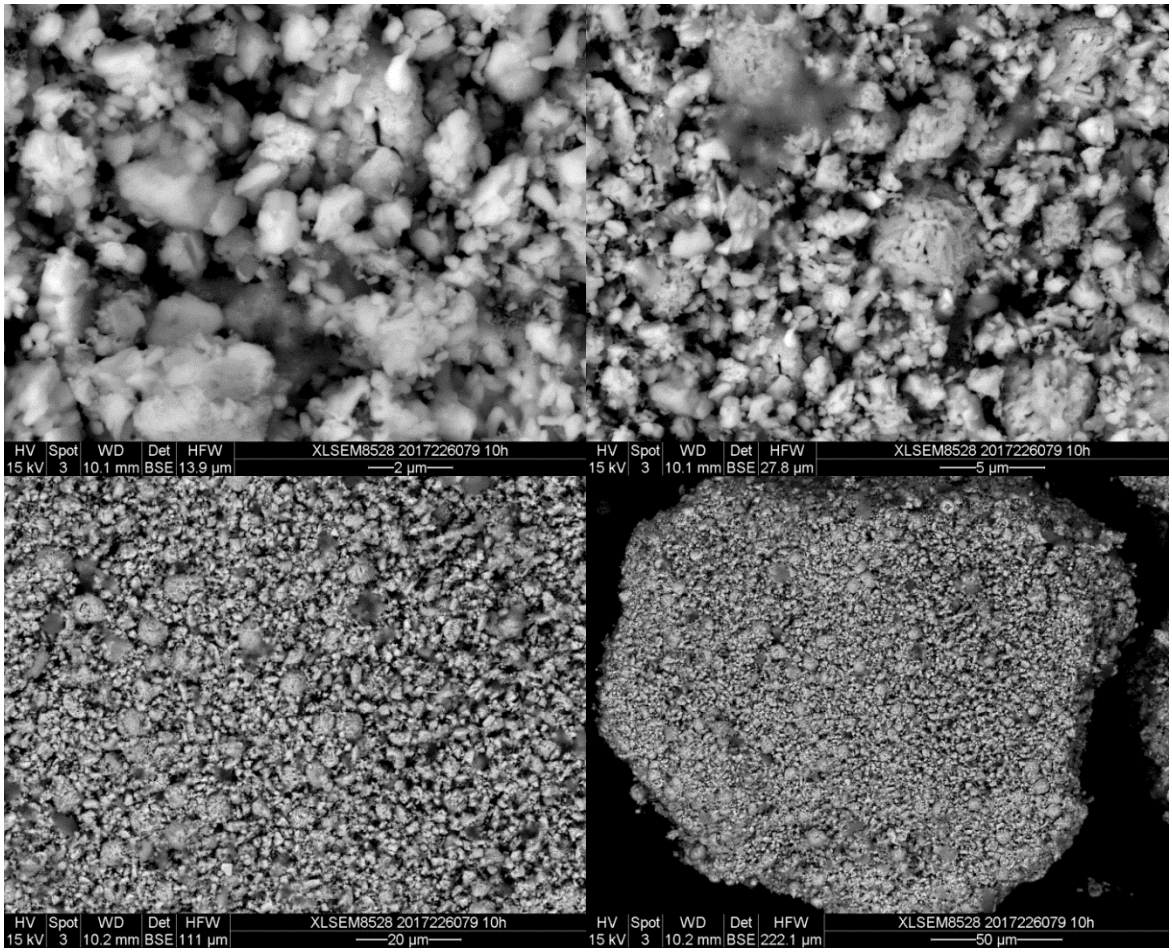

Figure A.14 – SEM images of spent catalyst (TOS = 10 h).

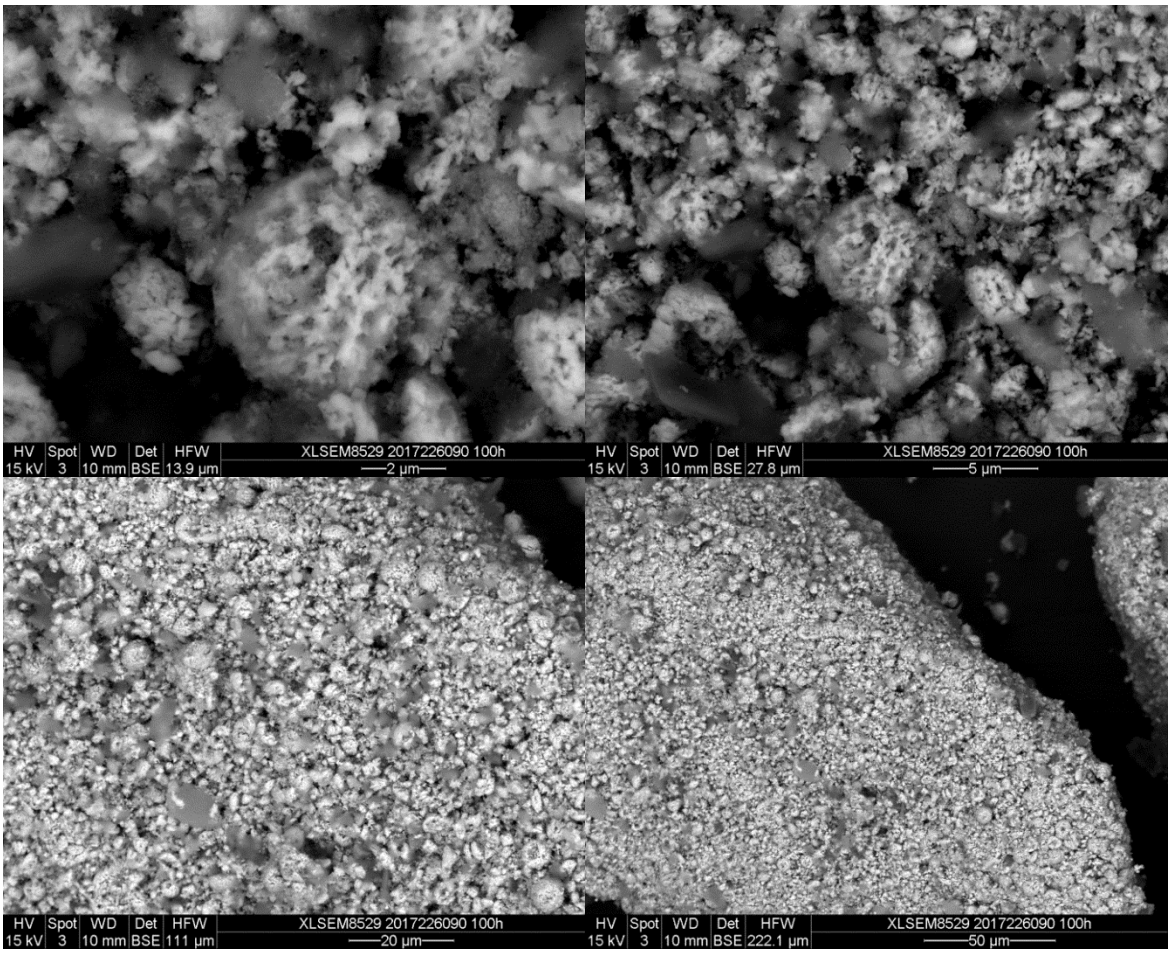

Figure A.15 – SEM images of spent catalyst (TOS = 100 h).

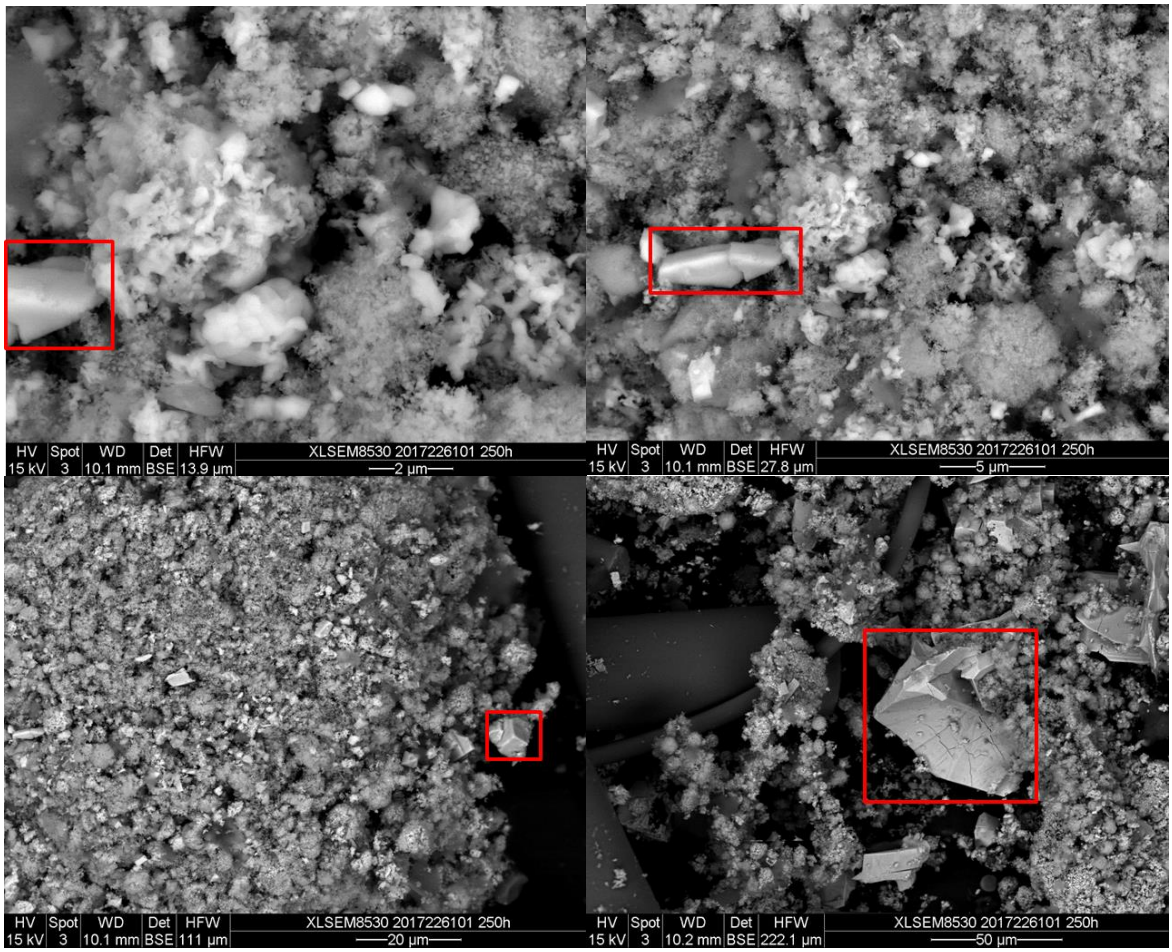

Figure A.16 – SEM images of spent catalyst (TOS = 250 h). Marked crystals are MoO_3.

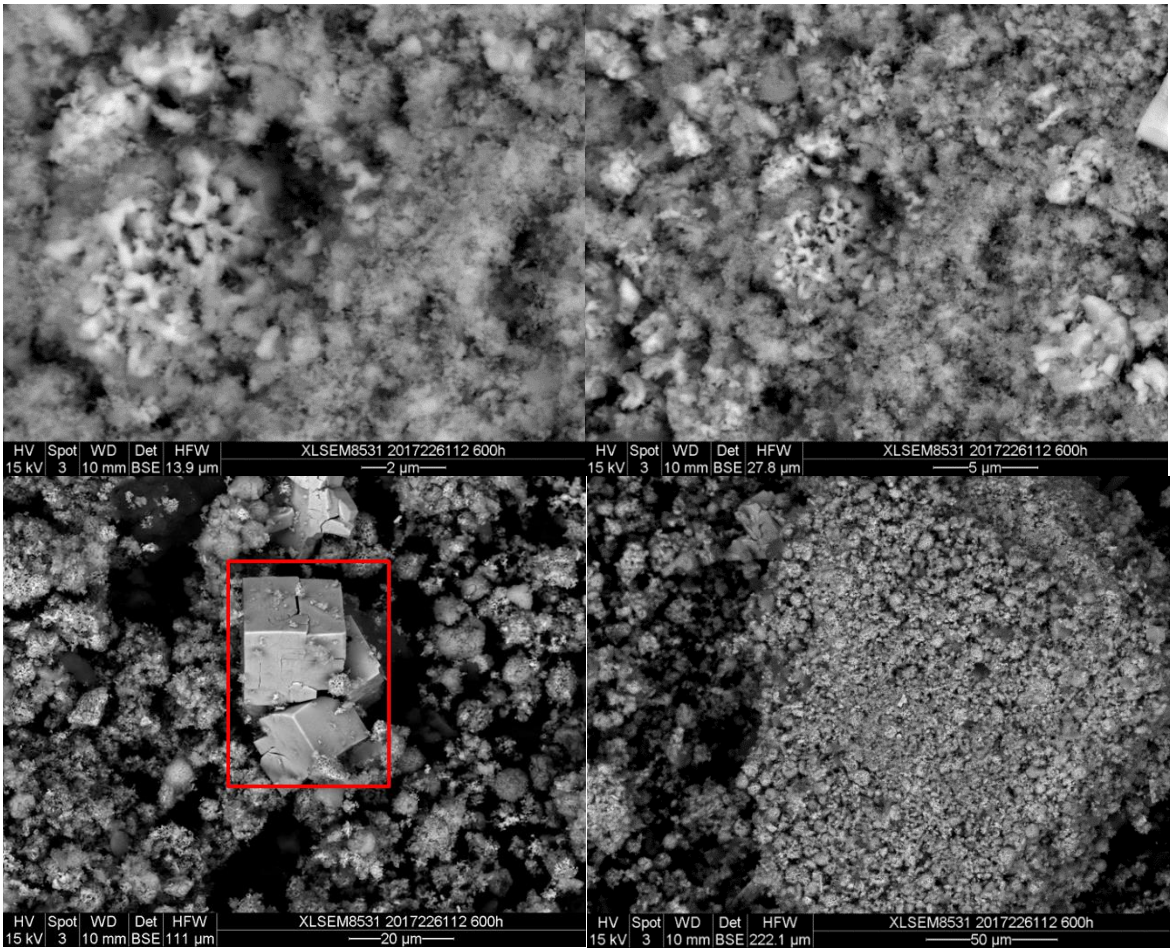

Figure A.17 – SEM images of spent catalyst (TOS = 600 h). Marked crystal is MoO_3.

A-6 STEM

High-angle annular dark-field images and elemental mapping images.

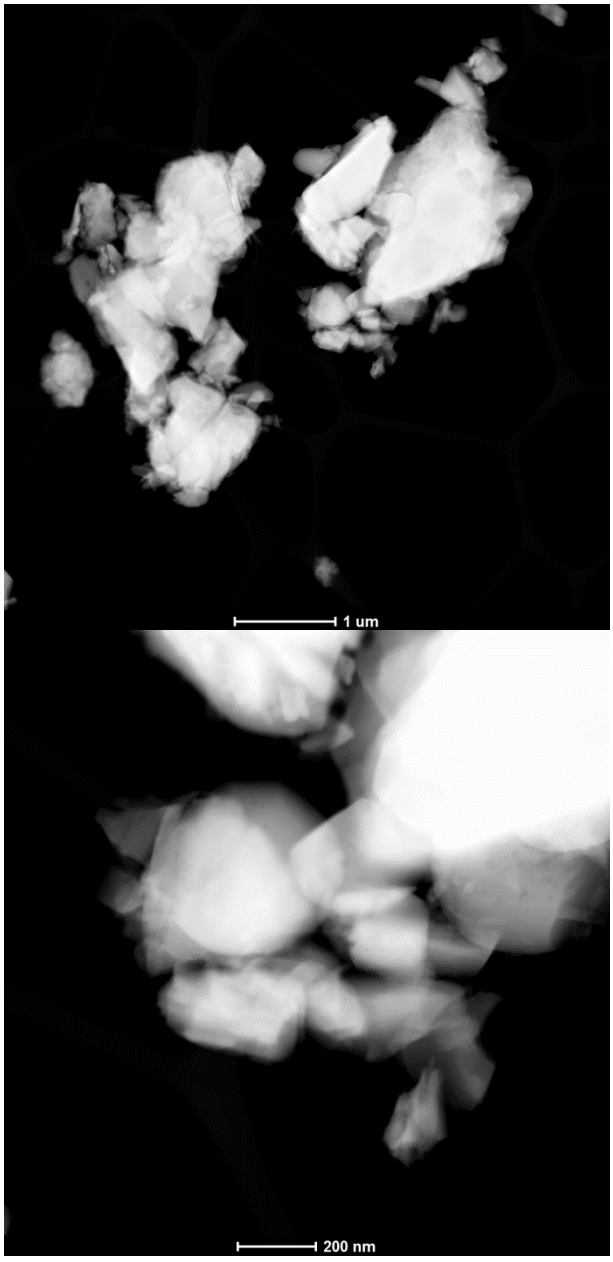

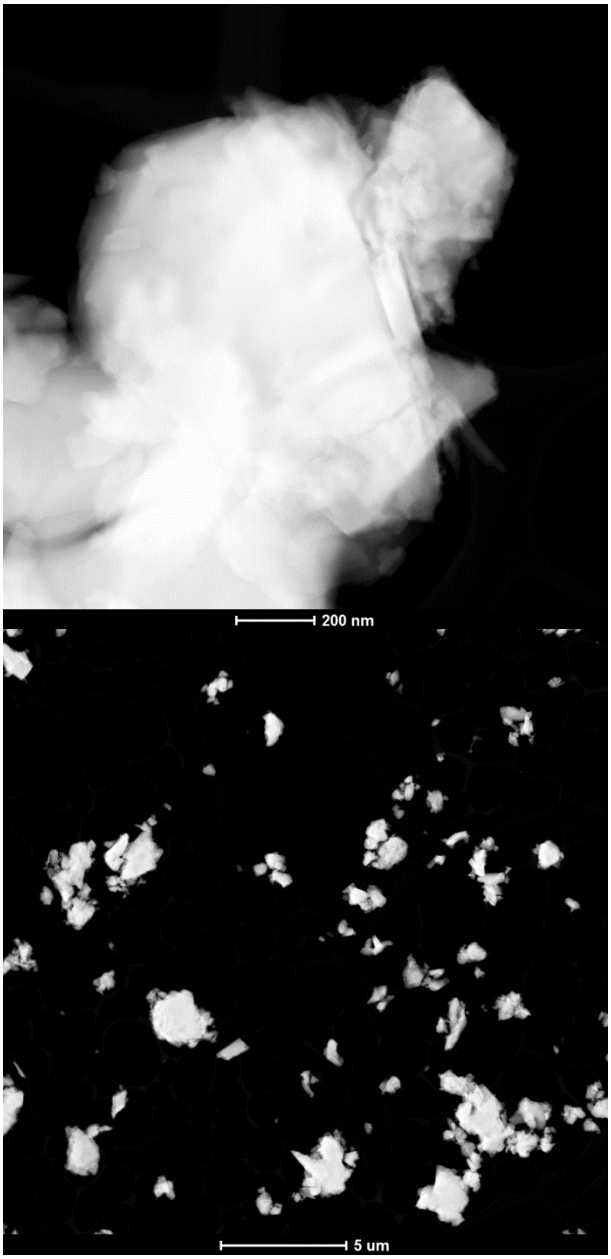

Figure A.18 – STEM-HAADF images of fresh catalyst.

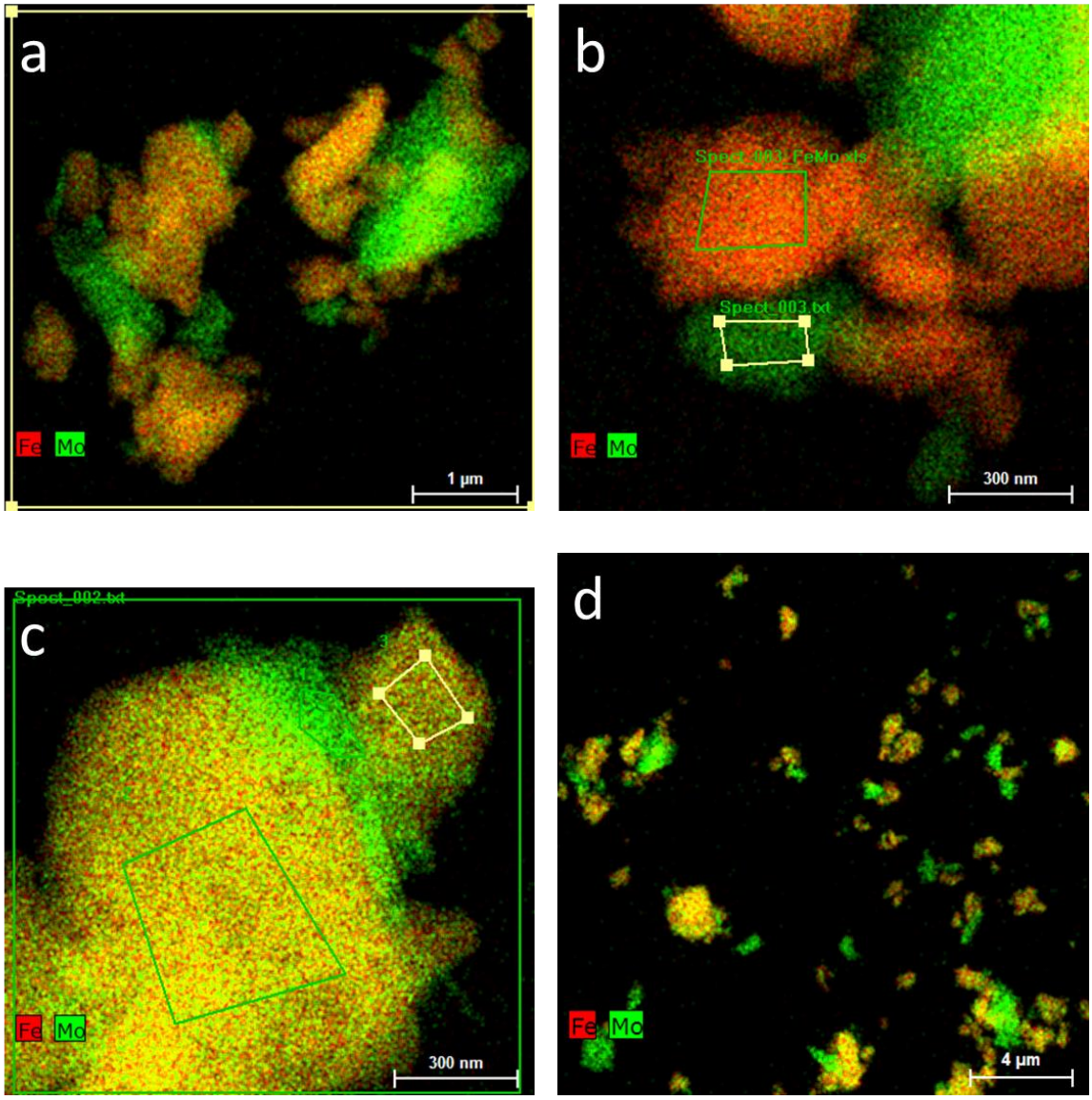

Figure A.19 – STEM elemental mapping of fresh catalyst. Mo/Fe ratio: b: spect_003_FeMo = 1.66 and, b: spect_003 = 64.9, c1 = 14.7, c2 = 1.55 and c3 = 1.64.

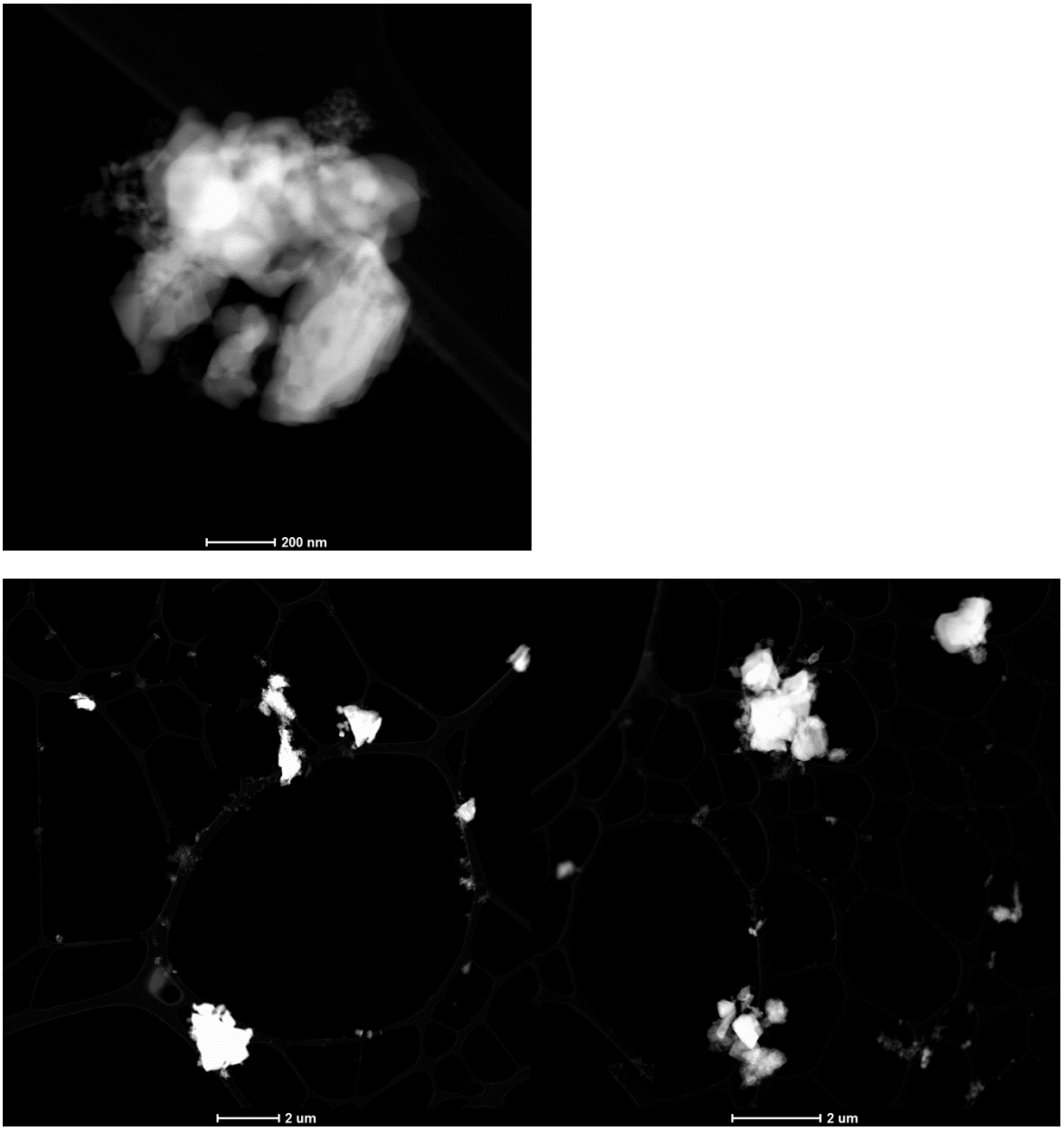

Figure A.20 – STEM-HAADF images of spent catalyst (TOS = 10 h).

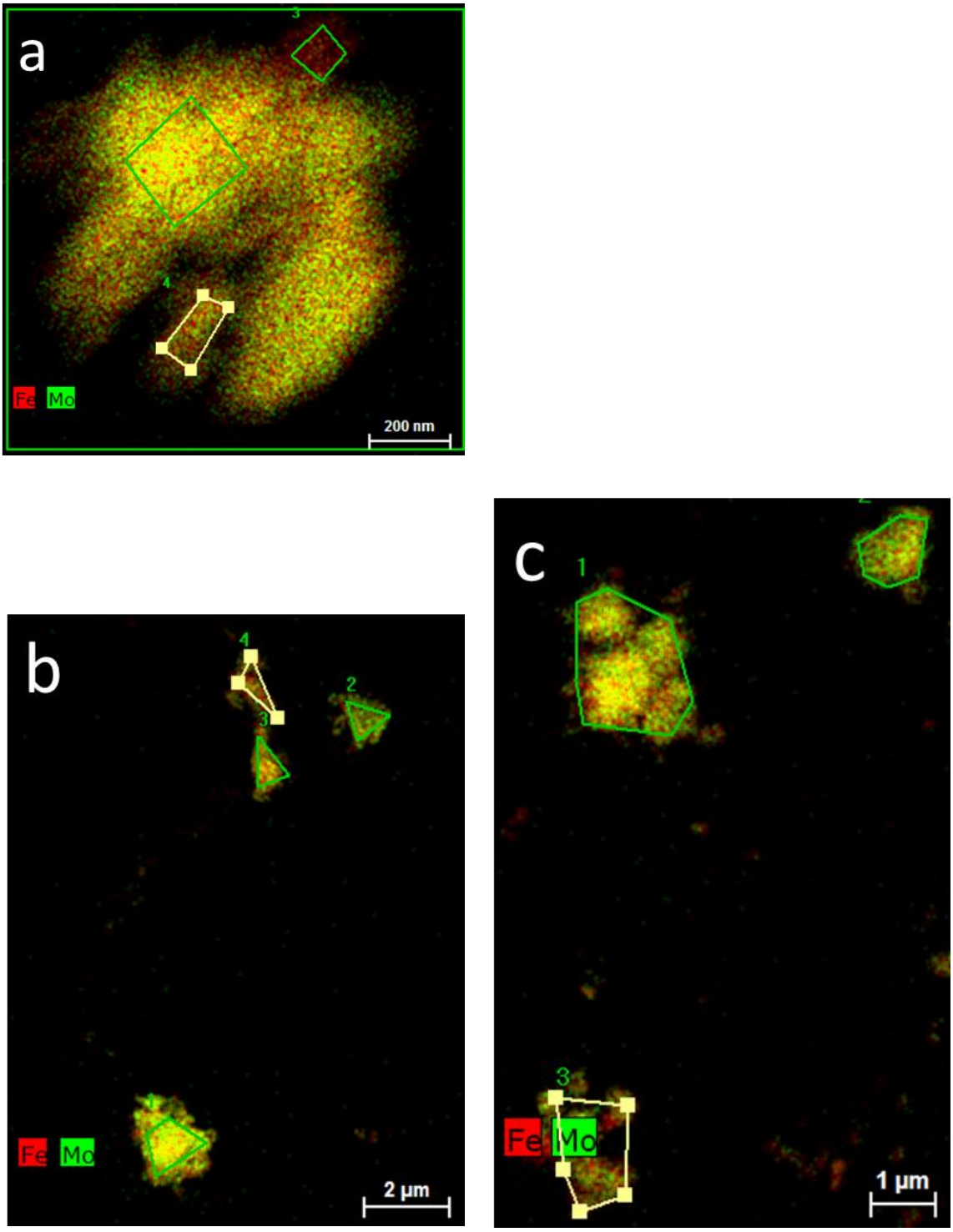

Figure A.21 - STEM elemental mapping of spent catalyst (TOS = 10 h). Mo/Fe ratio: a total = 1.12, a2 = 1.25, a3 = 0.13, a4 = 1.00, b1 = 1.33, b2 = 1.44, b3 = 1.05, b4 = 0.90, c1 = 1.31, c2 = 1.49 and c3 = 1.24.

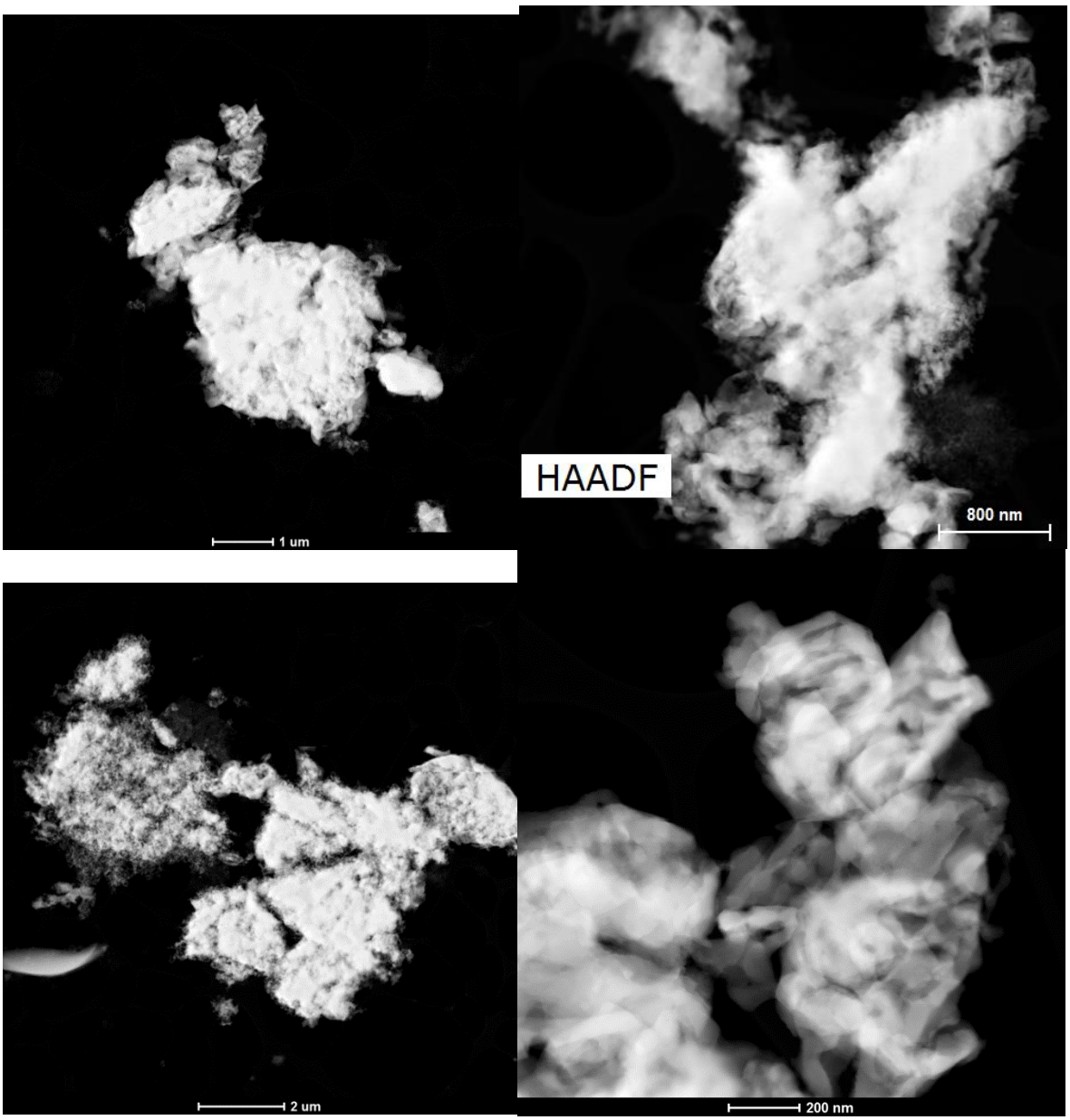

Figure A.22 – STEM-HAADF images of spent catalyst (TOS = 100 h).

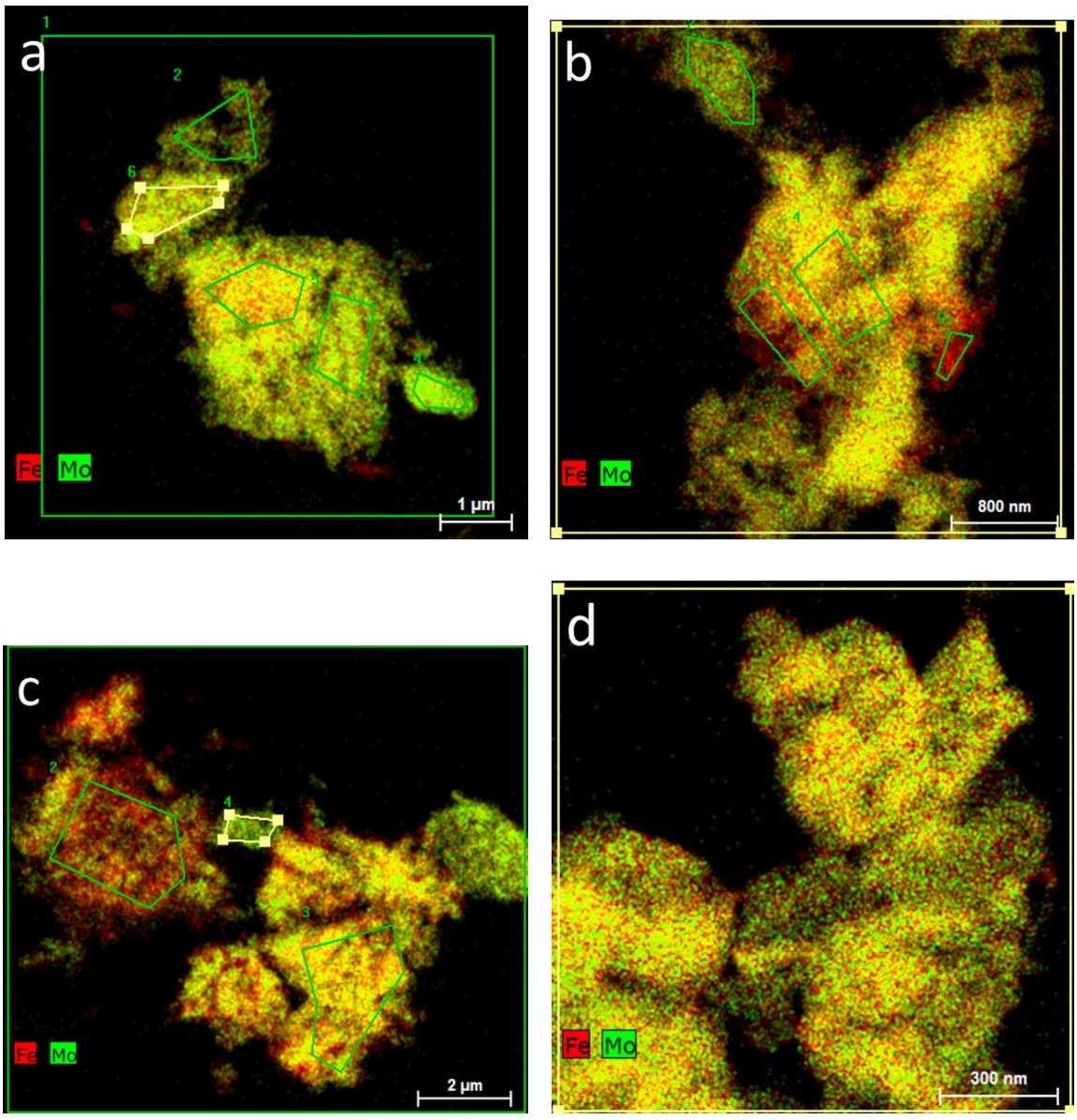

Figure A.23 - STEM elemental mapping of spent catalyst (TOS = 100 h). Mo/Fe ratio: a total = 0.81, a2 = 0.83, a3 = 0.65, a4 = 1.36, a5 = 0.81, a6 = 0.84, b total = 0.68, b2 = 0.92, b3 = 0.45, b5 = 0.057, c total = 0.46, c2 = 0.29, c3 = 0.51, c4 = 0.91, c4 = 0.91 and d total = 0.83.

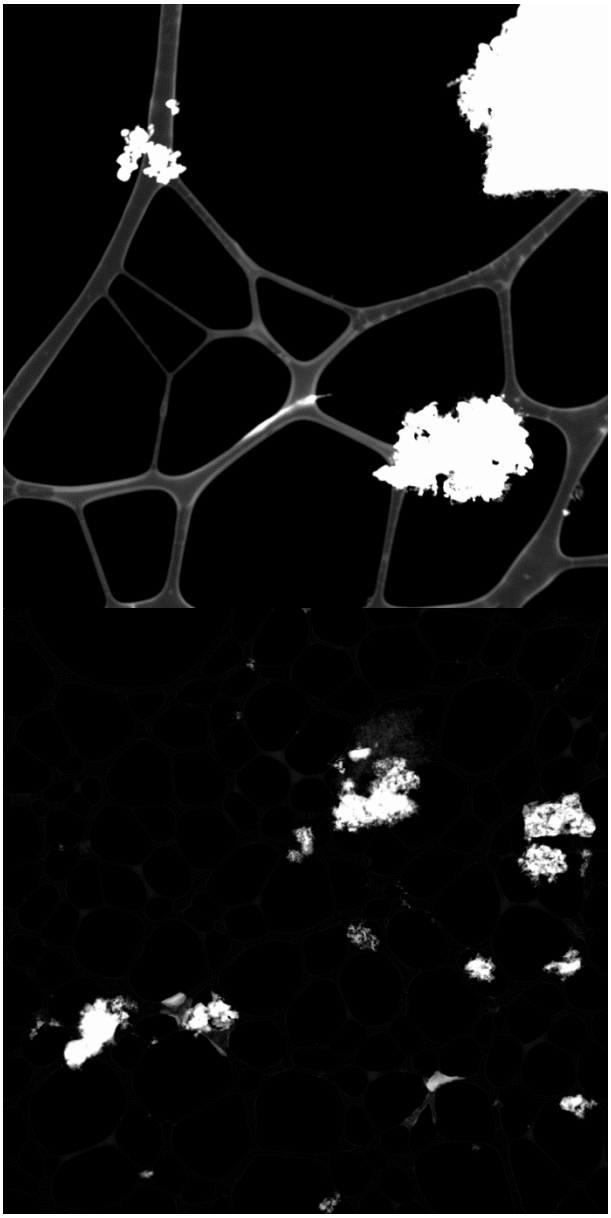

Figure A.24 – STEM-HAADF images of spent catalyst (TOS = 250 h).

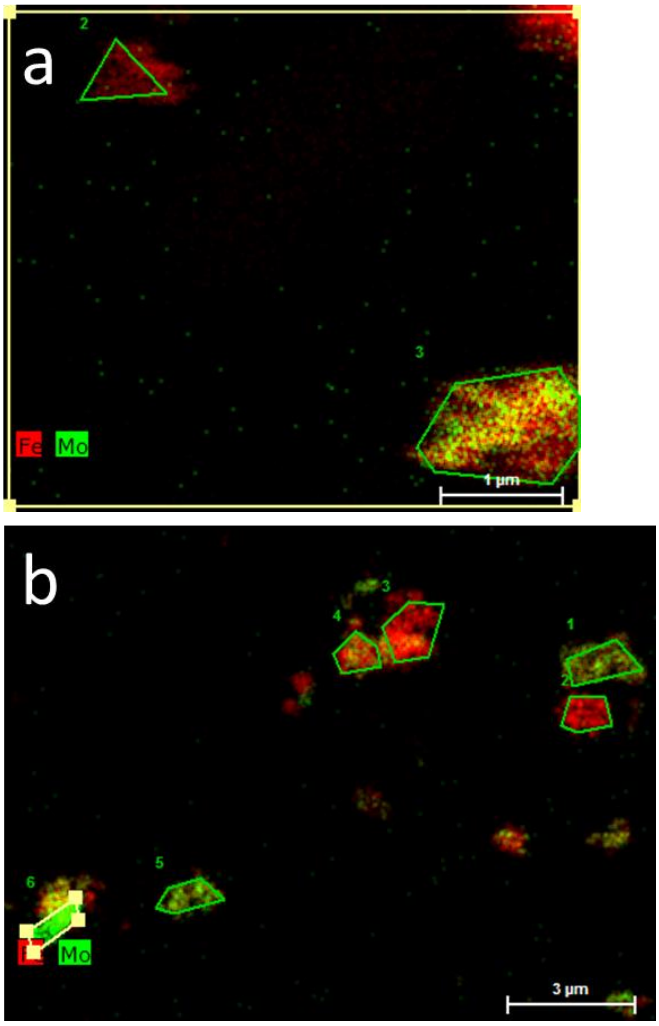

Figure A.25 - STEM elemental mapping of spent catalyst (TOS = 250 h). Mo/Fe ratio: a2 = Fe, a3 = 0.43, b1 = 0.66, b2 = 0.0026, b3 = 0.069, b4 = 0.26, b5 = 0.86 and b6 = 4.42.

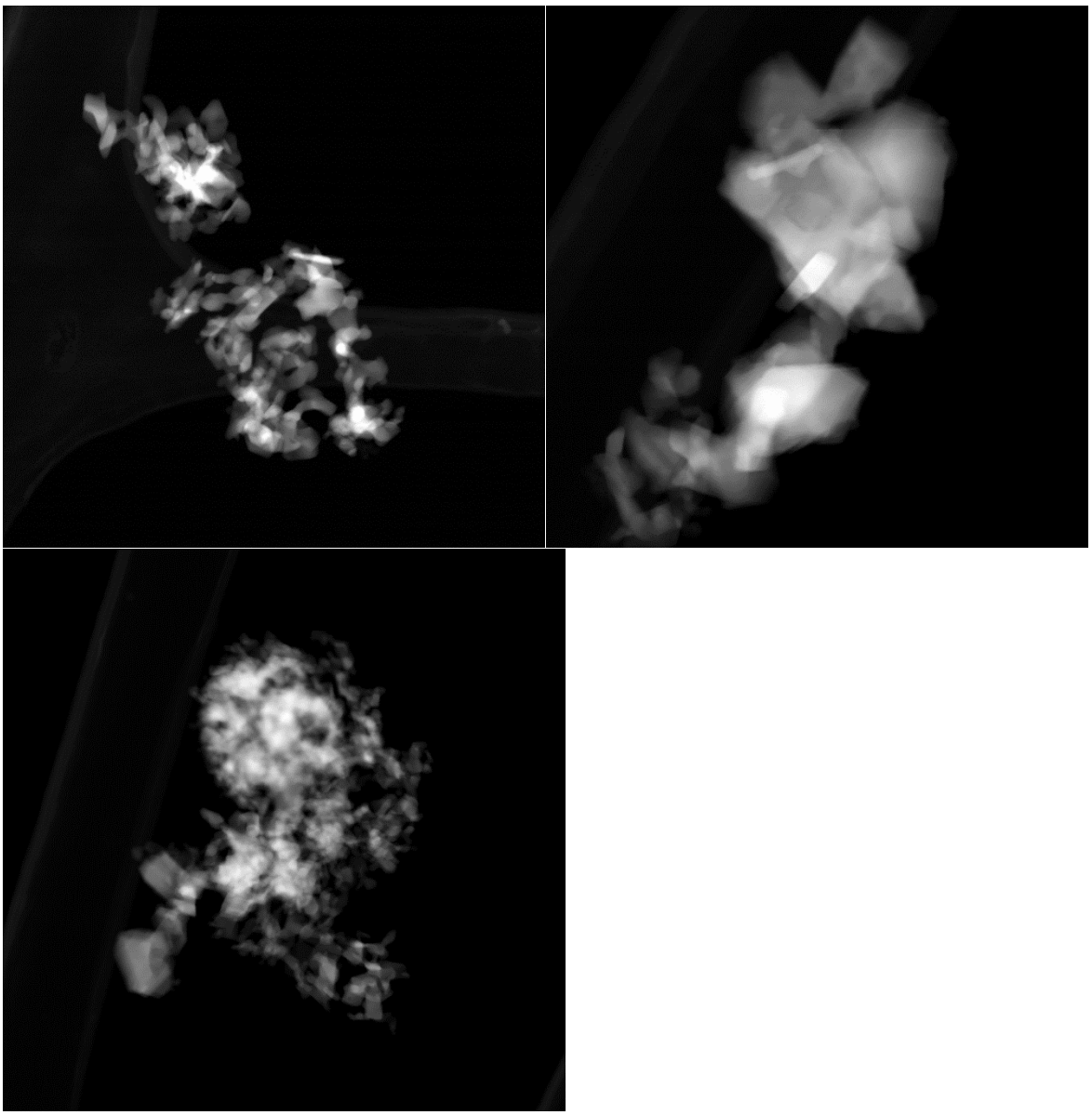

Figure A.26 – STEM-HAADF images of spent catalyst (TOS = 600 h).

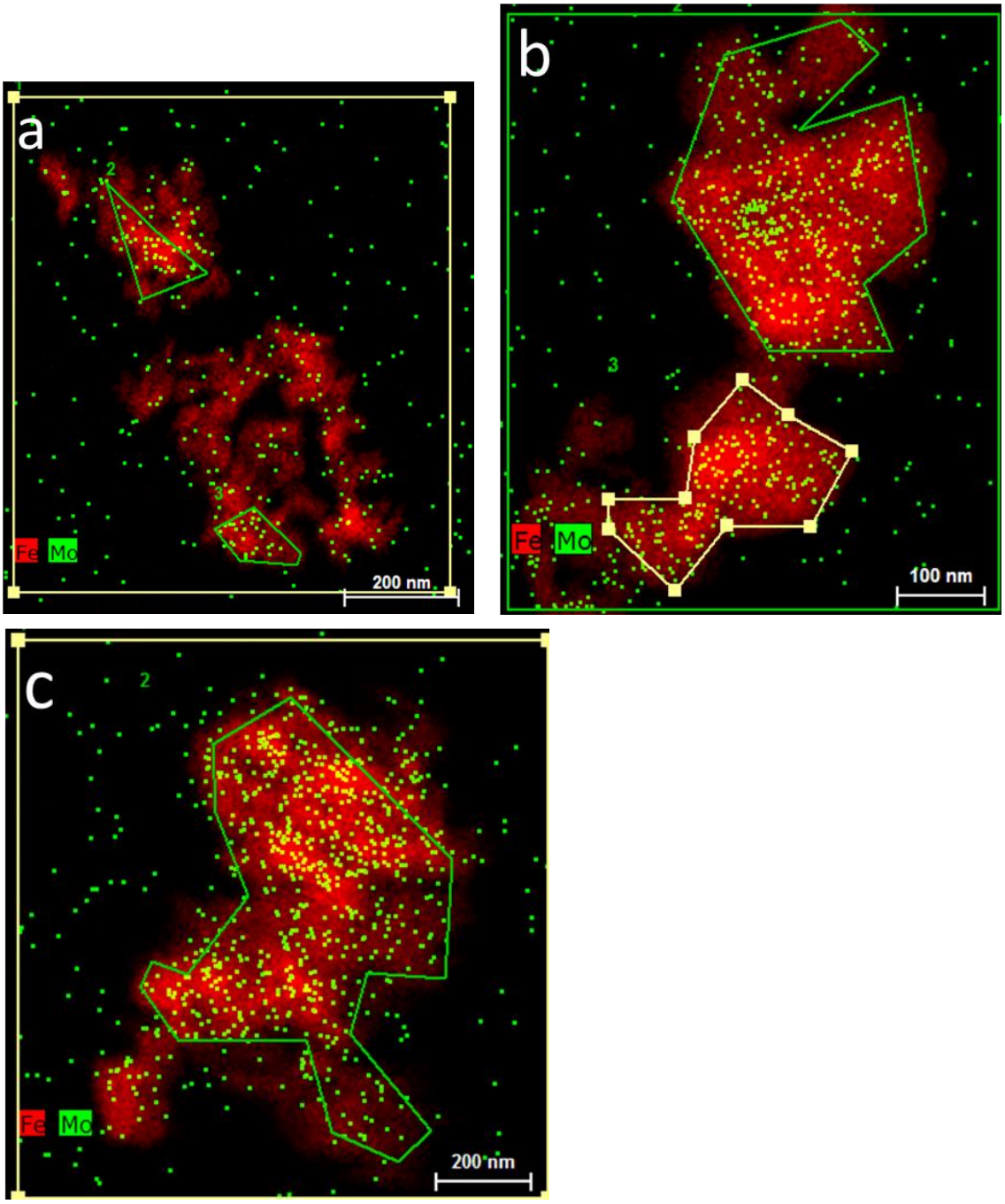

Figure A.27 - STEM elemental mapping of spent catalyst (TOS = 600 h). Mo/Fe ratio: a2 = 0.0094, a3 = 0.0041, b2 = 0.0057, b3 = 0.004 and c2 = 0.0090.

A-7 XPS

Spectra with respect to Molybdenum, Iron and Oxygen.

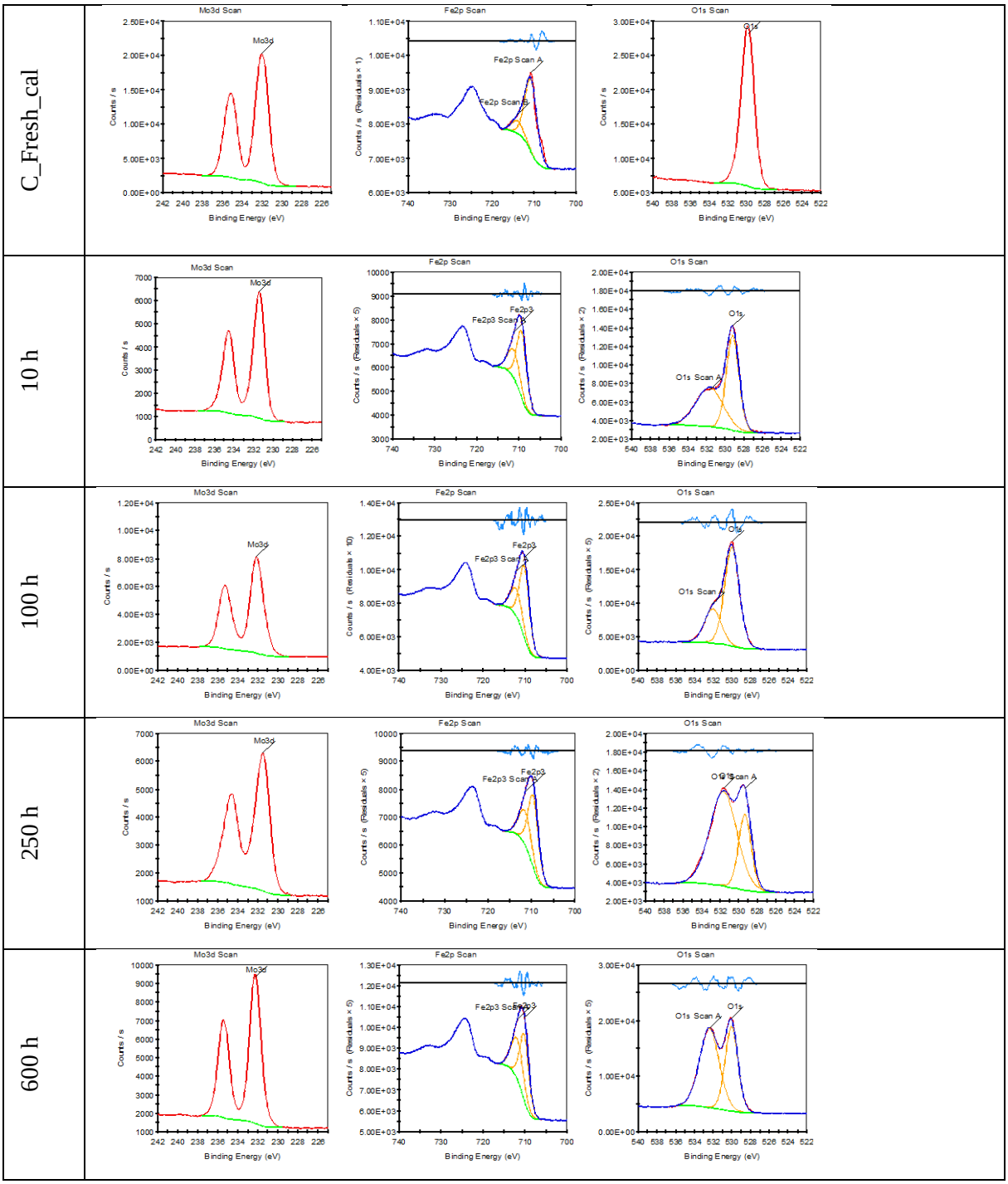

Figure A.28 – XPS spectra with respect to molybdenum, iron and oxygen for fresh and spent catalyst. Shirley background is shown.

Appendix B

B-1 Single pellet reactor setup

Figure B.1 shows the fresh cylindrical shaped industrial iron molybdate pellet. Furthermore, the figure shows the reactor setup where a pellet is slit on a thermocouple and centered in the reactor by two blocks.

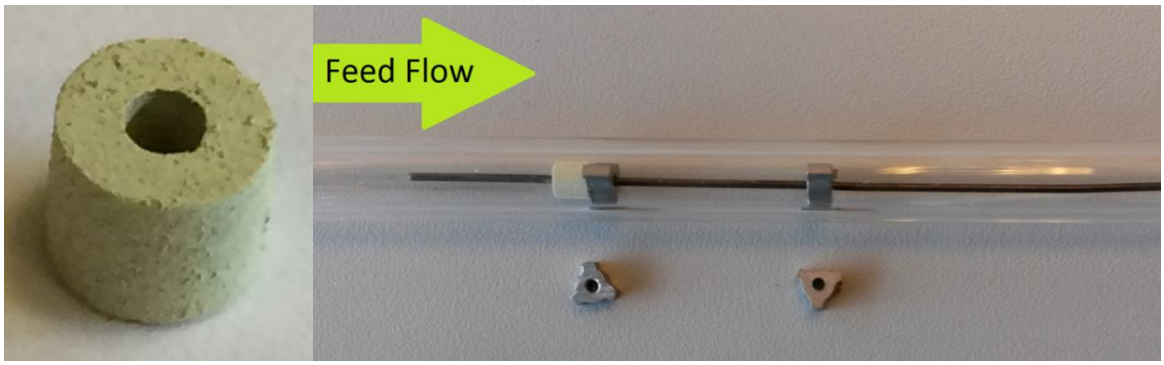

Figure B.1 – Left: Fresh industrial catalyst pellet. Right: Single pellet reactor with pellet in position.

B-2 SEM images and EDS analysis

In the following SEM images and EDS analysis are shown for a fresh and some representative depleted pellets. SEM images where not taken for all the depleted pellets.

Fresh catalyst	
Mo/Fe: Area 1 = 2.86 Area 2 = 2.42	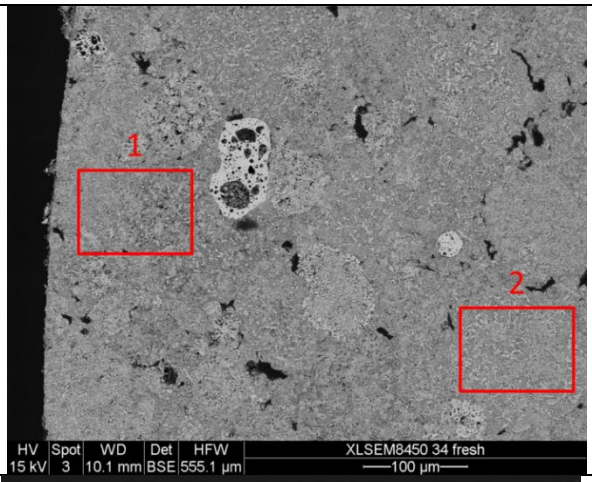
Mo/Fe: Area 1 = 2.43	
*Axial cross section	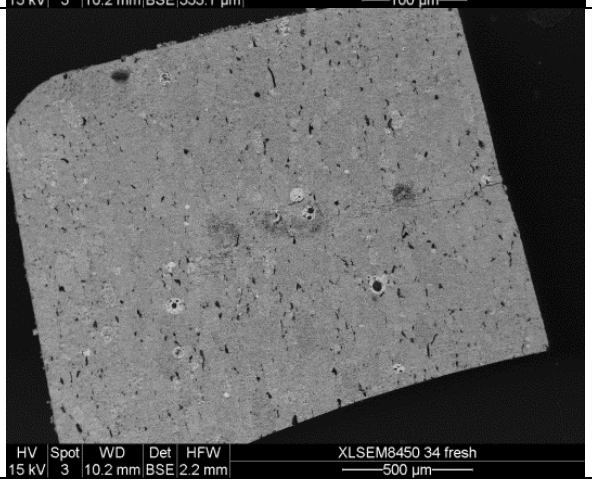

Figure B.2 – SEM-EDS of fresh catalyst pellet.

1 Reaction conditions: MeOH = 4.4 %, H_2O = 0 % O_2 = 10 % in N_2 Temp. = 250 °C	
TOS = 45 hours Mo/Fe Area 1 = 1.61 Area 2 = 2.40	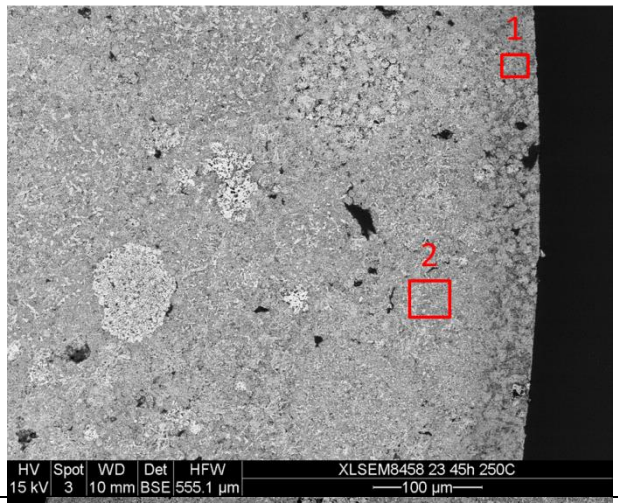
TOS = 78 hours Mo/Fe Area 1 = 1.55 Area 2 = 2.63 Area 3 = 2.63	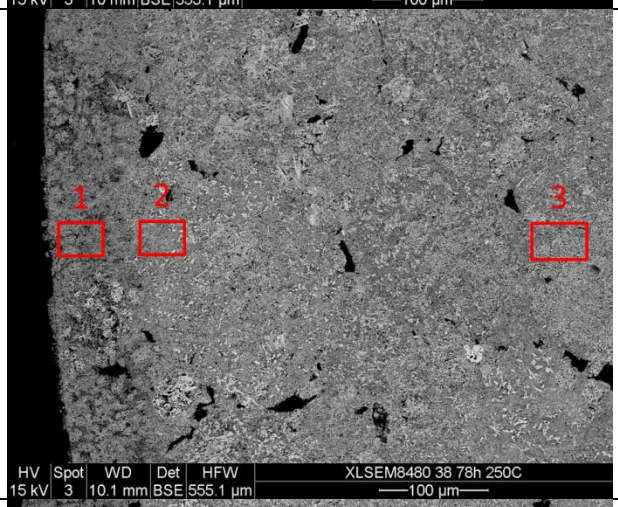
TOS = 122 hours Mo/Fe Area 1 = 1.63 Area 2 = 2.64 Area 3 = 2.42	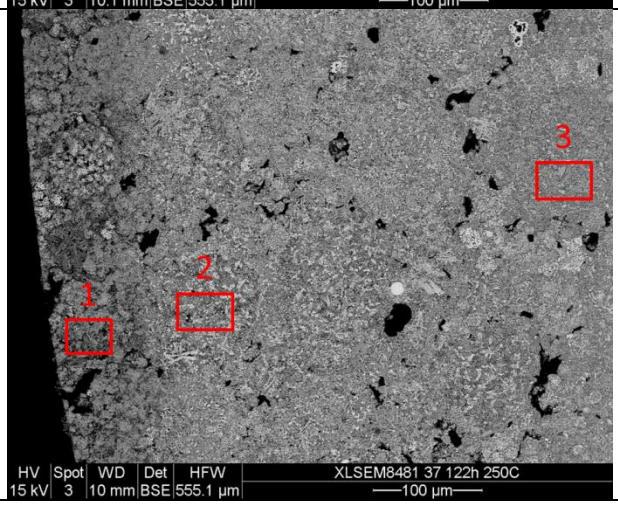

Figure B.3 - SEM-EDS of depleted catalyst pellet: MeOH = 4.4 %, H_2O = 0 % O_2 = 10 % in N_2 Temp. = 250 °C

2 Reaction conditions: MeOH = 4.5 %, H_2O = 0 % O_2 = 10 % in N_2 Temp. = 300 °C	
TOS = 43 hours Mo/Fe Area 1 = 1.53 Area 2 = 1.53 Area 3 = 2.69	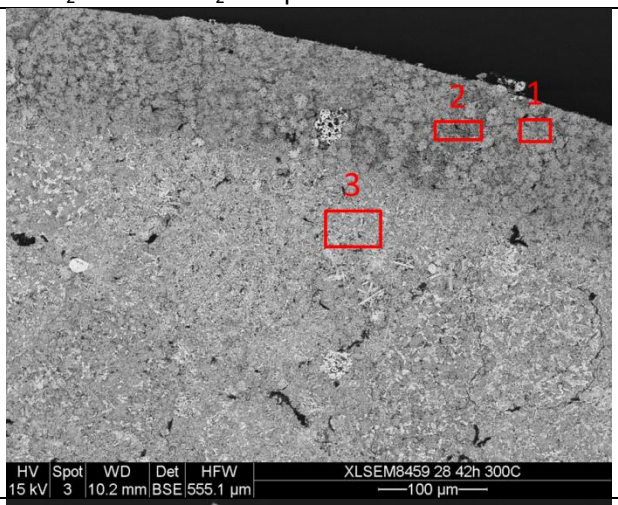
TOS = 43 hours Axial cross section	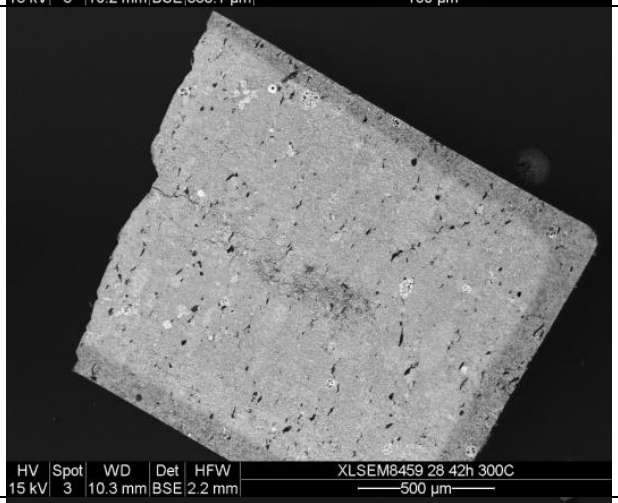
TOS = 71 hours Mo/Fe Area 1 = 1.52 Area 2 = 2.41	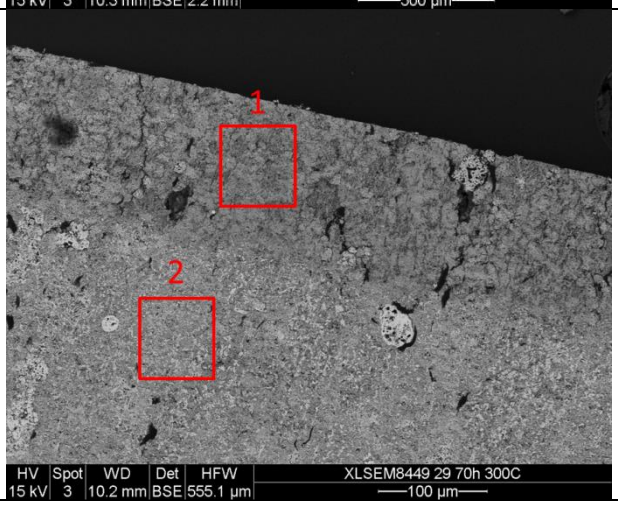

TOS = 136 hours Mo/Fe Area 1 = 1.42 Area 2 = 1.55 Area 3 = 1.66	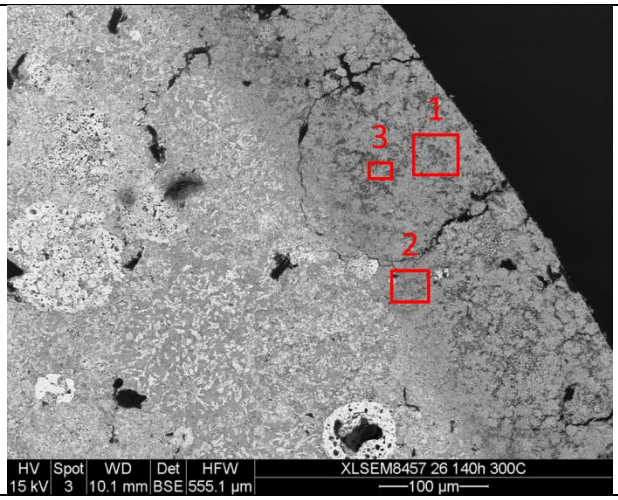

Figure B.4 - SEM-EDS of depleted catalyst pellet: MeOH = 4.5 %, H_2O = 0 % O_2 = 10 % in N_2 Temp. = 300 °C

3 Reaction conditions: MeOH = 4.4 %, H_2O = 0 % O_2 = 10 % in N_2 Temp. = 350 °C	
TOS = 41 hours	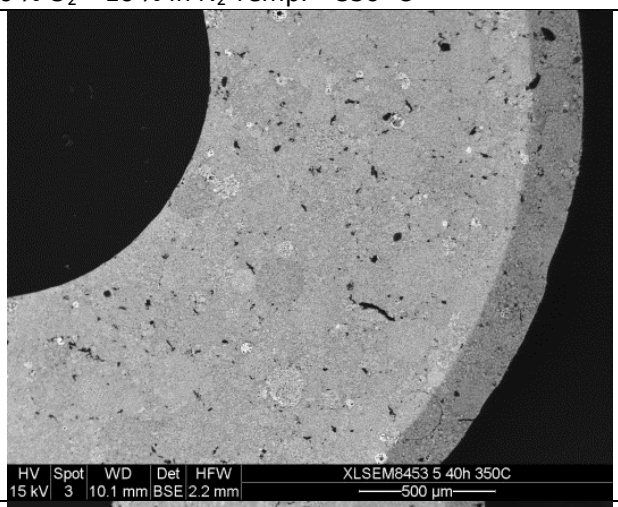
TOS = 41 hours Axial cross section	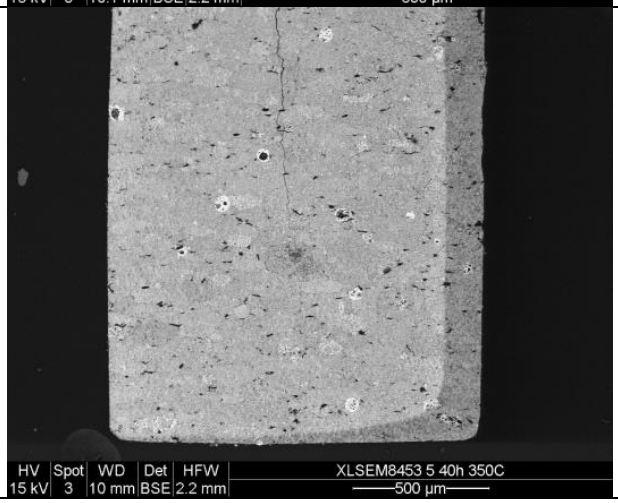

TOS = 71 hours	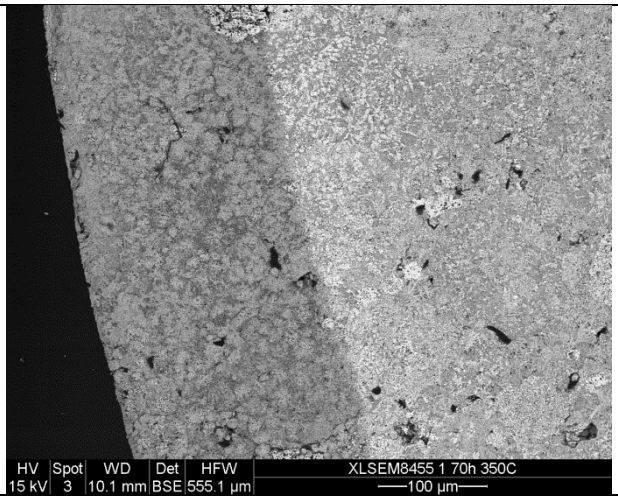
TOS = 159 hours Mo/Fe Area 1 = 1.06 Area 2 = 1.18 Area 3 = 3.03 Area 4 = 2.51	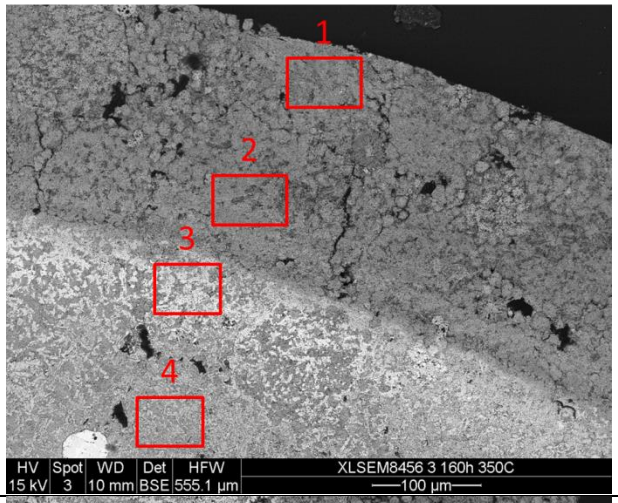
TOS = 238 hours Mo/Fe Area 1 = 1.04 Area 2 = 2.92 Area 3 = 2.88	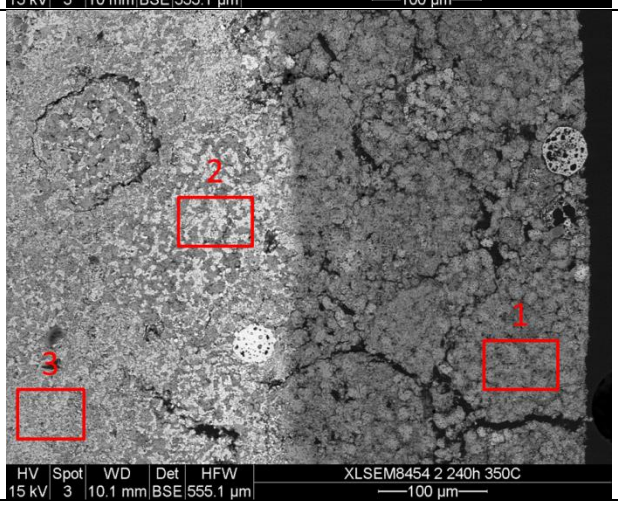

Figure B.5 - SEM-EDS of depleted catalyst pellet: MeOH = 4.4 %, H_2O = 0 % O_2 = 10 % in N_2 Temp. = 350 °C

4 Reaction conditions: MeOH = 4.0 %, H_2O = 4.1 % O_2 = 10 % in N_2 Temp. = 300 °C	
TOS = 102 hours	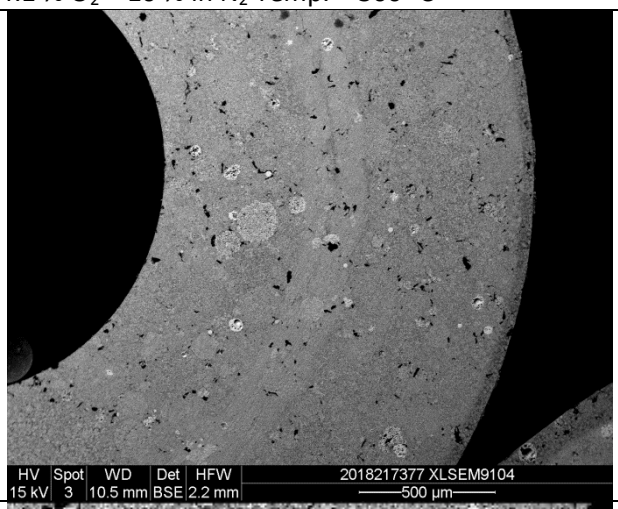
TOS = 102 hours Mo/Fe Area 1 = 1.73 Area 2 = 2.65 Area 3 = 2.54	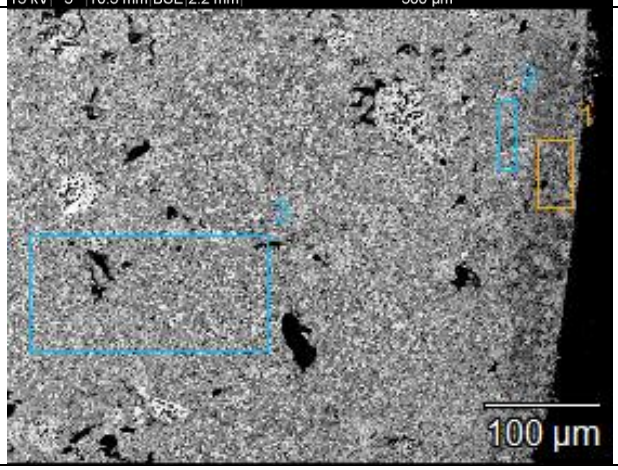

Figure B.6 - SEM-EDS of depleted catalyst pellet: MeOH = 4.0 %, H_2O = 4.1 % O_2 = 10 % in N_2 Temp. = 300 °C

5 Reaction conditions: MeOH = 3.99 %, H_2O = 10.17 % O_2 = 10 % in N_2 Temp. = 301 °C	
TOS = 73 hours Mo/Fe Area 1 = 1.61 Area 2 = 1.56 Area 3 = 1.60 Area 4 = 2.82 Area 5 = 2.65	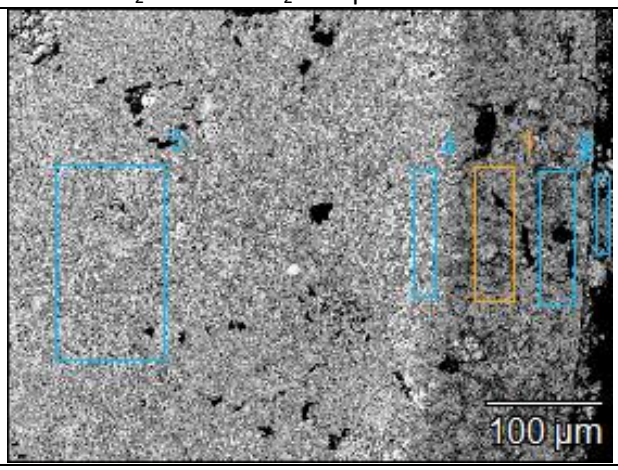

Figure B.7 - SEM-EDS of depleted catalyst pellet: MeOH = 3.99 %, H_2O = 10.17 % O_2 = 10 % in N_2 Temp. = 301 °C

6 Reaction conditions: MeOH = 1.6 %, H_2O = 0 % O_2 = 10 % in N_2 Temp. = 300 °C	
TOS = 67 hours	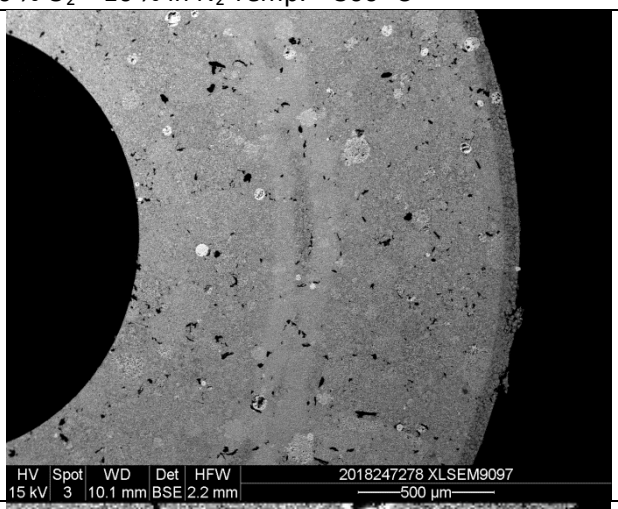
TOS = 67 hours Mo/Fe Area 1 = 1.71 Area 2 = 2.28 Area 3 = 2.56	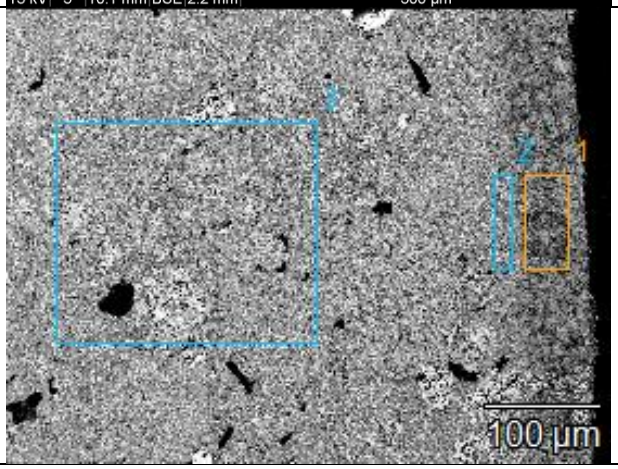

Figure B.8 - SEM-EDS of depleted catalyst pellet: MeOH = 1.6 %, H_2O = 0 % O_2 = 10 % in N_2 Temp. = 300 °C

9 Reaction conditions: MeOH = 4.2 %, H_2O = 9.3 % O_2 = 10 % in N_2 Temp. = 350 °C	
TOS = 73 hours	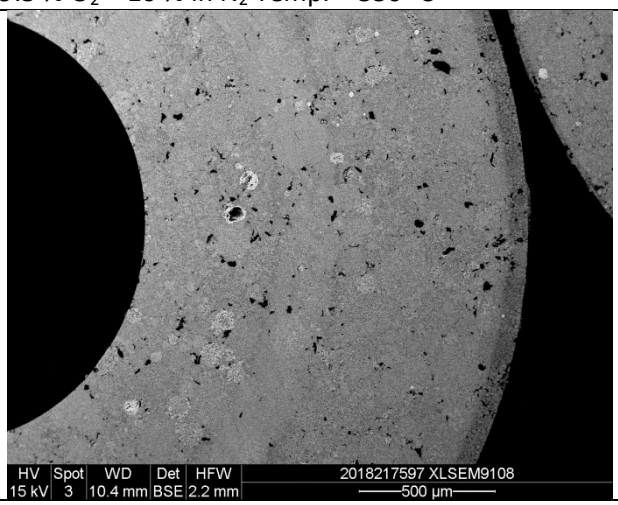

Figure B.9 - SEM-EDS of depleted catalyst pellet: MeOH = 4.2 %, H_2O = 9.3 % O_2 = 10 % in N_2 Temp. = 350 °C

11 Reaction conditions: MeOH = 1.7 %, H_2O = 0 % O_2 = 10 % in N_2 Temp. = 350 °C	
TOS = 122 hours	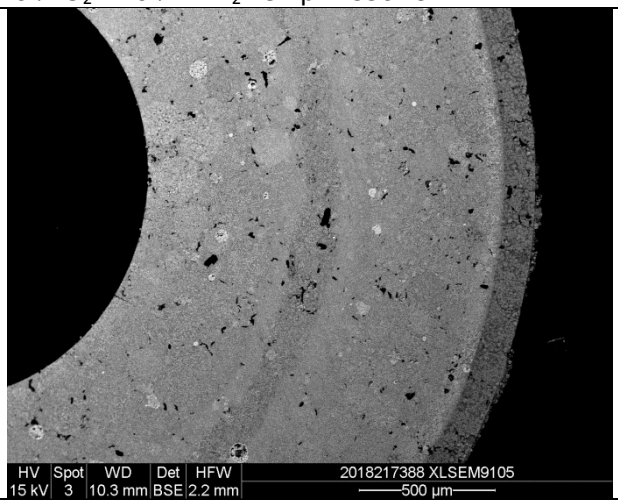

Figure B.10 - SEM-EDS of depleted catalyst pellet: MeOH = 1.7 %, H_2O = 0 % O_2 = 10 % in N_2 Temp. = 350 °C

12 Reaction conditions: MeOH = 3.3 %, H_2O = 0 % O_2 = 2.5 % in N_2 Temp. = 300 °C	
TOS = 288 hours	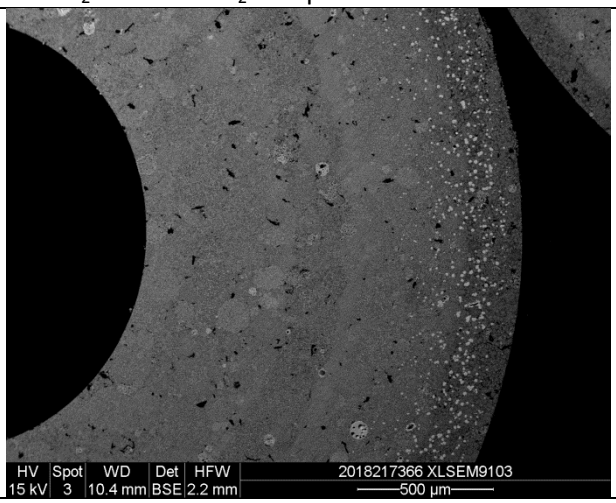

Figure B.11 - SEM-EDS of depleted catalyst pellet: MeOH = 3.3 %, H_2O = 0 % O_2 = 2.5 % in N_2 Temp. = 300 °C

13 Reaction conditions: MeOH = 3.8 %, H_2O = 0 % O_2 = 10 % in N_2 Temp. = 300 °C	
TOS = 27 hours Mo/Fe Area 1 = 1.67 Area 2 = 2.85 Area 3 = 2.65	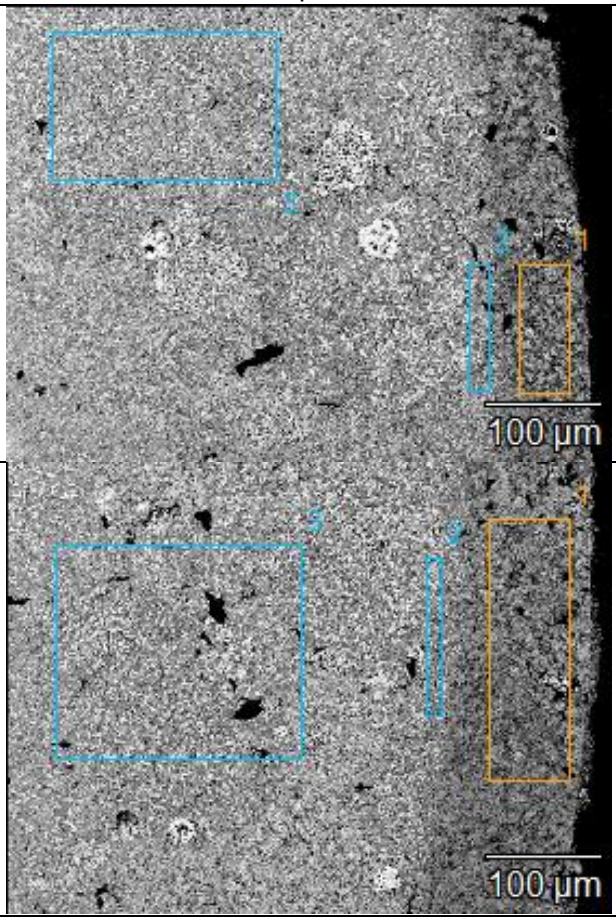
TOS = 68 hours Mo/Fe Area 1 = 1.63 Area 2 = 2.48 Area 3 = 2.62	

TOS = 167 hours Mo/Fe Area 1 = 1.66 Area 2 = 2.46 Area 3 = 2.63 Area 4 = 2.58	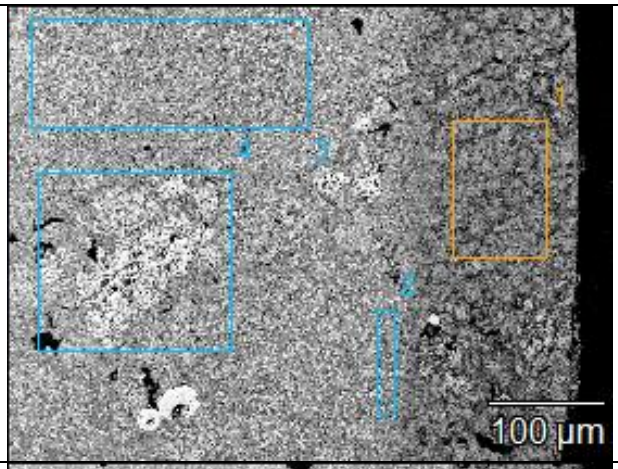
TOS = 289 hours Mo/Fe Area 1 = 1.67 Area 2 = 2.86 Area 3 = 2.58 Area 4 = 2.72 Area 5 = 2.65	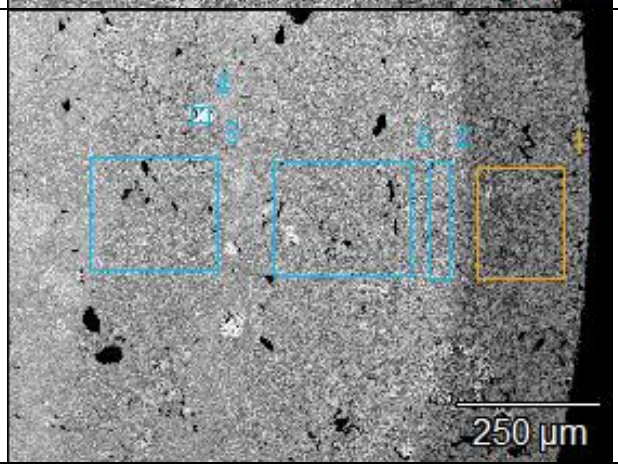

Figure B.12 - SEM-EDS of depleted catalyst pellet: MeOH = 3.8 %, H_2O = 0 % O_2 = 10 % in N_2 Temp. = 300 °C

B-3 X-ray micro computed tomography

Figure B.13 shows cross-sections obtained by virtual cutting of the 3D data recorded with X-ray micro computed tomography (µ-CT) on the full pellet. The cross-sections are taken at positions ranging from ¼ to ¾ through a spent pellet starting at the position closest to the reactor inlet. The reaction conditions for this studied pellet were TOS: 64 h, 350 °C, MeOH = 4.4 %, H_2O = 0 % O_2 = 10 % in N_2. The depletion layer on the outer surface is clearly visible and a negligible depletion on the inner surface can be observed at ¼ height. Furthermore, the depletion layer shows approximately the same thickness all around at the pellet outer surface.

A tomography movie of the pellet shown in Figure B.13 is available for download with the ESI.

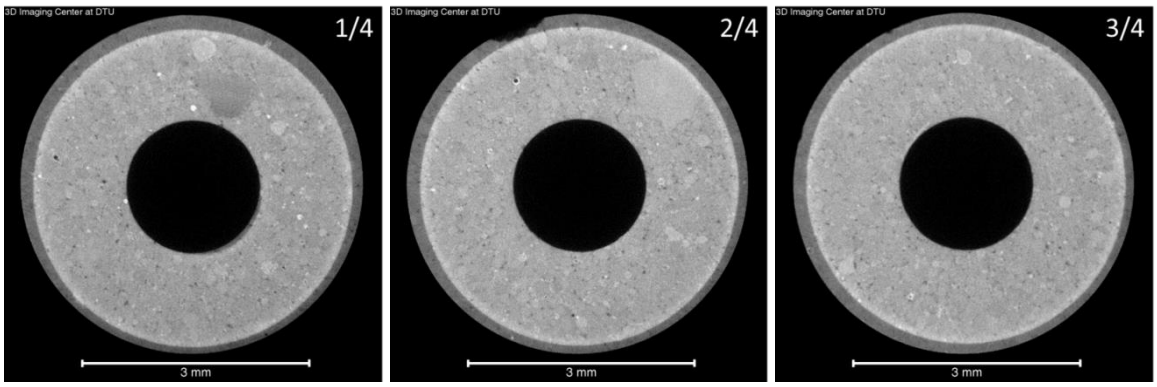

Figure B.13 – Cross-sections of 3D µ-CT data at heights ranging from ¼ to ¾ through height of a spent pellet. ¼ refers to a cut at ¼ of the full pellet height seen from the position closest to the reactor inlet, while ¾ refers to a cut ¼ away from the pellet position closest to the reactor outlet (Conditions: 4.4 % MeOH, 0 % H_2O, 10 % O_2 in N_2, 350 °C and TOS = 64 hours).

B-4 Mass loss measurements at varying oxygen concentration

Figure B.14 Shows that there is no clear effect by decreasing the O_2 concentration from 10 % to 2.5 %.

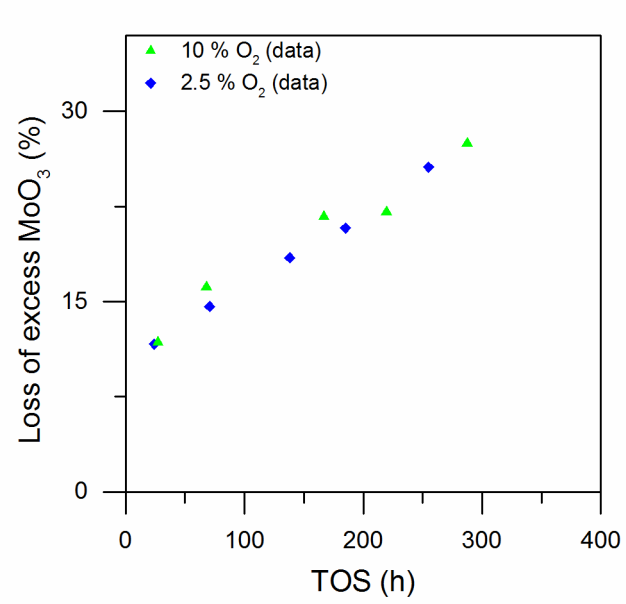

Figure B.14 – Mass loss of excess MoO_3 in pellet at increasing TOS shown for two different O_2 contents. Mo/Fe = 2.6. Flow rate = 3000 ml/min (1 bar, 273.15 K). At O_2 = 10 %: MeOH 3.75 %, H_2O = 0 % in N_2 at 302 °C. At O_2 = 2.5 %: MeOH = 3.50 %, H_2O = 0 % in N_2 at 301

B-5 Detailed derivation of single pellet model

For the concentration of components in the particle, a shell balance can be set up over the pellet. The pellet has a cylindrical shape with a hole in the middle. However, the balance is set up assuming an infinite cylindrical shape, with no influence from the top and bottom surface. r is the position where 0 is at the center of the cylindrical pellet, R_h is at the inner surface of the pellet and R_p is at the outer surface of the pellet. The balance is done from r to $r+\Delta r$ with the face area S ($2r\cdot\pi\cdot L$) during the time Δt. In the volume $S\Delta r$ reaction takes place over the catalyst and the concentration changes in the free volume of the pellet ($S\Delta r\varepsilon(r)$) in time Δt:

$$j_i\big|_r S\Delta t - j_i\big|_{r+\Delta r} S\Delta t + r_i S\Delta r\Delta t = (C_i\big|_{t+\Delta t} - C_i\big|_t)S\Delta r\varepsilon(r) \tag{B.1}$$

The flux of component i can be calculated by Fick's first law:

$$j_i = -D_{AB}\frac{dC_i}{dr} \tag{B.2}$$

Due to the porous nature of the catalyst pellet the diffusion coefficient is replaced by the effective diffusivity given by:

$$D_e = D_{AB}\frac{\varepsilon}{\tau} \tag{B.3}$$

As Mo is volatilized and removed from the catalyst the porosity will change. The porosity can be estimated from the volume of the excess MoO_3 as follows:

$$\varepsilon = \varepsilon^0 + \frac{\left(C^0_{MoO_3} - C_{MoO_3}\right)M_{MoO_3}}{\rho_{MoO_3}} \tag{B.4}$$

The effective diffusion coefficient (B.3) is dependent on the porosity. The effect of the changing porosity can be written as:

$$D_e = D_e^0\frac{\varepsilon(r)}{\varepsilon^0} \tag{B.5}$$

By inserting (B.2)-(B.5) in (B.1) and dividing with $S\Delta r\Delta t$ and setting the limits as $\Delta r \to 0$ and $\Delta t \to 0$, the equation becomes:

$$\frac{\partial\left(D_{e,i}^{0} \frac{\varepsilon(r)}{\varepsilon^{0}} \frac{\partial C_i}{\partial r}(r) \right)}{\partial r} + r_i = \frac{\partial C_i}{\partial t}\varepsilon(r) \tag{B.6}$$

Equation (B.6) can be rewritten as follows:

$$\frac{D_{e,\mathrm{i}}^{0}}{\varepsilon^{0}} \frac{\partial C_i}{\partial r} \frac{\partial \varepsilon}{\partial r} + \frac{D_{e,\mathrm{i}}^{0}}{\varepsilon^{0}} \frac{\partial^2 C_i}{\partial r^2}\varepsilon(r) + \frac{1}{(r)} \frac{D_{e,\mathrm{i}}^{0}}{\varepsilon^{0}} \frac{\partial C_i}{\partial r}\varepsilon(r) + r_i = \frac{\partial C_i}{\partial t}\varepsilon(r) \tag{B.7}$$

B-5.1 Dimensionless form

The single pellet model (table 3.1) equations (2.3-2.11) can be written in a dimensionless form upon introduction of the following dimensionless parameters:

$$\tau = \frac{t}{t_0},\ t_0 = \frac{L_p^2 \varepsilon^0}{D_{e,Ref}},\ z = \frac{r - R_h}{L_p}\ ,\ \tilde{C}_i = \frac{C_i}{C_{MeOH}^{b}},\ \tilde{r}_{hole} = \frac{R_h}{L_p}, L_p = R_p - R_h \tag{B.8)(B.9)(B.10) (B.11)(B.12) (B.13}$$

$$D_{e,i} = \frac{D_{e,i}}{D_{e,Ref}},\ \varphi_{MeOH} = L_p \sqrt{\frac{k_{MeOH}\rho_{FeMo}\varepsilon^0}{D_{e,MeOH,Ref}}} \tag{B.14)(B.15}$$

$$\varphi_{+} = L_p \sqrt{\frac{k^{+} C_{MeOH}^{b} \varepsilon^0}{D_{e,MeOH,Ref}}},\ \varphi_{-} = L_p \sqrt{\frac{k^{-}\varepsilon^0}{D_{e,MeOH,Ref}}} \tag{B.16)(B.17}$$

The system becomes:

Table B.1 – Equations in dimensionless forms for calculation of the profiles in the pellet with respect to MeOH, H_2O, volatile Mo species and solid MoO_3.

Profile	
$D_{e,i}\frac{\partial C_i}{\partial z}\frac{\partial \varepsilon}{\partial z}+D_{e,i}\frac{\partial^2 C_i}{\partial z^2}\varepsilon(z)+\frac{D_{e,i}}{\tilde{r}_{hole}+z}\frac{\partial C_i}{\partial z}\varepsilon(z)+\tilde{r}_i=\frac{\partial C_i}{\partial \tau}\varepsilon(z)$	(B.18)

Rate of formation	
$\tilde{r}_{MeOH}=-\frac{\varphi_{MeOH}^2 C_{MeOH}}{1+k_1 C_{MeOH}+k_2 C_{H_2O}}$	(B.19)
$\tilde{r}_{H_2O}=\frac{\varphi_{MeOH}^2 C_{MeOH}}{1+k_1 C_{MeOH}+k_2 C_{H_2O}}$	(B.20)
$\tilde{r}_{Mo(g)}=\frac{\varphi_{+}^2 a_{MoO_3} C_{MeOH}^{n_{MeOH}}}{1+K_3 C_{H_2O}}-\varphi_{-}^2 C_{Mo(g)}^{n_{Mo(g)}}$	(B.21)
$\tilde{r}_{MoO_3}=-\frac{\varphi_{+}^2 a_{MoO_3} C_{MeOH}^{n_{MeOH}}}{1+K_3 C_{H_2O}}+\varphi_{-}^2 C_{Mo(g)}^{n_{Mo(g)}}$	(B.22)

Boundary conditions for MeOH, H_2O and Mo(g)	
$C_i(\tau,1)=1$	(B.23)
$\frac{\partial C_i(\tau,0)}{\partial z}=0$	(B.24)

Initial conditions for MeOH, H_2O and Mo(g)	
$C_i(\tau=0,z)=0$	(B.25)

Initial conditions for MoO_3	
$C_i(\tau=0,z)=1$	(B.26)

B-5.2 Discretization (Method of Lines)

The single pellet system is solved using the method of lines to discretize the derivatives with respect to distance (z) into $N+1$ steps $\left(\Delta z = \frac{1}{N}\right)$. At the boundaries ($z=0$ and $z=1$) the values are known from the boundary conditions.

The derivative with respect to the position (z) is calculated by the expressions:

$$\frac{dC_{A,\mathrm{i}}}{dz} = \frac{C_{A,i+1} - C_{A,i-1}}{2\Delta z}, \quad \frac{d^2C_{A,\mathrm{i}}}{dz^2} = \frac{C_{A,i+1} - 2C_{A,i} + C_{A,i-1}}{(\Delta z)^2} \tag{B.27) (B.28}$$

Since the porosity at a given position is a function of the MoO_3 concentration $\left(C_{MoO_3}\right)$ the porosity is discretized as follows:

$$\varepsilon_i = \varepsilon^0 + (1 + C_{MoO_3,i})\beta_{MoO_3} \Rightarrow$$
$$\frac{d\varepsilon_i}{dz} = \frac{\varepsilon^0 + (1 - C_{MoO_3,i+1})\beta_{MoO_3} - \varepsilon^0 + (1 - C_{MoO_3,i-1})\beta_{MoO_3}}{2\Delta z} = \beta_{MoO_3}\frac{C_{MoO_3,i-1} - C_{MoO_3,i+1}}{2\Delta z} \tag{B.29}$$

Where β_{MoO_3} is the dimensionless parameter:

$$\beta_{MoO_3} = \frac{C^0_{MoO_3} M_{MoO_3}}{\rho_{MoO_3}} \tag{B.30}$$

Discretized boundary conditions

For the first discretized boundary condition the concentration at $C_{A,N+1}$, is equal to the known bulk concentration of the relevant gaseous species (B.36). For the second discretized boundary condition at $C_{A,1}$ the discretized derivative becomes $\frac{C_{A,2} - C_{A,0}}{2\Delta z} = 0$. The concentration at $C_{A,2}$ is within the pellet system. However, the concentration at $C_{A,0}$ is outside the pellet system and must be calculated. For the derivate to be equal to zero the concentration at $C_{A,0}$ must be equal to the concentration at $C_{A,2}$ (B.37). With respect to the calculation at $C_{A,1}$ the concentration at $C_{A,0}$ is replaced by $C_{A,2}$.

The single pellet system becomes:

Table B.2 – Equations in dimensionless form and discretized using method of lines the profiles in the pellet with respect to MeOH, H_2O, volatile Mo species and solid MoO_3. *i* is the respective component and *j* is the discretization step.

Profile	
$D_{e,j}\beta_{MoO_3}\frac{C_{MoO_3,i-1}-C_{MoO_3,i+1}}{2\Delta z}\frac{C_{j,i+1}-C_{j,i-1}}{2\Delta z}+D_{e,j}\frac{C_{j,i+1}-2C_{j,i}+C_{j,i-1}}{(\Delta z)^2}\varepsilon_i$ $+\frac{D_{e,j}}{\tilde{r}_{hole}+\Delta z\cdot(i-1)}\frac{C_{j,i+1}-C_{j,i-1}}{2\Delta z}\varepsilon_i+\tilde{r}_i=\frac{\partial C_{j,i}}{\partial\tau}\varepsilon_i$	(B.31)
Rate of formation	
$\tilde{r}_{MeOH}=-\frac{\varphi_{MeOH}^2 C_{MeOH}}{1+k_1 C_{MeOH}+k_2 C_{H_2O}}$	(B.32)
$\tilde{r}_{H_2O}=\frac{\varphi_{MeOH}^2 C_{MeOH}}{1+k_1 C_{MeOH}+k_2 C_{H_2O}}$	(B.33)
$\tilde{r}_{Mo(g)}=\frac{\varphi_+^2 a_{MoO_3,i} C_{MeOH,i}^{n_{MeOH}}}{1+K_3 C_{H_2O,i}}-\varphi_-^2 C_{Mo(g),i}^{n_{Mo(g)}}$	(B.34)
$\tilde{r}_{MoO_3}=-\frac{\varphi_+^2 a_{MoO_3,i} C_{MeOH,i}^{n_{MeOH}}}{1+K_3 C_{H_2O,i}}+\varphi_-^2 C_{Mo(g),i}^{n_{Mo(g)}}$	(B.35)
Boundary conditions for MeOH, H_2O and Mo(g)	
$C_j(\tau,1)=C_{j,N+1}=C_j^s$	(B.36)
$\frac{\partial C_j(\tau,0)}{\partial z}=\frac{dC_{j,1}}{dz}=\frac{C_{j,2}-C_{j,0}}{2\Delta z}=0\Rightarrow C_{j,2}=C_{j,0}$	(B.37)
Initial conditions for MeOH, H_2O and Mo(g)	
$C_{MoO_3}(\tau=0,z)=C_{MoO_3,1}\cdots C_{MoO_3,N+1}=0$	(B.38)
Initial conditions for MoO_3	
$C_{MoO_3}(\tau=0,z)=C_{MoO_3,1}\cdots C_{MoO_3,N+1}=1$	(B.39)

B-5.3 Arrhenius plot of the reverse volatilization rate constant (k_-)

Since the forward volatilization rate constant, k_+, is kept constant at all temperatures, the backward rate, k_-, constant decreases with increasing temperature, yielding faster overall volatilization at increased temperature.

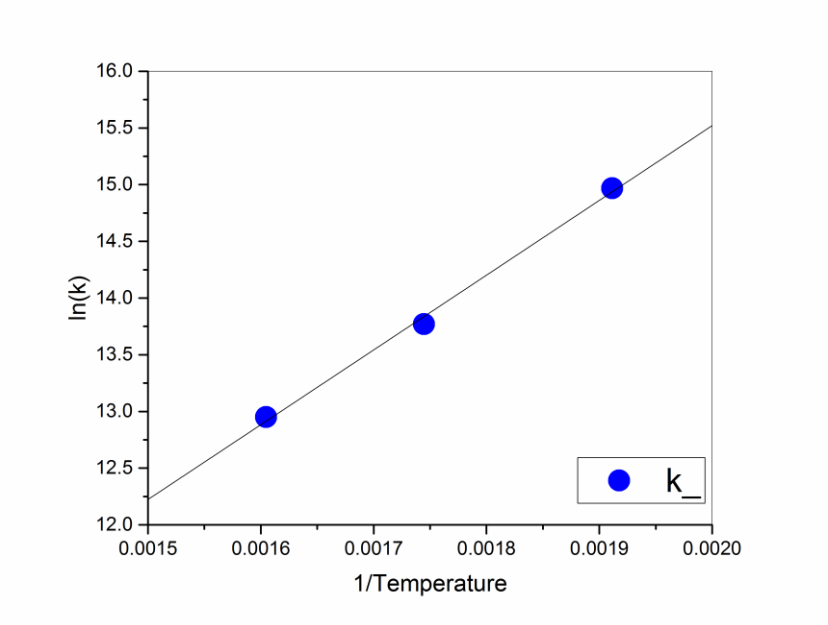

Figure B.15 – Arrhenius plot of the fitted reverse rate of volatilization rate constant.

Appendix C

C-1 Mass transfer coefficient and pellet surface area

The various correlations which have been applied in order to estimate mass transfer coefficients and diffusion coefficient, required in the model, are presented below.

The mass transfer coefficient of the volatile Mo-species is given by:

$$k_g = \frac{Sh\ D_{AB}}{d_p} \tag{C.1}$$

Where k_g is the mass transfer coefficient of the volatile Mo-species (m/s), Sh is the Sherwood number, d_p is the diameter of the catalyst pellet (m) (equivalent diameter of sphere of the same volume) and D_{AB} is the diffusion coefficient (m^2/s).

For the cylindrical hollow (ring shaped) catalyst pellet the surface area is given by:

$$A = 2\pi\left(\frac{d_R^2}{4} - \frac{d_r^2}{4}\right) + \pi h_p\left(d_R + d_r\right) \tag{C.2}$$

Where A is the surface area (m^2), d_R is the outer diameter of the pellet and d_r is the diameter of the hole in the pellet and h_p is the length of the pellet, all in (m).

The equivalent diameter of the pellet is given by:

$$d_p = \sqrt{\frac{A}{\pi}} \tag{C.3}$$

The Sherwood number can be calculated by:

$$Sh = J_D\, Sc^{1/3} Re \tag{C.4}$$

Where J_D is the Colburn factor. Sc is the Schmidt number and Re is the Reynolds number given by:

$$Sc = \frac{v_{gas}}{D_{AB}} \; Re = \frac{d_p U}{v_{gas}} \tag{C.5}$$

Where v is the kinetic viscosity (m^2/s) and U is the superficial gas velocity (m/s).

For (Re > 10) the following mass transfer correlation for flow through packed beds in terms of the Colburn *J* factor as a function of Reynolds number can be applied:

$$\varepsilon J_D = \frac{0.765}{Re^{0.82}} + \frac{0.365}{Re^{0.386}} \tag{C.6}$$

Where ε is the void fraction in the packed bed.

C-2 Dimensionless model

The system is written in dimensionless form by introducing the parameters (C.7) (C.8).

$$\sigma_i = \frac{Q_i}{V\varepsilon} \frac{L_p^2 \varepsilon^0}{D_{e,\mathrm{MeOH},ref}}, \; \sigma_p = \frac{A_p D_{e,Mo(g)}}{L_p \varepsilon} \frac{L_p^2 \varepsilon^0}{D_{e,\mathrm{MeOH},ref}} \tag{C.7) (C.8}$$

$$\sigma_{dep} = \frac{k_g A_p}{\varepsilon} \frac{L_p^2 \varepsilon^0}{D_{e,\mathrm{MeOH},ref}}, \; C_{Mo,dep} = \frac{C_{Mo,dep}}{C^0_{MoO_3}}, \; \beta_{dep} = \frac{1}{1-\varepsilon_{dep}} \frac{M_{MoO_3}}{\rho_{MoO_3}} \tag{C.9) (C.10) (C.11}$$

The system becomes:

$$\frac{\partial C^b_{Mo(g)}}{\partial \tau} = \sigma_{in} C^{in}_{Mo(g)} - \sigma_{out} C^b_{Mo(g)} - \sigma_{dep} (C_{Mo(g)} - C_{Mo(g),sat}) \tag{C.12}$$

$$\frac{\partial C^b_{Mo(g)}}{\partial \tau} = \sigma_{in} C^{in}_{Mo(g)} - \sigma_{out} C^b_{Mo(g)} - \sigma_p \frac{\partial C_{Mo(g)}}{\partial z} \tag{C.13}$$

$$\frac{\partial C_{Mo,dep}}{\partial \tau} = \sigma_{dep} (C_{Mo(g)} - C_{Mo(g),sat}) \tag{C.14}$$

With the initial conditions for all CSTR's:

$$C^b_{Mo(g)}(0) = 0, \; C_{Mo,dep}(0) = 0 \tag{C.15) (C.16}$$

The void space calculation in dimensionless form is given by:

$$\varepsilon = \varepsilon_0 - C_{Mo,dep}\beta_{dep} \tag{C.17}$$

C-3 Dynamic viscosity

The dynamic viscosity μ of the gas throughout the reactor is assumed only to vary with temperature T and follow the correlation:

$$\mu = k \cdot T^n \tag{C.18}$$

Where k and n are constants 1.0722 (Pa·s/K$^{0.5}$) and 0.5 respective.

C-4 Boundary conditions at inner pellet surface

The single pellet model previously derived (see chapter 3), does not take volatilization from the inner surface of the ring-shaped catalyst pellet into account, due to blocking of this surface by a thermocouple in the experiments used to measure the loss of Mo. However, volatilization from the inner surface occurs in an industrial reactor. To include this, the boundary condition at the inner surface ($r = R_h$) in the pellet model is changed to allow a gradient at this surface similar to the gradient at the outer surface as follows:

$$C_i(t, \mathrm{R}_h) = C_i^b \tag{C.19}$$

Where $C_i(t, \mathrm{R}_h)$ is the concentration of component i at the inner surface at time t and C_i^b is the concentration of component i in the bulk gas phase (both in mol/m^3).

C-5 Calculation of hydraulic diameter of the pellets

Li and Ma reported a procedure to calculate the hydraulic diameter of a non-spherical particles in a packed bed:

L. Li, W. Ma, "Experimental Study on the Effective Particle Diameter of a Packed Bed with Non-Spherical Particles," *Transport in Porous Media*, vol. 89, pp. 35-48, 2011.

The hydraulic diameter of the pellets is calculated following this procedure.

The pellets are shaped as cylinders with a hole. Outer diameter = 4.55 mm, hole diameter = 1.70 mm and length = 4.00 mm, yielding a pellet volume of 54.5 mm^3 and a surface area of 105.1 mm^2.

The shape factor of the particle ψ is calculated as follows:

$$\psi = \frac{A_{sp}}{A_p} = \frac{\pi^{\frac{1}{3}}(6V_p)^{\frac{2}{3}}}{A_p} = \frac{\pi^{\frac{1}{3}}(6 \cdot 54.5mm^3)^{\frac{2}{3}}}{105.1m^2} = 0.66 \quad \text{(C.20)}$$

Where V_p is the volume of the particle, A_p is the surface area of the particle and A_{sp} is thee surface area of the equivalent-volume sphere.

The Sauter mean diameter d_{sd} can be calculated as follows:

$$d_{sd} = \frac{6V_p}{A_p} = \frac{6 \cdot 54.5mm^3}{105.1m^2} = 3.11mm \quad \text{(C.21)}$$

The equivalent particle diameter (hydraulic diameter) d_{eq} is calculated as follows:

$$d_{eq} = \psi d_{sd} = 0.66 \cdot 3.1mm = 2.06mm \quad \text{(C.22)}$$

The calculated hydraulic diameter is calculated to 2.06 mm for the pellets.